Placental Cell Responses to Trichloroethylene Metabolite *S*-(1, 2-dichlorovinyl)-l-cysteine Exposure

by

Elana R. Elkin

A dissertation submitted in partial fulfillment
of the requirements for the degree of
Doctor of Philosophy
(Toxicology)
in the University of Michigan
2019

Doctoral Committee:

Professor Rita Loch-Caruso, Chair
Assistant Professor Dave Bridges
Assistant Professor Justin Colacino
Assistant Professor Mara Duncan
Professor Craig Harris

Elana R. Elkin

elkinela@umich.edu

ORCID iD: 0000-0001-8637-1731

Dedication

This dissertation is dedicated to H.T.R. and all others who selflessly contribute in order to further scientific research for the greater good.

And to those who contributed with or without their knowledge and/or consent.

To the trees and animals

To Peggy Adams and Ms. Terwilliger

To my family and friends

And to my partner in crime

COBY

Acknowledgements

I graciously acknowledge all the people that have supported me during my time here at University of Michigan. I would like to extend special thanks to my mentor and advisor, Dr. Rita Loch-Caruso, for her excellent mentorship and for the honor of allowing me to work in her lab. I would also like to thank members of my committee, Dr. Dave Bridges, Dr. Justin Colacino, Dr. Craig Harris, and Dr. Mara Duncan, for their guidance, support, time and expertise throughout the course of my doctoral studies. And for allowing me to work with them in their respective laboratories.

I would also like to thank all the present and past Loch-Caruso lab members who have offered their support and advice with experimental design, interpretation and training. I would also like thank them for engaging conversions about science and for making the Loch-Caruso lab an enjoyable place to work: Anthony Su, Dr. Sean Harris, Kyle Campbell, Dr. Kelly Hogan, Dr. Iman Hassan Dr. Hae-Ryung Park, Dr. Marisol Castillo-Castrejon, undergraduate lab assistants Eva Antibi-Lerman and Monica Smolinski, and our fearless lab manager Faith Bjork.

I'd like to especially extend my gratitude to Dr. Marie O'Neill for sending me on an adventure to Mexico and for encouraging me to pursue my doctoral studies, Dr. Kelly Bakulski for countless hours teaching me how to use R and for helping me make sense of my data; Dr. Randy Armant for graciously allowing me to work on placental tissues in his lab at Wayne State University, as well has his lab manager, Brian Kilburn; Dr. Shawn Xu of the University of Michigan Life Sciences Institute for giving me my first opportunity to work in a laboratory; Bridges Lab Manager, JeAnna Redd and lab members Molly Mullcahy and Archie for teaching me western blotting and many other important things; and Liz Ronan for providing me with essential Snapchat entertainment.

Completing my graduate studies at the University of Michigan has involved many collaborations and I would like to thank Maureen Kachman, Charles Evans, Angela Wiggins and Kari Bonds of the University of Michigan's Metabolomics Core, Maureen Sartor and Alla Karnovsky of the Bioinformatics Core, Sydney Bridges of the Nutrition Obesity Research Center, Larisa Yeomans of the University of Michigan Biochemical Nuclear Magnetic Resonance Core, Joel Whitfield of the University of Michigan Immunology Core, Ann Marie Deslauriers, Michael Pihalja and Sean Linkes of the University of Michigan Flow Cytometry Core and the staff of the DNA Sequencing Core.

Lastly, I would like to thank my family and friends especially my mom, Ellen Elkin, my dad, Dr. Neal Elkin and my siblings, Jonathan and Emily Elkin, my aunt, Margaret Bronson and our lifetime family friends, Addie Levine and Harvey Goldstein for putting up with me for a really long time.

This work would not have been possible without funding from the University of Michigan Horace H. Rackham School of Graduate Studies (One-term Dissertation Fellowship; Student Research Grant-Candidate; Student Research Grant-Pre-candidate; Travel Award), University of Michigan Mcubed research grant provided to Dr. Rita Loch-Caruso, Ruth L. Kirschstein Institutional Training Grant [ETEP] provided to Dr. Rita Loch-Caruso from the National Institute of Environmental Health (NIEHS)/National Institute of Health (NIH), The Puerto Rico Testsite for Exploring Contamination Threats [PROTECT] provided to Dr. Rita Loch-Caruso from the Superfund Research Program of the NIEHS, Michigan Lifestage Environmental Exposures and Disease (M-LEEaD) Center (Short Term Seed Pilot Grant) provided to Dr. Rita Loch-Caruso and funding from Wayne State University (Office of the Vice

President for Research; Center for Urban Responses to Environmental Stressors; Urban Health Waters).

Table of Contents

Dedication ii

Acknowledgements iii

List of Figures ix

Abstract x

Chapter I. Introduction 1

Pregnancy Complications and Adverse Birth Outcomes: A Global Public Health Crisis 1

Contributions of Environmental Contaminants to Risks of Adverse Birth Outcomes 2

Trichloroethylene: A pervasive and persistent environmental contaminant 3

Vulnerable Populations and Routes of Exposure 4

Trichloroethylene Metabolism 5

Trichloroethylene and DCVC-Mediated Adverse Health Outcomes 5

Evidence of DCVC-induced mitochondrial toxicity, lipid peroxidation and apoptosis in 6

Evidence of Maternal Trichloroethylene Exposure Associated with Adverse Birth Outcomes 7

Placenta as a Target of Trichloroethylene Toxicity 9

Role of Placenta in Pregnancy Impairment 10

Evidence of Mitochondrial Dysfunction in Pregnancy Disorders 11

Role of Apoptosis in Placental Disorders Involving Poor Placentation 12

HTR-8/SVneo Cell Line: An *in vitro* model of first-trimester extravillous trophoblast cells 13

Research Objectives and Overarching Hypothesis 13

References 20

Chapter II. Trichloroethylene Metabolite *S*-(1,2-Dichlorovinyl)-L-Cysteine Induces Lipid Peroxidation-Associated Apoptosis via the Intrinsic and Extrinsic Apoptotic Pathways in HTR-8/SVneo Cells 30

Abstract 30

Introduction 31
Materials and Methods 33
Results 42
Discussion 46
References 65
Chapter III. Short Duration Exposure to the Trichloroethylene Metabolite *S*-(1,2-Dichlorovinyl)-L-Cysteine Causes Compensatory Changes in Energy Metabolism in HTR-8/SVneo Cells 75
Abstract 75
Introduction 76
Materials and Methods 79
Results 86
Discussion 95
References 114
Chapter IV. Exposure to the Trichloroethylene Metabolite *S*-(1,2-Dichlorovinyl)-L-Cysteine for Short Durations Causes Progressive Mitochondrial Dysfunction in HTR-8/SVneo Trophoblasts 120
Abstract 120
Introduction 121
Materials and Methods 124
Results 132
Discussion 136
References 150
Chapter V. Transcriptional Profiling of the Trichloroethylene Metabolite *S*-(1,2-Dichlorovinyl)-L-Cysteine Revealed Activation of the EIF2α/ATF4 Integrated Stress Response in the HTR-8/SVneo Trophoblast Cell Line 157
Abstract 157
Introduction 158
Materials and Methods 160
Results 169
Discussion 173
References 190
Chapter VI. Conclusions 196
References 205

Appendix.. 208

List of Figures

Figure 1.1. Trichloroethylene Metabolism..... 16
Figure 1.2. Illustrated depiction of chorionic anchoring villi and extravillous trophoblast invasion of the uterus..... 17
Figure 1.3. Visualization of HTR-8/SVneo cells..... 18
Figure 1.4. Overall summary of dissertation specific aims..... 19
Figure 2.1. Effects of DCVC on apoptosis..... 57
Figure 2.2. DCVC effects on caspase activity. 58
Figure 2.3. Effect of tBID inhibitor pre-treatment on DCVC-stimulated caspase 3+7 activity..... 59
Figure 2.4. DCVC effects on cell mRNA expression of genes implicated in apoptosis signaling..... 60
Figure 2.5. Visualization of DCVC-induced gene expression changes in intrinsic and extrinsic apoptosis pathways..... 61
Figure 2.6. Effects of DCVC on lipid peroxidation..... 62
Figure 2.7. Effect of antioxidant co-treatment on DCVC-stimulated caspase 3+7 activity..... 63
Figure 2.8. Intrinsic and extrinsic apoptosis pathways..... 64
Figure 3.1. Effects of DCVC on cytotoxicity..... 103
Figure 3.2. DCVC-induced changes in key cellular energy status indictors..... 106
Figure 3.3. Effects of DCVC on energy metabolism pathways in HTR-8/SVneo cells..... 109
Figure 3.4. DCVC-induced changes in amino acid transporter levels..... 110
Figure 3.5. Energy pathway metabolite ratios..... 111
Figure 3.6. Proposed DCVC-induced energy metabolism alterations HTR-8/SVneo cells..... 113
Figure 4.1. Effects of DCVC on extracellular acidification rate (ECAR), oxygen consumption rate (OCR) and mitochondrial functional parameters..... 145
Figure 4.2. Effects of DCVC mitochondrial DNA content..... 146
Figure 4.3. Effects of DCVC mitochondrial membrane potential..... 147
Figure 4.4. Effect of antioxidant co-treatment on DCVC-induced changes in membrane potential depolarization and OCR..... 148
Figure 4.5. Proposed DCVC-induced mitochondrial dysfunction in HTR-8/SVneo cells..... 149
Figure 5.1. Summary of DCVC effects on differential gene expression in HTR-8/SVneo cells..... 181
Figure 5.2. Effects of DCVC concentration and exposure duration on transcriptional response..... 182
Figure 5.3. Identification of significantly enriched biological processes after 12 h treatment with DCVC..... 183
Figure 5.4. DCVC-induced Integrated Stress Response activation following 12 h treatment with DCVC..... 185
Figure 5.5. DCVC effects on protein synthesis..... 186
Figure 5.6. Effects of DCVC on cell cycle progression..... 187
Figure 5.7. Effects of DCVC on cellular proliferation..... 188
Figure 5.8. Summary of DCVC-induced activation of the Integrated Stress Response. 189
Figure 6.1. Integrated model depicting proposed responses to DCVC exposure in HTR-8/SVneo cells..... 204
Figure A.1. Effects of trichloroacetate (TCA) and dichloroacetate (DCA) treatment on cell viability..... 208
Figure A.2. Mitochondrial OCR function parameters..... 209
Figure A.3. Effects of acute DCVC treatment on OCR and ECAR..... 210
Figure A.4. Non-mitochondrial OCR..... 211
Figure A.5. Identification of significantly enriched biological processes after 6 h treatment with DCVC..... 212

Abstract

The placenta provides the critical interface between mother and fetus, regulating fetal *in utero* development through the exchange of hormones nutrients, waste, and oxygen. Given its critical role, abnormalities of the placenta substantially increase the risk of adverse birth outcomes. Although exposure to environmental contaminants is increasingly thought to elevate risk for adverse birth outcomes, the mechanism(s) by which toxicants adversely impact pregnancy remain largely unknown. Recent epidemiology studies found that maternal exposure to trichloroethylene (TCE), an industrial solvent and pervasive environmental contaminant, was associated with increased risk for low birth weight and preterm birth. This thesis investigated the effects of the TCE metabolite *S*-(1, 2-dichlorovinyl)-L-cysteine on extravillous trophoblasts, specific cells that play a pivotal role in tissue and maternal spiral artery remodeling during placental development.

DCVC effects on placental cells were studied using the HTR-8/SVneo immortalized extravillous trophoblast cell line. Following exposure to 5-20 μM DCVC for 6 or 12 h, targeted metabolomics detected changes in intracellular concentrations of metabolites from different energy metabolism pathways. Although no change in ATP levels were observed, glucose metabolism perturbations were detected that included a time-dependent accumulation of glucose-6-phosphate+frutose-6-phosphate (G6P+F6P), as well as independent shunting of glucose intermediates. Furthermore, DCVC treatment stimulated compensatory utilization of glycerol, lipid and amino acid amino metabolism to provide intermediate substrates entering downstream

glycolysis or the tricarboxylic cycle. In addition, transcriptomics analysis revealed hundreds of differentially expressed genes with exposure to 20 μM DCVC for 12 h (FDR<0.1 and fold-change < -1.5 or >1.5). Furthermore, gene set enrichment analyses demonstrated that the most substantially altered molecular signaling pathway was the EIF2α/ATF4 Integrated Stress Response (ISR), accompanied by decreased global protein synthesis. However, no changes in cell cycle progression or proliferation were detected, suggesting that a generally successful adaptive process occurred after 12 h of DCVC treatment.

In order to further investigate DCVC effects, HTR-8/SVneo cells were treated with 10-20 μM DCVC for mitochondrial bioenergentics experiments, or 10-100 μM DCVC for apoptosis experiments. Using the Seahorse XF Analyzer allowed evaluation of key aspects of mitochondrial function with concurrent real-time monitoring of oxygen consumption rates and extracellular acidification rates. Elevated basal oxygen consumption rate, mitochondrial proton leak and sustained energy coupling deficiency occurred after 6 h of exposure to 20 μM DCVC, whereas 12 h of exposure to DCVC decreased mitochondrial-dependent basal, ATP-linked and maximum oxygen consumption rates. Moreover, mitochondrial membrane potential dissipated after 12 h of exposure to 20 μM DCVC, as detected with the TMRE fluorochrome. The antioxidant (±)-α-tocopherol attenuated DCVC-stimulated mitochondrial membrane depolarization and caspase 3+7 activity but failed to rescue oxygen consumption perturbations. Furthermore, evaluation of DCVC-stimulated apoptosis revealed that DCVC simultaneously activated the mitochondrial-mediated and cell surface receptor-mediated apoptotic pathways, most likely via co-regulatory p53 signaling. Finally, mitochondria-centered crosstalk between the two activated pathways appeared to amplify the effect on the overall apoptotic response. Taken together, these findings showed progressive defects in mitochondrial function and suggest

mitochondria as the primary intracellular targets for DCVC-mediated cytotoxicity in placental cells.

Collectively, the series of studies presented in this thesis detail responses to the TCE metabolite DCVC in placental cells, contributing to our understanding of the toxicological mechanism of action of TCE. These new insights support epidemiology studies by providing plausible biological explanations for observed association with pregnancy complications and adverse birth outcomes.

Chapter I. Introduction

Pregnancy Complications and Adverse Birth Outcomes: A Global Public Health Crisis

Pregnancy complications and adverse birth outcomes are relatively common occurrences associated with a myriad of adverse birth outcomes ranging from minor conditions to untimely mortality for mothers and infants. Approximately 15 million or 11% of babies born yearly around the world are born before 37 weeks gestation and are categorized as preterm (WHO 2014). According to the World Health Organization, complications from preterm birth are the number one leading cause of death in children under 5 years of age, and 75% of these deaths are preventable (WHO 2014). In the United States, 8% or 315,000 babies born each year are classified as having low birth weights of less than 5.5 pounds (Martin 2015). Disorders related to preterm birth and low birth weight were the second leading of all infant mortality, whereas maternal pregnancy complications were the fourth leading cause, accounting for 17% and 6.1%, respectively, of U.S. infant deaths in 2016 (Heron 2018). Additionally, placental, cord and membrane complications accounted for an additional 3.6% of infant deaths (Heron 2018).The resulting health complications of preterm birth cost the United States an estimated twenty six billion dollars a year (Behrman et al. 2007). The widespread prevalence of pregnancy complications and unfavorable birth outcomes, and the potential severity and longevity of resulting health consequences, make these detrimental outcomes both an urgent and significant global public crisis.

Contributions of Environmental Contaminants to Risks of Adverse Birth Outcomes

Despite considerable scientific scrutiny and identification of risk factors associated with adverse birth outcomes, such as genetic factors, infections, contraindicated maternal behaviors and chronic maternal conditions, the precise pathophysiology underlying most pregnancy complications and adverse birth outcomes remains poorly understood (March of Dimes 2012). Exposure to environmental contaminants are increasingly thought to contribute to adverse birth outcomes. Indeed, epidemiological studies have detected associations between maternal exposures to environmental contaminants and increased risk for adverse birth outcomes (Ferguson et al. 2013; Porpora et al. 2019). For example, studies have associated exposure to fine air particulate matter (PM 2.5) with increased risk of pre-eclampsia and preterm birth (Jedrychowski et al. 2012; Liu et al. 2017). Exposures to water and soil contaminants have also been associated with poor gestational outcomes. Specifically, exposure to relatively low concentrations of lead and cadmium revealed an associated increase of preterm birth and small head circumference (Taylor et al. 2015; Taylor et al. 2016). Similarly, maternal exposure to polyfluoroalkyl substances (PFAS) was positively associated with preterm (Sagiv et al. 2018). Although some studies have established links between environmental contaminants and adverse birth outcomes, many studies have reported conflicting results on the same contaminants (Ferguson et al. 2013). For example, despite dozens of studies on the subject, an association between maternal environmental tobacco smoke exposure and preterm birth remains inconclusive (Elkin and O'Neill 2017). Despite reasonable evidence that maternal exposure to environmental contaminants contribute to elevated risks of adverse birth outcomes, further investigation into the biological plausibility and specific toxicological mechanism of different environmental contaminants is warranted.

Trichloroethylene: A pervasive and persistent environmental contaminant

Currently ranked as number sixteen on the U.S. Agency for Toxic Substances and Disease Registry's Substance Priority List, trichloroethylene (TCE) is an anthropogenic volatile organic compound with a long legacy of environmental contamination that peaked in the 1980s (Chiu et al. 2013; NTP 2015). Additionally, TCE continues to makes its way into the environment with approximately 1.9 million pounds of TCE being released in 2015(EPA 2017b). Although most TCE released into the environment vaporizes into air where it is quickly broken down, TCE persists as a contaminant in groundwater and soil (ATSDR 2014b). Because TCE is 50% denser than water, it can linger in groundwater for decades, potentially putting many people at risk of exposure from legacy contamination (ATSDR 2014b). In fact, an estimated one-third of all municipal water supplies in the United States have at least trace amounts of trichloroethylene (Jollow et al. 2009).

Originally commercialized in the 1920s as an oral anesthetic, TCE's potent solvent properties were quickly discovered and harnessed, propelling TCE to become one of the most commonly used industrial and dry-cleaning solvents by mid-century (Waters et al. 1977). Today, over 80% of TCE production is used as a chemical intermediate in closed-system refrigerant manufacturing processes, specifically HFC-134a, a refrigerant used in car air conditioning systems (ATSDR 2016; NTP 2015). The other current primary use of TCE is as a vaporized metal degreaser, although the Environmental Protection Agency (EPA) has proposed to ban this use as recently as 2017 (Chiu et al. 2013; EPA 2017a; Waters et al. 1977). As a result of its long-standing pervasive usage and its chemical properties, TCE is a ubiquitous persistent environmental contaminant found in soil, air and water (Chiu et al. 2013), including it presence in 1055 of 1750 current and former EPA-designated National Priorities List Superfund sites,

(ATSDR 2016; ATSDR 2017; EPA 2017b; EPA 2018). Because industrial usage and persistent environmental contamination of TCE continue, exposure remains a potential threat to human health.

Vulnerable Populations and Routes of Exposure

Use of TCE is regulated by law in most post-industrial countries. In the United States, the Environmental Protection Agency has set a maximum contaminant level of 5 ppb in drinking water (ATSDR 2014a). Similarly, the U.S. Occupational Safety and Health Administration (OSHA) has set a permissible exposure limit (PEL) of 100 ppm for TCE in air averaged over an 8-hour workday and an acceptable maximum of 300 ppm for no more than 5 minutes of any 2-hour period (ATSDR 2014a). Despite these regulations, exposure to TCE remains a concern for workers who are exposed at their workplaces and for residents who live near industries that continue to use TCE or who live near TCE-contaminated sites. Whereas community-level TCE exposure may occur through ingestion of contaminated drinking water, both occupational and community populations are vulnerable to TCE exposure through inhalation of TCE vapor-polluted air (Kim et al. 2014; Yu 2007). For example, a recent study detected blood concentrations of TCE that were 50 times higher in people exposed through residential vapor intrusion (>1.6 μg M^{-3} indoor air concentration) compared with residents of households with no detectable TCE vapor intrusion (Archer et al. 2015). Likewise, a recent occupational study detected TCE concentrations up to 229 ppm in 80 full-shift workers exposed through metal, optical lens and circuit board cleaning processes in factory settings. TCE was detected with personal aerosolized monitoring devices worn by the test subjects (Walker et al. 2016).

Trichloroethylene Metabolism

TCE's lipophilic, nonpolar and volatile properties allow it to be quickly absorbed into the blood stream from the lungs, gastrointestinal tract and skin (Lash et al. 2000a). Once in the blood stream, the chemical distributes most rapidly to highly perfused organs such as the liver, kidney and lungs where it is biotransformed (Lash et al. 2000a). There are two major metabolic pathways for TCE in mammals (Fig. 1.1). Occurring primarily in the liver, the major metabolic pathway is TCE oxidation by the cytochrome P450 family of enzymes (CYP1A2, CYP2E1 and CYP3A4) to chloral or oxalic acid. These latter metabolites are then biotransformed in multiple steps to the three key metabolites: chloral hydrate (CH), dichloroacetate (DCA), and trichloroacetate (TCA) (Lash et al. 2000a; Yu 2007). In the other important metabolic pathway, TCE is conjugated to glutathione as S-(1,2-dichlorovinyl) glutathione (DCVG). The DCVG is further metabolized to S-(1,2-dichlorovinyl)-L-cysteine (DCVC) and ultimately metabolized to either S-(1,2-dichlorovinyl)thiol (DCVT) or N-acetyl-S-(1,2-dichlorovinyl)-L-cysteine (NAcDCVC) (Lash et al. 2000a; Yu 2007). TCE has a relatively short plasma half-life of 3-4 days in humans depending on exposure duration and concentration. Although some TCE is exhaled in its parent form, most TCE is metabolized with execration and/or elimination from the body in bile and urine (Forkert et al. 2003; Lash et al. 2000a).

Trichloroethylene and DCVC-Mediated Adverse Health Outcomes

TCE has been extensively studied as a renal and liver toxicant because these organs are the primary sites of TCE metabolism in the body (Chiu et al. 2013; Lash et al. 2000a; Lash et al. 2006; Waters et al. 1977). TCE was recently re-classified by the National Toxicology Program (NTP) and International Agency for Research on Cancer (IARC) from a probable human

carcinogen to a known human (Guha et al. 2012; NTP 2015; Rusyn et al. 2014). This re-classification was based on epidemiology studies associating TCE exposure with elevated risk of renal cancer (Chiu et al. 2013; Scott and Jinot 2011) and experiments demonstrating that the TCE metabolite DCVC caused nephrotoxicity in human and animal renal tubular epithelial cells (Jaffe et al. 1984; Lash et al. 2000b). Other acute and chronic TCE-induced health effects that have been reported in epidemiology and animal studies include neurotoxicity, hepatotoxicity, nephrotoxicity, respiratory distress, and gastrointestinal irritation (Chiu et al. 2013; Lock and Reed 2006; Ramdhan et al. 2008; Reif et al. 2003; Rufer et al. 2010; Yu 2007).

Evidence of DCVC-induced mitochondrial toxicity, lipid peroxidation and apoptosis in

Dating back to the 1980s, multiple studies investigating mechanisms of DCVC toxicity in real proximal tubular cells have reported involvement of mitochondria, the primary energy-producing organelle in the cell. Mitochondrial toxicity is particularly challenging to evaluate because the organelle performs many different functions within a cell. As a result, mitochondrial toxicity is typically investigated *in vitro* by measuring numerous aspects of mitochondrial function using different laboratory assays and analytical techniques. Mitochondrial membrane potential depolarization is one of the best-established and reliable indicators of mitochondrial toxicity (Perry et al. 2011). At least four studies have measured DCVC-induced mitochondrial membrane depolarization in kidney cells. In general, it was found that the higher the DCVC concentration, the shorter the time required to depolarize the mitochondrial membrane. Lash et al. and van de Water et al. used 1 mM and 100 µM DCVC, respectively, in primary rat renal cells, and reported continuously measured depolarization beginning at 30 min and 1 h (Lash and Anders 1987; van de Water et al. 1994). Xu et al. used human renal tubal cells treated with 50 µM DCVC and visually observed depolarization at 4 h (Xu et al. 2008), Additionally, Chen et al.

reported mitochondrial membrane depolarization in a pig-derived renal cell line after exposure to 1 mM DCVC for 4 h. Moreover, several of the above-mentioned studies also reported other indicators of DCVC-induced mitochondrial toxicity including decreased oxygen consumption rates (Lash and Anders 1987; van de Water et al. 1995), elevated mitochondrial-sequestered calcium concentrations (van de Water et al. 1993; van de Water et al. 1994), and altered mitochondrial morphology (Chen et al. 2001; Van de Water et al. 1996).

In addition to mitochondrial toxicity, DCVC induces lipid peroxidation- reactive oxygen species damage to lipid molecules,-in the renal proximal tubular cells (Beuter et al. 1989; Chen et al. 1990; Groves et al. 1991). Lipid peroxidation can cause mitochondrial membrane potential collapse if it damages lipids contains within the mitochondrial membrane (Stark 2005). Furthermore, mitochondria and lipid peroxidation are both involved in the regulation of apoptotic pathways leading to programing cell death (Ayala et al. 2014; Simon et al. 2000), and DCVC initiates apoptosis in proximal tubular cells of humans and rodents (Chen et al. 2001; Lash et al. 2001; Van de Water et al. 1996; Xu et al. 2008). Taken together, the evidence to date indicates that mitochondrial dysfunction, lipid peroxidation and apoptosis play central roles in DCVC-mediated TCE cytotoxicity. For this reason, these cell functions were investigated as targets of DCVC toxicity in placental cells in this thesis.

Evidence of Maternal Trichloroethylene Exposure Associated with Adverse Birth Outcomes

Although many different studies have established TCE as a potent renal and liver toxicant (Chiu et al. 2013), TCE effects on pregnancy and birth outcomes remain understudied and inconclusive. Epidemiological studies investigating a potential TCE effect on pregnancy and birth outcomes have reported contradictory findings. For example, an early study found no

association between maternal TCE exposure and low birth weight (Lagakos et al. 1986). However, more recent studies reported positive associations between maternal TCE exposure and low birth weight and preterm birth (Forand et al. 2012; Ruckart et al. 2014). Most notably, a cross-sectional study concerning TCE exposure at the Camp Lejeune, NC, Superfund site found an association between TCE exposure and small-for-gestation-age (SGA) with an odds-ratio of 1.5 (95%CI: 1.2, 1.9) (Ruckart et al., 2014). Additionally, our laboratory recently published an animal study demonstrating potential pregnancy-related TCE toxicity in rats including reduced fetal weights and increased oxidative stress markers (Loch-Caruso et al. 2018). The discrepancies may be attributed to differences in exposure assessment methods, study size and statistical modeling.

Perhaps the most debatable aspect of pregnancy-related TCE toxicity involves conflicting evidence on whether or not TCE induces cardiotoxicity in developing fetuses. Although multiple laboratory animal studies spanning several decades have affirmatively reported TCE-induced cardiac abnormalities (Das and Scott 1994; Johnson et al. 2003; Rufer et al. 2010), other studies have reported that TCE causes no effects on fetal cardiac development (Carney et al. 2006; Fisher et al. 2001). Furthermore, two systematic reviews concluded there was inadequate evidence to demonstrate that maternal TCE exposure is associated with and/or causes congenital heart defects (Bukowski 2014; Watson et al. 2006). However, the most recent systematic review conducted by EPA scientists reported affirmative evidence (Makris et al. 2016). While more epidemiology studies are needed, there is sufficient evidence for toxicological interrogation of the biological plausibility of an association between maternal TCE exposure and gestational disorders.

Placenta as a Target of Trichloroethylene Toxicity

Although the kidney has been the focus of much research related to DCVC-mediated TCE toxicity, other highly perfused organs such as the placenta may also be targets for toxicity because of high-volume blood flow and other characteristics. For example, placental structure consisting of a large surface area and a thin interface separating maternal and fetal circulation provides an ideal environmental for maternal transfer of compounds (Burton and Fowden 2015). Moreover, hundreds of environmental compounds have been measured in umbilical cord blood confirming placental transfer (Aylward et al. 2014; Morello-Frosch et al. 2016) and in placental tissue confirming the potential for placental accumulation (Consortium et al. 2014). The placenta is readily exposed to circulating compounds. Additionally, it expresses many enzymes required for biotransformation of exogenous compounds including TCE metabolizing enzymes cytochrome P450, glutathione-S-transferase and beta-lyase (Lee et al. 2013; Myllynen et al. 2005), thereby increasing the risk of tissue-generated metabolites. With regards to TCE, several studies have demonstrated that TCE and a few of its cytochrome P450 pathway metabolites including TCA and DCA cross the placenta (Ghantous et al. 1986; Laham 1970).

Much attention has been paid to the cytochrome P450 oxidation pathway's key metabolites TCA and DCA as mediators of TCE-induced toxicity. However, preliminary experiments conducted by the Loch-Caruso Lab on TCA and DCA found no significant indications of toxicity in placental cells (Fig. A.1) (Hassan 2015). The glutathione conjugation pathway metabolite DCVC has also been the subject of research into TCE's potential mechanism of toxicity, especially in renal proximal tubular cells (Caldwell and Keshava 2006; Lash et al. 2000a; Lash et al. 2000b). In contrast to TCA and DCA, the Loch-Caruso lab has found significant evidence of DCVC toxicity in placental cells (Hassan 2015). These experiments were

part of the rationale for further investigating DCVC-induced toxic responses in extravillous trophoblasts.

Role of Placenta in Pregnancy Impairment

The placenta is a transient and multifaceted organ specially adapted to carryout multiple life-supporting functions for the fetus including oxygen and nutrient exchange, immune protection, hormonal synthesis and compound metabolism (Burton and Fowden 2015). Abnormal placental function can play a key role in the development of pregnancy complications and adverse birth outcomes (Ilekis et al. 2016). For example, placental insufficiency, which is defined as deficient nutrient and metabolic waste exchange between mother and fetus resulting from placental abnormalities, is known to cause intrauterine growth restriction (Baschat 2004; Gagnon 2003). Additionally, placental insufficiency may contribute to early parturition (Morgan 2014; Morgan 2016). For example, pregnancy disorders involving placental deficiencies such as pre-eclampsia have been associated or observed, respectively with adverse birth outcomes in several recent epidemiology and pathology studies (Davies et al. 2016; Nijman et al. 2016; Oshvandi et al. 2018).

Placental development early during the first-trimester is particularly important for establishing the maternal blood supply to the placenta. During the first-trimester, extravillous trophoblasts of fetal origin invade into the maternal uterine wall from the chorionic villi and facilitate critical remodeling of the spiral arteries necessary to accommodate increased maternal blood flow to the placenta (Fig. 1.2) (Burton and Jauniaux 2015; Pijnenborg et al. 1981). Furthermore, as pregnancy progresses to the second and third trimesters, the extravillous trophoblasts form cell columns at the tips of chorionic villi that anchor the villi to the maternal basal plate and stabilize them in the intervillous space (Kaufmann and Castellucci 1997).

Dysfunctional trophoblasts may jeopardize the fetal blood supply and result in abnormal placental development, potentially leading to adverse gestational outcomes (Norwitz 2007). In this thesis, impaired extavillous trophoblasts cells were investigated as a possible mechanism for TCE injury to the placenta.

Evidence of Mitochondrial Dysfunction in Pregnancy Disorders

Optimal mitochondrial functioning is critical for placental cells because of their sizable energy requirements for carrying out early pregnancy biological processes such tissue remodeling (Mando et al. 2014; Murray 2012; Vaughan and Fowden 2016). Mitochondrial dysfunction associated with first-trimester pregnancy disorders involving poor placentation has been well-studied. The most widely-reported aspects of mitochondrial function associated with abnormal placentae are mitochondrial-generated ROS including lipid peroxidation and mitochondrial DNA content (Gupta et al. 2005; Holland et al. 2017). For instance, pre-eclamptic and intrauterine growth-restricted pregnancies have increased placental lipid peroxidation and serum circulating lipid peroxidation byproducts compared to normal pregnancies (Atamer et al. 2005; Biri et al. 2007; Gupta et al. 2005; Karowicz-Bilinska et al. 2007; Madazli et al. 2002). With regards to mitochondrial copy number and pregnancy disorders, studies have provided conflicting evidence (Holland et al. 2017). Several studies reported decreased placental mitochondrial content in term IUGR pregnancies (Mando et al. 2014; Poidatz et al. 2015), while other studies reported increased content (Lattuada et al. 2008; Mando et al. 2014). One of the latter studies even reported decreased mitochondrial content in isolated cytotrophoblasts and increased content in tissue (Mando et al. 2014). Nevertheless, a consistent finding in published studies is some type of alteration in mitochondrial content with pregnancy disorders compared to normal pregnancies. Finally, perturbations of mitochondrial oxygen consumption rate, electron

transport, and proton leak were reported in pre-eclamptic human placental tissues (Holland et al. 2018; Xu et al. 2018). To date, there is considerable evidence supporting the theory that mitochondrial disruptions play a role in the pathophysiology of early pregnancy disorders. Thus, this thesis investigated DCVC-induced mitochondrial dysfunction as a mechanism by which TCE contributes to pregnancy complications and adverse birth outcomes.

Role of Apoptosis in Placental Disorders Involving Poor Placentation

Apoptotic cell death can severely impair tissue development and function if stimulated to occur excessively and prematurely. Apoptosis is defined as programed cell death which is specifically characterized by signal-induced, energy-dependent breakdown and condensation of nuclei, and fragmented cellular components packaged into apoptotic vesicles in preparation for phagocytosis by immune system cells (Sharp et al. 2010). During pregnancy, normal apoptosis plays a vital role in implantation, placentation and remodeling of decidual tissue and maternal spiral arteries in early pregnancy (Sharp et al. 2010; Smith et al. 1997b). However, aberrant and widespread apoptosis is strongly associated with several pregnancy disorders specifically characterized by poor placentation such as pre-eclampsia and intrauterine growth restriction (DiFederico et al. 1999; Genbacev et al. 1999; Reister et al. 2001; Smith et al. 1997a). This aberrant apoptosis drives major pathological features of these pregnancy disorders including insufficient extravillous trophoblast invasion into the maternal decidua and inadequate remodeling of the spiral arteries (Aardema et al. 2001; Brosens et al. 1972; Caniggia et al. 1999; Kadyrov et al. 2006; Meekins et al. 1994; Pennington et al. 2012). Additionally, increased expression of apoptosis-inducing genes has been reported in association with recurrent miscarriages and failure of blastocyst implantation (Jurisicova et al. 2003; Rull et al. 2013). Because a growing body of evidence ties excessive apoptosis to abnormal placental

development, apoptosis in placental extravillous trophoblasts could be a mechanism by which DCVC contributes to poor placentation and early pregnancy disorders if it occurs *in vivo*.

HTR-8/SVneo Cell Line: An *in vitro* model of first-trimester extravillous trophoblast cells

The HTR-8/SVneo cell line models extravillous cytotrophoblasts *in vitro* (Graham et al. 1993) (Fig. 1.3). HTR-8/SVneo cells were originally derived from first trimester female human cytotrophoblast cells and immortalized with simian virus 40 large T antigen (Graham et al. 1993). HTR-8/SVneo cells retain key molecular and functional characteristics of extravillous trophoblasts such as invasive and proliferative capacities that change in response to stress and oxygen availability, expression of adhesion molecules and a mesenchymal proteomic phenotype (Hannan et al. 2010; Kilburn et al. 2000; Liu et al. 2016; Szklanna et al. 2017). In addition, HTR-8/SVneo cells express specific markers that uniquely identify extravillous trophoblasts including cytokeratin 7 (CK7) and α5β1 integrin, and, when grown on Matrigel, histocompatibility antigen, class I, G (HLA-G) (Irving et al. 1995; Khan et al. 2011; Kilburn et al. 2000; Takao et al. 2011).

Overall, HTR-8/SVneo cells have proven useful in modeling extravillous trophoblasts because primary first-trimester placental tissue tends to have limited availability for research purposes.

Research Objectives and Overarching Hypothesis

Pregnancy complications and resulting adverse birth outcomes remain a monumental global public health challenge. Currently, the biological mechanisms underlying pregnancy complications are poorly characterized. The primary research goal of this thesis was to identify and elucidate biologically plausible toxicological mechanisms by which environmental contaminants that may interfere with pregnancy, specifically focusing on TCE**.**

TCE is a common environmental contaminant detected in thousands of hazardous waste sites across the United States. Because of its continued use and widespread persistent environmental contamination, TCE exposure poses a threat to human health through ingestion of contaminated drinking water and inhalation of the volatilized chemical. Recent epidemiological studies report associations between maternal TCE exposure and adverse birth outcomes, in contradiction to earlier studies. TCE toxicity to the placenta may contribute to adverse birth outcomes due to the placenta's critical role during gestation. Specifically, extravillous trophoblasts, placental cells that invade into the uterine wall and play pivotal roles in placental development, may be targets of toxicity. This thesis investigated the effects of the trichloroethylene metabolite *S*-(1, 2-dichlorovinyl)-L-cysteine (DCVC) on extravillous trophoblasts. The overarching hypothesis is that short-term exposure to the TCE metabolite DCVC disrupts normal cellular energy metabolism, mitochondrial activity and alters molecular signaling pathways resulting in reduced physiological adaptability and aberrant apoptosis in early human placental cells. An overview of the specific aims is outlined in figure 1.4. The specifics aims for this thesis are:

1) Demonstrate that the trichloroethylene metabolite *S*-(1,2-dichlorovinyl)-L-cysteine induces apoptosis and lipid peroxidation in human placental cells.

2) Demonstrate that exposure to the trichloroethylene metabolite *S*-(1, 2-dichlorovinyl)-L-cysteine triggers changes in cellular energy metabolism in human placental cells.

3) Demonstrate that exposure to the trichloroethylene metabolite *S*-(1, 2-dichlorovinyl)-L-cysteine promotes mitochondrial dysfunction in human placental cells.

4) Show that the trichloroethylene metabolite *S*-(1,2-dichlorovinyl)-L-cysteine stimulates genome-wide differential gene expression resulting in stress-related adaptations in human placental cells.

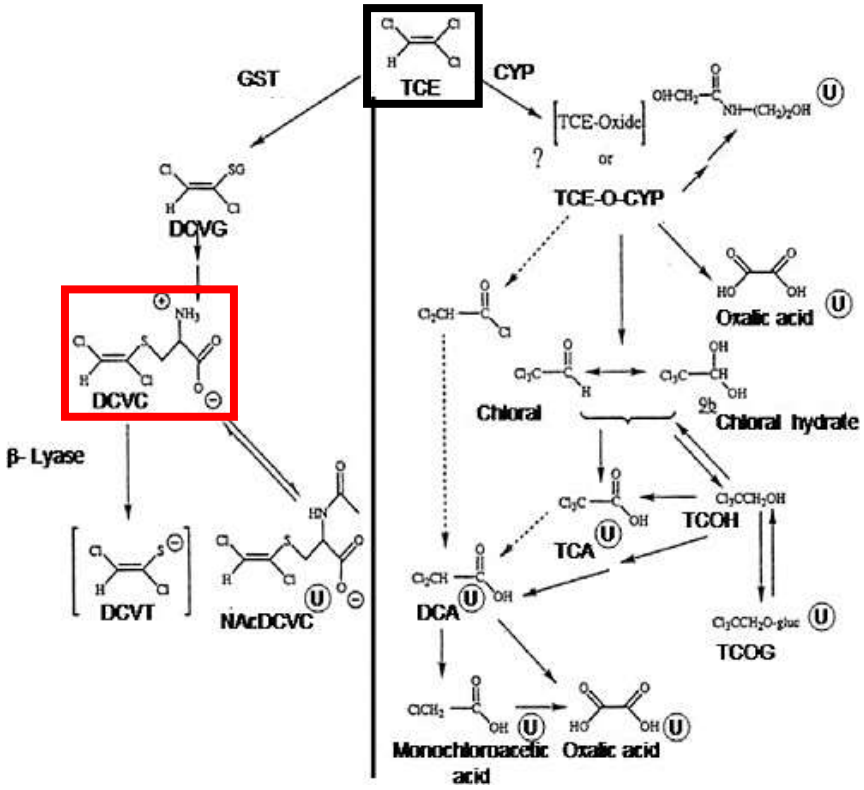

Figure 1.1. Trichloroethylene Metabolism.
Metabolism of TCE by cytochrome P450-dependent oxidation and glutathione pathway conjugation pathway. The parent compound is outlined in a black box and the metabolite of interest is outlined in a red box. Abbreviations: CYP, cytochrome P-450; DCA, dichloroacetic acid; DCVC, S-(1,2-dichlorovinyl)-L-cysteine; DCVG, S-(1,2-dichlorovinyl)glutathione; DCVT, S-(1,2-dichlorovinyl)thiol; GST, glutathione S-transferase; NAcDCVC, N-acetyl-S-(1,2-dichlorovinyl)-L-cysteine; TCA, trichloroacetic acid; TCE, trichloroethylene; TCE-O-CYP, trichloroethylene-oxide-cytochrome P-450 complex; TCOH, trichloroethanol; TCOG, trichloroethanol glucuronide; NAT, Nactyltransferase. Figure modified from National Research Council Publication (2006).

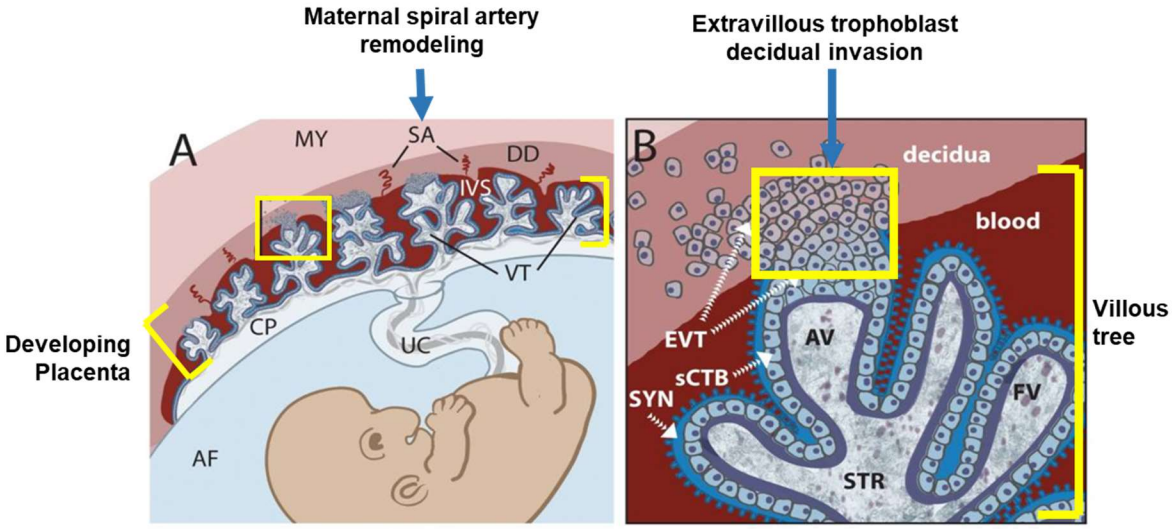

Figure 1.2. Illustrated depiction of chorionic anchoring villi and extravillous trophoblast invasion of the uterus.
During the process of placentation, extravillous trophoblasts of fetal origin invade the maternal uterine wall, facilitating tissue remodeling and widening of uterine spiral arteries necessary to accommodate increased blood flow to the uterus and tissue expansion as the pregnancy progresses. Insufficient trophoblast invasion resulting from toxicity can jeopardize normal placental development is a key pathological feature of pregnancy complications such as preeclampsia and intrauterine growth restriction. Figure modified from Robbins et al. (2010).

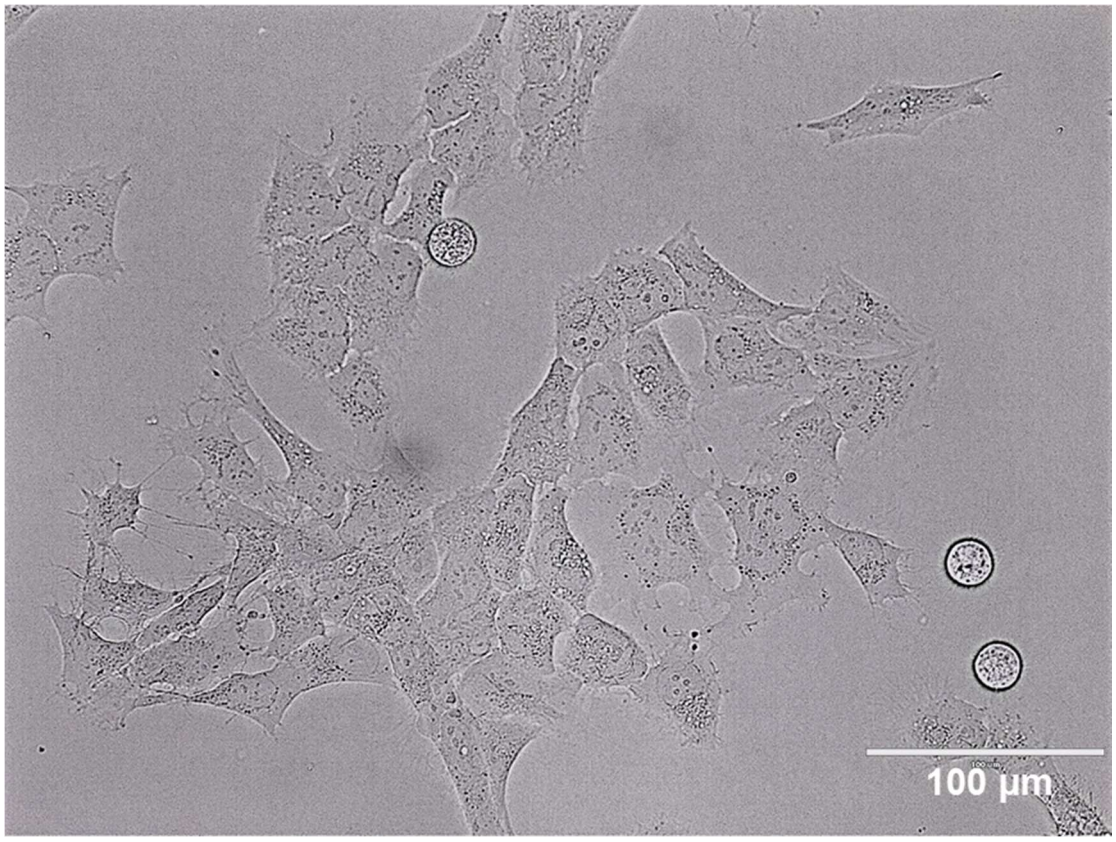

Figure 1.3. Visualization of HTR-8/SVneo cells.
The HTR-8/SVneo cell line is widely used to model cellular responses of first-trimester extravillous trophoblasts *in vitro*. The cell line was originally derived from first trimester female human cytotrophoblast cells and immortalized with simian virus 40 large T antigen (Graham et al. 1993). Multiple studies have reported that HTR-8/SVneo cells retain key molecular and functional characteristics of extravillous trophoblasts. The photo was taken with an EVOS fl inverted microscope with a 40X objective. Image shown with a 100 µm scale bar.

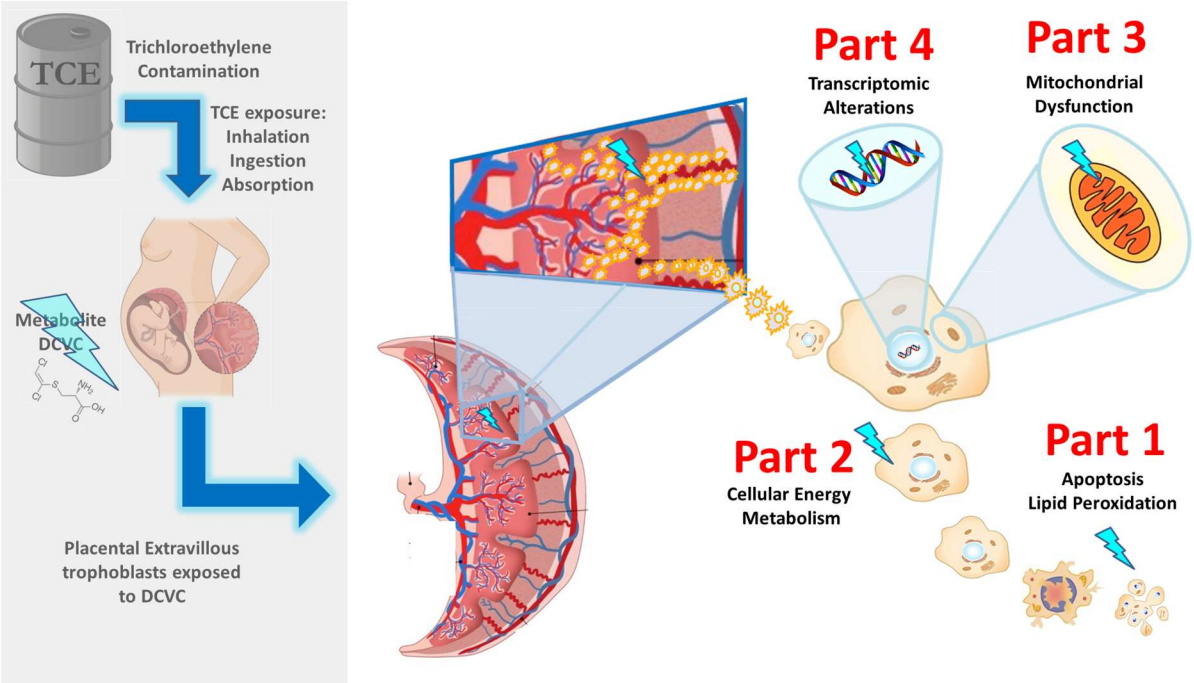

Figure 1.4. Overall summary of dissertation specific aims.
Part 1 investigated the effects of DCVC on apoptosis and lipid peroxidation in HTR-8/SVneo cells. Part 2 profiled DCVC-induced changes in macronutrient and energy metabolism pathway utilization. Part 3 evaluated DCVC-stimulated mitochondrial dysfunction. Part 4 analyzed DCVC-induced transcriptomic alterations and pathway enrichment analysis. Graphical depiction of the placenta was modified from an image found at: http://ib.bioninja.com.au/higher-level/topic-11-animal-physiology/114-sexual-reproduction/placenta.html.

References

Aardema M.W., Oosterhof H., Timmer A., van Rooy I., Aarnoudse J.G. 2001. Uterine artery doppler flow and uteroplacental vascular pathology in normal pregnancies and pregnancies complicated by pre-eclampsia and small for gestational age fetuses. *Placenta.* **22**:405-411.

Archer N.P., Bradford C.M., Villanacci J.F., Crain N.E., Corsi R.L., Chambers D.M., et al. 2015. Relationship between vapor intrusion and human exposure to trichloroethylene. *J Environ Sci Health A Tox Hazard Subst Environ Eng.* **50**:1360-1368.

Atamer Y., Kocyigit Y., Yokus B., Atamer A., Erden A.C. 2005. Lipid peroxidation, antioxidant defense, status of trace metals and leptin levels in preeclampsia. *Eur J Obstet Gynecol Reprod Biol.* **119**:60-66.

ATSDR. 2014a. Public health statement: Trichloroethylene. Available: http://www.atsdr.cdc.gov/ToxProfiles/tp19-c1-b.pdf.

ATSDR. 2014b. Toxicological profile for trichloroethylene. Available: http://www.atsdr.cdc.gov/toxprofiles/tp19.pdf 2016].

ATSDR. 2016. Public health statement on trichloroethylene.Agency for Toxic Substances and Disease Registry.

ATSDR. 2017. 2017 substance priority list.U.S. Agency for Toxic Substances and Disease Registry.

Ayala A., Munoz M.F., Arguelles S. 2014. Lipid peroxidation: Production, metabolism, and signaling mechanisms of malondialdehyde and 4-hydroxy-2-nonenal. *Oxid Med Cell Longev.* **2014**:360438.

Aylward L.L., Hays S.M., Kirman C.R., Marchitti S.A., Kenneke J.F., English C., et al. 2014. Relationships of chemical concentrations in maternal and cord blood: A review of available data. *J Toxicol Environ Health B Crit Rev.* **17**:175-203.

Baschat A.A. 2004. Fetal responses to placental insufficiency: An update. *BJOG.* **111**:1031-1041.

Behrman R.E., Butler A.S., Committee on Understanding Premature B., Assuring Healthy O., Board on Health Sciences P., Medicine I.o. 2007. Preterm birth:National Academies Press.

Beuter W., Cojocel C., Muller W., Donaubauer H.H., Mayer D. 1989. Peroxidative damage and nephrotoxicity of dichlorovinylcysteine in mice. *J Appl Toxicol.* **9**:181-186.

Biri A., Bozkurt N., Turp A., Kavutcu M., Himmetoglu O., Durak I. 2007. Role of oxidative stress in intrauterine growth restriction. *Gynecol Obstet Invest.* **64**:187-192.

Brosens I.A., Robertson W.B., Dixon H.G. 1972. The role of the spiral arteries in the pathogenesis of preeclampsia. *Obstet Gynecol Annu.* **1**:177-191.

Bukowski J. 2014. Critical review of the epidemiologic literature regarding the association between congenital heart defects and exposure to trichloroethylene. *Critical reviews in toxicology.* **44**:581-589.

Burton G.J., Fowden A.L. 2015. The placenta: A multifaceted, transient organ. *Philos Trans R Soc Lond B Biol Sci.* **370**:20140066.

Burton G.J., Jauniaux E. 2015. What is the placenta? *Am J Obstet Gynecol.* **213**:S6 e1, S6-8.

Caldwell J.C., Keshava N. 2006. Key issues in the modes of action and effects of trichloroethylene metabolites for liver and kidney tumorigenesis. *Environ Health Perspect.* **114**:1457-1463.

Caniggia I., Grisaru-Gravnosky S., Kuliszewsky M., Post M., Lye S.J. 1999. Inhibition of tgf-beta 3 restores the invasive capability of extravillous trophoblasts in preeclamptic pregnancies. *J Clin Invest.* **103**:1641-1650.

Carney E.W., Thorsrud B.A., Dugard P.H., Zablotny C.L. 2006. Developmental toxicity studies in crl:Cd (sd) rats following inhalation exposure to trichloroethylene and perchloroethylene. *Birth Defects Res B Dev Reprod Toxicol.* **77**:405-412.

Chen Q., Jones T.W., Brown P.C., Stevens J.L. 1990. The mechanism of cysteine conjugate cytotoxicity in renal epithelial cells. Covalent binding leads to thiol depletion and lipid peroxidation. *J Biol Chem.* **265**:21603-21611.

Chen Y., Cai J., Anders M.W., Stevens J.L., Jones D.P. 2001. Role of mitochondrial dysfunction in s-(1,2-dichlorovinyl)-l-cysteine-induced apoptosis. *Toxicol Appl Pharmacol.* **170**:172-180.

Chiu W.A., Jinot J., Scott C.S., Makris S.L., Cooper G.S., Dzubow R.C., et al. 2013. Human health effects of trichloroethylene: Key findings and scientific issues. *Environ Health Perspect.* **121**:303-311.

Consortium N.C.s.S.P., Nanes J.A., Xia Y., Dassanayake R., Jones R.M., Li A., et al. 2014. Selected persistent organic pollutants in human placental tissue from the united states. *Chemosphere.* **106**:20-27.

Das R.M., Scott J.E. 1994. Trichloroethylene-induced pneumotoxicity in fetal and neonatal mice. *Toxicol Lett.* **73**:227-239.

Davies E.L., Bell J.S., Bhattacharya S. 2016. Preeclampsia and preterm delivery: A population-based case-control study. *Hypertens Pregnancy.* **35**:510-519.

DiFederico E., Genbacev O., Fisher S.J. 1999. Preeclampsia is associated with widespread apoptosis of placental cytotrophoblasts within the uterine wall. *Am J Pathol.* **155**:293-301.

Elkin E.R., O'Neill M.S. 2017. Trends in environmental tobacco smoke (ets) exposure and preterm birth: Use of smoking bans and direct ets exposure assessments in study designs. *Chem Res Toxicol.* **30**:1376-1383.

EPA. 2017a. Trichloroethylene (tce); regulation of use in vapor degreasing under tsca §6(a) (rin 2070-ak11).

EPA. 2017b. Tri explorer: Release trends report.Environmental Protection Agency.

EPA. 2018. National priorities list.

Ferguson K.K., O'Neill M.S., Meeker J.D. 2013. Environmental contaminant exposures and preterm birth: A comprehensive review. *J Toxicol Environ Health B Crit Rev.* **16**:69-113.

Fisher J.W., Channel S.R., Eggers J.S., Johnson P.D., MacMahon K.L., Goodyear C.D., et al. 2001. Trichloroethylene, trichloroacetic acid, and dichloroacetic acid: Do they affect fetal rat heart development? *Int J Toxicol.* **20**:257-267.

Forand S.P., Lewis-Michl E.L., Gomez M.I. 2012. Adverse birth outcomes and maternal exposure to trichloroethylene and tetrachloroethylene through soil vapor intrusion in new york state. *Environ Health Perspect.* **120**:616-621.

Forkert P.G., Lash L., Tardif R., Tanphaichitr N., Vandevoort C., Moussa M. 2003. Identification of trichloroethylene and its metabolites in human seminal fluid of workers exposed to trichloroethylene. *Drug Metab Dispos.* **31**:306-311.

Gagnon R. 2003. Placental insufficiency and its consequences. *Eur J Obstet Gynecol Reprod Biol.* **110 Suppl 1**:S99-107.

Genbacev O., DiFederico E., McMaster M., Fisher S.J. 1999. Invasive cytotrophoblast apoptosis in pre-eclampsia. *Hum Reprod.* **14 Suppl 2**:59-66.

Ghantous H., Danielsson B.R., Dencker L., Gorczak J., Vesterberg O. 1986. Trichloroacetic acid accumulates in murine amniotic fluid after tri- and tetrachloroethylene inhalation. *Acta Pharmacol Toxicol (Copenh).* **58**:105-114.

Graham C.H., Hawley T.S., Hawley R.G., MacDougall J.R., Kerbel R.S., Khoo N., et al. 1993. Establishment and characterization of first trimester human trophoblast cells with extended lifespan. *Experimental cell research.* **206**:204-211.

Groves C.E., Lock E.A., Schnellmann R.G. 1991. Role of lipid peroxidation in renal proximal tubule cell death induced by haloalkene cysteine conjugates. *Toxicol Appl Pharmacol.* **107**:54-62.

Guha N., Loomis D., Grosse Y., Lauby-Secretan B., El Ghissassi F., Bouvard V., et al. 2012. Carcinogenicity of trichloroethylene, tetrachloroethylene, some other chlorinated solvents, and their metabolites. *Lancet Oncol.* **13**:1192-1193.

Gupta S., Agarwal A., Sharma R.K. 2005. The role of placental oxidative stress and lipid peroxidation in preeclampsia. *Obstet Gynecol Surv.* **60**:807-816.

Hannan N.J., Paiva P., Dimitriadis E., Salamonsen L.A. 2010. Models for study of human embryo implantation: Choice of cell lines? *Biology of reproduction.* **82**:235-245.

Hassan I. 2015. The effects of trichloroethylene on adverse birth outcomes. Ann Arbor, MI:University of Michigan.

Heron M. 2018. Deaths: Leading causes for 2016. *Natl Vital Stat Rep.* **67**:1-77.

Holland O., Dekker Nitert M., Gallo L.A., Vejzovic M., Fisher J.J., Perkins A.V. 2017. Review: Placental mitochondrial function and structure in gestational disorders. *Placenta.* **54**:2-9.

Holland O.J., Cuffe J.S.M., Dekker Nitert M., Callaway L., Kwan Cheung K.A., Radenkovic F., et al. 2018. Placental mitochondrial adaptations in preeclampsia associated with progression to term delivery. *Cell Death Dis.* **9**:1150.

Ilekis J.V., Tsilou E., Fisher S., Abrahams V.M., Soares M.J., Cross J.C., et al. 2016. Placental origins of adverse pregnancy outcomes: Potential molecular targets: An executive workshop summary of the eunice kennedy shriver national institute of child health and human development. *Am J Obstet Gynecol.* **215**:S1-S46.

Irving J.A., Lysiak J.J., Graham C.H., Hearn S., Han V.K., Lala P.K. 1995. Characteristics of trophoblast cells migrating from first trimester chorionic villus explants and propagated in culture. *Placenta.* **16**:413-433.

Jaffe D.R., Gandolfi A.J., Nagle R.B. 1984. Chronic toxicity of s-(trans-1,2-dichlorovinyl)-l-cysteine in mice. *J Appl Toxicol.* **4**:315-319.

Jedrychowski W.A., Perera F.P., Maugeri U., Spengler J., Mroz E., Flak E., et al. 2012. Prohypertensive effect of gestational personal exposure to fine particulate matter. Prospective cohort study in non-smoking and non-obese pregnant women. *Cardiovasc Toxicol.* **12**:216-225.

Johnson P.D., Goldberg S.J., Mays M.Z., Dawson B.V. 2003. Threshold of trichloroethylene contamination in maternal drinking waters affecting fetal heart development in the rat. *Environ Health Perspect.* **111**:289-292.

Jollow D.J., Bruckner J.V., McMillan D.C., Fisher J.W., Hoel D.G., Mohr L.C. 2009. Trichloroethylene risk assessment: A review and commentary. *Critical reviews in toxicology.* **39**:782-797.

Jurisicova A., Antenos M., Varmuza S., Tilly J.L., Casper R.F. 2003. Expression of apoptosis-related genes during human preimplantation embryo development: Potential roles for the harakiri gene product and caspase-3 in blastomere fragmentation. *Molecular human reproduction.* **9**:133-141.

Kadyrov M., Kingdom J.C., Huppertz B. 2006. Divergent trophoblast invasion and apoptosis in placental bed spiral arteries from pregnancies complicated by maternal anemia and early-onset preeclampsia/intrauterine growth restriction. *Am J Obstet Gynecol.* **194**:557-563.

Karowicz-Bilinska A., Kedziora-Kornatowska K., Bartosz G. 2007. Indices of oxidative stress in pregnancy with fetal growth restriction. *Free Radic Res.* **41**:870-873.

Kaufmann P., Castellucci M. 1997. Extravillous trophoblast in humans: A review. *Placenta.* **18**:21-65.

Khan G.A., Girish G.V., Lala N., Di Guglielmo G.M., Lala P.K. 2011. Decorin is a novel vegfr-2-binding antagonist for the human extravillous trophoblast. *Mol Endocrinol.* **25**:1431-1443.

Kilburn B.A., Wang J., Duniec-Dmuchowski Z.M., Leach R.E., Romero R., Armant D.R. 2000. Extracellular matrix composition and hypoxia regulate the expression of hla-g and integrins in a human trophoblast cell line. *Biology of reproduction.* **62**:739-747.

Kim I., Ha J., Lee J.H., Yoo K.M., Rho J. 2014. The relationship between the occupational exposure of trichloroethylene and kidney cancer. *Ann Occup Environ Med.* **26**:12.

Lagakos S., Wessen B., Zelen M. 1986. An analysis of contaminated well water and health eff ects in woburn, massachusetts *Journal of the American Statistical Association.* **81**:583-596.

Laham S. 1970. Studies on placental transfer. Trichlorethylene. *IMS Ind Med Surg.* **39**:46-49.

Lash L.H., Anders M.W. 1987. Mechanism of s-(1,2-dichlorovinyl)-l-cysteine- and s-(1,2-dichlorovinyl)-l-homocysteine-induced renal mitochondrial toxicity. *Molecular pharmacology.* **32**:549-556.

Lash L.H., Fisher J.W., Lipscomb J.C., Parker J.C. 2000a. Metabolism of trichloroethylene. *Environ Health Perspect.* **108 Suppl 2**:177-200.

Lash L.H., Parker J.C., Scott C.S. 2000b. Modes of action of trichloroethylene for kidney tumorigenesis. *Environ Health Perspect.* **108 Suppl 2**:225-240.

Lash L.H., Hueni S.E., Putt D.A. 2001. Apoptosis, necrosis, and cell proliferation induced by s-(1,2-dichlorovinyl)-l-cysteine in primary cultures of human proximal tubular cells. *Toxicol Appl Pharmacol.* **177**:1-16.

Lash L.H., Putt D.A., Parker J.C. 2006. Metabolism and tissue distribution of orally administered trichloroethylene in male and female rats: Identification of glutathione- and cytochrome p-450-derived metabolites in liver, kidney, blood, and urine. *J Toxicol Environ Health A.* **69**:1285-1309.

Lattuada D., Colleoni F., Martinelli A., Garretto A., Magni R., Radaelli T., et al. 2008. Higher mitochondrial DNA content in human IUGR placenta. *Placenta.* **29**:1029-1033.

Lee H.J., Jeong S.K., Na K., Lee M.J., Lee S.H., Lim J.S., et al. 2013. Comprehensive genome-wide proteomic analysis of human placental tissue for the chromosome-centric human proteome project. *J Proteome Res.* **12**:2458-2466.

Liu C., Sun J., Liu Y., Liang H., Wang M., Wang C., et al. 2017. Different exposure levels of fine particulate matter and preterm birth: A meta-analysis based on cohort studies. *Environ Sci Pollut Res Int.* **24**:17976-17984.

Liu L., Wang Y., Shen C., He J., Liu X., Ding Y., et al. 2016. Benzo(a)pyrene inhibits migration and invasion of extravillous trophoblast htr-8/svneo cells via activation of the erk and jnk pathway. *J Appl Toxicol.* **36**:946-955.

Loch-Caruso R., Hassan I., Harris S.M., Kumar A., Bjork F., Lash L.H. 2018. Trichloroethylene exposure in mid-pregnancy decreased fetal weight and increased placental markers of oxidative stress in rats. *Reprod Toxicol.* **83**:38-45.

Lock E.A., Reed C.J. 2006. Trichloroethylene: Mechanisms of renal toxicity and renal cancer and relevance to risk assessment. *Toxicol Sci.* **91**:313-331.

Madazli R., Benian A., Aydin S., Uzun H., Tolun N. 2002. The plasma and placental levels of malondialdehyde, glutathione and superoxide dismutase in pre-eclampsia. *J Obstet Gynaecol.* **22**:477-480.

Makris S.L., Scott C.S., Fox J., Knudsen T.B., Hotchkiss A.K., Arzuaga X., et al. 2016. A systematic evaluation of the potential effects of trichloroethylene exposure on cardiac development. *Reprod Toxicol.* **65**:321-358.

Mando C., De Palma C., Stampalija T., Anelli G.M., Figus M., Novielli C., et al. 2014. Placental mitochondrial content and function in intrauterine growth restriction and preeclampsia. *American journal of physiology Endocrinology and metabolism.* **306**:E404-413.

March of Dimes P., Save the Children, WHO. 2012. Born too soon: The global action report on preterm birth. Geneva:World Health Organization.

Martin J.A., Hamilton, B. E., Osterman, M. J. K., et al. 2015. Births: Final data for 2013. . Available: http://www.cdc.gov/nchs/data/nvsr/nvsr64/nvsr64_01.pdf 2016].

Meekins J.W., Pijnenborg R., Hanssens M., McFadyen I.R., van Asshe A. 1994. A study of placental bed spiral arteries and trophoblast invasion in normal and severe pre-eclamptic pregnancies. *Br J Obstet Gynaecol.* **101**:669-674.

Morello-Frosch R., Cushing L.J., Jesdale B.M., Schwartz J.M., Guo W., Guo T., et al. 2016. Environmental chemicals in an urban population of pregnant women and their newborns from san francisco. *Environ Sci Technol.* **50**:12464-12472.

Morgan T. 2014. Placental insufficiency is a leading cause of preterm labor. *NewReviews.* **15**:5618-e5525.

Morgan T.K. 2016. Role of the placenta in preterm birth: A review. *Am J Perinatol.* **33**:258-266.

Murray A.J. 2012. Oxygen delivery and fetal-placental growth: Beyond a question of supply and demand? *Placenta.* **33 Suppl 2**:e16-22.

Myllynen P., Pasanen M., Pelkonen O. 2005. Human placenta: A human organ for developmental toxicology research and biomonitoring. *Placenta.* **26**:361-371.

Nijman T.A., van Vliet E.O., Benders M.J., Mol B.W., Franx A., Nikkels P.G., et al. 2016. Placental histology in spontaneous and indicated preterm birth: A case control study. *Placenta.* **48**:56-62.

Norwitz E.R. 2007. Defective implantation and placentation: Laying the blueprint for pregnancy complications. *Reprod Biomed Online.* **14 Spec No 1**:101-109.

NRC. 2006. Assessing the human health risks of trichloroethylene: Key scientific issues. Washington D.C.:The National Academies Press.

NTP. 2015. Monograph on trichloroethylene Available: https://ntp.niehs.nih.gov/ntp/roc/monographs/finaltce_508.pdf 2016].

Oshvandi K., Jadidi A., Dehvan F., Shobeiri F., Cheraghi F., Sangestani G., et al. 2018. Relationship between pregnancy-induced hypertension with neonatal and maternal complications. *International Journal of Pediatrics.* **6**:8587-8594.

Pennington K.A., Schlitt J.M., Jackson D.L., Schulz L.C., Schust D.J. 2012. Preeclampsia: Multiple approaches for a multifactorial disease. *Dis Model Mech.* **5**:9-18.

Perry S.W., Norman J.P., Barbieri J., Brown E.B., Gelbard H.A. 2011. Mitochondrial membrane potential probes and the proton gradient: A practical usage guide. *Biotechniques.* **50**:98-115.

Pijnenborg R., Bland J.M., Robertson W.B., Dixon G., Brosens I. 1981. The pattern of interstitial trophoblastic invasion of the myometrium in early human pregnancy. *Placenta.* **2**:303-316.

Poidatz D., Dos Santos E., Duval F., Moindjie H., Serazin V., Vialard F., et al. 2015. Involvement of estrogen-related receptor-gamma and mitochondrial content in intrauterine growth restriction and preeclampsia. *Fertil Steril.* **104**:483-490.

Porpora M.G., Piacenti I., Scaramuzzino S., Masciullo L., Rech F., Panici P.B. 2019. Environmental contaminants exposure and preterm birth: A systematic review. *Toxics.* **7**:1-16.

Ramdhan D.H., Kamijima M., Yamada N., Ito Y., Yanagiba Y., Nakamura D., et al. 2008. Molecular mechanism of trichloroethylene-induced hepatotoxicity mediated by cyp2e1. *Toxicol Appl Pharmacol.* **231**:300-307.

Reif J.S., Burch J.B., Nuckols J.R., Metzger L., Ellington D., Anger W.K. 2003. Neurobehavioral effects of exposure to trichloroethylene through a municipal water supply. *Environ Res.* **93**:248-258.

Reister F., Frank H.G., Kingdom J.C., Heyl W., Kaufmann P., Rath W., et al. 2001. Macrophage-induced apoptosis limits endovascular trophoblast invasion in the uterine wall of preeclamptic women. *Lab Invest.* **81**:1143-1152.

Robbins J.R., Skrzypczynska K.M., Zeldovich V.B., Kapidzic M., Bakardjiev A.I. 2010. Placental syncytiotrophoblast constitutes a major barrier to vertical transmission of listeria monocytogenes. *PLoS pathogens.* **6**:e1000732.

Ruckart P.Z., Bove F.J., Maslia M. 2014. Evaluation of contaminated drinking water and preterm birth, small for gestational age, and birth weight at marine corps base camp lejeune, north carolina: A cross-sectional study. *Environ Health.* **13**:99.

Rufer E.S., Hacker T.A., Flentke G.R., Drake V.J., Brody M.J., Lough J., et al. 2010. Altered cardiac function and ventricular septal defect in avian embryos exposed to low-dose trichloroethylene. *Toxicol Sci.* **113**:444-452.

Rull K., Tomberg K., Koks S., Mannik J., Mols M., Sirotkina M., et al. 2013. Increased placental expression and maternal serum levels of apoptosis-inducing trail in recurrent miscarriage. *Placenta.* **34**:141-148.

Rusyn I., Chiu W.A., Lash L.H., Kromhout H., Hansen J., Guyton K.Z. 2014. Trichloroethylene: Mechanistic, epidemiologic and other supporting evidence of carcinogenic hazard. *Pharmacol Ther.* **141**:55-68.

Sagiv S.K., Rifas-Shiman S.L., Fleisch A.F., Webster T.F., Calafat A.M., Ye X., et al. 2018. Early-pregnancy plasma concentrations of perfluoroalkyl substances and birth outcomes in project viva: Confounded by pregnancy hemodynamics? *Am J Epidemiol.* **187**:793-802.

Scott C.S., Jinot J. 2011. Trichloroethylene and cancer: Systematic and quantitative review of epidemiologic evidence for identifying hazards. *Int J Environ Res Public Health.* **8**:4238-4272.

Sharp A.N., Heazell A.E., Crocker I.P., Mor G. 2010. Placental apoptosis in health and disease. *Am J Reprod Immunol.* **64**:159-169.

Simon H.U., Haj-Yehia A., Levi-Schaffer F. 2000. Role of reactive oxygen species (ros) in apoptosis induction. *Apoptosis : an international journal on programmed cell death.* **5**:415-418.

Smith S.C., Baker P.N., Symonds E.M. 1997a. Increased placental apoptosis in intrauterine growth restriction. *Am J Obstet Gynecol.* **177**:1395-1401.

Smith S.C., Baker P.N., Symonds E.M. 1997b. Placental apoptosis in normal human pregnancy. *Am J Obstet Gynecol.* **177**:57-65.

Stark G. 2005. Functional consequences of oxidative membrane damage. *J Membr Biol.* **205**:1-16.

Szklanna P.B., Wynne K., Nolan M., Egan K., Ainle F.N., Maguire P.B. 2017. Comparative proteomic analysis of trophoblast cell models reveals their differential phenotypes, potential uses and limitations. *Proteomics.* **17**:1700037-1700042.

Takao T., Asanoma K., Kato K., Fukushima K., Tsunematsu R., Hirakawa T., et al. 2011. Isolation and characterization of human trophoblast side-population (sp) cells in primary villous cytotrophoblasts and htr-8/svneo cell line. *PloS one.* **6**:e21990.

Taylor C.M., Golding J., Emond A.M. 2015. Adverse effects of maternal lead levels on birth outcomes in the alspac study: A prospective birth cohort study. *BJOG.* **122**:322-328.

Taylor C.M., Golding J., Emond A.M. 2016. Moderate prenatal cadmium exposure and adverse birth outcomes: A role for sex-specific differences? *Paediatr Perinat Epidemiol.* **30**:603-611.

van de Water B., Zoetewey J.P., de Bont H.J., Mulder G.J., Nagelkerke J.F. 1993. The relationship between intracellular ca2+ and the mitochondrial membrane potential in isolated proximal tubular cells from rat kidney exposed to the nephrotoxin 1,2-dichlorovinyl-cysteine. *Biochem Pharmacol.* **45**:2259-2267.

van de Water B., Zoeteweij J.P., de Bont H.J., Mulder G.J., Nagelkerke J.F. 1994. Role of mitochondrial ca2+ in the oxidative stress-induced dissipation of the mitochondrial membrane potential. Studies in isolated proximal tubular cells using the nephrotoxin 1,2-dichlorovinyl-l-cysteine. *J Biol Chem.* **269**:14546-14552.

van de Water B., Zoeteweij J.P., de Bont H.J., Nagelkerke J.F. 1995. Inhibition of succinate:Ubiquinone reductase and decrease of ubiquinol in nephrotoxic cysteine s-conjugate-induced oxidative cell injury. *Molecular pharmacology.* **48**:928-937.

Van de Water B., Kruidering M., Nagelkerke J.F. 1996. F-actin disorganization in apoptotic cell death of cultured rat renal proximal tubular cells. *Am J Physiol.* **270**:F593-603.

Vaughan O.R., Fowden A.L. 2016. Placental metabolism: Substrate requirements and the response to stress. *Reprod Domest Anim.* **51 Suppl 2**:25-35.

Walker D.I., Uppal K., Zhang L., Vermeulen R., Smith M., Hu W., et al. 2016. High-resolution metabolomics of occupational exposure to trichloroethylene. *Int J Epidemiol.* **45**:1517-1527.

Waters E.M., Gerstner H.B., Huff J.E. 1977. Trichloroethylene. I. An overview. *J Toxicol Environ Health.* **2**:671-707.

Watson R.E., Jacobson C.F., Williams A.L., Howard W.B., DeSesso J.M. 2006. Trichloroethylene-contaminated drinking water and congenital heart defects: A critical analysis of the literature. *Reprod Toxicol.* **21**:117-147.

WHO. 2014. Preterm birth factsheet. Vol. 2015:World Health Organization.

Xu F., Papanayotou I., Putt D.A., Wang J., Lash L.H. 2008. Role of mitochondrial dysfunction in cellular responses to s-(1,2-dichlorovinyl)-l-cysteine in primary cultures of human proximal tubular cells. *Biochem Pharmacol.* **76**:552-567.

Xu Z., Jin X., Cai W., Zhou M., Shao P., Yang Z., et al. 2018. Proteomics analysis reveals abnormal electron transport and excessive oxidative stress cause mitochondrial dysfunction in placental tissues of early-onset preeclampsia. *Proteomics Clin Appl.* **12**:e1700165.

Yu D. 2007. Trichloroethylene toxicity. Available: http://www.atsdr.cdc.gov/csem/tce/docs/tce.pdf 2016].

Chapter II. Trichloroethylene Metabolite *S*-(1,2-Dichlorovinyl)-L-Cysteine Induces Lipid Peroxidation-Associated Apoptosis via the Intrinsic and Extrinsic Apoptotic Pathways in HTR-8/SVneo Cells

Abstract

Trichloroethylene (TCE), a prevalent environmental contaminant, is a potent renal and hepatic toxicant through metabolites such as *S*-(1,2-dichlorovinyl)-L-cysteine (DCVC). However, effects of TCE on other target organs such as the placenta have been minimally explored. Because elevated apoptosis and lipid peroxidation in placenta have been observed in pregnancy disorders involving poor placentation, we evaluated the effects of DCVC exposure on apoptosis and lipid peroxidation in a human extravillous trophoblast cell line, HTR-8/SVneo. We exposed the cells *in vitro* to 10-100 μM DCVC for various time points up to 24 h. Following exposure, we measured apoptosis using flow cytometry, caspase activity using luminescence assays, gene expression using qRT-PCR, and lipid peroxidation using a malondialdehyde quantification assay. DCVC significantly increased apoptosis in time- and concentration-dependent manners ($p<0.05$). DCVC also significantly stimulated caspase 3+7, 8 and 9 activities after 12 h ($p<0.05$), suggesting that DCVC stimulates the activation of both the intrinsic and extrinsic apoptotic signaling pathways simultaneously. Pre-treatment with the tBID inhibitor Bl-6C9 partially reduced DCVC-stimulated caspase 3+7 activity, signifying crosstalk between the two pathways. Additionally, DCVC treatment increased lipid peroxidation in a concentration-dependent manner. Co-treatment with the antioxidant peroxyl radical scavenger (±)-α-tocopherol attenuated caspase 3+7 activity, suggesting that lipid peroxidation mediates DCVC-induced

apoptosis in extravillous trophoblasts. Our findings suggest that DCVC-induced apoptosis and lipid peroxidation in extravillous trophoblasts could contribute to poor placentation if similar effects occur *in vivo* in response to TCE exposure, indicating that further studies into this mechanism are warranted.

Introduction

Trichloroethylene (TCE) is a chlorinated volatile organic solvent most commonly used in chemical production and as an industrial metal degreaser (Chiu et al. 2013; NTP 2015; Waters et al. 1977). Ranked as number sixteen on the U.S. Agency for Toxic Substances and Disease Registry's Priority List of Hazardous Substances, TCE is a common environmental contaminant found in approximately 800 Environmental Protection Agency-designated Superfund sites (ATSDR 2015; Chiu et al. 2013). Despite being classified as a "known human carcinogen," (Guha et al. 2012; NTP 2015), approximately 1.9 million pounds of TCE were released into the environment in 2015 (EPA 2017). Because of its continued use and widespread persistent environmental contamination, TCE exposure continues to pose a threat to human health through ingestion of contaminated drinking water and inhalation of the volatilized chemical.

Although TCE is most commonly recognized as a renal and liver toxicant (Chiu et al. 2013), its effects during pregnancy are not well understood. TCE-induced fetal cardiotoxicity is particularly controversial: for example, some laboratory animal studies reported TCE effects (Das and Scott 1994; Johnson et al. 2003; Rufer et al. 2010) and other studies reported no cardiac defects (Carney et al. 2006; Fisher et al. 2001). Furthermore, two systematic literature reviews concluded there was insufficient evidence to support an association between TCE exposure and congenital heart abnormalities (Bukowski 2014; Watson et al. 2006). With regard to other pregnancy outcomes, an earlier study found no association between maternal TCE exposure and

low birth weight (Lagakos et al. 1986), but more recent epidemiology studies report positive associations of TCE exposure during pregnancy with decreased fetal weight and preterm birth (Forand et al. 2012) (Ruckart et al. 2014).

Placental toxicity could potentially mediate adverse birth outcomes such as preterm birth and decreased birth weight (Ilekis et al. 2016). In particular, emerging recent studies implicate placental insufficiency, defined as inadequate maternal-fetal nutrient and waste exchange resulting from placental abnormalities, as a potential cause of premature labor (Morgan 2014; Morgan 2016). Furthermore, a recent epidemiology study found a significant association between pre-eclampsia and preterm birth (Davies et al. 2016). Because it is highly perfused, the placenta is readily exposed to circulating TCE and its metabolites, and may be a target for TCE toxicity (Laham 1970). Moreover, the placenta is capable of metabolizing compounds, which puts it at risk for tissue generation of toxic TCE metabolites (Burton and Fowden 2015).

Previous studies have shown that TCE exerts its toxic effects primarily through its metabolites (Lash et al. 2014). For example, exposure to the glutathione conjugation pathway metabolite S-(1, 2-dichlorovinyl)-L-cysteine (DCVC) is toxic *in vitro* to renal proximal tubular cells, the main putative target in the kidney, of rats, mice and humans (Chen et al. 2001; Darnerud et al. 1989; Lash and Anders 1986; Lash et al. 2001; Xu et al. 2008). Furthermore, numerous studies demonstrated that DCVC induces mitochondrial dysfunction, excessive reactive oxygen species generation and subsequent lipid peroxidation in kidney cells (Chen et al. 1990; Chen et al. 2001; Lash and Anders 1986; Lash et al. 2003; van de Water et al. 1994; van de Water et al. 1995; Xu et al. 2008). Similarly, our lab recently showed that DCVC induces a loss of mitochondrial membrane potential and increases ROS generation in the first trimester extravillous trophoblast HTR-8/SVneo cell line (Hassan et al. 2016). Taken together, the

evidence indicates that mitochondrial dysfunction and aberrant ROS-generating lipid peroxidation play central roles in DCVC-mediated TCE cytotoxicity (Lash and Anders 1986).

Mitochondria and lipid peroxidation are involved in the regulation of apoptotic pathways (Ayala et al. 2014; Simon et al. 2000), and multiple studies have demonstrated that DCVC initiates apoptosis in proximal tubular cells of humans and rodents (Chen et al. 2001; Lash et al. 2001; Van de Water et al. 1996; Xu et al. 2008). Apoptosis is a highly organized form of cell death that is tightly regulated by two primary signaling pathways depending upon the stimulus: the mitochondrial-dependent or intrinsic pathway and the cell surface death receptor-mediated or extrinsic pathway. Apoptosis is especially critical during pregnancy (Straszewski-Chavez et al. 2005). During placental development, apoptosis plays an important role in removing damaged cells without injuring surrounding tissues (Sharp et al. 2010; Smith et al. 1997b; Straszewski-Chavez et al. 2005). Despite its role in normal placentation, evidence suggests that an abnormal increase in apoptosis of extravillous trophoblasts contributes to multiple placental pathologies including intrauterine growth restriction and pre-eclampsia (DiFederico et al. 1999; Genbacev et al. 1999; Smith et al. 1997a). The present study investigated the effects of DCVC on the two primary apoptosis signaling pathways and lipid peroxidation in the human extravillous trophoblast cell line HTR-8/SVneo.

Materials and Methods

Chemicals and reagents

The trichloroethylene metabolite S-(1, 2-dichlorovinyl)-L-cysteine (DCVC) was synthesized by the University of Michigan Medicinal Chemistry Core according to procedures described by McKinney et al. (McKinney et al. 1959). Purity (98.7%) was determined by HPLC analysis. A stock solution was prepared in PBS and identity was confirmed by proton nuclear

magnetic resonance spectroscopy performed at the University of Michigan Biochemical Nuclear Magnetic Resonance Core. Phosphate buffered saline (PBS) and 0.25% trypsin were purchased from Invitrogen Life Technologies (Carlsbad, CA, USA). BI-6C9 tBID inhibitor**,** *tert*-butyl hydroperoxide (TBHP) and (±)-α-tocopherol were purchased from Sigma-Aldrich (St. Louis, MO). Camptothecin was purchased from Cayman Chemical (Ann Arbor, MI). RPMI 1640 culture medium with L-glutamine and without phenol red, 10,000 U/mL penicillin/10,000 µg/mL streptomycin (P/S) solution, and fetal bovine serum (FBS) were purchased from Thermo Fisher Scientific (Waltham, MA, USA).

Cell culture and treatment

The HTR-8/SVneo cell line, a gift from Dr. Charles H. Graham (Queen's University, Kingston, Ontario, Canada), models first-trimester extravillous cytotrophoblasts *in vitro* (Graham et al. 1993). HTR-8/SVneo cells were originally derived from first trimester female human cytotrophoblast cells and immortalized with simian virus 40 large T antigen (Graham et al. 1993). HTR-8/SVneo cells were cultured as previously described (Hassan et al. 2016; Tetz et al. 2013). Briefly, cells were cultured between passages 71-87 in RPMI 1640 medium supplemented with 10% FBS and 1% P/S at 37°C in a 5% CO_2 humidified incubator. Cells were maintained in RPMI 1640 growth medium with 10% FBS and 1% P/S prior to and during experiments to ensure optimal cell growth (Graham et al. 1993). Cells were grown to 70-90% confluence at least 24 h after subculture before starting any experiment.

A stock solution of 1 mM DCVC was prepared in PBS and stored in 1-ml aliquots at -20°C to minimize freeze/thaw cycles. Prior to each experiment, a DCVC stock solution aliquot was quickly thawed in a 37°C water bath and then diluted in RPMI 1640 medium with 10% FBS and 1% P/S to final exposure concentrations of 10-100 µM DCVC. The DCVC concentrations

were selected for the current study to include the mean peak blood concentration of 13.4 μM *S*-(1,2-dichlorovinyl)glutathione, the stable precursor of DCVC, measured in female volunteers exposed to 100 ppm of TCE by inhalation for 4 h (Lash et al. 1999), with higher concentrations consistent with DCVC-induced cytotoxicity in human placental cells and human proximal tubular cells *in vitro* (Hassan et al. 2016; Xu et al. 2008).

Cell line validation

HTR-8/SVneo cells were seeded at a density of 400,000 cells per well in a 6-well cell culture plate and allowed to adhere for 24 h. Cells were treated with RPMI 1640 medium alone for 24 h. Following exposure, DNA was extracted using QIAamp® DNA Mini Kit (Qiagen; Hilden, Germany). DNA samples were frozen at -20ºC and transported to the University of Michigan DNA Sequencing Core for completion of the cell line validation process using microsatellite genotyping. At the core, AmpFLSTR Identifiler Plus PCR Amplification Kit run on an 3730XL Genetic Analyzer purchased from Applied Biosystems (Waltham, MA) was utilized to identify human genomic DNA for 8 tetranucleotide repeat loci and the Amelogenin gender determination marker. The short tandem repeat profile generated for our cells was compared to the short tandem repeat profile for HTR-8/SVneo (ATCC® CRL-3271™) published by American Type Culture Collection (Manassas, VA) (ATCC 2015). The short tandem repeat profile was an exact match: Amelogenin gender determination marker: X, CSF1PO: 12, D13S317: 9,12, D16S539: 13D5S818: 12, D7S820: 12, TH01: 6,9.3, vWA: 13,18, TPOX: 8 (ATCC 2015).

Apoptosis assessment with flow cytometry

HTR-8/SVneo cells were seeded at a density of 50,000 cells per well in a 24-well plate and allowed to adhere for 24 h prior to treatment. Cells were treated with medium alone

(control), DCVC (10, 20, 50 and 100 μM), or 4 μM camptothecin (positive control) in triplicate. After 12 or 24 h of exposure, viable, early apoptotic, late-apoptotic, and necrotic cells were measured using the Annexin V FITC Assay Kit (Cayman Chemical). This assay uses two staining solutions simultaneously: annexin V, which exclusively binds to phosphatidylserines externalized on the plasma membrane during apoptosis, and propidium iodide (PI), which enters the cell when the plasma membrane is compromised in late-apoptotic and necrotic cells. The assay was performed according to the manufacturer's protocol with modifications. Following exposure, cells were treated with 0.25% trypsin-EDTA and incubated for 2 min to detach adherent cells. Following incubation, trypsin was deactivated with cell culture medium and triplicate wells were pooled into one 5-ml round-bottom fluorescence-activated cell sorting tube per treatment group. Cells were washed with 1 ml Annexin V Binding Buffer and resuspended with 500 μl Annexin V FITC/Propidium Iodide Staining Solution diluted in Binding Buffer, incubated for 10 min at room temperature and transported to the University of Michigan Flow Cytometry Core for analysis. Early apoptotic, late apoptotic and necrotic cells were quantified using a FACSAria II Flow Cytometer (BD Biosciences; San Jose, CA). Quantification and dye-based visualization were performed using BD FACSDiva Software (BD Sciences; San Jose, CA) for PC. Cell aggregates and cellular debris were excluded using the forward scatter and side scatter modes and the analysis was performed using 10,000 events per sample. Annexin V-FITC was detected using the 488 nm laser, while PI was detecting using the 561 nm laser.

Measurement of caspase 3+7, 8 and 9 activity

HTR-8/SVneo cells were seeded at a density of 10,000 cells per well in a 96-well white, clear-bottom plate and allowed to adhere for 24 h prior to treatment. Cells were treated in quadruplicate with RPMI 1640 medium alone (control) or DCVC (20 or 100 μM). Following 3,

6, 12, or 24 h treatments, caspase activity was measured using luminescence-based Caspase-Glo 3/7, 8 and 9 Assays (Promega; Madison, WI) following the manufacturer's recommended protocols. Caspase assays utilize luminogenically engineered caspase substrates that are specific to each type of caspase being measured based on specific amino acid sequences embedded within the substrates: DEVD (Asp-Glu-Val-Asp) for caspase 3+7, LETD (Leu-Glu-Thr-Asp) for caspase 8, and LEHD (Leu-Glu-His-Asp) for caspase 9. Following cleavage of the substrates, the product generated, aminoluciferin, reacts with luciferase to produce light proportional to the amount of caspase activity (Niles et al. 2008). Briefly, for Caspase-Glo 3/7, 8 and 9 assays, respectively, 100 µL Caspase-Glo substrate in Caspase-Glo buffer was added to cell cultures and incubated at room temperature for 1 h following DCVC treatment. In order to reduce non-specific background signal, MG-132, a proteasome inhibitor, was added to caspase 8 and 9 cell cultures only. Following incubation, luminescence signal was measured on Glomax Multi Plus Detection System (Promega).

Apoptosis PCR array

We evaluated changes in the gene expression of 84 genes specifically involved in apoptosis using the commercially available Apoptosis PCR Array manufactured by SABiosciences (Valencia, CA). HTR-8/SVneo cells were seeded at a density of 400,000 cells per well in a 6-well cell culture plate and allowed to adhere for 24 h. Following the adjustment period, the cells were treated with RPMI 1640 medium alone (control) or DCVC **(**20, 50 and 100 µM**)** and exposed for 24 h. The concentrations of 20, 50 and 100 µM were chosen to span a range of concentrations from no effect to effective concentrations that induced apoptosis in our earlier experiment. Following exposure, cell lysates were homogenized using QIA shredder (Qiagen; Hilden, Germany) and RNA was extracted using the RNeasy Plus Mini Kit (Qiagen)

following the manufacture's recommended protocol. RNA samples were frozen at -20ºC and transported to the University of Michigan DNA Sequencing Core for completion of the Apoptosis PCR Array. At the core, cDNA was synthesized using the RT2 First Strand Kit (SABiosciences; Valencia, CA) following the manufacturer's recommended protocol. For the array, cDNA from the culture medium-only control, 20 μM DCVC, 50 μM DCVC and 100 μM DCVC treatment groups was analyzed using the Applied Biosystems 7900HT Sequence Detection System following the SABiosciences recommended protocol. Fold changes were calculated from ΔCT values (gene of interest CT value – average of all housekeeping gene CT values) using the ΔΔCT method. Mean ΔCT values were compared between groups using paired t-tests from the Limma package of Bioconductor (Smyth 2004). The resulting P-values were adjusted for multiplicity using the Benjamini and Hochberg false discovery rate method (Benjamini and Hochberg 1995).

Real-time quantitative PCR (qRT-PCR) validation

We validated the findings of the PCR-based array using qRT-PCR for genes with significant differential mRNA expression at least 2 fold higher or 0.5 fold lower than control following 100 μM DCVC treatment for 24 h. These genes included: Harakiri, BCl-2 interaction protein (*HRK*), BCL2-related protein A1 (*BCL2A1*), growth arrest and DNA-damage-inducible, alpha (*GADD45α*), DNA fragmentation factor alpha polypeptide (*c*), Receptor-interacting serine-threonine kinase 2 (*RIPK2*), nuclear factor kappa B subunit 1 (*NFKB1*), caspase 1 (*CASP1*) caspase 4 (*CASP4*), BCL2-antagonist/killer 1 (*BAK1*), and TNF receptor-associated factor 3 (*TRAF3*). We also tested differential expression of the tumor suppressor protein p53 (*TP53*) and TNF receptor superfamily, member 6 (*FAS*) genes because they showed a trend towards upregulation in the PCR-based array. Primary sequences are shown in Supplemental Table 1.

Primary sequences for *BCL2A1, DFFA, RIPK2, TRAF3, NFKB1, TP53, CASP1, BAK1, FAS AND CASP4* were obtained from the online primer sequence database PrimerBank (Spandidos et al. 2010). *HRK* primer sequence was obtained from Zaker et al. (Zaker et al. 2016). *GADD45α* primer sequence was obtained from Zhang et al. (Zhang et al. 2011). qRT-PCR was performed on the above genes using samples from cells treated with RPMI 1640 medium alone (control), or DCVC (20 and 100 μM) for 24 h. qRT-PCR reactions were prepared with SYBR Green Mastermix (SABiosciences) and custom synthesized primers (Integrated DNA Technologies; Coralville, IA), and run on a Bio-Rad (Hercules, CA) CFX96 Real Time C1000 thermal cycler following the manufacturer's recommended protocols. mRNA levels of each gene of interest were normalized to β-2-microglobulin (*B2M*) mRNA levels.

Visualization of intrinsic and extrinsic apoptosis pathways

We used PathVisio software (version 3.2.4) to visualize DCVC-induced gene expression changes in the intrinsic and extrinsic apoptotic pathways. Pathways were constructed from WikiPathways (Apoptosis-Homo Sapiens) (Kelder et al. 2012; Zambon et al. 2017) with modifications from Kegg Pathway Database (Apoptosis [map04210] and NOD-like receptor [map04621]-Homo sapiens signaling pathways) (Kanehisa et al. 2017) and other sources from the literature (Amaral et al. 2010; Gao and Abu Kwaik 2000; Graupner et al. 2011; Haupt et al. 2003; Inohara et al. 1997; McCarthy et al. 1998; Nishizaki et al. 2014; Perfettini et al. 2004; Roth et al. 2003). Genes found to be differentially expressed in either the 84-gene qRT-PCR array experiments or in qRT-PCR experiments were included in the visualization (except *CD70* and *IGR1F*).

ROS lipid peroxidation assessment

We investigated the effect of DCVC treatment on the degradation of membrane lipids by ROS by measuring a lipid peroxidation by-product, malondialdehyde (MDA). HTR-8/SVneo cells were seeded at a density of 150,000 cells per well in 12-well plates and allowed to adhere for 24 h prior to treatment. Cells were treated with medium alone (control), DCVC (10, 20, and 50 μM), or 20 μM *tert*-butyl hydroperoxide (TBHP) (positive control) for 12 h**.** MDA was measured using a Lipid Peroxidation (MDA) Assay Kit (Sigma-Aldrich) according to the manufacturer's protocol. The assay uses the reaction of MDA with thiobarbituric acid (TBA) to form an MDA-TBA adduct product proportional to the amount of MDA present in the samples. Briefly, cells were lysed using MDA lysis buffer containing butylated hydroxytoluene. Insoluble material was removed by centrifugation and lysates were transferred to microcentrifuge tubes. TBA solution was added to the lysate and incubated at 95ºC for 1 h. Lysate was cooled to room temperature with an ice bath for 10 min and plated on a 96-well plate for analysis. MDA concentration was measured colorimetrically (OD = 532 nm) using a SpectraMax M2e Multi-Mode Microplate Reader (Molecular Devices; Sunnyvale, CA).

Modulation of DCVC-stimulated caspase 3+7 activity

In order to investigate the role of aberrant ROS generation on DCVC-stimulated caspase 3+7 activity, the antioxidant peroxyl radical scavenger (±)-α-tocopherol was used to block lipid peroxidation. HTR-8/SVneo cells were seeded at a density of 10,000 cells per well in a 96-well white, clear-bottom plate and allowed to adhere for 24 h prior to treatment. Cells were treated in quadruplicate with medium alone (control) or DCVC (20 μM) plus (±)-α-tocopherol (50 μM). The cells were pre-treated for 15 min with (±)-α-tocopherol prior to co-treatment with DCVC for 12 h. We used a concentration of 50 μM (±)-α-tocopherol because it was previously shown by

our lab to attenuate DCVC-stimulated IL-6 release in HTR-8/SVneo cells (Hassan et al. 2016). In addition, it showed a protective role in TCE-induced human epidermal keratinocytes at a concentration of one order of magnitude higher (50 mM) (Zhu et al. 2005). Caspase 3+7 activity was measured with Caspase-Glo 3/7 Assay as previously described.

We explored the involvement of the truncated BID protein, tBID, as a source of cross talk between the two pathways. HTR-8/SVneo cells were seeded and cultured as previously described. Cells were treated in triplicate with medium alone (control), DCVC (20 μM) or DCVC plus tBID inhibitor BI-6C9 (10 μM). We used a concentration of 10 μM BI-6C9 because it was shown in a previous study to moderately inhibit BID-induced apoptosis without cytotoxicity (Becattini et al. 2004). The cells were pre-treated for 1 h prior with BI-6C9, followed by treatment with DCVC for 12 h. Caspase 3+7 activity was measured with Caspase-Glo 3/7 Assays as previously described.

Statistical Analysis

All experiments were performed independently in at least triplicate and repeated at least three times. The technical replicates were averaged within each experiment, and these values were analyzed using student's t-test, one-way or two-way analysis of variance (ANOVA), followed by Tukey's or Dunnett's post-hoc test for comparison of means using GraphPad Prism software (GraphPad Software Inc., San Diego, CA, USA). Data are expressed as means ± SEM. N=number of independent experiments. $P < 0.05$ was considered statistically significant.

Results

Effect of DCVC treatment on apoptosis

Because our laboratory previously demonstrated that DCVC treatment impacts cell viability, we investigated the effects of DCVC exposure on a specific form of cell death, apoptosis. Early apoptosis, late apoptosis, and necrosis were quantified in HTR-8/SVneo cells with annexin V-FITC and propidium iodide fluorescence indicators using flow cytometry (Fig. 2.1). Statistically significant concentration-dependent increases of total apoptosis were observed after 24 h but not 12 h of DCVC exposure (ANOVA interaction effect, $P=0.001$, Fig. 2.1). No statistically significant treatment-related differences were observed with 12 h of exposure, but treatment with 50 and 100 μM DCVC increased total apoptosis in a concentration-dependent manner at 24 h. Following 24-h treatment, total apoptosis increased from 6.38% (control) to 14.73% and 23.48% with 50 and 100 μM DCVC treatment, respectively ($P<0.001$). The 100 μM DCVC treatment increased apoptosis 2.3 fold at 24 h compared with 12 h ($P<0.0001$).

Effect of DCVC treatment on caspase activity

We measured the effects of DCVC on caspase activity to evaluate the involvement of the intrinsic and extrinsic apoptotic pathways in DCVC-induced apoptosis (Fig. 2.2). Caspases 3 and 7, which are downstream executor caspases activated by both the intrinsic and extrinsic pathways, showed time- and concentration-dependent increases in activity following DCVC exposure for 12 and 24 h (ANOVA time and treatment interaction, $P<0.0001$, Fig. 2.2A). Caspases 3+7 measured after 3 and 6 h of DCVC treatment showed no significant changes in activity. In contrast, treatment with 20 and 100 μM DCVC increased caspase 3+7 activity by 86.2% ($P=0.0015$) and 187.5% ($P<0.001$) at 12 h, and 88.6% ($P<0.001$) and 155.5% ($P<0.001$) at 24 h, respectively, compared with time-matched controls. Likewise, increases of caspase 3+7

activity were observed at 12 h and 24 h compared to earlier time points, ranging from 2.4 to 3.5 fold within each DCVC treatment ($P<0.0001$).

Caspase 9, an initiator caspase specific to the mitochondria-mediated intrinsic pathway, showed time- and concentration-dependent increases in activity following DCVC exposure (ANOVA time and treatment interaction, $P<0.0001$, Fig. 2.2B). Caspase 9 activity measured after 3 and 6 h of DCVC treatment showed no changes in activity level compared to time-matched controls. However, caspase 9 activity measured at 12 h showed a 56.3% increase in activity compared to time-matched control for 100 µM DCVC, whereas activity measured at 24 h showed 41.4% and 69.6% increases in activity compared to time-matched controls ($P<0.0001$). The 20 µM DCVC treatment increased caspase 9 activity 1.32 fold at 12 h compared to 6 h ($P=0.0228$) and 1.42 fold at 24 h compared to 12 h ($P<0.0001$). Similarly, 100 µM DCVC treatment increased caspase 9 activity 1.66 fold at 12 h compared to 6 h and 1.29 fold at 24 h compared to 12 h ($P<0.0001$).

Caspase 8, an initiator caspase specific to the cell surface receptor-mediated extrinsic pathway, showed time- and concentration-dependent increases in activity following DCVC exposure (ANOVA time and treatment interaction, $P<0.0001$, Fig. 2.2C). Caspase 8 activity measured after 3 and 6 h post-DCVC treatment showed no significant differences in activity compared to time-matched controls. However, caspase 8 activity measured at 12 h showed 36.5% ($P=0.029$) and 72.0% ($P<0.0001$) increases in activity compared to time-matched control for 20 and 100 µM DCVC, respectively, and activity measured at 24 h showed 30.6% ($P=0.0002$) and 70.2% ($P<0.0001$) increases in activity compared to time-matched control. The 20 µM DCVC treatment increased caspase 8 activity 1.86 fold at 12 h compared to 6 h and 1.39

fold at 24 h compared to 12 h (P<0.0001). The 100 μM DCVC treatment increased caspase 8 activity 2.39 fold at 12 h compared to 6 h and 1.43 fold at 24 h compared to 12 h (P<0.0001).

Inhibition of DCVC-stimulated caspase 3+7 by tBID protein inhibitor

In order to ascertain whether the DCVC mechanism of cytotoxicity involves interaction between the intrinsic and extrinsic apoptosis pathways, we used BI-6C9, which inhibits tBID-mediated cross talk between the two pathways. HTR-8/SVneo cells were pre-treated for 1 h with 10 μM BI-6C9 followed by treatment with 20 μM DCVC for 12 h. BI-6C9 pre-treatment attenuated DCVC-induced caspase 3+7 activity by 60.77% compared to cells treated with DCVC without the inhibitor (ANOVA interaction between DCVC and BI-6C9 treatments, P=0.028; Fig 2.3).

Apoptosis PCR array and qRT-PCR Validation

Because there are potentially hundreds of genes involved in the activation of apoptosis in cells, we used a commercially available PCR-based apoptosis array to screen 84 apoptosis-related genes for DCVC-induced changes in mRNA expression following treatment with 100 μM DCVC for 24 h (Supplement Table 2; P<0.05). Using this array, we identified ten genes that were significantly upregulated at least 2 fold or significantly downregulated at least 0.5 fold compared to control, and two other genes that showed a trend towards upregulation (Fig 2.4; P<0.05). We used qRT-PCR to follow up on these array results. In agreement with the PCR-based array results, 20 and 100 μM DCVC increased mRNA expression of the BCL-2 family genes *HRK*, *BAK1* and *BCL2A1* by 13.1 and 19.4 fold, 1.3 and 1.4 fold, and 7.6 and 8.0 fold, respectively, compared to control (P<0.05). Tumor suppressor gene *TP53* showed 1.7 and 1.3 fold increases in mRNA expression following 24-h treatment with 20 and 100 μM DCVC, respectively (P<0.05). Cell cycle arrest gene *GADD45α* expression increased 9.8 and 9.7 fold,

while *FAS* death receptor gene increased 1.8 fold with 20 and 100 μM DCVC treatments, respectively, compared to control ($P<0.05$). Inflammatory response genes *NFKB1*, *RIPK2*, and *CASP4* were upregulated 2.0 and 1.8 fold, 2.0 and 1.6 fold, and 1.7 and 2.5 fold, respectively, while *CASP1* was downregulated 0.5 and 0.2 fold, respectively, compared to control ($P<0.05$). Contrary to the array data, *TRAF3* and *DFFA* did not yield a significant increase in expression, although *DFFA* showed a trend towards upregulation of 1.5 fold compared to control with 100 μM DCVC treatment ($P=0.0582$). Relevant genes significantly up or down regulated in the apoptosis array and/or qRT-PCR are shown in Figure 2.5.

Effect of DCVC treatment on ROS lipid peroxidation

In order to further investigate the mechanism of DCVC-induced cytotoxicity, we evaluated the effects of DCVC on lipid peroxidation in HTR-8/SVneo cells by measuring cellular malondialdehyde concentrations, a byproduct and proxy measurement for lipid peroxidation. We detected a significant concentration-dependent increase in cellular malondialdehyde concentration following 24-h exposure to 10, 20 and 50 μM DCVC compared to control (Fig 2.6; $P<0.05$).

Attenuation of DCVC-stimulated caspase 3+7 activity by an antioxidant

To test the hypothesis that lipid peroxidation mediates DCVC-stimulated caspase 3+7 activity and apoptosis, we co-treated HTR-8/SVneo cells with either 20 μM DCVC only or 20 μM DCVC plus (±)-α-tocopherol (50 μM), an antioxidant peroxyl radical scavenger. Co-treatment with (±)-α-tocopherol significantly attenuated DCVC-stimulated caspase 3+7 activity by 80% compared to cells treated only with 20 μM DCVC for 12 h (ANOVA interaction between DCVC and α-tocopherol treatments, $P=0.0103$; Fig 2.7).

Discussion

Trichloroethylene continues to be a pervasive environmental contaminant in soil and groundwater despite reduction of improper disposal of the parent compound in recent decades. When TCE is ingested or inhaled, it is metabolized by two primary pathways into harmful metabolites, one of which is S-(1, 2-dichlorovinyl)-L-cysteine (DCVC), the focus of the current study. Although DCVC has been studied and established as a renal toxicant and carcinogen (Lash et al. 2014), epidemiological and animal studies linking TCE to pregnancy complications and adverse birth outcomes thus far remain inconclusive (Chiu et al. 2013), prompting our laboratory to examine DCVC as a placental toxicant. The general objectives of the current study were to further test the biological plausibility of DCVC as a placental toxicant and to examine its possible mechanism of action. In this study, we demonstrated that DCVC induced lipid peroxidation-associated apoptosis in placental cells through activation of both the intrinsic and extrinsic signaling pathways, providing new insights into the biological plausibility of DCVC-induced placental injury and the cytotoxic mechanism of action of DCVC.

Our laboratory previously reported that DCVC decreased cell viability and increased cytotoxicity in HTR-8/SVneo, an immortalized cell line that retains key molecular and functional characteristics of extravillous trophoblasts and which serves as an *in vitro* model for these cells (Hannan et al. 2010; Hassan et al. 2016; Khan et al. 2011; Kilburn et al. 2000). The present study extends those findings with evidence that DCVC directly induced aberrant apoptosis, a specific form of cell death, in the same HTR-8/SVneo cell type. These findings are consistent with previous reports that DCVC exposure induces apoptosis in kidney proximal tubular cells of humans and rodents (Chen et al. 2001; Lash et al. 2001; Van de Water et al. 1996; Xu et al. 2008). In addition, aberrant and widespread apoptosis of extravillous trophoblasts has been

observed in several pregnancy-related disorders specifically characterized by poor placentation such as pre-eclampsia and intrauterine growth restriction (DiFederico et al. 1999; Genbacev et al. 1999; Reister et al. 2001). Aberrant placental apoptosis is linked to major pathological features of these pregnancy disorders including insufficient extravillous trophoblast invasion into the maternal decidua and inadequate remodeling of the spiral arteries needed to accommodate increased maternal blood flow to the placenta (Aardema et al. 2001; Brosens et al. 1972; Caniggia et al. 1999; Kadyrov et al. 2006; Meekins et al. 1994; Pennington et al. 2012). Because a growing body of evidence ties excessive apoptosis to impaired trophoblast invasion and inadequate remodeling of the spiral arties commonly observed with pregnancy-related disorders, our results suggest that DCVC-induced apoptosis in extravillous trophoblasts could be a mechanism by which TCE contributes to poor placentation and early pregnancy disorders if it occurs *in vivo*.

In order to gain further insight into the cytotoxic mechanism of action, we evaluated specific signaling pathways involved in DCVC-stimulated apoptosis. Depending upon the stimulus, there are two well-characterized pathways that are capable of inducing apoptosis: the extrinsic and intrinsic pathways, as illustrated in Figure 2.8 (Ashkenazi, 2008; Beesoo et al., 2014). The intrinsic pathway is activated by non-receptor stress stimuli such as hypoxia, damaged DNA and ROS (Elmore 2007). These stimuli induce apoptosis through interactions with the BCL-2 family of mitochondrial proteins including BAX and BAK, which control mitochondrial membrane permeability. Upon activation, the pro-apoptotic BCL-2 family proteins dimerize to increase the permeability of the mitochondrial membrane, allowing cytochrome c to leak into the cytoplasm and prompting activation of the intrinsic pathway-specific initiator caspase 9 (Elmore 2007). In contrast, the extrinsic pathway is stimulated when

specific tumor necrosis factor (TNF) superfamily cytokines bind to TNF cell surface death receptors, prompting cytoplasmic adapter proteins to form complexes that activate extrinsic pathway-specific initiator caspase 8 (Elmore 2007; Straszewski-Chavez et al. 2005). Following activation of caspase 8 and 9, both apoptosis pathways converge in a common pathway when caspases 8 and 9 activate executioner caspases 3 and 7, ultimately leading to the cleavage of cellular proteins and destruction of the cell (Elmore 2007; Levy and Nelson 2000). In the current study, we showed that DCVC exposure simultaneously activated both major apoptosis pathways, as indicated by caspase 8 and 9 activity results, in time- and concentration-dependent manners. We chose to measure caspase enzymatic activity as an endpoint that reflects caspase zymogen activation as well as enzyme abundance (Niles et al. 2008). Although western blot analysis would provide specific information on protein expression, a study that compared the sensitivity and specificity of Caspase Glo assays to western blot analysis demonstrated a strong correlation between activity levels measured by Caspase Glo 3+7, 8, and 9 assays and western blot detection of active caspase enzymes (Alvero et al. 2008).

To our knowledge, our study is the first to demonstrate that DCVC is capable of activating both the intrinsic and extrinsic apoptosis pathways simultaneously, as indicated by the caspase results, as part of its cytotoxicity mechanism. Interestingly, these results only partially agree with a previous study that reported involvement of the mitochondrial-mediated intrinsic but not extrinsic pathway in DCVC-induced apoptosis (Xu et al. 2008). The differences between the study findings may be attributed to the different cell types and/or exposure concentrations examined. For example, contrary to our study, Xu et al. investigated the effects of DCVC in concentrations up to 300 μM in primary human proximal tubular cells.

Because our results clearly showed that DCVC exposure activated both intrinsic and extrinsic apoptosis signaling pathways in HTR-8/SVneo cells, we examined potential interactions between the two pathways by evaluating cross talk between the pathways. The best characterized source of cross talk between the two pathways involves the truncated protein tBID. The pathway interaction typically occurs when extrinsic pathway-specific caspase 8 cleaves the cytosolic BCL-2 protein family member BID into its truncated form, tBID. tBID then translocates across the mitochondrial membrane and engages the intrinsic pathway by dimerizing with BCL-2 family proteins and increasing mitochondrial membrane permeability (Li et al. 1998; Wei et al. 2000). Our results indicated that pre-treatment with the tBID inhibitor Bl-6C9 partially attenuated DCVC-induced downstream activation of caspases 3+7, demonstrating that cross talk between the two pathways contributes to the DCVC mechanism of stimulating apoptosis in placental cells.

In agreement with these results, we further observed that DCVC treatment stimulated an increase in caspase 3+7 activity that was more than double the increase in activity observed in either caspase 8 or 9 when compared to control. As reported in previous studies, the latter results strongly suggest that the cross talk occurring between the two pathways amplifies the effect on the common terminal pathway, which may also explain the magnitude of the DCVC-induced apoptotic response (Chou et al. 1999; Kuwana et al. 1998). Although multiple studies have established that first-trimester extravillous trophoblasts are capable of undergoing apoptosis via either the intrinsic or extrinsic pathways (Belkacemi et al. 2009; Belkacemi et al. 2011; Huang et al. 2014), to our knowledge, our study is the first to demonstrate a simultaneous pathway activation involving tBID-mediated cross talk in response to exposure to an exogenous chemical stimulant.

To elucidate the specific signaling mechanism of DCVC-induced apoptosis in placental cells, we evaluated expression of apoptosis-related genes using a targeted PCR-based array and qRT-PCR. The DCVC-induced gene expression changes for the extrinsic and intrinsic apoptotic pathways are summarized in Figure 2.6. We detected a notable DCVC-stimulated increase in *TP53* (p53) tumor suppressor gene expression consistent with previous studies (Chen et al. 2002; Rehman et al. 2013). The p53 protein activates apoptosis through multiple transcription-dependent and independent mechanisms involving both apoptosis pathways (Amaral et al. 2010; Haupt et al. 2003). In fact, the effect of DCVC on p53 may explain, at least in part, why both pathways are activated in DCVC-induced apoptosis. For example, we observed a significant upregulation of the p53 transcriptional target *FAS*, a gene encoding a TNF family death receptor, indicating involvement of p53 in extrinsic pathway regulation. On the other hand, we also observed a significant gene upregulation of *BAK1*, another p53 transcriptional target which codes for a BCL-2 family protein, indicating simultaneous involvement of p53 in intrinsic pathway regulation (Graupner et al. 2011; Perfettini et al. 2004). Additionally, p53 regulates the intrinsic pathway in a non-transcriptional manner by directly translocating into the mitochondria following stress-induced upregulation and cytosolic accumulation of the protein (Amaral et al. 2010; Haupt et al. 2003). Once inside the mitochondria, p53 forms an antagonist complex with anti-apoptotic Bcl-XL, releasing pro-apoptotic BAX and BAK1 to dimerize and increase mitochondrial membrane permeability (Amaral et al. 2010; Perfettini et al. 2004).

In addition to p53-associated apoptosis, we observed that DCVC treatment substantially increased the expression of another p53 transcriptionally regulated gene, *GADD45α*, which induces cell cycle arrest in response to stress stimuli (Hollander et al. 1993; Papathanasiou et al. 1991). Although previous studies failed to reach a consensus on the role of *GADD45α* in

apoptosis signaling (Sheikh et al. 2000), *GADD45α*-mediated gene expression has been implicated in physiological irregularities and insufficient trophoblast invasion in pre-eclamptic placentas (Liu et al. 2014; X Liu et al. 2016; Xiong et al. 2009; Xiong et al. 2013). Because DCVC exposure increased *GADD45α* gene expression by a magnitude of nearly ten-fold, our findings suggest that this gene may play a pivotal role in DCVC-induced placental cell cytotoxicity: however, further investigation is needed to clarify this role.

Several other salient apoptosis-related genes demonstrated differential DCVC-stimulated expression in the current study. For example, DNA fragmentation factor gene, *DFFA*, a common pathway caspase 3 cleavage target that promotes DNA fragmentation, showed a trend in upregulation following DCVC exposure. In addition, *CASP4*, the gene coding for caspase 4, was significantly upregulated, while *CASP1* was significantly downregulated. Caspases 1 and 4 are part of a family of caspases that are strongly implicated in inflammatory processes and responses to pathogens (McIlwain et al. 2015). Although their role in the induction of apoptosis is not fully understood (Denes et al. 2012), several studies have suggested that caspase 4 participates in endoplasm-reticulum stress-induced apoptosis in neuronal cells (Hitomi et al. 2004; Li et al. 2013; Yamamuro et al. 2011). More research in needed to clarify the function of caspases 1 and 4 expression in placental cells. Lastly, *HRK,* which showed a large 19-fold increase in expression, belongs to a BCL-2 subfamily of genes called BH3-only because they only contain one domain in common with other BCL-2 family genes. This subfamily of genes plays a pivotal role in the induction of intrinsic apoptosis because they travel freely in the cytoplasm until they are activated by receptor-free stimuli. Upon activation, they translocate into the mitochondria and interact with other mitochondrial-sequestered BCL-2 proteins like BAK1, directly stimulating the mitochondrial components of the intrinsic pathway (Inohara et al. 1997).

Interestingly, a previous study also reported an increase *HRK* mRNA expression in abnormally fragmented pre-implantation embryos (Jurisicova et al. 2003). These results may indicate that HRK plays an important role in regulating both normal and pathological cell death during early pregnancy.

Because our prior study showed that DCVC increases ROS generation in HTR-8/SVneo cells, we tested the hypothesis that aberrant ROS generation contributes to DCVC-induced apoptosis. We found that DCVC treatment increased malondialdehydes in HTR-8/SVneo cells, a byproduct and proxy measure for lipid peroxidation. These results are consistent with previous studies that indicate DCVC causes lipid peroxidation in kidney tubular cells of humans and rodents (Beuter et al. 1989; Chen et al. 1990; Groves et al. 1991). Lipid peroxidation occurs when reactive oxygen species, including free radicals, attack carbon double bonds in lipids resulting in lipid peroxyl radicals and hydroperoxides (Ayala et al. 2014). This process damages lipid membranes within the cell and affects their ability to function properly, especially the plasma and mitochondrial membranes. Membrane damage caused by lipid peroxidation is capable of inducing a loss of mitochondrial membrane potential because it destroys the selective barrier and ion transport properties of the membrane (Stark 2005). Our finding that DCVC induced lipid peroxidation offers a possible mechanistic explanation for a DCVC-induced loss of mitochondrial membrane potential in HTR-8/SVneo cells, previously reported by our lab (Hassan et al. 2016).

Consistent with our finding of DCVC-induced lipid peroxidation, we observed a significant increase in *NFKB1* gene expression in placental cells, as well as its upstream regulator *RIPK2* (McCarthy et al. 1998). NFKB1 (nuclear factor kappa-light-chain-enhancer of activated B cells) is a transcription factor primarily involved in inflammatory responses to a

variety of stimuli, most notably, reactive oxygen species (ROS) (Schreck et al. 1991). NFKB1 directly regulates the transcription levels of many cytokines such as the pro-inflammatory cytokine interleuken-6 (IL-6) (Libermann and Baltimore 1990). Our result indicating a DCVC-induced increase in *NFKB1* gene expression is consistent with our previous study that showed DCVC caused an ROS-mediated increase in IL-6 production (Hassan et al. 2016). Our *NFKB1* gene expression results are particularly significant because increased NFKB1 activity and concomitant aberrant ROS generation have been observed both in early pre-eclamptic pregnancies *in vivo* and in trophoblast-like cells *in vitro* (Luppi et al. 2006; Vaughan and Walsh 2012). Additionally, we observed the upregulation of another *NFKB1* transcriptional target *BCL2A1*, an anti-apoptotic BCL-2 family gene. The exact nature of the upregulation of this gene remains unclear but it is likely related to a stress response-induced biological feedback system.

Consistent with lipid peroxidation, we demonstrated that the antioxidant peroxyl radical scavenger (±)-α-tocopherol attenuated DCVC-induced increase caspase 3+7 activity. These results suggest that DCVC-stimulated apoptotic activity is dependent on increased ROS generation and lipid peroxidation. These data agree with prior findings that increased ROS generation is capable of inducing apoptosis (Myatt and Cui 2004; Simon et al. 2000; Smith et al. 1999). Lipid peroxidation activity has been observed in pregnancy complications that involve poor placentation. For example, multiple studies reported that pre-eclamptic pregnancies have increased placental lipid peroxidation and serum circulating lipid peroxidation byproducts compared to normal pregnancies (Atamer et al. 2005; Gupta et al. 2005; Madazli et al. 2002). Studies have also implicated lipid peroxidation as a pathological feature of intrauterine growth restriction (Biri et al. 2007; Karowicz-Bilinska et al. 2007). The evidence presented in the

current study suggests that increased ROS generation and lipid peroxidation are involved in the mechanism by which DCVC exposure placental toxicity.

Multiple studies have reported that HTR-8/SVneo cells retain key functional characteristics of extravillous trophoblasts such as invasive and proliferative capacities which change in response to stress and oxygen availability, expression of adhesion molecules and a mesenchymal proteomic phenotype (Hannan et al. 2010; Kilburn et al. 2000; L Liu et al. 2016; Szklanna et al. 2017). In addition, several studies have also shown that HTR-8/SVneo cells express specific markers that uniquely identify extravillous trophoblasts including cytokeratin 7 (CK7) and α5β1 integrin, and when grown on matrigel, histocompatibility antigen, class I, G (HLA-G) (Irving et al. 1995; Khan et al. 2011; Kilburn et al. 2000; Takao et al. 2011). Overall, HTR-8/SVneo cells have proven useful in modeling first-trimester extravillous trophoblasts because primary first-trimester placental tissue tends to have limited availability for research purposes. Regardless, *in vitro* cultured cells lack cell signaling and tissue interactions that would otherwise be present in *in vivo* models. Thus, *in vivo* studies are needed to further validate our results. In addition, HTR-8/SVneo is an immortalized cell line. Even though HTR-8/SVneo were originally derived from first-trimester non-cancerous placental cells, the process of immortalization changes cells to allow them to be cultured for extended periods of time (Graham et al. 1993). Moreover, cell culture conditions may also be responsible for reported changes in the genetic and epigenetic profiles of HTR-8/SVneo cells (Bilban et al. 2010; Novakovic et al. 2011). For these reasons, the mechanisms of cytotoxicity of DCVC should be further investigated in primary first-trimester extravillous trophoblasts.

The current study includes DCVC concentrations selected for relevance to human exposure. Although the EPA's maximum contaminant level (MCL) for drinking water is 5 μg/L

or parts-per-billion of TCE (NTP 2015), some people may regularly be exposed to TCE levels in drinking water that exceed the EPA MCL (ATSDR 2016). Moreover, the Occupational Safety and Health Administration (OSHA) Permissible Exposure Limit (PEL) is 100 ppm averaged over an 8-hour work day (ATSDR 2016). We suggest that the 10 µL and 20 µL DCVC concentrations used in our study are relevant to occupational exposures because the average peak concentration in blood of female volunteers exposed to 100 ppm TCE by inhalation for 4 h was 13.4 µM for the metabolic precursor to DCVC, *S*-(1,2-dichlorovinyl)glutathione (Lash et al. 1999). Moreover, the most recent human physiologically based pharmacokinetic models are in good agreement with human data of the latter study, though the need for further study was noted (EPA 2011). Adding support that the concentrations used in our study are plausible for some occupational exposures, a recent study detected concentrations up to 229 ppm using personal aerosolized TCE exposure of 80 workers (29% women) (Walker et al. 2016). We measured a number of significant effects on HTR-8/SVneo cells at the 20 µL DCVC treatment level, including increased caspase 3, 7, 8 and 9 activation, increased malondialdehyde formation, and increased expression of multiple apoptosis and inflammatory-related genes, suggesting that DCVC stimulated apoptosis, lipid peroxidation, and pro-inflammatory responses at a concentration relevant for human exposure. Additionally, we included higher DCVC concentrations in our study that allowed us to characterize DCVC-induced cell death more completely. The concentrations of 50 µM and 100 µM DCVC are still within an order of magnitude of occupationally relevant concentrations, and similar to (Hassan et al. 2016) or less than those used in previously published *in vitro* studies, with multiple studies using concentrations up to 500 µM and 1 mM DCVC (Chen et al. 2001; Lash et al. 2001; Lash et al. 2003; van de Water et al. 1995; Xu et al. 2008).

In summary, we detected significant DCVC-induced cytotoxic effects in placental cells utilizing concentrations that encompass those detected of the DCVC precursor in human serum samples (Lash et al. 1999). We demonstrated that the TCE metabolite DCVC stimulated activation of both the intrinsic and extrinsic apoptotic signaling pathways, culminating in aberrant apoptosis in a first-trimester extravillous trophoblast cell line. In addition, we demonstrated that DCVC-induced lipid peroxidation-associated apoptosis. To our knowledge, our study is the first to report that DCVC induces apoptosis via two signaling pathways simultaneously and that cross talk occurs between the two pathways. Our findings contribute to the biological plausibility of DCVC-induced placental toxicity, indicating that further studies into matter are warranted.

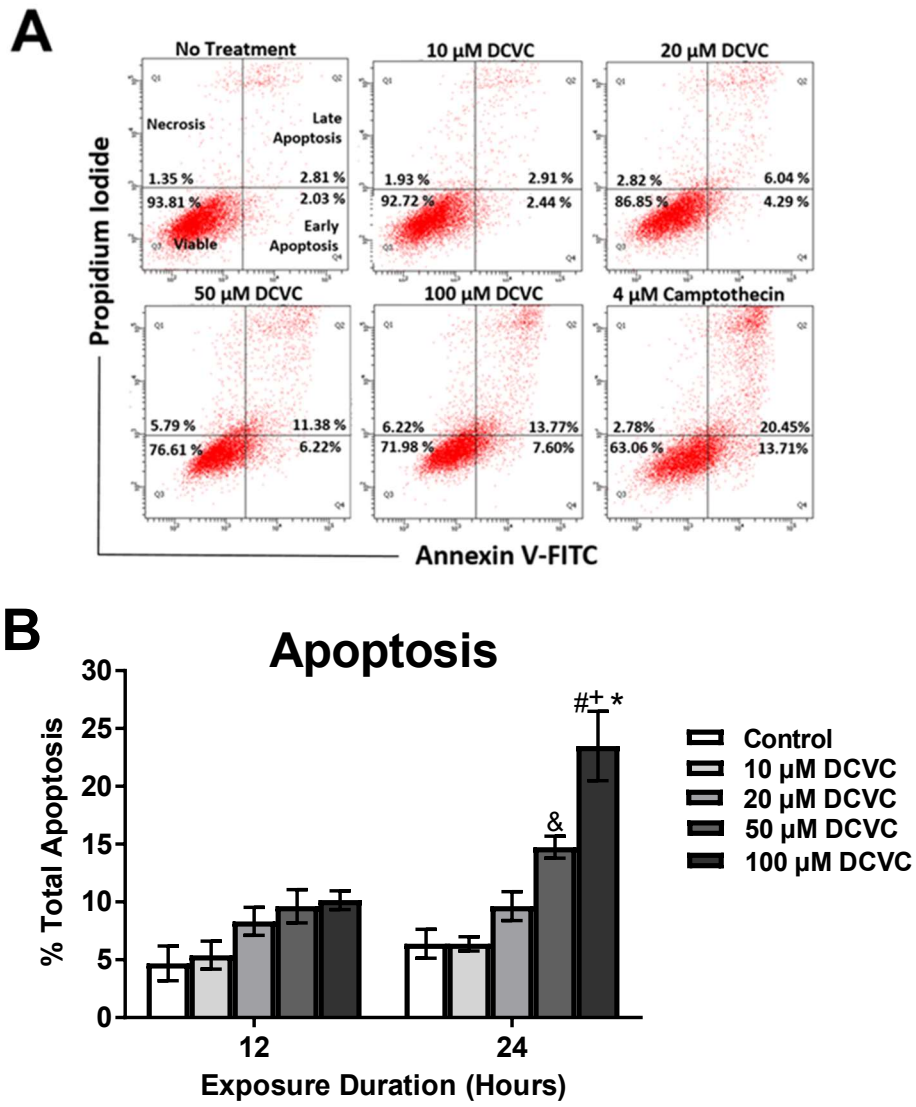

Figure 2.1. Effects of DCVC on apoptosis.
Cells were treated for 12 h or 24 h with 0 (no treatment control), 10, 20, 50, or 100 µM DCVC. A) Annexin V-FITC and propidium iodide fluorescence indicators were used to quantify apoptosis using flow cytometry. The dot plots are representative of each experiment at 24 h. B) Graphical representation of total apoptosis (early+late apoptosis). Bars represent means±SEM. Data were analyzed by two-way ANOVA (interaction between time and treatment, P=0.001) with posthoc Tukey multiple comparisons. $^{\#}$Significantly different compared to all 12 h time points (P<0.0022). $^{\&}$Significantly different compared to control and 10 µM DCVC at 24 h time point (P<0.0088). $^{+}$Significantly different compared to control, 10 and 20 µM DCVC at 24 h time point (P<0.0001). *Significantly different compared to 50 µM DCVC at 24 h time (P=0.005). N=4 independent experiments for 12 h and N=5 independent experiments for 24 h, with 3 replicates per treatment in each experiment. All experiments were performed in triplicate. Camptothecin (4 µM) was included as a positive control and increased total apoptosis 32.89% +/-15.23% at 12 h and 39.11% +/- 6.36 at 24 h.

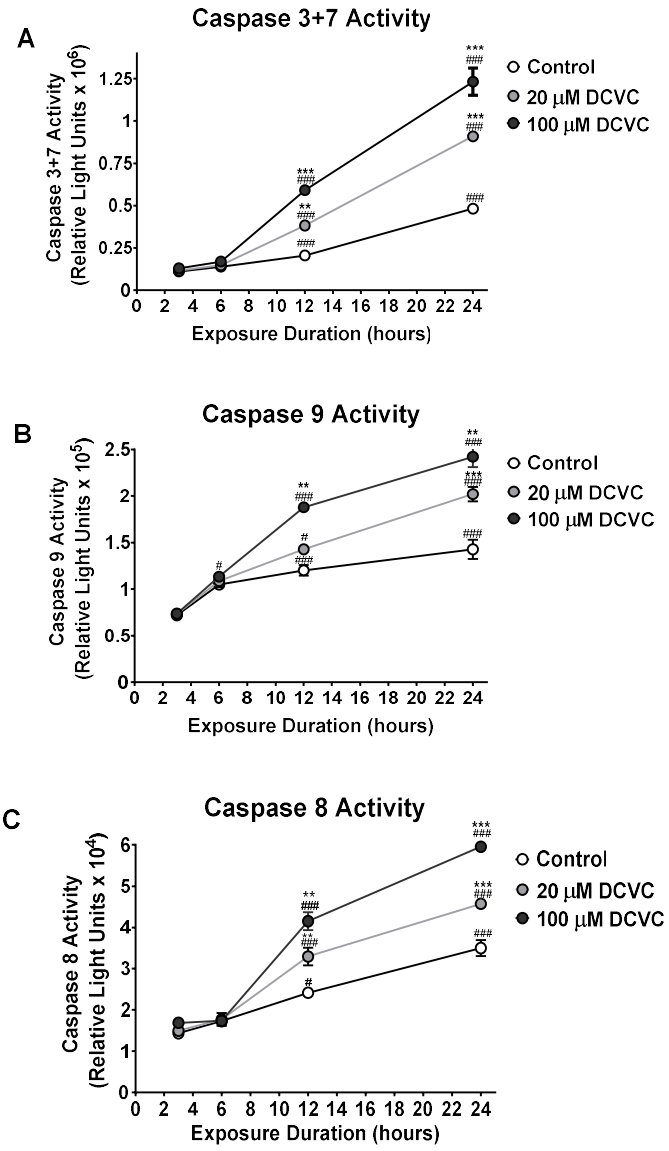

Figure 2.2. DCVC effects on caspase activity.
Cells were treated for 3, 6, 12 or 24 h with 0 (control), 20 or 100 μM DCVC. Caspase activity was measured using the Caspase Glo® luminescence assays. A) Time course of caspase 3+7 activity. B) Caspase 9 activity. C) Caspase 8 activity. Symbols represent means±SEM. N=3 independent experiments. Data were analyzed by two-way ANOVA (interaction between time and treatment, $P<0.0001$) with posthoc Tukey multiple comparisons. Given the very large number of significant mean comparisons, only significant comparisons within a treatment across time points and within a time point across treatments are indicated. Asterisks indicate significant differences with all lower concentrations within a single time point across treatments: * $P<0.05$, ** $P<0.005$, *** $P<0.0001$. Pound signs indicate significantly different compared with all earlier time points for same treatment: $^{\#}P<0.05$, $^{\#\#\#}P<0.0001$. N= 3 independent experiments, with 5 replicates per treatment in each experiment.

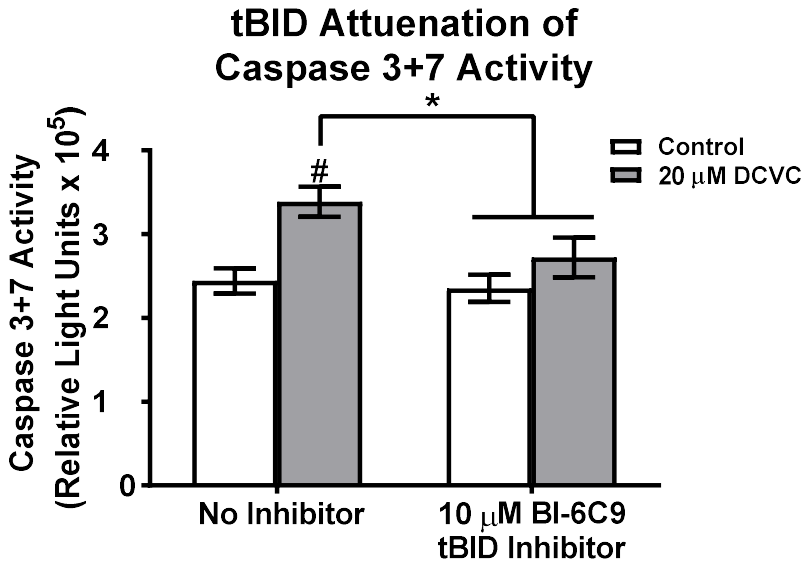

Figure 2.3. Effect of tBID inhibitor pre-treatment on DCVC-stimulated caspase 3+7 activity.
Cells were exposed to 20 μM DCVC for 12 h without pretreatment or after pretreatment with the tBID inhibitor BI-6C9 (10 μM for 1 h). Controls were not exposed to DCVC. Bars represent means±SEM. Data were analyzed by two-way ANOVA (interaction between DCVC and BI-6C9 treatments, P=0.028), followed by Tukey's multiple comparison of means. # Significantly different compared to control with no inhibitor (P=0.001). * Significantly different compared to 20 μM DCVC with no inhibitor (P<0.010). N= 3 independent experiments, with 5 replicates per treatment in each experiment

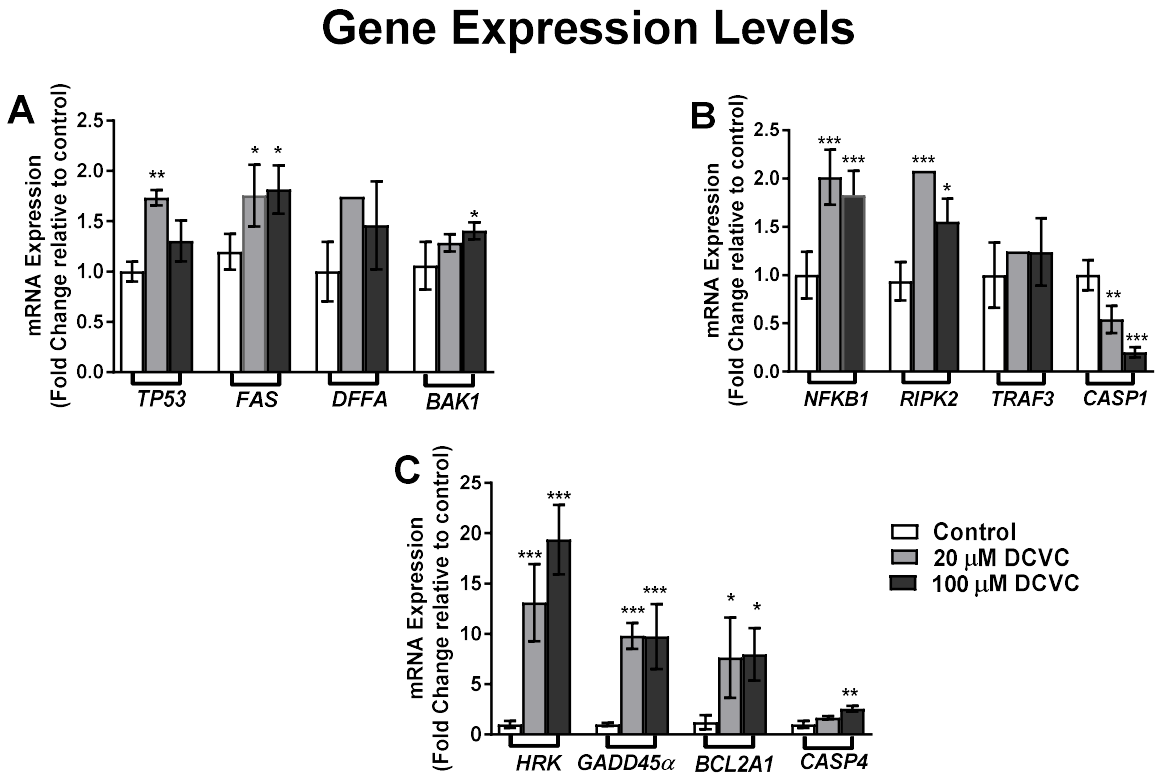

Figure 2.4. DCVC effects on cell mRNA expression of genes implicated in apoptosis signaling.
Based on the results of an apoptosis PCR array, we identified ten genes that were significantly upregulated by at least 2 fold or downregulated at least 0.5 fold compared to control, following treatment with 100 μM DCVC for 24 h. The PCR array data results were confirmed using qRT-PCR. Two other genes were also included in the qRT-PCR analysis because they showed a trend of upregulation. Cells were exposed to 0 (control), 20 μM DCVC or 100 μM DCVC for 24 h followed by qRT-PCR analysis. A) The mRNA expression of *TP53*, *FAS*, *DFFA* and *BAK1*. B) The mRNA expression of *NFKB1*, *RIPK2*, *TRAF3* and *CASP1*. B) The mRNA expression of *HRK*, *GADD45α*, *BCL2A1* and *CASP4*. Bars represent means±SEM. * Significantly different compared to control ($P<0.05$). ** Significantly different compared to control ($P<0.01$). *** Significantly different compared to control ($P<0.001$). Data were analyzed by one-way ANOVA with posthoc Dunnett's multiple comparison. N= 3-6 independent experiments, with 3 replicates per treatment in each experiment. qRT-PCR samples were plated in duplicate.

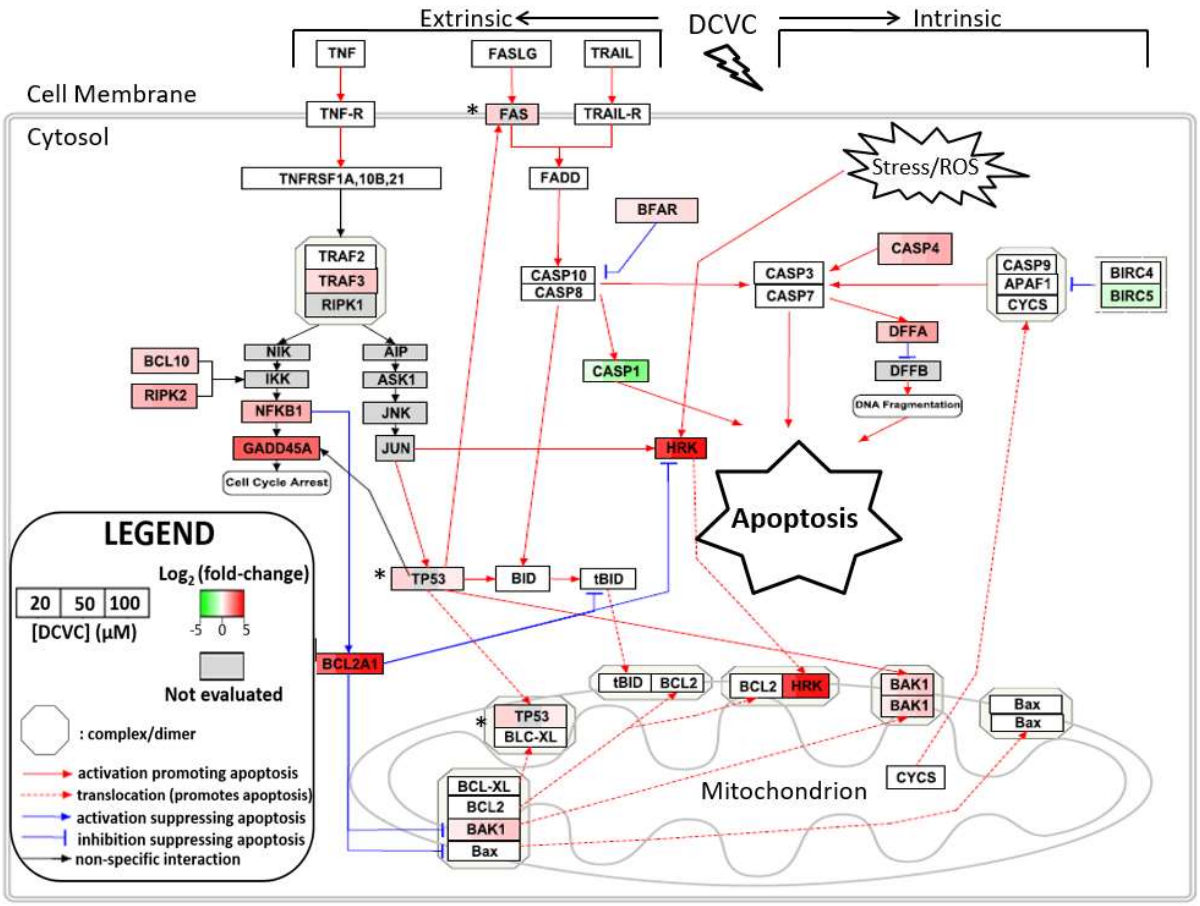

Figure 2.5. Visualization of DCVC-induced gene expression changes in intrinsic and extrinsic apoptosis pathways.
In order to elucidate the gene expression patterns that regulate the apoptosis observed in cells after treatment with DCVC, we mapped gene expression changes for extrinsic and intrinsic apoptosis pathways using Pathvisio software. Gene expression changes (log2 fold-change/control) are shown with red=upregulation, green=downregulation, grey=gene not evaluated. All gene expression data were obtained from an 84-gene qRT-PCR array except that genes indicated with an asterisk (*) had expression data obtained from separate qRT-PCR experiments. Two genes, *IGF1R* and *CD70,* were differentially expressed in the array but are not included in the diagram. This figure was constructed in part from Wikipathways: Apoptosis (Homo sapiens) (Zambon et al. 2017).

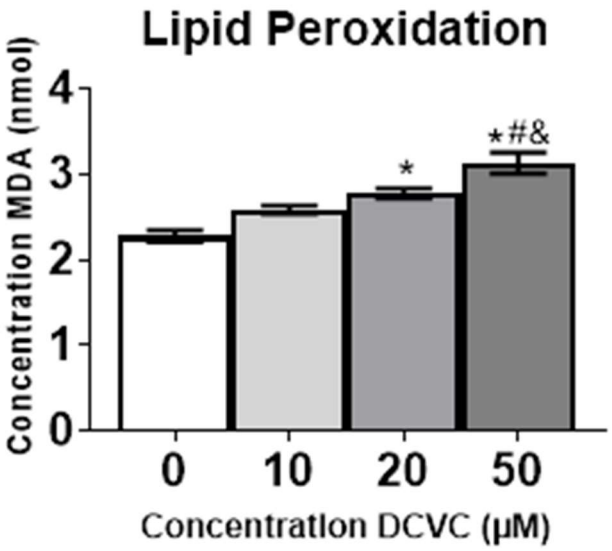

Figure 2.6. Effects of DCVC on lipid peroxidation.
Cells were treated for 24 h with 0 (control), 10, 20, and 50 µM DCVC or 20 µM tert-butyl hydroperoxide (positive control). As a proxy measure for lipid peroxidation, malondialdehyde (MDA) concentrations were quantified using thiobarbituric acid (TBA), which generates a MDA-TBA adduct when in contact with MDA. The MDA concentrations were quantified colorimetrically (OD = 532). Bars represent means±SEM. *Significantly different compared to control ($P<0.004$). $^{\#}$Significantly different compared to 10 µM DCVC ($P=0.0020$). $^{\&}$Significantly different compared 20 µM DCVC ($P= 0.0389$). Data were analyzed by one-way ANOVA with posthoc Tukey multiple comparisons. N=4 independent experiments. N= 4 independent experiments, with 3 replicates per treatment in each experiment. TBHP (20 µM) was used as a positive control (2.87 nmol +/- 0.167 nmol).

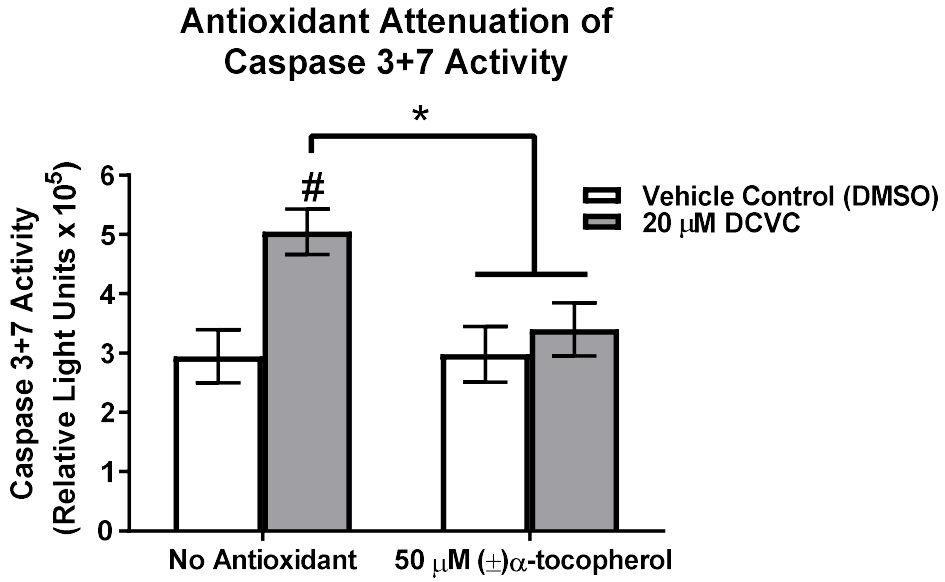

Figure 2.7. Effect of antioxidant co-treatment on DCVC-stimulated caspase 3+7 activity. Cells were untreated (media only control) for 12 h or exposed to 20 μM DCVC without or with 50 μM (±)α-tocopherol pre-treatment for 15 min followed by co-treatment for 12 h. Bars represent means±SEM. Data were analyzed by two-way ANOVA (interaction between DCVC and α-tocopherol treatments, P=0.0103), followed by Tukey's multiple comparison of means. # Significantly different compared to control with no (±)α-tocopherol treatment (P=0.0016). * Significantly different compared to 20 μM DCVC with no (±)α-tocopherol treatment (P<0.0075). N= 3 independent experiments, with 4 replicates per treatment in each experiment.

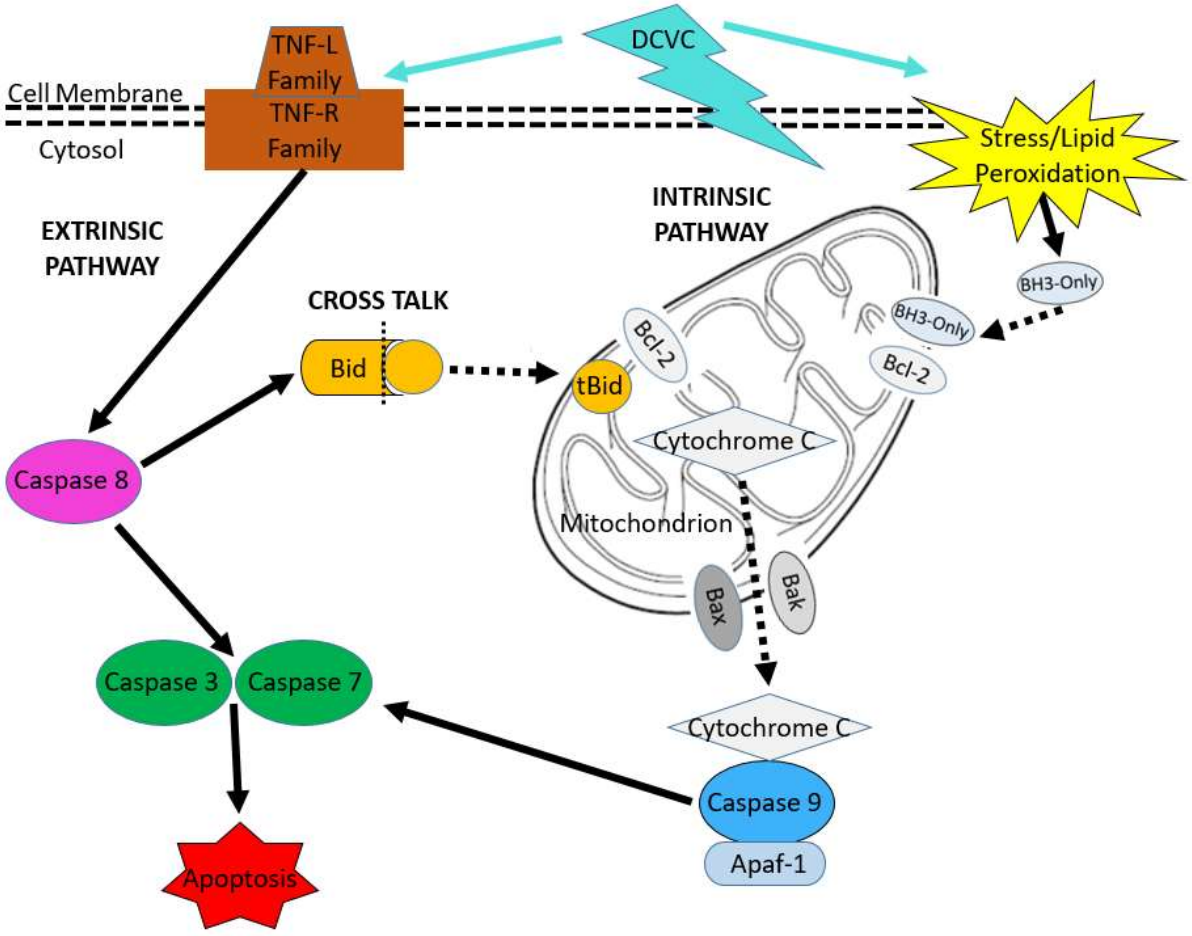

Figure 2.8. Intrinsic and extrinsic apoptosis pathways.
The mitochondria-mediated intrinsic pathway is activated in response to stress stimuli. BCL-2 family proteins with the BH3-only domain such as HRK translocate into mitochondria and dimerize with anti-apoptotic BCL-2, releasing pro-apoptotic BAK and BAX, which increase mitochondrial membrane permeability. In response, mitochondrial components such as cytochrome c leak out and bind to caspase 9 and APAF-1 to form the apoptosome. This complex activates caspases 3 and 7, which execute apoptosis. The extrinsic pathway is activated when TNF family ligands bind to receptors and activate caspase 8, which then activates caspases 3 and 7. Cross talk occurs when extrinsic pathway protein caspase 8 cleaves BID into truncated tBID. tBID translocates into the mitochondria and dimerizes with BCL-2 family proteins, engaging the intrinsic pathway.

References

Aardema M.W., Oosterhof H., Timmer A., van Rooy I., Aarnoudse J.G. 2001. Uterine artery doppler flow and uteroplacental vascular pathology in normal pregnancies and pregnancies complicated by pre-eclampsia and small for gestational age fetuses. *Placenta.* **22**:405-411.

Alvero A.B., Montagna M.K., Mor G. 2008. Correlation of caspase activity and in vitro chemo-response in epithelial ovarian cancer cell lines. *Methods Mol Biol.* **414**:79-82.

Amaral J.D., Xavier J.M., Steer C.J., Rodrigues C.M. 2010. The role of p53 in apoptosis. *Discov Med.* **9**:145-152.

Atamer Y., Kocyigit Y., Yokus B., Atamer A., Erden A.C. 2005. Lipid peroxidation, antioxidant defense, status of trace metals and leptin levels in preeclampsia. *Eur J Obstet Gynecol Reprod Biol.* **119**:60-66.

ATCC. 2015. Atcc product sheet: Htr8/svneo (atcc® crl3271™).American Type Culture Collection.

ATSDR. 2015. 2015 priority list of hazardous substances. Available: http://www.atsdr.cdc.gov/spl/ [accessed February 25, 2016 2016].

ATSDR. 2016. Public health statement on trichloroethylene.Agency for Toxic Substances and Disease Registry.

Ayala A., Munoz M.F., Arguelles S. 2014. Lipid peroxidation: Production, metabolism, and signaling mechanisms of malondialdehyde and 4-hydroxy-2-nonenal. *Oxid Med Cell Longev.* **2014**:360438.

Becattini B., Sareth S., Zhai D., Crowell K.J., Leone M., Reed J.C., et al. 2004. Targeting apoptosis via chemical design: Inhibition of bid-induced cell death by small organic molecules. *Chem Biol.* **11**:1107-1117.

Belkacemi L., Chen C.H., Ross M.G., Desai M. 2009. Increased placental apoptosis in maternal food restricted gestations: Role of the fas pathway. *Placenta.* **30**:739-751.

Belkacemi L., Desai M., Nelson D.M., Ross M.G. 2011. Altered mitochondrial apoptotic pathway in placentas from undernourished rat gestations. *Am J Physiol Regul Integr Comp Physiol.* **301**:R1599-1615.

Benjamini Y., Hochberg Y. 1995. Controlling the false discovery rate: A practical and powerful approach to multiple testing. *Journal of the Royal Statistical Society Series B (Methodological).* **57**:289– 300.

Beuter W., Cojocel C., Muller W., Donaubauer H.H., Mayer D. 1989. Peroxidative damage and nephrotoxicity of dichlorovinylcysteine in mice. *J Appl Toxicol.* **9**:181-186.

Bilban M., Tauber S., Haslinger P., Pollheimer J., Saleh L., Pehamberger H., et al. 2010. Trophoblast invasion: Assessment of cellular models using gene expression signatures. *Placenta.* **31**:989-996.

Biri A., Bozkurt N., Turp A., Kavutcu M., Himmetoglu O., Durak I. 2007. Role of oxidative stress in intrauterine growth restriction. *Gynecol Obstet Invest.* **64**:187-192.

Brosens I.A., Robertson W.B., Dixon H.G. 1972. The role of the spiral arteries in the pathogenesis of preeclampsia. *Obstet Gynecol Annu.* **1**:177-191.

Bukowski J. 2014. Critical review of the epidemiologic literature regarding the association between congenital heart defects and exposure to trichloroethylene. *Critical reviews in toxicology.* **44**:581-589.

Burton G.J., Fowden A.L. 2015. The placenta: A multifaceted, transient organ. *Philos Trans R Soc Lond B Biol Sci.* **370**:20140066.

Caniggia I., Grisaru-Gravnosky S., Kuliszewsky M., Post M., Lye S.J. 1999. Inhibition of tgf-beta 3 restores the invasive capability of extravillous trophoblasts in preeclamptic pregnancies. *J Clin Invest.* **103**:1641-1650.

Carney E.W., Thorsrud B.A., Dugard P.H., Zablotny C.L. 2006. Developmental toxicity studies in crl:Cd (sd) rats following inhalation exposure to trichloroethylene and perchloroethylene. *Birth Defects Res B Dev Reprod Toxicol.* **77**:405-412.

Chen Q., Jones T.W., Brown P.C., Stevens J.L. 1990. The mechanism of cysteine conjugate cytotoxicity in renal epithelial cells. Covalent binding leads to thiol depletion and lipid peroxidation. *J Biol Chem.* **265**:21603-21611.

Chen S.J., Wang J.L., Chen J.H., Huang R.N. 2002. Possible involvement of glutathione and p53 in trichloroethylene- and perchloroethylene-induced lipid peroxidation and apoptosis in human lung cancer cells. *Free Radic Biol Med.* **33**:464-472.

Chen Y., Cai J., Anders M.W., Stevens J.L., Jones D.P. 2001. Role of mitochondrial dysfunction in s-(1,2-dichlorovinyl)-l-cysteine-induced apoptosis. *Toxicol Appl Pharmacol.* **170**:172-180.

Chiu W.A., Jinot J., Scott C.S., Makris S.L., Cooper G.S., Dzubow R.C., et al. 2013. Human health effects of trichloroethylene: Key findings and scientific issues. *Environ Health Perspect.* **121**:303-311.

Chou J.J., Li H., Salvesen G.S., Yuan J., Wagner G. 1999. Solution structure of bid, an intracellular amplifier of apoptotic signaling. *Cell.* **96**:615-624.

Darnerud P.O., Brandt I., Feil V.J., Bakke J.E. 1989. Dichlorovinyl cysteine (dcvc) in the mouse kidney: Tissue-binding and toxicity after glutathione depletion and probenecid treatment. *Arch Toxicol.* **63**:345-350.

Das R.M., Scott J.E. 1994. Trichloroethylene-induced pneumotoxicity in fetal and neonatal mice. *Toxicol Lett.* **73**:227-239.

Davies E.L., Bell J.S., Bhattacharya S. 2016. Preeclampsia and preterm delivery: A population-based case-control study. *Hypertens Pregnancy.* **35**:510-519.

Denes A., Lopez-Castejon G., Brough D. 2012. Caspase-1: Is il-1 just the tip of the iceberg? *Cell Death Dis.* **3**:e338.

DiFederico E., Genbacev O., Fisher S.J. 1999. Preeclampsia is associated with widespread apoptosis of placental cytotrophoblasts within the uterine wall. *Am J Pathol.* **155**:293-301.

Elmore S. 2007. Apoptosis: A review of programmed cell death. *Toxicol Pathol.* **35**:495-516.

EPA. 2011. Toxicological review of trichloroethylene (cas no. 79-01-6). Washtingon D.C.:National Center for Environmental Assessment.

EPA. 2017. Tri explorer: Release trends report.Environmental Protection Agency.

Fisher J.W., Channel S.R., Eggers J.S., Johnson P.D., MacMahon K.L., Goodyear C.D., et al. 2001. Trichloroethylene, trichloroacetic acid, and dichloroacetic acid: Do they affect fetal rat heart development? *Int J Toxicol.* **20**:257-267.

Forand S.P., Lewis-Michl E.L., Gomez M.I. 2012. Adverse birth outcomes and maternal exposure to trichloroethylene and tetrachloroethylene through soil vapor intrusion in new york state. *Environ Health Perspect.* **120**:616-621.

Gao L., Abu Kwaik Y. 2000. Hijacking of apoptotic pathwaysby bacterial pathogens. *Microbes Infect.* **2**:1705-1719.

Genbacev O., DiFederico E., McMaster M., Fisher S.J. 1999. Invasive cytotrophoblast apoptosis in pre-eclampsia. *Hum Reprod.* **14 Suppl 2**:59-66.

Graham C.H., Hawley T.S., Hawley R.G., MacDougall J.R., Kerbel R.S., Khoo N., et al. 1993. Establishment and characterization of first trimester human trophoblast cells with extended lifespan. *Experimental cell research.* **206**:204-211.

Graupner V., Alexander E., Overkamp T., Rothfuss O., De Laurenzi V., Gillissen B.F., et al. 2011. Differential regulation of the proapoptotic multidomain protein bak by p53 and p73 at the promoter level. *Cell Death Differ.* **18**:1130-1139.

Groves C.E., Lock E.A., Schnellmann R.G. 1991. Role of lipid peroxidation in renal proximal tubule cell death induced by haloalkene cysteine conjugates. *Toxicol Appl Pharmacol.* **107**:54-62.

Guha N., Loomis D., Grosse Y., Lauby-Secretan B., El Ghissassi F., Bouvard V., et al. 2012. Carcinogenicity of trichloroethylene, tetrachloroethylene, some other chlorinated solvents, and their metabolites. *Lancet Oncol.* **13**:1192-1193.

Gupta S., Agarwal A., Sharma R.K. 2005. The role of placental oxidative stress and lipid peroxidation in preeclampsia. *Obstet Gynecol Surv.* **60**:807-816.

Hannan N.J., Paiva P., Dimitriadis E., Salamonsen L.A. 2010. Models for study of human embryo implantation: Choice of cell lines? *Biology of reproduction.* **82**:235-245.

Hassan I., Kumar A.M., Park H.R., Lash L.H., Loch-Caruso R. 2016. Reactive oxygen stimulation of interleukin-6 release in the human trophoblast cell line htr-8/svneo by the trichlorethylene metabolite s-(1,2-dichloro)-l-cysteine. *Biology of reproduction.* **95**:66.

Haupt S., Berger M., Goldberg Z., Haupt Y. 2003. Apoptosis - the p53 network. *J Cell Sci.* **116**:4077-4085.

Hitomi J., Katayama T., Eguchi Y., Kudo T., Taniguchi M., Koyama Y., et al. 2004. Involvement of caspase-4 in endoplasmic reticulum stress-induced apoptosis and abeta-induced cell death. *J Cell Biol.* **165**:347-356.

Hollander M.C., Alamo I., Jackman J., Wang M.G., McBride O.W., Fornace A.J., Jr. 1993. Analysis of the mammalian gadd45 gene and its response to DNA damage. *J Biol Chem.* **268**:24385-24393.

Huang Y., Dong F., Du Q., Zhang H., Luo X., Song X., et al. 2014. Swainsonine induces apoptosis through mitochondrial pathway and caspase activation in goat trophoblasts. *Int J Biol Sci.* **10**:789-797.

Ilekis J.V., Tsilou E., Fisher S., Abrahams V.M., Soares M.J., Cross J.C., et al. 2016. Placental origins of adverse pregnancy outcomes: Potential molecular targets: An executive workshop summary of the eunice kennedy shriver national institute of child health and human development. *Am J Obstet Gynecol.* **215**:S1-S46.

Inohara N., Ding L., Chen S., Nunez G. 1997. Harakiri, a novel regulator of cell death, encodes a protein that activates apoptosis and interacts selectively with survival-promoting proteins bcl-2 and bcl-x(l). *EMBO J.* **16**:1686-1694.

Irving J.A., Lysiak J.J., Graham C.H., Hearn S., Han V.K., Lala P.K. 1995. Characteristics of trophoblast cells migrating from first trimester chorionic villus explants and propagated in culture. *Placenta.* **16**:413-433.

Johnson P.D., Goldberg S.J., Mays M.Z., Dawson B.V. 2003. Threshold of trichloroethylene contamination in maternal drinking waters affecting fetal heart development in the rat. *Environ Health Perspect.* **111**:289-292.

Jurisicova A., Antenos M., Varmuza S., Tilly J.L., Casper R.F. 2003. Expression of apoptosis-related genes during human preimplantation embryo development: Potential roles for the harakiri gene product and caspase-3 in blastomere fragmentation. *Molecular human reproduction.* **9**:133-141.

Kadyrov M., Kingdom J.C., Huppertz B. 2006. Divergent trophoblast invasion and apoptosis in placental bed spiral arteries from pregnancies complicated by maternal anemia and early-onset preeclampsia/intrauterine growth restriction. *Am J Obstet Gynecol.* **194**:557-563.

Kanehisa M., Furumichi M., Tanabe M., Sato Y., Morishima K. 2017. Kegg: New perspectives on genomes, pathways, diseases and drugs. *Nucleic Acids Res.* **45**:D353-D361.

Karowicz-Bilinska A., Kedziora-Kornatowska K., Bartosz G. 2007. Indices of oxidative stress in pregnancy with fetal growth restriction. *Free Radic Res.* **41**:870-873.

Kelder T., van Iersel M.P., Hanspers K., Kutmon M., Conklin B.R., Evelo C.T., et al. 2012. Wikipathways: Building research communities on biological pathways. *Nucleic Acids Res.* **40**:D1301-1307.

Khan G.A., Girish G.V., Lala N., Di Guglielmo G.M., Lala P.K. 2011. Decorin is a novel vegfr-2-binding antagonist for the human extravillous trophoblast. *Mol Endocrinol.* **25**:1431-1443.

Kilburn B.A., Wang J., Duniec-Dmuchowski Z.M., Leach R.E., Romero R., Armant D.R. 2000. Extracellular matrix composition and hypoxia regulate the expression of hla-g and integrins in a human trophoblast cell line. *Biology of reproduction.* **62**:739-747.

Kuwana T., Smith J.J., Muzio M., Dixit V., Newmeyer D.D., Kornbluth S. 1998. Apoptosis induction by caspase-8 is amplified through the mitochondrial release of cytochrome c. *J Biol Chem.* **273**:16589-16594.

Lagakos S., Wessen B., Zelen M. 1986. An analysis of contaminated well water and health eff ects in woburn, massachusetts *Journal of the American Statistical Association.* **81**:583-596.

Laham S. 1970. Studies on placental transfer. Trichlorethylene. *IMS Ind Med Surg.* **39**:46-49.

Lash L.H., Anders M.W. 1986. Cytotoxicity of s-(1,2-dichlorovinyl)glutathione and s-(1,2-dichlorovinyl)-l-cysteine in isolated rat kidney cells. *J Biol Chem.* **261**:13076-13081.

Lash L.H., Putt D.A., Brashear W.T., Abbas R., Parker J.C., Fisher J.W. 1999. Identification of s-(1,2-dichlorovinyl)glutathione in the blood of human volunteers exposed to trichloroethylene. *J Toxicol Environ Health A.* **56**:1-21.

Lash L.H., Hueni S.E., Putt D.A. 2001. Apoptosis, necrosis, and cell proliferation induced by s-(1,2-dichlorovinyl)-l-cysteine in primary cultures of human proximal tubular cells. *Toxicol Appl Pharmacol.* **177**:1-16.

Lash L.H., Putt D.A., Hueni S.E., Krause R.J., Elfarra A.A. 2003. Roles of necrosis, apoptosis, and mitochondrial dysfunction in s-(1,2-dichlorovinyl)-l-cysteine sulfoxide-induced cytotoxicity in primary cultures of human renal proximal tubular cells. *J Pharmacol Exp Ther.* **305**:1163-1172.

Lash L.H., Chiu W.A., Guyton K.Z., Rusyn I. 2014. Trichloroethylene biotransformation and its role in mutagenicity, carcinogenicity and target organ toxicity. *Mutat Res Rev Mutat Res.* **762**:22-36.

Levy R., Nelson D.M. 2000. To be, or not to be, that is the question. Apoptosis in human trophoblast. *Placenta.* **21**:1-13.

Li C., Wei J., Li Y., He X., Zhou Q., Yan J., et al. 2013. Transmembrane protein 214 (tmem214) mediates endoplasmic reticulum stress-induced caspase 4 enzyme activation and apoptosis. *J Biol Chem.* **288**:17908-17917.

Li H., Zhu H., Xu C.J., Yuan J. 1998. Cleavage of bid by caspase 8 mediates the mitochondrial damage in the fas pathway of apoptosis. *Cell.* **94**:491-501.

Libermann T.A., Baltimore D. 1990. Activation of interleukin-6 gene expression through the nf-kappa b transcription factor. *Mol Cell Biol.* **10**:2327-2334.

Liu L., Wang Y., Shen C., He J., Liu X., Ding Y., et al. 2016. Benzo(a)pyrene inhibits migration and invasion of extravillous trophoblast htr-8/svneo cells via activation of the erk and jnk pathway. *J Appl Toxicol.* **36**:946-955.

Liu X., Mu H., Luo X., Xiao X., Ding Y., Yin N., et al. 2014. Expression of gadd45alpha in human early placenta and its role in trophoblast invasion. *Placenta.* **35**:370-377.

Liu X., Deng Q., Luo X., Chen Y., Shan N., Qi H. 2016. Oxidative stress-induced gadd45alpha inhibits trophoblast invasion and increases sflt1/seng secretions via p38 mapk involving in the pathology of pre-eclampsia. *J Matern Fetal Neonatal Med.* **29**:3776-3785.

Luppi P., Tse H., Lain K.Y., Markovic N., Piganelli J.D., DeLoia J.A. 2006. Preeclampsia activates circulating immune cells with engagement of the nf-kappab pathway. *Am J Reprod Immunol.* **56**:135-144.

Madazli R., Benian A., Aydin S., Uzun H., Tolun N. 2002. The plasma and placental levels of malondialdehyde, glutathione and superoxide dismutase in pre-eclampsia. *J Obstet Gynaecol.* **22**:477-480.

McCarthy J.V., Ni J., Dixit V.M. 1998. Rip2 is a novel nf-kappab-activating and cell death-inducing kinase. *J Biol Chem.* **273**:16968-16975.

McIlwain D.R., Berger T., Mak T.W. 2015. Caspase functions in cell death and disease. *Cold Spring Harb Perspect Biol.* **7**.

McKinney L.L., Picken Jr. J.C., Weakley F.B., Eldridge A.C., Campbell R.E., Cowan J.C., et al. 1959. Possible toxic factor of trichloroethylene-extracted soybean oil meal3. *Journal of the American Chemical Society.* **81**:909-915.

Meekins J.W., Pijnenborg R., Hanssens M., McFadyen I.R., van Asshe A. 1994. A study of placental bed spiral arteries and trophoblast invasion in normal and severe pre-eclamptic pregnancies. *Br J Obstet Gynaecol.* **101**:669-674.

Morgan T. 2014. Placental insufficiency is a leading cause of preterm labor. *NewReviews.* **15**:5618-e5525.

Morgan T.K. 2016. Role of the placenta in preterm birth: A review. *Am J Perinatol.* **33**:258-266.

Myatt L., Cui X. 2004. Oxidative stress in the placenta. *Histochem Cell Biol.* **122**:369-382.

Niles A.L., Moravec R.A., Riss T.L. 2008. Caspase activity assays. *Methods Mol Biol.* **414**:137-150.

Nishizaki T., Kanno T., Tsuchiya A., Kaku Y., Shimizu T., Tanaka A. 2014. 1-[2-(2-methoxyphenylamino)ethylamino]-3-(naphthalene-1- yloxy)propan-2-ol may be a promising anticancer drug. *Molecules.* **19**:21462-21472.

Novakovic B., Gordon L., Wong N.C., Moffett A., Manuelpillai U., Craig J.M., et al. 2011. Wide-ranging DNA methylation differences of primary trophoblast cell populations and derived cell lines: Implications and opportunities for understanding trophoblast function. *Molecular human reproduction.* **17**:344-353.

NTP. 2015. Monograph on trichloroethylene Available: https://ntp.niehs.nih.gov/ntp/roc/monographs/finaltce_508.pdf 2016].

Papathanasiou M.A., Kerr N.C., Robbins J.H., McBride O.W., Alamo I., Jr., Barrett S.F., et al. 1991. Induction by ionizing radiation of the gadd45 gene in cultured human cells: Lack of mediation by protein kinase c. *Mol Cell Biol.* **11**:1009-1016.

Pennington K.A., Schlitt J.M., Jackson D.L., Schulz L.C., Schust D.J. 2012. Preeclampsia: Multiple approaches for a multifactorial disease. *Dis Model Mech.* **5**:9-18.

Perfettini J.L., Kroemer R.T., Kroemer G. 2004. Fatal liaisons of p53 with bax and bak. *Nat Cell Biol.* **6**:386-388.

Rehman M.U., Tahir M., Quaiyoom Khan A., Khan R., Lateef A., Hamiza O.O., et al. 2013. Diosmin protects against trichloroethylene-induced renal injury in wistar rats: Plausible role of p53, bax and caspases. *Br J Nutr.* **110**:699-710.

Reister F., Frank H.G., Kingdom J.C., Heyl W., Kaufmann P., Rath W., et al. 2001. Macrophage-induced apoptosis limits endovascular trophoblast invasion in the uterine wall of preeclamptic women. *Lab Invest.* **81**:1143-1152.

Roth W., Kermer P., Krajewska M., Welsh K., Davis S., Krajewski S., et al. 2003. Bifunctional apoptosis inhibitor (bar) protects neurons from diverse cell death pathways. *Cell Death Differ.* **10**:1178-1187.

Ruckart P.Z., Bove F.J., Maslia M. 2014. Evaluation of contaminated drinking water and preterm birth, small for gestational age, and birth weight at marine corps base camp lejeune, north carolina: A cross-sectional study. *Environ Health.* **13**:99.

Rufer E.S., Hacker T.A., Flentke G.R., Drake V.J., Brody M.J., Lough J., et al. 2010. Altered cardiac function and ventricular septal defect in avian embryos exposed to low-dose trichloroethylene. *Toxicol Sci.* **113**:444-452.

Schreck R., Rieber P., Baeuerle P.A. 1991. Reactive oxygen intermediates as apparently widely used messengers in the activation of the nf-kappa b transcription factor and hiv-1. *EMBO J.* **10**:2247-2258.

Sharp A.N., Heazell A.E., Crocker I.P., Mor G. 2010. Placental apoptosis in health and disease. *Am J Reprod Immunol.* **64**:159-169.

Sheikh M.S., Hollander M.C., Fornance A.J., Jr. 2000. Role of gadd45 in apoptosis. *Biochem Pharmacol.* **59**:43-45.

Simon H.U., Haj-Yehia A., Levi-Schaffer F. 2000. Role of reactive oxygen species (ros) in apoptosis induction. *Apoptosis : an international journal on programmed cell death.* **5**:415-418.

Smith S.C., Baker P.N., Symonds E.M. 1997a. Increased placental apoptosis in intrauterine growth restriction. *Am J Obstet Gynecol.* **177**:1395-1401.

Smith S.C., Baker P.N., Symonds E.M. 1997b. Placental apoptosis in normal human pregnancy. *Am J Obstet Gynecol.* **177**:57-65.

Smith S.C., Guilbert L.J., Yui J., Baker P.N., Davidge S.T. 1999. The role of reactive nitrogen/oxygen intermediates in cytokine-induced trophoblast apoptosis. *Placenta.* **20**:309-315.

Smyth G.K. 2004. Linear models and empirical bayes methods for assessing differential expression in microarray experiments. *Statistical applications in genetics and molecular biology.* **3**:Article3.

Spandidos A., Wang X., Wang H., Seed B. 2010. Primerbank: A resource of human and mouse pcr primer pairs for gene expression detection and quantification. *Nucleic Acids Res.* **38**:D792-799.

Stark G. 2005. Functional consequences of oxidative membrane damage. *J Membr Biol.* **205**:1-16.

Straszewski-Chavez S.L., Abrahams V.M., Mor G. 2005. The role of apoptosis in the regulation of trophoblast survival and differentiation during pregnancy. *Endocr Rev.* **26**:877-897.

Szklanna P.B., Wynne K., Nolan M., Egan K., Ainle F.N., Maguire P.B. 2017. Comparative proteomic analysis of trophoblast cell models reveals their differential phenotypes, potential uses and limitations. *Proteomics.* **17**:1700037-1700042.

Takao T., Asanoma K., Kato K., Fukushima K., Tsunematsu R., Hirakawa T., et al. 2011. Isolation and characterization of human trophoblast side-population (sp) cells in primary villous cytotrophoblasts and htr-8/svneo cell line. *PloS one.* **6**:e21990.

Tetz L.M., Cheng A.A., Korte C.S., Giese R.W., Wang P., Harris C., et al. 2013. Mono-2-ethylhexyl phthalate induces oxidative stress responses in human placental cells in vitro. *Toxicol Appl Pharmacol.* **268**:47-54.

van de Water B., Zoeteweij J.P., de Bont H.J., Mulder G.J., Nagelkerke J.F. 1994. Role of mitochondrial ca2+ in the oxidative stress-induced dissipation of the mitochondrial membrane potential. Studies in isolated proximal tubular cells using the nephrotoxin 1,2-dichlorovinyl-l-cysteine. *J Biol Chem.* **269**:14546-14552.

van de Water B., Zoeteweij J.P., de Bont H.J., Nagelkerke J.F. 1995. Inhibition of succinate:Ubiquinone reductase and decrease of ubiquinol in nephrotoxic cysteine s-conjugate-induced oxidative cell injury. *Molecular pharmacology.* **48**:928-937.

Van de Water B., Kruidering M., Nagelkerke J.F. 1996. F-actin disorganization in apoptotic cell death of cultured rat renal proximal tubular cells. *Am J Physiol.* **270**:F593-603.

Vaughan J.E., Walsh S.W. 2012. Activation of nf-kappab in placentas of women with preeclampsia. *Hypertens Pregnancy.* **31**:243-251.

Walker D.I., Uppal K., Zhang L., Vermeulen R., Smith M., Hu W., et al. 2016. High-resolution metabolomics of occupational exposure to trichloroethylene. *Int J Epidemiol.* **45**:1517-1527.

Waters E.M., Gerstner H.B., Huff J.E. 1977. Trichloroethylene. I. An overview. *J Toxicol Environ Health.* **2**:671-707.

Watson R.E., Jacobson C.F., Williams A.L., Howard W.B., DeSesso J.M. 2006. Trichloroethylene-contaminated drinking water and congenital heart defects: A critical analysis of the literature. *Reprod Toxicol.* **21**:117-147.

Wei M.C., Lindsten T., Mootha V.K., Weiler S., Gross A., Ashiya M., et al. 2000. Tbid, a membrane-targeted death ligand, oligomerizes bak to release cytochrome c. *Genes Dev.* **14**:2060-2071.

Xiong Y., Liebermann D.A., Tront J.S., Holtzman E.J., Huang Y., Hoffman B., et al. 2009. Gadd45a stress signaling regulates sflt-1 expression in preeclampsia. *J Cell Physiol.* **220**:632-639.

Xiong Y., Liebermann D.A., Holtzman E.J., Jeronis S., Hoffman B., Geifman-Holtzman O. 2013. Preeclampsia-associated stresses activate gadd45a signaling and sflt-1 in placental explants. *J Cell Physiol.* **228**:362-370.

Xu F., Papanayotou I., Putt D.A., Wang J., Lash L.H. 2008. Role of mitochondrial dysfunction in cellular responses to s-(1,2-dichlorovinyl)-l-cysteine in primary cultures of human proximal tubular cells. *Biochem Pharmacol.* **76**:552-567.

Yamamuro A., Kishino T., Ohshima Y., Yoshioka Y., Kimura T., Kasai A., et al. 2011. Caspase-4 directly activates caspase-9 in endoplasmic reticulum stress-induced apoptosis in sh-sy5y cells. *J Pharmacol Sci.* **115**:239-243.

Zaker F., Amirizadeh N., Nasiri N., Razavi S.M., Teimoori-Toolabi L., Yaghmaie M., et al. 2016. Gene expression and methylation pattern in hrk apoptotic gene in myelodysplastic syndrome. *Int J Mol Cell Med.* **5**:90-99.

Zambon A., Hanspers K., Pico A., Kalafati M., van Iersel M.P., nuno, et al. 2017. Wikipathways: Apoptosis (homo sapiens) Available: http://www.wikipathways.org/index.php/Pathway:WP254 2017].

Zhang X.Y., Qu X., Wang C.Q., Zhou C.J., Liu G.X., Wei F.C., et al. 2011. Over-expression of gadd45a enhances radiotherapy efficacy in human tca8113 cell line. *Acta Pharmacol Sin.* **32**:253-258.

Zhu Q.X., Shen T., Ding R., Liang Z.Z., Zhang X.J. 2005. Cytotoxicity of trichloroethylene and perchloroethylene on normal human epidermal keratinocytes and protective role of vitamin e. *Toxicology.* **209**:55-67.

Chapter III. Short Duration Exposure to the Trichloroethylene Metabolite *S*-(1,2-Dichlorovinyl)-L-Cysteine Causes Compensatory Changes in Energy Metabolism in HTR-8/SVneo Cells

Abstract

Trichloroethylene (TCE) is a widespread environmental contaminant, resulting from decades of application as an industrial solvent, improper disposal and remediation challenges. Consequently, TCE exposure continues to constitute a risk to human health. Despite epidemiological evidence associating exposure with adverse birth outcomes, the effects of TCE and its metabolite *S*-(1, 2-dichlorovinyl)-L-cysteine (DCVC) on the placenta remain undetermined. Flexible and efficient macronutrient and energy metabolism pathway utilization is essential for placental cell physiological adaptability in their specialized roles in pregnancy and. Because DCVC is known to compromise cellular energy status and disrupt energy metabolism in renal proximal tubular cells, this study investigated the effects of DCVC on cellular energy status and energy metabolism pathways in placental cells. Human extravillous trophoblast cells, HTR-8/SVneo, were exposed to 5-20 μM DCVC for 6 or 12 h. After establishing concentration and exposure duration thresholds for DCVC-induced cytotoxicity, targeted metabolomics was used to evaluate overall energy status and metabolite concentrations from energy metabolism pathways. The data revealed glucose metabolism perturbations including a time-dependent accumulation of glucose-6-phosphate+frutose-6-phosphate (G6P+F6P) as well as independent shunting of glucose intermediates that diminished with time, with modest energy status decline but in the absence of significant changes in ATP concentrations. Furthermore, metabolic

profiling suggested that DCVC stimulated compensatory utilization of glycerol, lipid and amino acid amino metabolism to provide intermediate substrates entering downstream in the glycolytic pathway or the tricarboxylic cycle. Taken together, these results suggest that DCVC caused metabolic perturbations necessitating adaptations in macronutrient and energy metabolism pathway utilization in order to maintain adequate ATP levels.

Introduction

TCE is a volatile organic compound that originates exclusively from human activities. Originally commercialized in the 1920s as an oral anesthetic, its potent solvent properties were quickly discovered and harnessed, propelling TCE to become one of the most commonly used industrial and dry-cleaning solvents by mid-century (Waters et al. 1977). Today, over 80% of TCE production is utilized as a chemical intermediate in closed-system refrigerant manufacturing processes, specifically HFC-134a, a refrigerant used in car air conditioning systems (ATSDR 2016; NTP 2015). The remaining TCE produced is used primarily as a vaporized metal degreaser, although the Environmental Protection Agency (EPA) has proposed to ban this use as recently as 2017 (Chiu et al. 2013; EPA 2017b; Waters et al. 1977). As a result of its long-standing pervasive usage and its chemical properties, TCE is a ubiquitous persistent environmental contaminant found in soil, air and water (Chiu et al. 2013). TCE is currently ranked as number sixteen on the U.S. Agency for Toxic Substances and Disease Registry's Substance Priority List. Despite being detected in 1055 of 1750 current and former EPA-designated National Priorities List Superfund sites, TCE continues to makes its way into the environment with approximately 1.9 million pounds of TCE released in 2015 (ATSDR 2016; ATSDR 2017; EPA 2017a; EPA 2018). Because industrial usage and persistent environmental

contamination of TCE continue, exposure through inhalation, ingestion and skin contact remains a potential threat to human health.

TCE has as a long history of study as a potential organ-specific toxicant (Waters et al. 1977). In particular, there is extensive literature on TCE toxicity to liver and kidney, and TCE was recently re-classified by the National Toxicology Program (NTP) and International Agency for Research on Cancer (IARC) as a known human carcinogen based on substantial evidence that it causes kidney cancer in humans (Guha et al. 2012; NTP 2015; Rusyn et al. 2014). In addition to recognition as a renal and liver toxicant (Chiu et al. 2013), TCE has been implicated in adverse pregnancy outcomes. Although an early study found no association between maternal TCE exposure and low birth weight (Lagakos et al. 1986), more recent studies reported positive associations between maternal TCE exposure and low birth weight and preterm birth (Forand et al. 2012; Ruckart et al. 2014).

The precise underlying mechanisms of adverse birth outcomes such as low birth weight and preterm birth remain murky at best despite considerable scientific scrutiny (March of Dimes 2012). Because the placenta is critical for support and protection of the fetus during pregnancy, placental disruption may play a key role in the development of adverse birth outcomes (Ilekis et al. 2016). For example, there is evidence that placental insufficiency, with deficient nutrient and metabolic waste exchange between mother and fetus, may contribute to early parturition (Morgan 2014; Morgan 2016). Similarly, recent epidemiology studies found significant associations between pre-eclampsia and increased risk of preterm birth and/or low birth weight (Davies et al. 2016; Oshvandi et al. 2018).

As a metabolically active organ in direct contact with maternal circulation, the placenta is a likely target organ for toxicity(Goodman et al. 1982). Due to high blood volume and a large

surface area, the placenta is readily exposed to maternal serum-circulating TCE and it metabolites (Burton and Fowden 2015; Laham 1970). Moreover, the placenta expresses many enzymes required for TCE biotransformation including cytochrome P450, glutathione-S-transferase and beta-lyase (Lee et al. 2013; Myllynen et al. 2005) The presence of these enzymes greatly increases the risk of tissue-generated harmful TCE metabolites.

The weight of evidence indicates that biotransformation is required for TCE-mediated cytotoxicity (Lash et al. 2014). The glutathione pathway-derived metabolite *S*-(1, 2-dichlorovinyl)-L-cysteine (DCVC) causes cytotoxicity in kidney proximal tubular cells mediated by reactive oxygen species and mitochondrial dysfunction (Chen et al. 1990; Chen et al. 2001; Lash and Anders 1986; Lash et al. 2003; van de Water et al. 1994; van de Water et al. 1995; Xu et al. 2008). Moreover, Lash et al. demonstrated that DCVC causes a decrease in the total adenine nucleotide pool, compromised cellular energy status and tricarboxylic acid cycle perturbations in kidney cells (Lash and Anders 1986; Lash and Anders 1987). Similarly, we recently reported that DCVC increased reactive species regeneration, lipid peroxidation and mitochondrial-mediated apoptosis *in vitro* utilizing a first trimester extravillous trophoblast cell line (Elkin et al. 2018; Hassan et al. 2016). Together, the evidence suggests that cellular processes and structures responsible for generating ATP may be impacted by DCVC exposure.

Placental cells have sizable energy requirements for carrying out pregnancy biological processes such tissue remodeling, steroid hormone synthesis, and maintenance of homeostasis amid changing environmental conditions (Mando et al. 2014; Murray 2012; Vaughan and Fowden 2016). ATP is required for those processes as well as many others such as active transport, transcription and translation (Fisher et al. 1987; Lager and Powell 2012). ATP is generated anaerobically by macronutrients through metabolism of glucose, lipids and proteins

through glycolysis and aerobically through oxidative phosphorylation. Because of the need to maintain adequate ATP, flexible and efficient utilization of macronutrients and energy metabolism pathways are essential. Based on the high energy requirements of the placenta and previous studies that identified DCVC impacts cellular energy status and ATP stability, this study investigated the effects of DCVC on cellular energy status and energy metabolism pathways in human extravillous trophoblasts.

Materials and Methods

Chemicals and Reagents

S-(1, 2-dichlorovinyl)-L-cysteine (DCVC), a trichloroethylene glutathione conjugation pathway metabolite, was synthesized in powder form by the University of Michigan Medicinal Chemistry Core as previously described (McKinney et al. 1959)**.** High-performance liquid chromatography (HPLC) analysis was used to determine purity (98.7%). A stock solution of 1 mM DCVC was prepared by dissolving DCVC in phosphate buffered saline and stored in small aliquots at −20°C to minimize freeze/thaw cycles. The chemical purity of the DCVC stock solution was confirmed periodically by nuclear magnetic resonance (NMR).

RPMI 1640 culture medium with L-glutamine and without phenol red, 10,000 U/mL penicillin/10,000 µg/mL streptomycin (P/S) solution, and fetal bovine serum (FBS) were purchased from Gibco, a division of Thermo Fisher Scientific (Waltham, MA, USA). Phosphate buffered saline (PBS), Hank's Balanced Salt Solution (HBSS) and 0.25% trypsin were purchased from Invitrogen Life Technologies (Carlsbad, CA, USA). Dimethyl sulfoxide (DMSO) was purchased from Torcis Biosciences (Bristol, UK).

Cell Culture and Treatment

The HTR-8/SVneo cells were obtained from Dr. Charles H. Graham (Queen's University, Kingston, Ontario, Canada). This cell line was derived from first-trimester human placentae and immortalized with simian virus 40 large T antigen (Graham et al. 1993). The cell line expresses markers of an extravillous trophoblast phenotype and has a female genotype. HTR-8/SVneo cells were cultured as previously described (Hassan et al. 2016; Tetz et al. 2013). Briefly, cells were cultured between passages 78–87 in RPMI 1640 medium supplemented with 10% FBS and 1% P/S at 37°C in a 5% CO_2 humidified incubator. Cells were sustained in RPMI 1640 growth medium with 10% FBS and 1% P/S prior to and during experiments to ensure optimal cell growth as previously described (Graham et al. 1993). Cells were grown to 70–90% confluence for 24 h after subculture prior to beginning each experiment.

Just before each experiment, a DCVC stock solution aliquot was quickly thawed in a 37°C water bath and then diluted in RPMI 1640 medium with 10% FBS and 1% P/S to final exposure concentrations of 5–20 μM DCVC. The DCVC concentrations selected for study include plausible metabolite concentrations in human blood with occupational exposure to the parent compound, trichloroethylene (Lash et al. 1999). Additionally, we selected concentrations previously determined to lack overt cytotoxicity in HTR-8/SVneo cells at the times points used in the present study (Hassan et al. 2016).

Cell Line Validation

Genomic DNA was extracted from HTR-8/SVneo cellsQIAamp® DNA Mini Kit (Qiagen; Hilden, Germany). Microsatellite genotyping was performed using AmpFLSTR Identifier Plus PCR Amplification Kit run on a 3730XL Genetic Analyzer (Applied Biosystems; Waltham, MA, USA). The short tandem repeat profile generated for our cells was compared to

the short tandem repeat profile for HTR-8/SVneo (ATCC® CRL-3271™) published by American Type Culture Collection (Manassas, VA, USA) (ATCC 2015).The short tandem repeat profile was a match: CSF1PO: 12, D13S317: 9,12, D16S539: 13D5S818: 12, D7S820: 12, TH01: 6,9.3, vWA: 13,18, TPOX: 8, Amelogenin gender determination marker: X (ATCC 2015).

Measurement of cytotoxicity

Cytotoxicity was measured with the MultiTox-Glo Multiplex Cytotoxicity Kit performed according to the manufacturer's protocol (Promega; Madison, WI), which sequentially measures the relative number of live and dead cells in a single assay. Live cells were measured with the cell-permanent fluorescent compound glycyl-phenylalanyl-aminoflourocoumarin (GF-AFC), and dead cells were measured with the luminescent cell-impermeable compound alanyl-alanyl-phenylalanyl-aminoluciferin (AAF-Glo). Briefly, HTR-8/SVneo cells were seeded at 10,000 cells per well in a white, clear-bottom 96-well plate and incubated for 24 h. Cells were treated with medium alone (Control) or DCVC (5, 10, or 20 μM) for 12, 24 or 48 h. Following exposure, GF-AFC was added directly to the media and incubated for 1 h. Fluorescence signal (emission: 400; excitation: 505) for viable cells was measured with a SpectraMax M2e Multi-Mode Microplate Reader (Molecular Devices). After viability quantification, AAF-Glo was added to the media and incubated at room temperature for 10 minutes. Luminescence signal for dead cells was quantified using the Glomax Multi Plus detection system (Promega). In order to normalize the data, the relative live-to-dead cell ratios were calculated by dividing the average live cell fluorescence signal by the average dead cell luminescence signal per treatment group for each time point. Camptothecin (4 μM) was included as a positive control at each time point.

Bicinchoninic acid (BCA) assay

In order to normalize metabolomics and western blot experiments, total protein concentration per well was measured calorimetrically using the Pierce Bicinchoninic Acid (BCA) Assay Kit (Thermo Fisher Scientific) performed according to the manufacturer's recommended protocol. Briefly, cells were lysed with RIPA lysis buffer containing a protease inhibitor cocktail. Cell lysates from each sample (10 μM) were transferred to a 96-well clear-bottomed plate, combined with working buffer (200 μM) and incubated for 30 minutes at 37°C. Following incubation, protein concentrations were determined with a SpectraMax M2e Multi-Mode Microplate Reader (OD=562 nm) (Molecular Devices) based on comparison to a bovine serum albumin-derived standard curve ranging between 0.0625-2 mg/ml.

Quantification of targeted metabolomics

Targeted metabolomics was used to quantify a panel of energy metabolism pathway-related metabolites and amino acids. HTR-8/SVneo cells were seeded at a density of 1.6 million cells per plate in tissue culture (TC)-treated 100 mm dishes and allowed to adhere and acclimate for 48 h. Cells were then treated with medium alone (Control) or DCVC (20 μM) for 6 or 12 h. Following the exposure period, cell culture medium was aspirated, and then cells were briefly washed with 0.15 M ammonium acetate to remove excess medium, rapidly flash frozen with liquid nitrogen, and stored at -80°C. Samples were transported on ice to the University of Michigan Metabolomics Core for further processing.

Samples were prepared as previously described by Lorenz et al. (2011). Briefly, cells were treated with an extraction solvent containing isotope-labeled internal standards. The

extraction solvent contained a mixture of chloroform, water and methanol in a ratio of 1:1:8. Cells were lysed and scraped to create a homogenized mixture containing extracted metabolites. Metabolites were detected with reverse-phase liquid chromatography-mass spectrometry (LC-MS) on an Agilent system consisting of a 1290 UPLC coupled with a 6520 Quadrupole-Time-of-flight (QTOF) mass spectrometer operated in ESI- mode (Agilent Technologies, Santa Clara, CA, USA). Data were processed using MassHunter Quantitative analysis version B.07.00. Glycolytic, tricarboxylic acid and pentose phosphate pathway metabolites were normalized to the nearest isotope-labeled internal standard and quantitated using two replicated injections of 5 standards to create a highly accurate linear calibration curve. Glycolytic, tricarboxylic acid and pentose phosphate pathway metabolites were reported with specific intracellular concentrations normalized to total protein mass per dish, as measured with the BCA assay. Amino acids, lipids and other metabolites in the analysis were normalized to the nearest internal standard and the peak areas were used for differential analysis between groups. These metabolites were reported as relative response (RR) normalized to total protein mass per samples (Lorenz et al. 2011). For each time point, 5 independent experiments were conducted.

Immunoblotting protein analysis

HTR-8/SVneo cells were seeded at a density of 400,000 cells per well in a clear 6-well culture plate and allowed to attach for 24 h. Following the acclimation period, cells were treated with medium alone (control) or DCVC (20 μM) for 12 h. Cells were lysed in RIPA lysis buffer and centrifuged at 14,000 rpm for 10 minutes at 4°C. Lysates were heated with loading buffer at 85°C for 3 minutes. Samples were loaded into commercially available Novex 4–20% Tris-Glycine Mini Gel cassettes (Invitrogen) and proteins were separated by polyacrylamide gel

electrophoresis run at 125V for 1.5 h. SeeBlue Plus2 pre-stained protein standard (Invitrogen) was included as a visual molecular weight reference. Following separation, proteins were transferred onto nitrocellulose membranes at 75V for 4 h at a temperature of 4°C. Membranes were blotted at room temperature using small neutral amino acid transporter type 2 (ASCT2) antibody [molecular weight 75; catalog no. 8057; Cell Signaling Technologies; Research Resource Identifier (RRID): AB_10891440], large amino acid transporter heavy subunit (4F2hc/CD98) antibody (molecular weight 75-120; catalog no. 13180; Cell Signaling Technologies; RRID: AB_2687475), L-type neutral amino acid transporter 1 (LAT1) antibody (molecular weight 39; catalog no. 5347; Cell Signaling Technologies; RRID: AB_10695104) and AMP-activated protein kinase alpha subunit-phosphorylated (p-AMPKα) or non-phosphorylated (AMPKα) antibodies [molecular weight 62; catalog nos. 2535 or 2793; Cell Signaling Technologies; Research Resource Identifier (RRID): AB_10705605 or AB_915794]. Antibody complexes were detected by Alexa Fluor anti-mouse and anti-rabbit fluorescent-conjugated antibodies (Invitrogen) and visualized using an Odyssey CLx image scanner (Li-Cor Biosciences; Lincoln, NE, USA). Blots were quantified using Image Studio software version 5.2 and normalized to Revert Total Protein Stain (Li-Cor Biosciences). Three to four independent experiments were performed and each experiment was performed in triplicate.

PFK activity enzyme assay

Phosphofructokinase 1 (PFK1) activity was measured in cells treated for 12 h with medium alone (control) or 20 μM DCVC. PFK1 activity was measured with a commercially available colorimetric activity assay. The assay was performed according to the manufacturer's protocol (Sigma-Aldrich). Briefly, following DCVC exposure, reaction mixture (comprised of

PFK1 assay buffer, PFK1 enzyme mix, PFK1 enzyme developer, ATP and PFK1 substrate) was added to each well containing NADH standards, samples or sample blanks. After an initial 5-minute incubation at 37°C, the first absorbance measurement was recorded. Subsequent measurements were taken every seven minutes until the value of the most active sample was greater than the value of the highest standard (28 to 35 minutes). Calorimetric absorbance (OD=450 nm) was measured with a SpectraMax M2e Multi-Mode Microplate Reader (Molecular Devices). PFK1 activity was calculated using the following formula: PFK1 Activity = [(Amount of NADH generated between T_{Intial} and T_{final} as determined by standard curve) x (Sample Dilution Tactor)]/[(Reaction Time) x (Sample volume)]. Three independent experiments were performed and each experiment was performed in triplicate.

Statistical Analysis

All experiments were performed independently and repeated three to five times. When applicable, technical replicates were averaged within each experiment. These data were analyzed using student t-tests or one-way or two-way analysis of variance (ANOVA followed by Tukey's post-hoc test for comparison of means (GraphPad Prism version 7; GraphPad Software Inc; San Diego, CA, USA). Experiments containing different time points and treatment were analyzed with two-way ANOVA. Experiments only containing one time point and two treatment groups including Western blots and PFK activity assay were analyzed using Student's *t*-tests. Metabolomics data were log2 transformed due to non-normal Gaussian distribution. After transformation, the data were normally distributed prior to statistical analysis using two-way ANOVA. Data are expressed as means ± SEM. N=number of independent experiments. $P < 0.05$ was considered statistically significant in all experiments.

Results

DCVC cytotoxicity

Because the objective of this study was to investigate energy metabolism under non-cytolethal conditions, we measured cytotoxicity at lower concentrations (5-20 μM DCVC) and for a larger range of time points (12-48 h) than previously reported by Hassan et al. (2016). DCVC stimulated cytotoxicity in time- and concentration-dependent manners after 24 and 48 h exposure but not 12 h (ANOVA interaction effect, $P<0.0001$, Fig. 3.1). After 24 h of exposure, only 20 μM DCVC decreased the live-to-dead cell ratio significantly by 51% ($P = 0.002$). However, after 48 h of exposure, both 10 and 20 μM DCVC reduced the live-to-dead cell ratio by 55% and 67%, respectively ($P <0.0008$). These experiments validated previous findings that exposure to 20 μM DCVC for 24 h is cytotoxic to HTR-8/SVneo cells (Hassan et al. 2016) while establishing an exposure duration threshold of 48 h for cytotoxicity with 10 μM DCVC.

DCVC-induced changes in cellular energy status indicators

We focused our investigation on cellular energy metabolism because DCVC was previously shown to deplete ATP concentrations and compromise cellular energy status in renal proximal tubular cells (Lash and Anders 1986). In order to evaluate the effect of DCVC on the overall energy status of treated HTR-8/SVneo cells, we used targeted metabolomics to measure concentrations of key energy metabolites.

Intracellular concentrations of key energy metabolites

The DCVC-induced changes in intracellular concentrations of selected key energy metabolites are summarized in figure 3.2A. DCVC exposure significantly increased most

adenylate and guanylate nucleotide concentrations, the primary energy drivers of physiological processes in cells. Exposure to 20 μM DCVC significantly increased AMP, ADP and GMP concentrations by at least 1.4 fold after 6 and 12 h exposures, whereas GDP and GTP concentrations increased significantly only after 12 h, compared to time-matched controls (Fig 3.2Ai; $P<0.05$). Interestingly, ATP concentrations did not change significantly despite changes in concentrations of other adenylate nucleotides. Phosphocreatine, a phosphate donor critical for rapid regeneration of ATP during high energy expenditure, decreased 1.6 fold after 12 h ($P=0.0002$) but was not significantly changed after 6 h (Fig 3.2Aii). Concomitantly, creatine byproduct concentrations increased nearly 2 fold at both 6 h and 12 h($P<0.01$). Lastly, NADH, an electron carrier that shuttles electrons from different pathways to the electron transport chain, increased significantly, contrary to the other energy-relevant metabolites, by 2.2 fold after 6 h ($P=0.0007$) but not 12 h exposure (Fig 3.2Aiii;. NAD+ concentrations did not significantly change at either time point. The significant DCVC-induced changes in key energy metabolite concentrations may indicate a disruption in cellular energy status.

Ratios of key energy metabolite couples

Ratios of key energy metabolite couples are shown in figure 3.2B, calculated from the concentrations reported in figure Fig 3.2A. Because these energy metabolites are normally maintained in narrow non-equilibrium concentrations for optimal physiologic function, changes in ratios of critical metabolite couples may indicate compromise of the intracellular mechanisms that maintain the concentrations (Guimaraes-Ferreira 2014; Hardie 2003). The ATP:AMP ratio decreased 72% and 62% after 6 and 12 h exposure to DCVC, respectively, whereas the ATP:ADP ratio decreased by 44% only after 12 h (Figs. 3.2Bi & ii; $P<0.01$). After 6 and 12 h

DCVC exposure, the phosphocreatine:creatine ratio decreased 55% and 65%, respectively (Figs. 3.2Biii; P <0.0001). On the other hand, the NADH:NAD+ ratio, demonstrating the opposite pattern, increased by 128% after 6 h, however, did not change after 12 h (Figs. 3.2Biv; P=0.0084). These fluctuating energy metabolite ratios indicate that short-duration DCVC treatment caused an overall mild decline in cellular energy status.

AMP-kinase phosphorylation

Because a decreased ATP:AMP ratio may reflect activation of the energy stress response AMP-kinase (AMPK) signaling pathway (Hardie 2003), we measured protein levels of phosphorylated (activated) and total AMPKα using western blot analysis (Fig. 3.2C). We did observed no significant treatment-related changes when comparing the ratio of p-AMPKα to AMPKα protein levels between non-treated control and DCVC-treated cells, suggesting that the increase in the AMP/ATP ratio was not sufficient to promote AMPK phosphorylation.

Profiling DCVC effect on energy metabolism pathway utilization

DCVC has previously been shown to alter concentrations of tricarboxylic acid cycle intermediates in renal proximal tubular cells (Lash and Anders 1987), prompting us to further investigate DCVC-induced effects on specific energy metabolism pathways and related pathways using targeted metabolomics to quantify a panel of metabolites unique to each pathway. Indeed, nine pathways had one or more metabolite concentrations significantly altered by exposure to 20 μM DCVC at either the 6-h or 12-h time points. An overview of DCVC-induced changes in energy metabolism pathways is summarized in figure 3.3A, with affected pathways in dark grey

boxes and notable impacted metabolites outlined in light grey rectangles. The outlined metabolite concentrations are individually displayed in figure 3.3B for each pathway.

Glucose metabolism pathway

DCVC had no significant effect on glucose concentrations compared to non-treated controls at either 6 or 12 h: however, glucose concentrations decreased from 6 to 12 h regardless of treatment (Fig 3.3Bi; $P<0.004$). Once glucose enters the cell via GLUT membrane transporters, it undergoes irreversible phosphorylation yielding glucose-6-phosphate (G6P), which is further isomerized to fructose-6-phosphate (F6P) (Chen and Kato 1985). Although our analysis was unable to differentiate between G6P and F6P, DCVC treatment increased G6P+F6P metabolites 1.4 and 2.4 fold at 6 h and 12 h, respectively, compared to time-matched controls (Fig 3.3Bi; $P\leq0.03$). These results demonstrate that 20 μM DCVC treatment caused a substantial time-dependent accumulation of F6P+G6P, indicating possible perturbation of downstream glucose catabolism.

Phosphofructokinase 1 Activity

Because a time-dependent accumulation of F6P+G6P was observed, we measured DCVC effects on activity of the enzyme phosphofructokinase 1 (PFK1), which catalyzes phosphorylation of F6P to frucose-1,6-bisphosphate. We observed no significant change in activity after 12 h of treatment with 20 μM DCVC, compared to time-matched controls (Fig 3.3C). These results indicate that F6P+G6P accumulation was not caused by reduced *in vitro* enzymatic activity.

Pentose phosphate, hexosamine and purine nucleotide pathways

Notably, the metabolic fate of the accumulated F6P+G6P is a critical branching point for glucose metabolism: although most molecules proceed through glycolysis, a small quantity shunt into the pentose phosphate pathway (PPP) and downstream purine nucleotide pathways (PNP), or into the hexosamine biosynthesis pathway (HBP) (Fig. 3.3B). Treatment with 20 μM DCVC significantly increased metabolite concentrations in each of these pathways: PPP five-carbon sugars (R5P+X5P) increased after 6 h but not 12 h (Fig. 3.3Bii; P=0.0004); PNP metabolites inosine and inosine monophosphate increased after 6 and 12 h, albeit a smaller increase after 12 h (Fig. 3Biii; P<0.04); and HBP metabolites N-acetyl-glucosamine-1-phosphate (NAcG1P) and uridine diphosphate N-acetyl-glucosamine increased after 6 h or both time points, respectively, compared to time-matched controls (Figs. 3.3iv; P<0.03). These elevated metabolite concentrations suggest that 20 μM DCVC treatment increased F6P+G6P shunting from the glycolytic pathway after 6 h, but not 12 h.

Glycolytic pathway

Despite increased shunting, the vast majority of F6P+G6P molecules are further phosphorylated into frucose-1,6-bisphosphate (F1,6bP) during the first committed and most heavily regulated glycolytic step. F1BP then splits into two molecules, glyceraldehyde-3-phosphate (Ga3P) and dihydroxyacetone phosphate (DHAP), which rapidly interconvert. Although F1,6bP concentrations did not change in 20 μM DCVC-exposed cells, Ga3P and DHAP concentrations increased by 2.5 and 2.8 fold after 6 h, and 1.8 and 2 fold after 12 h, respectively, compared with time-matched control cells (Fig. 3.3v; P<0.0003). The remaining downstream glycolytic metabolites, including 2-phosphoglycerate+3-phosphoglycerate

(2PG+3PG) and phosphoenolpyruvate (PEP), were not significantly altered by DCVC treatment. However, lactate, the terminal anaerobic glycolytic metabolite, increased by 1.4 fold with 20 μM DCVC after 6 h but not 12 h, compared to time-matched controls (Fig. 3.3Bv; P=0.04). These results demonstrate that 20 μM DCVC elevated Ga3P and DHAP intracellular concentrations, indicating a potential DCVC-induced compensatory mechanism occurring in up-stream glycolysis.

Tricarboxylic acid cycle

Under aerobic conditions, the final step of the glycolytic pathway converts pyruvate to acetyl CoA in preparation for entrance into tricarboxylic acid cycle (TCA). Treatment with 20 μM DCVC for 6 and 12 h increased acetyl CoA concentrations approximately 2.4 fold compared to time-matched controls (Fig. 3.3Bvi; P=0.01). Of the TCA metabolites measured in our panel, only malate had elevated concentrations with DCVC treatment after 12 h, compared to time-matched controls (Fig. 3.3Bvi; P=0.01). DCVC had no significant impact on the other TCA metabolites, citrate+isocitrate and succinate. In comparison to the other energy metabolic pathways examined, the TCA cycle appeared largely unaffected by DCVC treatment under our experimental conditions.

Alternative bioenergetics fuel sources

Glycerol metabolism pathway

Because DCVC increased Ga3P and DHAP concentrations along with G6P+F6P accumulations in the absence of changes in glycolytic downstream metabolites, we hypothesized that there may be alternative macronutrient source(s) providing glycolytic intermediates.

Importantly, DHAP is also a downstream metabolite in the glycerol metabolism pathway (Fig. 3.3Bvii), providing a crucial entry point at which glycerol derived from lipid molecules may enter the glycolytic pathway midstream. Indeed, concentrations of glycerol-3-phosphate (GL3P), an upstream metabolite of DHAP in the glycerol catabolism pathway, increased 1.5 fold in DCVC-exposed cells at 6 and 12 h compared to time-matched controls (Fig. 3.3Bvii $P<0.0001$). Moreover, free oleic fatty acid concentrations, possibly derived extracellularly or from β-oxidation, were increased 4 fold with DCVC treatment for 6 and 12 h, compared with time-matched controls (Fig. 3.3Bviii; $P<0.0001$). The DCVC-stimulated increases of intracellular GL3P, oleate and acetyl-coA concentrations may reflect the use of lipids as an alternative fuel source.

Amino acid metabolism and transport

Under certain conditions, amino acids can enter the glycolytic pathway as pyruvate, acetyl-CoA or other TCA intermediates. Treatment with 20 μM DCVC increased intracellular concentrations of multiple amino acids (Fig. 3.3Bix). Among the most important amino acids for energy metabolism, alanine concentrations were significantly elevated after 6 and 12 h, whereas glutamine and glutamate concentrations were only elevated after 6 h treatment with DCVC, compared to time-matched controls (Fig. 3.3Bix; $P<0.05$). Among essential amino acids, DCVC treatment increased tryptophan concentrations by nearly 4 fold after 6 and 12 h, whereas leucine+isoleucine concentrations increased 1.4 fold at 6 h only, and histidine increased 1.6 fold at 12 h only, compared to time-matched controls (Fig. 3.3Bix; $P<0.04$). These results suggest that DCVC may stimulate compensatory uptake and utilization of amino acids as macronutrient sources.

Membrane transporters involved in cellular uptake of extracellular free amino acids were investigated as potential contributors to the increased intracellular concentrations of energy-relevant amino acids. Western blotting revealed that treatment with 20 μM DCVC for 12 h stimulated a 1.7-fold increased abundance of the alanine, serine, cysteine transporter 2 (ASCT2) protein, an amino acid transporter responsible for transporting small neutral amino acids (Fig. 3.4A; P=0.047 compared to time-matched control). Protein expression of the 4F2 cell-surface antigen heavy chain (4F2hc) and L-type amino acid transporter 1 (LAT1) proteins that form a heterodimer transporter of large neutral amino acids, were not statistically significant, despite an apparent trend of DCVC-stimulated increases (Fig. 3.4B & C). These findings suggest that increased amino acid transport may contribute to the observed DCVC-induced increases in amino acid concentrations.

Energy pathway metabolite ratios

In order to confirm DCVC-induced alterations to energy metabolism pathways, we calculated metabolite ratios to determine metabolite flux in glucose metabolism, upstream glycolysis and other connected pathways. The metabolite ratios are graphically displayed in the context of the respective pathways they represent in figure 3.5.

G6P+F6P time-dependent accumulation

DCVC treatment for 12 h increased the glucose:G6P+F6P ratio compared to time-matched controls (Fig. 3.5A; P=0.01). Concomitantly, the downstream G6P+F6P:F1BP ratio decreased at 6 and 12 h (Fig. 3.5B; P=0.0003). These ratio changes indicate metabolite flux

favoring G6P+F6P, consistent with the finding that DCVC increased G6P+F6P intracellular concentration.

Pentose phosphate and hexosamine biosynthesis shunts

Following 12 h of exposure to 20 μM DCVC, the G6P+F6P:R5P+X5P ratio, representing the PPP, increased significantly (Fig.3.5C; P=0.005), whereas the G6P+F6P:NAcG1P ratio, representing the HBP, did not significantly change compared to time-matched controls. Following 6 h of exposure to 20μM DCVC, neither ratio was significantly altered, despite an apparent decreasing trend for both ratios, compared to time-matched controls.
These results may indicate potential DCVC-stimulated metabolic fluctuations favoring the PPP and HBP after 6 h, whereas the evidence indicates a reverse trend after 12 h with metabolic fluctuations favoring the glycolytic pathway.

Alternative bioenergetics fuel sources via glycerol metabolism

The calculated metabolite ratio for F1BP:Ga3P+DHAP decreased significantly with 20 μM DCVC treatment after 6 and 12 h, whereas the Ga3P+DHAP:2PG+3PG ratio increased only after 6 h, compared to time-match controls (Fig 3.5E & F; P<0.002). These results indicate DCVC-stimulated metabolic fluctuations favoring Ga3P and DHAP formation after 6 h that eased slightly after 12 h. Furthermore, 20 μM DCVC treatment increased the metabolite ratio of Ga3P+DAHP:GL3P after 6 h but not 12 h, compared to time-matched controls (Fig 3.5G; P=0.0008). Importantly, this latter ratio indicates DCVC-induced metabolite fluctuation towards the glycolytic pathway, especially after 6 h, consistent with glycerol metabolism intermediates entering glycolysis.

Discussion

Epidemiologic evidence has associated maternal TCE exposure with increased risk of adverse birth outcomes. However, the effects of TCE and its metabolite *S*-(1, 2-dichlorovinyl)-L-cysteine (DCVC) on the placenta remain largely undetermined. Because of previous evidence of DCVC-induced energy perturbations in kidney cells (Lash and Anders 1986; Lash and Anders 1987), and the importance of maintaining sufficient ATP levels for placental cell function (Vaughan and Fowden 2016), this study investigated the effects of non-cytolethal DCVC concentrations on cellular energy status, macronutrients and energy metabolism in placental cells. To our knowledge, the present study is the first to report DCVC-stimulated changes in energy metabolism pathway and macronutrient utilization in placental cells.

DCVC-induced changes to cellular energy status

The cellular energy status – indicated by ratios comparing intracellular concentrations of key energy metabolite couples – describes cells' ability to meet and maintain sufficient ATP levels in order to carry out energy-dependent processes (Hardie 2003; Tantama and Yellen 2014). Our targeted metabolomics analysis revealed many DCVC-induced changes to intracellular concentrations of energy-relevant metabolites and correlated ratios, together, indicating an apparent decline in cellular energy status, similar to a prior study conducted in rat kidney cells (Lash and Anders 1987). Importantly, we observed elevated ADP and AMP concentrations along with depressed ATP:ADP and ATP:AMP ratios compared to controls 6- and 12-h-post DCVC exposure. However, despite these findings, we observed no overall changes to ATP intracellular concentrations after 6 or 12 h, nor activation of the AMPK energy stress pathway after 12 h of exposure. Taken together, these results suggest that despite the

apparent cellular energy status decline, adaptive changes in energy production were sufficient to maintain ATP levels in HTR-8/SVneo cells under our exposure conditions.

In addition to cellular energy status, ratios of energy metabolite couples may also serve as predictors and/or regulators of metabolic activity (Hardie 2003; Tantama and Yellen 2014). During pregnancy, the ratio of ATP:ADP in placental tissue does not change in the first, second or third-trimesters under normal circumstances (Cindrova-Davies et al. 2015). However, a decreased ATP:ADP ratio was observed in primary cultures of cytotrophoblasts isolated from placentae of term pregnancies complicated with intrauterine growth restricted (IUGR) compared to normal term placentae (Crocker et al. 2003). Moreover, the decreased ratio in the same study also corresponded with higher susceptibility to spontaneous apoptosis in the cytotrophoblasts (Crocker et al. 2003), a defining characteristic of abnormal placental development (Sharp et al. 2010). The Crocker et al. study provides an example in which the ATP:ADP ratio is not only an indicator of energy status, but also appears to be a metabolic regulator or predictor of cell fate (Hardie 2003; Tantama and Yellen 2014). Although not directly tested, we suggest that the DCVC-induced changes in energy status ratios reported here may serve as early indicators and subsequent regulators of cell fate associated abnormal placental growth, as observed by others in IUGR.

DCVC-induced changes to macronutrients and energy metabolism pathways

To our knowledge, the current study is the first to use targeted metabolomics to evaluate DCVC-induced changes in cellular energy metabolism. Cellular energy metabolism pathways are tightly regulated and highly interconnected, enabling cells to precisely adjust macronutrient utilization and metabolism pathways catabolism for optimal ATP synthesis (Murray 2012;

Vaughan and Fowden 2016). This facilitates crucial plasticity necessary to meet the energy demands of the placenta amidst constantly changing environmental conditions (Illsley et al. 2010; Vaughan and Fowden 2016). In normal early pregnancies, anaerobic glycolysis fueled by glucose derived from maternal glandular histiotroph is the preferred source of energy over oxidative phosphorylation as outlined in figure 3.6A (Burton et al. 2002; Burton and Fowden 2015; Hoang et al. 2001; James et al. 2006). In the present study, we demonstrated DCVC-induced changes in intracellular metabolite concentrations from 9 interconnected metabolism pathways. Based on these concentrations altered by DCVC exposure and corresponding metabolite flux ratios, we present an integrated framework describing how DCVC may be altering bioenergetic fuel sources and pathway utilization following 6 and 12 h of exposure as summarized in figure 3.6B.

During glucose metabolism, we observed time-dependent elevated G6P+F6P concentrations in DCVC-treated cells and DCVC-stimulated ratio shifts for metabolites upstream (glucose: G6P+F6P), and downstream (G6P+F6P:F1BP), of G6P+F6P; both heavily favoring metabolite flux towards G6P+F6P. Together, these results indicated a time-progressive accumulation of G6P+F6P metabolites resulting from DCVC exposure between 6 and 12 h. Furthermore, we established that the time-progressive G6P+F6P accumulation was not caused by a change in PFK1 activity, the enzyme which converts F6P to F1BP. Considering that PFK1 is the most regulated glycolytic enzyme (Mor et al. 2011), there may be DCVC-induced changes to other regulatory mechanisms. For example, not only is F6P converted to F1BP via PFK1, but F6P is simultaneously converted by the enzyme PFK2 to fructose-2,6 bisphosphate (F2BP) for the purpose of feed-forward up-regulation of PFK1 activity (Berg et al. 2015). As a result of this complex regulation, determining the exact target of DCVC requires further investigation.

Nevertheless, the time-progressive G6P+F6P accumulation represents a significant DCVC-induced disruption in a key energy metabolism pathway.

Shunting of glucose metabolism intermediates were also detected, as indicated by elevated concentrations of R5P+X5P and NAcG1P from the PPP and HBP, respectively, following 6 h of DCVC exposure but not 12 h. Moreover, DCVC treatment stimulated metabolite ratios that shifted towards the PPP and HBP after 6 h, but not 12 h. Together, these results indicated DCVC-induced elevated G6P+F6P shunting away from glycolysis in favor of the PPP and HBP; a pattern that peaked at 6 h and diminished with time. Because G6P+F6P shunting towards the PPP and HBP decreased with time, whereas the G6P+F6P accumulation increased with time, these observations suggest opposing G6P+F6P metabolite fluctuations. Although not directed tested, diminished G6P+F6P shunting may have exacerbated the G6P+F6P accumulation between 6 and 12 h of DCVC exposure. Regardless, the opposing nature of these metabolite flux patterns likely suggests independent processes. However, the precise relationship between these observations required further experimental clarification outside of the scope this study. Despite the need for further investigation, the results presented here offer compelling evidence of DCVC-induced disruptions centered aroundG6P+F6P.

Interestingly, DCVC treatment revealed likely compensatory use of alternative macronutrient fuel sources based on evidence that DCVC treatment for 6 and 12 h increased intracellular concentrations of glycerol metabolism intermediates, lipids and energy-relevant amino acids, accompanied by changes in metabolite ratios favoring catabolic flux patterns. These results indicate that DCVC treatment stimulated increased utilization of secondary macronutrient fuel sources. Indeed, DCVC induced elevated Ga3P+DHAP and acetyl CoA concentrations. The latter metabolite changes frequently occur in association with increased of utilization alternative

macronutrient fuel sources because Ga3P+DHAP and acetyl CoA are entry points into energy metabolism for glycerol intermediates, some amino acids and and some lipids (Lipmann 1940; Pietrocola et al. 2015). Furthermore, because the lower glycolytic pathway and TCA cycle downstream of these entry points were largely unaffected by DCVC treatment, this pattern suggests a successful compensatory mechanism, likely related to increased energy demand and/or the previously described changes in glucose metabolism following treatment with DCVC. Increased utilization of alternative macronutrient fuel sources appears to be an important adaptation mechanism by which the cells maintain sufficient energy production, even when challenged by DCVC treatment.

DCVC treatment did not change TCA cycle metabolite concentrations included in our panel except for a slightly elevated malate concentration following 12 h of exposure. Contrary to a DCVC toxicity study in rat renal proximal tubular cells reported by Lash and Anders (1987), our results suggest that DCVC likely did not directly impact TCA metabolites, whereas Lash and Anders reported a substantial impact on succinate concentrations. Although the reasons remain uncertain, the different findings may be attributed to different cell types or the large difference in the DCVC concentrations used in each study: 20 μM DCVC in our study versus 1 mM DCVC in the study by Lash and Anders. Regardless, our results clearly indicate that TCA cycle metabolites were not the primary target of DCVC-induced changes in energy metabolism in HTR-8/SVneo cells at the concentrations and exposure durations tested here.

To our knowledge, the current study is the first to use targeted metabolomics to evaluate DCVC-induced changes in cellular energy metabolism for any cell type, although a previous study used a metabolomics approach to investigate TCE-induced changes to the metabolome in the context of embryogenesis (Vianta 2005). In agreement our results, increased histidine,

glutamine, isoleucine, and decreased phosphocreatine concentrations were reported in Japanese medaka fish exposed to 0-175 mg/L of TCE during embryogenesis: however, contrary to our results, ATP and glutamate and ATP concentrations decreased (Vianta 2005). Although the latter study in fish involved TCE exposure and not specifically DCVC, it is noteworthy that important energy-related metabolite concentrations were affected in the context embryogenesis, suggesting that TCE exposure may affect energy metabolism related to fetal development and/or pregnancy.

S-(1, 2-dichlorovinyl)-L-cysteine (DCVC) concentrations

Because the aim of the current study was to investigate the effects of non-cytolethal DCVC concentrations on energy in HTR-8/SVneo cells, we reaffirmed previous findings indicating that 24-h exposure to 20 μM DCVC or higher caused cell death, whereas 12-h exposure to 20 μM DCVC or lower was not lethal to the cells (Elkin et al. 2018; Hassan et al. 2016). Furthermore, we established a exposure duration threshold for detectable cell death at a lower concentration of DCVC: 10 μM following 48 h of exposure. Contrary to the current study, previous studies investigating energy and/or energy metabolism responses to DCVC treatment in different cell types mostly used lethal concentrations up to 1 mM, an order of magnitude higher than those used here (Lash and Anders 1986; Lash and Anders 1987; van de Water et al. 1995). Thus, the findings reported here contribute novel evidence of cellular energy responses to non-cytolethal DCVC concentrations.

The DCVC concentrations used in the present study are relevant to human occupational exposures based on levels of TCE that workers may encounter in an occupational setting. The Occupational Safety and Health Administration (OSHA) Permissible Exposure Limit (PEL) is 100 ppm averaged over an 8-hour work day(ATSDR 2016). In one study, female volunteers

exposed to the PEL of TCE for 4 h by inhalation had an average peak blood concentration of 13.4 μM for the metabolic precursor to DCVC, S-(1,2-dichlorovinyl) glutathione (Lash et al. 1999). This peak blood concentration is included within the range of concentrations used in our study of 5-20 μM DCVC. Moreover, another study detected TCE concentrations up to 229 ppm, more than twice the PEL, in 80 exposed workers (29% women) wearing personal aerosolized monitoring devices (Walker et al. 2016), demonstrating the exposure levels above the PEL are possible. Thus, our study contributes valuable evidence of the effects of plausible DCVC concentrations in human placental cells.

HTR-8/SVneo cells

In the current study, the widely-used immortalized first-trimester extravillous trophoblast cell line HTR-8/SVneo, was used to model the effects of DCVC treatment on the metabolome of extravillous trophoblasts. The use of this cell line has both advantages and limitation. For example, these cells express a combination of molecular markers that are distinct to extravillous trophoblasts such as cytokeratin 7 (CK7), and histocompatibility antigen, class I, G (HLA-G) (when grown on matrigel) (Irving et al. 1995; Khan et al. 2011; Kilburn et al. 2000; Takao et al. 2011). Moreover, these cells maintain many functional characteristics of extravillous trophoblasts (Hannan et al. 2010; Kilburn et al. 2000; Liu et al. 2016; Szklanna et al. 2017). On the other hand, although originally derived from first-trimester non-cancerous placental tissue, the immortalization processes alters the cells genetically to allow them to be cultured for extended time periods (Graham et al. 1993). Furthermore, *in vitro* cell culture condition may also explain genetic and epigenetic differences previous measured between HTR-8/SVneo cells and freshly isolated extravillous trophoblasts (Bilban et al. 2010; Novakovic et al. 2011). Generally,

our *in vitro* experiments don't reflect the full complicated *in vivo* dynamics within the fetal-uteroplacental unit and further studies in primary first-trimester extravillous trophoblasts, villous explants and other models are needed to confirm our results.

Summary and conclusion

In summary, we presented evidence detailing non-cytolethal DCVC-induced alterations to macronutrient and energy pathway metabolites in HTR-8/SVneo cells. Taken together, the results presented here suggest that DCVC caused metabolic perturbations necessitating adaptations in macronutrient and energy metabolism pathway utilization, while successfully maintaining sufficient ATP concentrations. Our findings demonstrate the biological plausibility of DCVC-induced placental injury and provide new insights into the toxicological mechanisms of action of TCE and its metabolite DCVC.

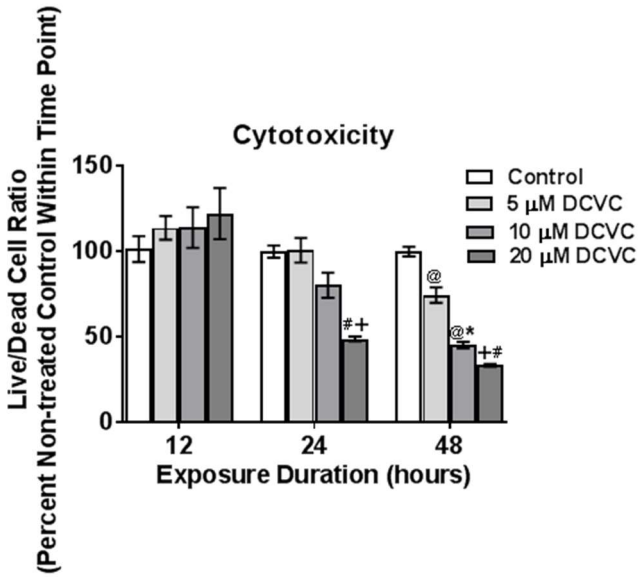

Figure 3.1. Effects of DCVC on cytotoxicity.
Cells were treated for 12, 24 or 48 h with medium alone (control), or with 5, 10, or 20 µM DCVC. The MultiTox-Glo Multiplex Cytotoxicity Kit (Promega) was used to sequentially measure the relative number of live and dead cells within a single well. Live cells were measured with cell-permanent glycyl-phenylalanyl-aminoflourocoumarin (GF-AFC) using a fluorescent signal. Dead cells were measured with cell-impermeable alanyl-alanyl-phenylalanyl-aminoluciferin (AAF-Glo) using a luminescent signal. Graphical representation shows live-to-dead cell ratios as percent control within each time point. Bars represent means ± SEM. Data were analyzed by two-way ANOVA (interaction between time and treatment, $P<0.0001$) with posthoc Tukey multiple comparisons prior to percent control conversion. Pound sign indicates significant difference compared to same treatment at all earlier time points: $^{\#}P< 0.0001$. At symbol indicates significant difference compared to same treatment at 12 h time point: $^{@}P<0.03$. Asterisk indicates significant difference compared to medium alone (control) within same time point: $^{*}P=0.0008$. Plus sign indicates significant difference compared to control and 5 µM DCVC within same time point: $^{+}P <0.02$. N= 3 independent experiments for each time point, with 3 replicates per treatment in each experiment. Camptothecin (4 µM) was included as a positive control and decreased the live-to-dead cell ratio by 55.6% ± 2.17% at 12 h, 80.68% ± 0.531% at 24 h, and 32.89% ± 0.039%% at 48 h.

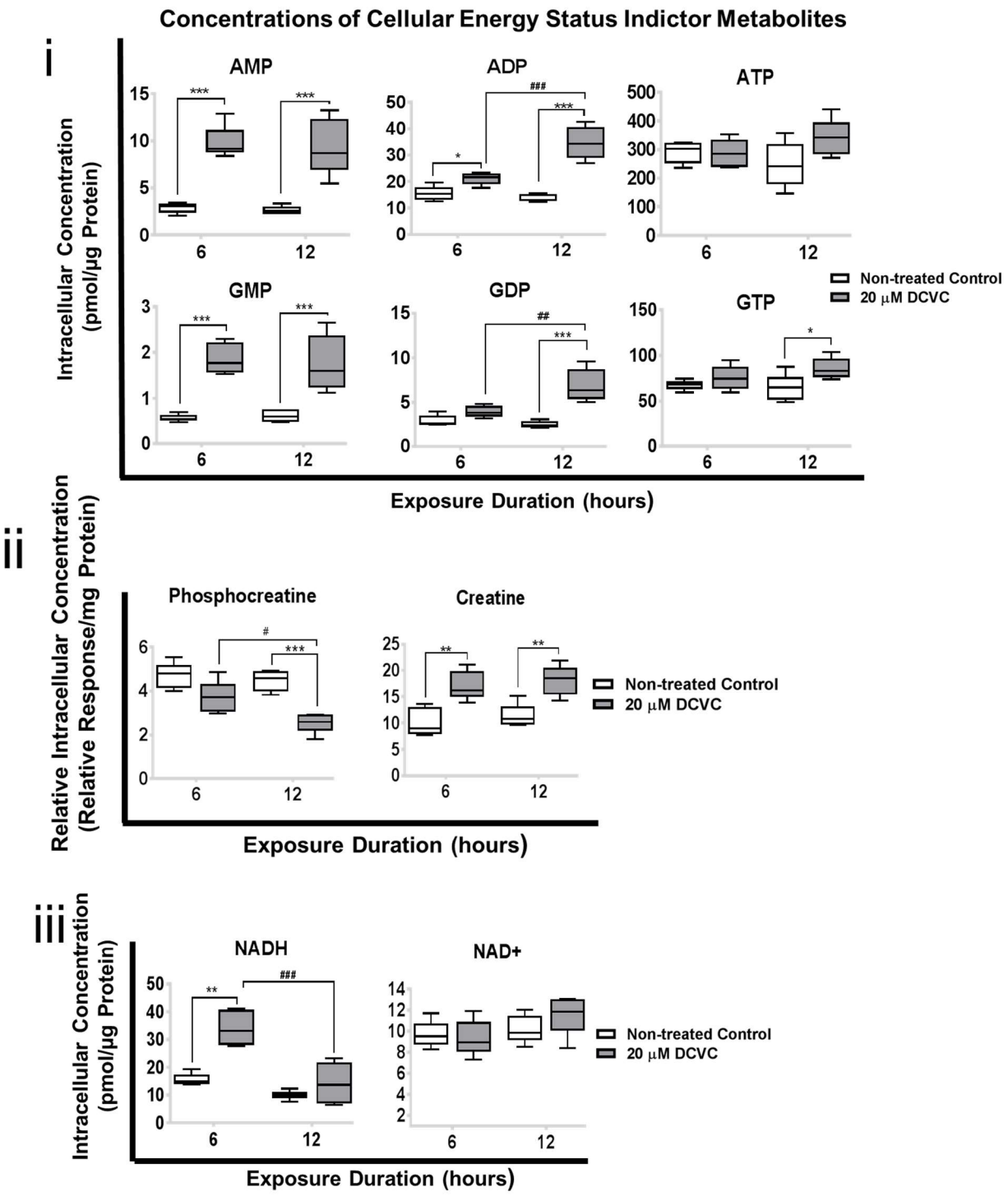
A
Concentrations of Cellular Energy Status Indictor Metabolites
i
AMP
ADP
ATP
GMP
GDP
GTP
Intracellular Concentration (pmol/µg Protein)
Non-treated Control
20 µM DCVC
Exposure Duration (hours)
ii
Phosphocreatine
Creatine
Relative Intracellular Concentration (Relative Response/mg Protein)
Non-treated Control
20 µM DCVC
Exposure Duration (hours)
iii
NADH
NAD+
Intracellular Concentration (pmol/µg Protein)
Non-treated Control
20 µM DCVC
Exposure Duration (hours)

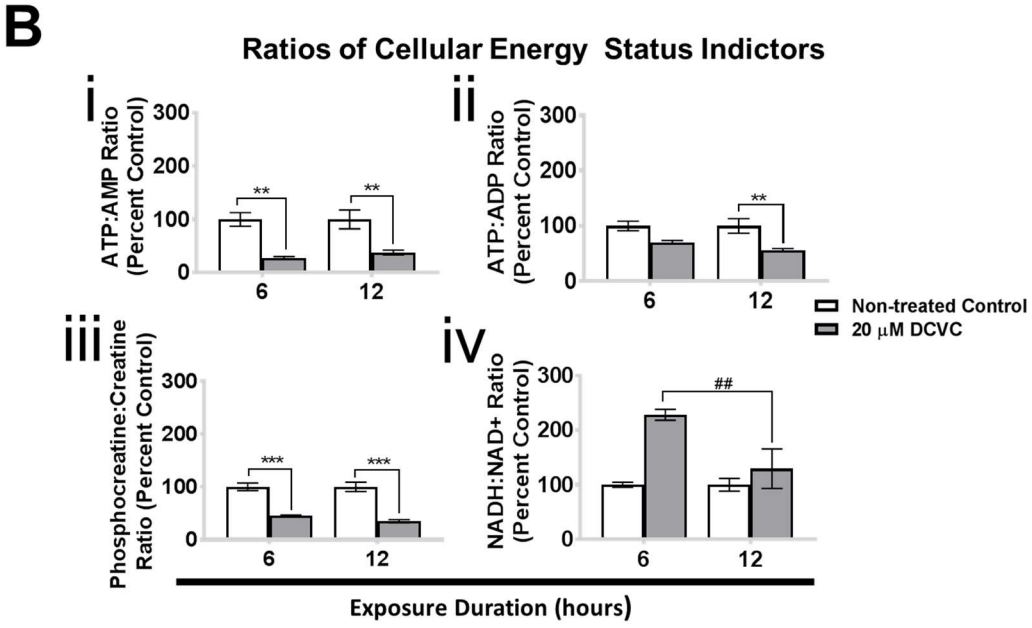
B
Ratios of Cellular Energy Status Indictors
i
ATP:AMP Ratio (Percent Control)
300
200
100
0
**
**
6
12
ii
ATP:ADP Ratio (Percent Control)
300
200
100
0
**
6
12
Non-treated Control
20 μM DCVC
iii
Phosphocreatine:Creatine Ratio (Percent Control)
300
200
100
0
***
***
6
12
iv
NADH:NAD+ Ratio (Percent Control)
300
200
100
0
##
6
12
Exposure Duration (hours)

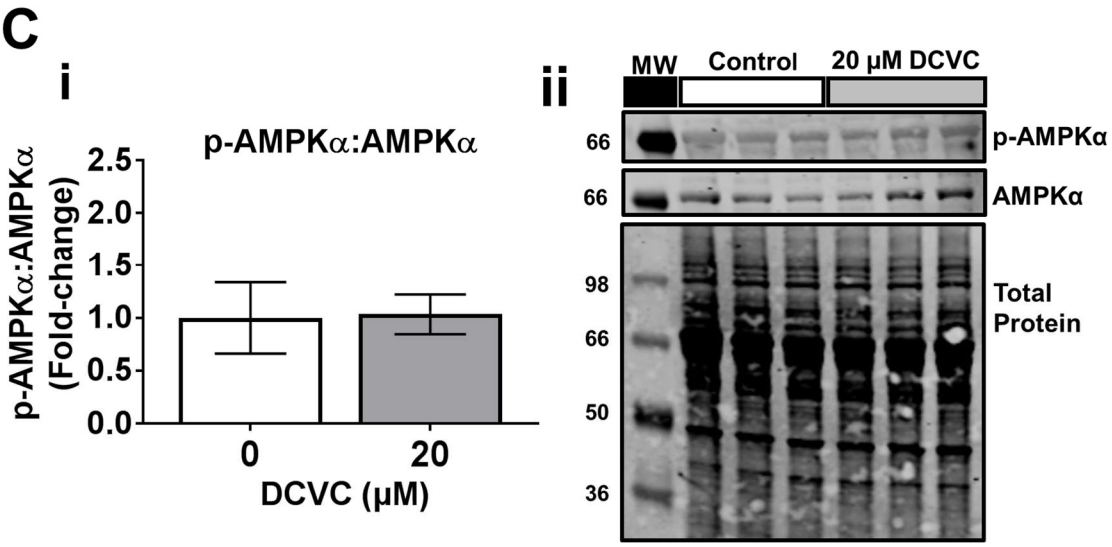
C
i
p-AMPKα:AMPKα
p-AMPKα:AMPKα (Fold-change)
2.5
2.0
1.5
1.0
0.5
0.0
0
20
DCVC (μM)
ii
MW
Control
20 μM DCVC
66
p-AMPKα
66
AMPKα
98
66
50
36
Total Protein

Figure 3.2. DCVC-induced changes in key cellular energy status indictors.
Cells were treated with medium alone (control) or 20 μM DCVC for 6 or 12 h. Targeted metabolomics were used to measure concentrations of energy status metabolites with reverse-phase liquid chromatography-mass spectrometry (LC-MS) as detailed in the methods section. A) Graphical representations of concentrations of: (i) adenylate and guanylate nucleotides (ii) phosphate donor and product phosphocreatine and creatine, and (iii) electron transporters NAD+ andNADH. Boxes represent first quartile, median and third quartile; whiskers represent minimum and maximum concentrations. B) Graphical representations of energy metabolite ratios derived from metabolite concentrations: (i) ATP:AMP, (ii) ATP:ADP, (iii) phosphocreatine:creatine and (iv) NADH:NAD+. Bars represent ratio means ± SEM. All data were analyzed by two-way ANOVA (interaction between time and treatment varied by metabolite, $P<0.05$) with posthoc Tukey multiple comparisons. Asterisks indicate significant differences compared to medium alone (control): $^{*}P<0.0419$, $^{**}P<0.0097$. $^{***}P<0.001$. Pound signs indicates significant differences compared to same treatment at all earlier time points: $^{\#}P=0.0116$, $^{\#\#}P=0.0026$, $^{\#\#\#}P<0.001$. N=5 independent experiments for each time point. D) AMPK signaling pathway was evaluated with western blotting analysis and normalized to total protein. (i) Graphical representation of p-AMPKα:p-AMPKα ratio and (ii) representative western blotting images. Bars represent means ± SEM. Data were analyzed with student t-tests. N= 3 independent experiment, with 3 replicates per treatment in each experiment.

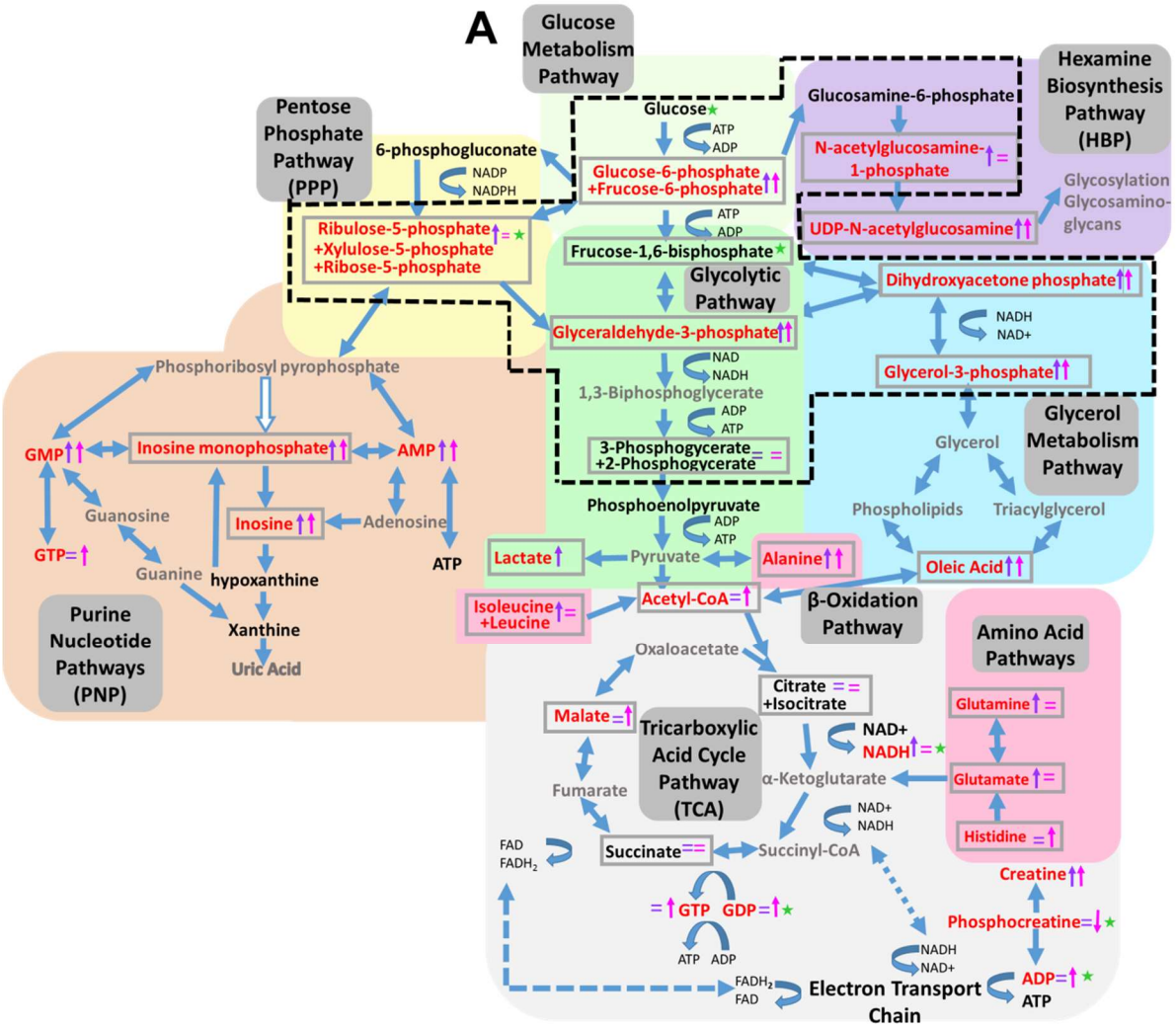

Key

- Direct downstream metabolite
- Indirect downstream metabolite
- Bidirectional metabolite
- Translocation
- ABC Not measured
- ABC No change in concentration between treatment groups within time point
- ABC Significant change in concentration between treatment groups within time point*
- 6 h: direction of concentration change*
- 6 h: No Change in concentration
- 12 h: direction of concentration change*
- 12 h: No Change in concentration
- ★ Significant change in concentration between time points within treatment group*
- Selected metabolite concentrations shown in 3B
- Calculated metabolite ratios shown in fig. 3.5
- *P<0.05

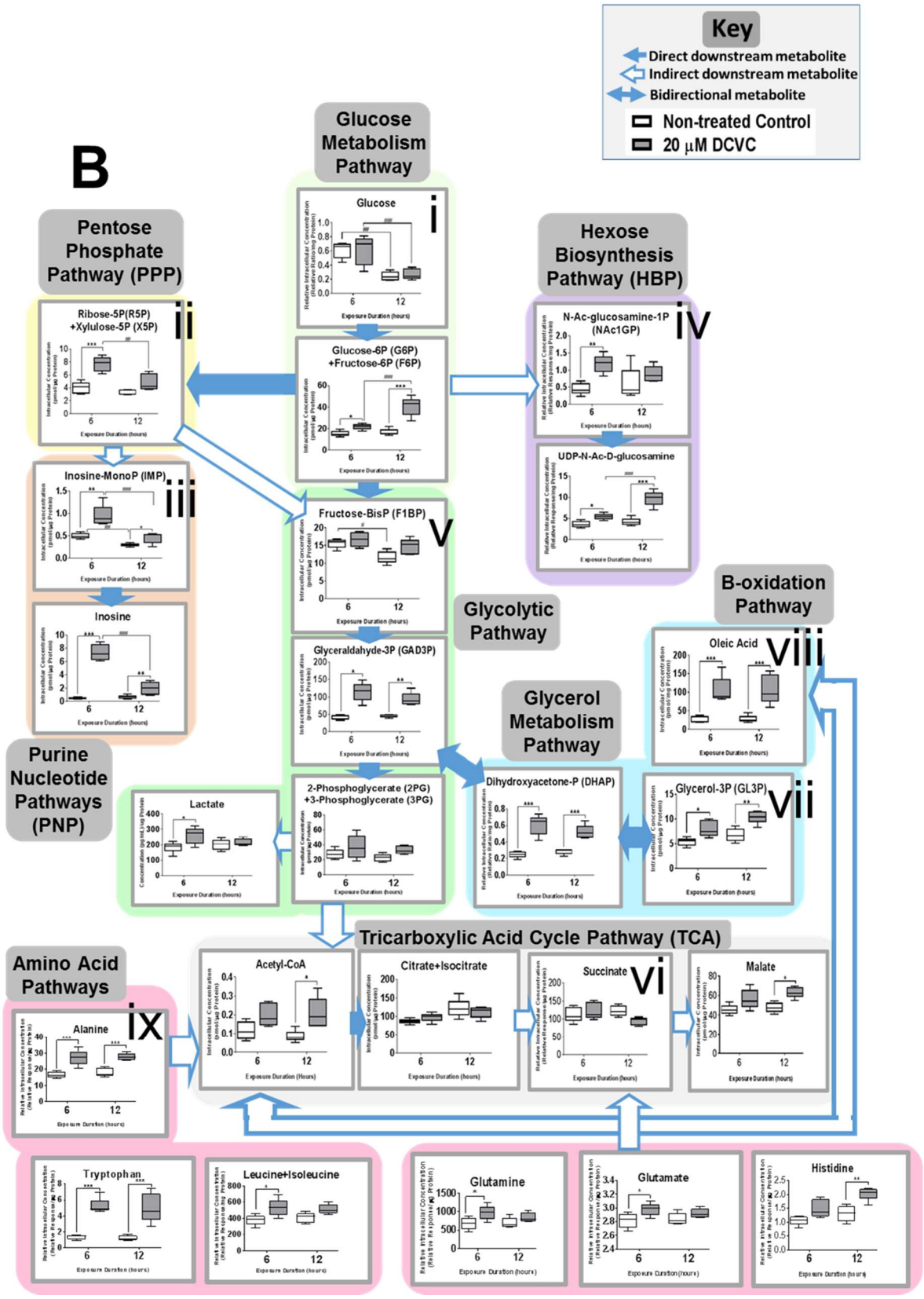
B
Key
Direct downstream metabolite
Indirect downstream metabolite
Bidirectional metabolite
Non-treated Control
20 μM DCVC
Glucose Metabolism Pathway
Pentose Phosphate Pathway (PPP)
Hexose Biosynthesis Pathway (HBP)
Glycolytic Pathway
Glycerol Metabolism Pathway
B-oxidation Pathway
Purine Nucleotide Pathways (PNP)
Amino Acid Pathways
Tricarboxylic Acid Cycle Pathway (TCA)
Glucose
i
Ribose-5P(R5P) +Xylulose-5P (X5P)
ii
Glucose-6P (G6P) +Fructose-6P (F6P)
N-Ac-glucosamine-1P (NAc1GP)
iv
UDP-N-Ac-D-glucosamine
Inosine-MonoP (IMP)
iii
Inosine
Fructose-BisP (F1BP)
v
Glyceraldahyde-3P (GAD3P)
2-Phosphoglycerate (2PG) +3-Phosphoglycerate (3PG)
Lactate
Dihydroxyacetone-P (DHAP)
Glycerol-3P (GL3P)
vii
Oleic Acid
viii
Acetyl-CoA
Citrate+Isocitrate
Succinate
vi
Malate
Alanine
ix
Tryptophan
Leucine+Isoleucine
Glutamine
Glutamate
Histidine
Exposure Duration (hours)

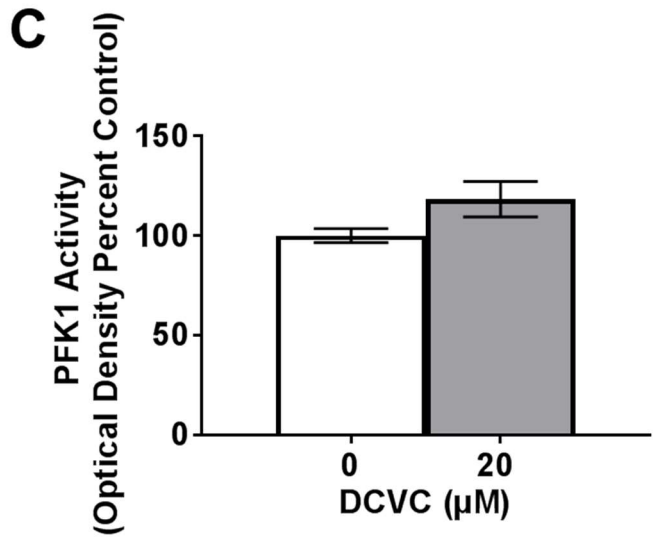

Figure 3.3. Effects of DCVC on energy metabolism pathways in HTR-8/SVneo cells. Cells were treated with medium alone (control) or 20 μM DCVC for 6 or 12 h. Targeted metabolomics were used to measure a panel of intracellular metabolites unique to specific energy metabolism pathways. Metabolite concentrations were quantified with LC-MS as detailed in the methods section. **A)** Overview of DCVC-induced changes in integrated energy metabolism pathways. Blue arrows indicate pathway directionality. Metabolite names in red indicate altered concentrations between treatment groups within same time point ($P<0.05$). Purple and pink symbols indicate direction of change in concentrations within 6 or 12 h time points, respectively. Green star symbols indicate altered concentrations between time points within same treatment group ($P<0.05$). All other symbols are indicated in figure legend. **B)** Graphical representations of selected metabolite concentrations grouped by energy metabolic pathway. Background color indicates corresponding pathway on integrated overview in 3A. Pathways represented include: **(i)** glucose metabolism, **(ii)** pentose phosphate pathway, **(iii)** purine pathways, **(vi)** hexosamine biosynthesis pathway, **(v)** glycolysis, **(vi)** TCA cycle pathway, **(vii)** glycerol metabolism pathway, **(viii)** β-oxidation pathway, and **(ix)** amino acid metabolism pathways. Boxes within each graph represent first quartile, median and third quartile; whiskers represent minimum and maximum. All data were log2 transformed prior to statistical analysis to achieve normal Gaussian distribution. Data were analyzed by two-way ANOVA (interaction between time and treatment varied depending on metabolite, $P<0.05$) with posthoc Tukey multiple comparisons. Asterisks indicate significant differences compared to medium alone (control): $^{*}P<0.05$, $^{**}P<0.01$, $^{***}P<0.001$. Pound signs indicate significant differences compared to same treatment at all earlier time points: $^{\#}P<0.05$, $^{\#\#}P<0.01$, $^{\#\#\#}P<0.001$. N=5 independent experiments for each time point. N=5 independent experiments for each time point. **C)** Graphical representation of phosphofructokinase 1 activity after 12 h DCVC treatment. PFK1 activity was measured with a commercially available enzyme activity assay kit (Sigma-Aldrich). Graphical representation of PFK1 activity as percent control absorbance. Bars represent means ± SEM. Data were analyzed with student t-test. N= 3 independent experiments, with 3 replicates per treatment in each experiment.

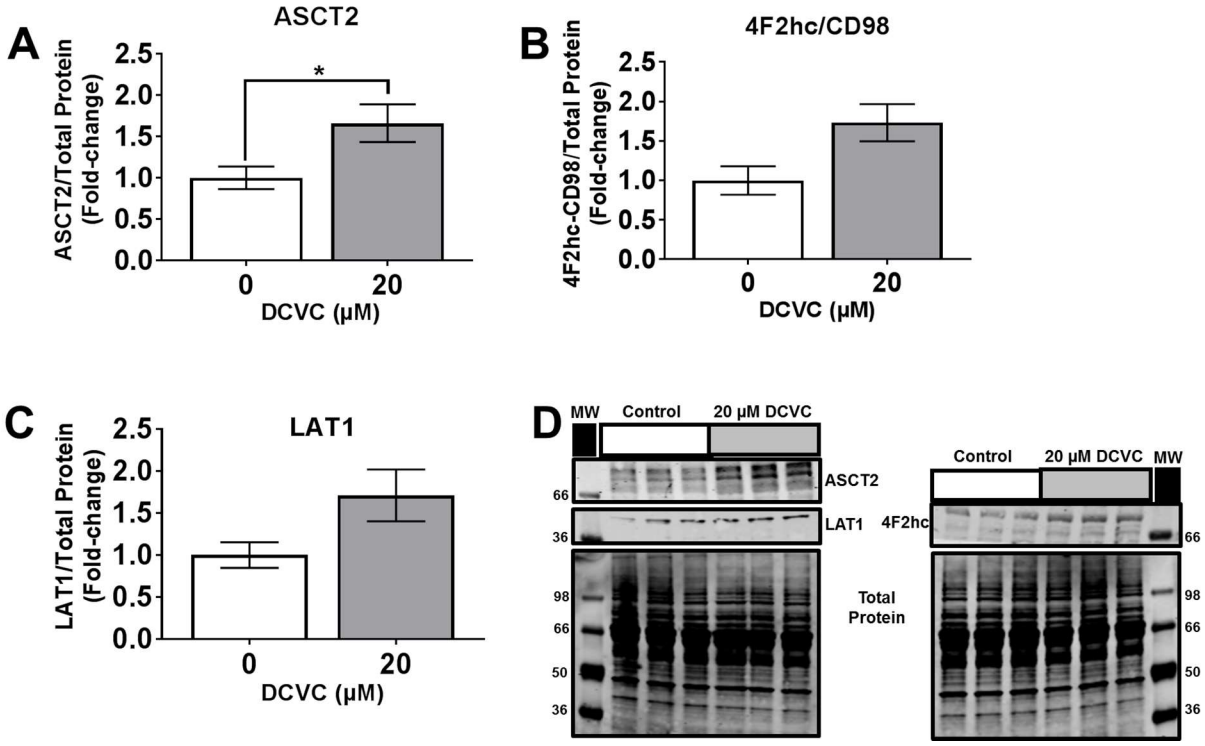

Figure 3.4. DCVC-induced changes in amino acid transporter levels.
Cells were treated with medium alone (control) or 20 μM DCVC for 12 h. Energy-relevant amino acid transporter levels were evaluated with western blotting analysis and normalized to total protein. Graphical representation of amino acid transporters as quantified using Odyssey CLx image scanner and Image Studio software. **A)** Small neutral amino acid transporter ASCT2. **B)** Large amino acid transporter heavy subunit 4F2hc. **C)** Large neutral amino acid transporter LAT1. **D)** Representative western blot images. Bars represent means ± SEM as percent control. Data were analyzed with student t-tests. Asterisks indicate significant difference compared to medium alone (control): * P=0.0474. N= 3 independent experiments, with 3 replicates per treatment in each experiment.

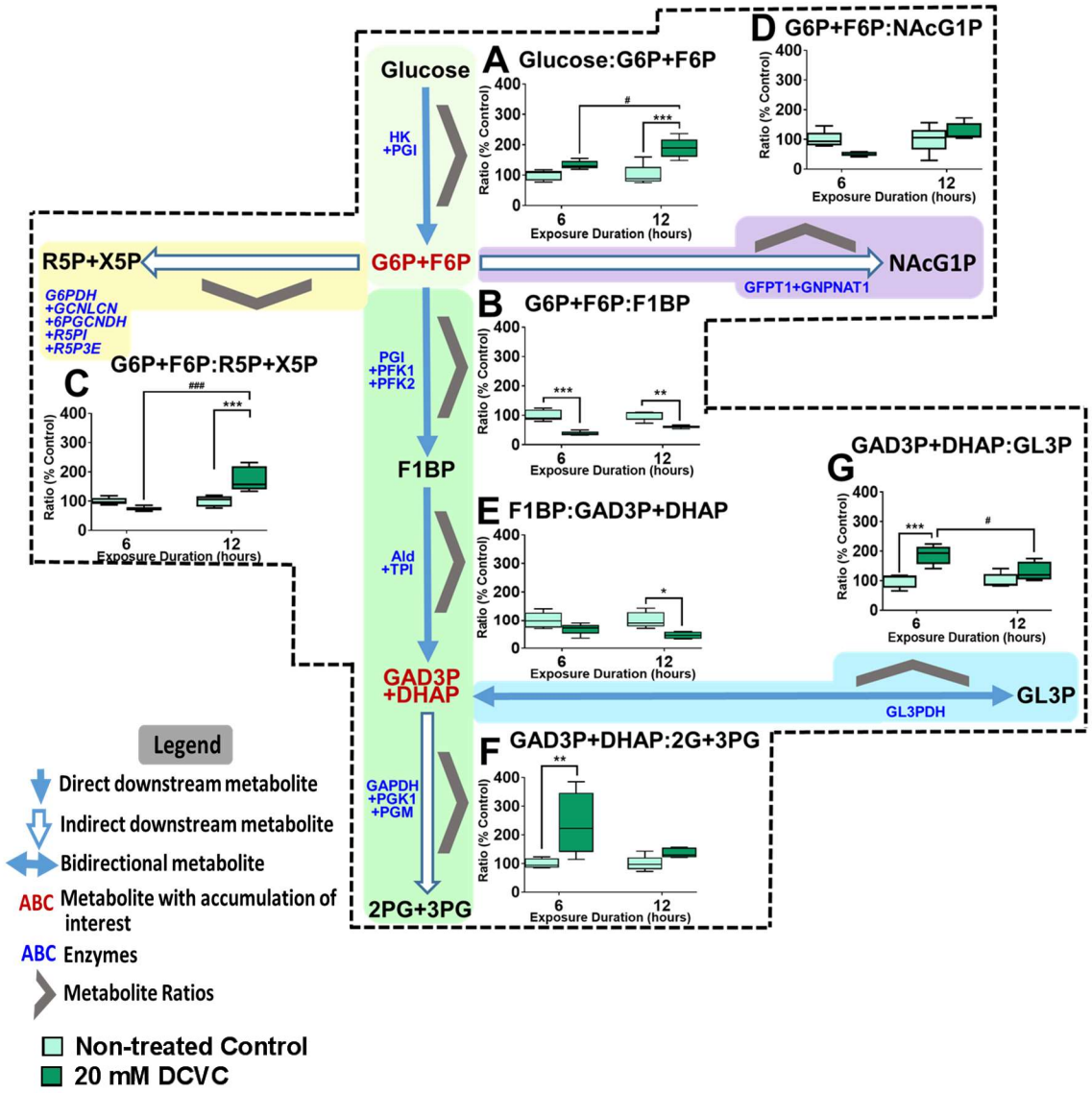

Figure 3.5. Energy pathway metabolite ratios.
Graphical representations of energy metabolite ratio calculated from metabolite concentrations representing upstream glycolysis, pentose phosphate pathway and glycerol metabolism pathway. **A)** Glucose:G6P+F6P ratio **B)** G6P+F6P:R5P+X5P ratio **C)** G6P+F6P:R5P+X5P ratio **D** G6P+F6P:NAcG1P ratio **E)** F1BP:Ga3P+DHAP ratio **F)** Ga3P+DHAP:2G+3PG ratio **E)** Ga3P+DHAP:GL3P ratio. Names in dark red indicate metabolites with noteworthy post-DCVC fluctuations. Boxes within each graph represent first quartile, median and third quartile; whiskers represent minimum and maximum. All data were log2 transformed prior to statistical analysis to achieve normal Gaussian distribution. Data were analyzed by two-way ANOVA (interaction between time and treatment varied depending on metabolite, $P<0.05$) with posthoc Tukey multiple comparisons. Asterisks indicate significant differences compared to medium alone (control): $^{*}P<0.05$, $^{**}P<0.01$, $^{***}P<0.001$. Pound signs indicate significant differences compared to same treatment at all earlier time points: $^{\#}P<0.05$, $^{\#\#}P<0.01$, $^{\#\#\#}P<0.001$.

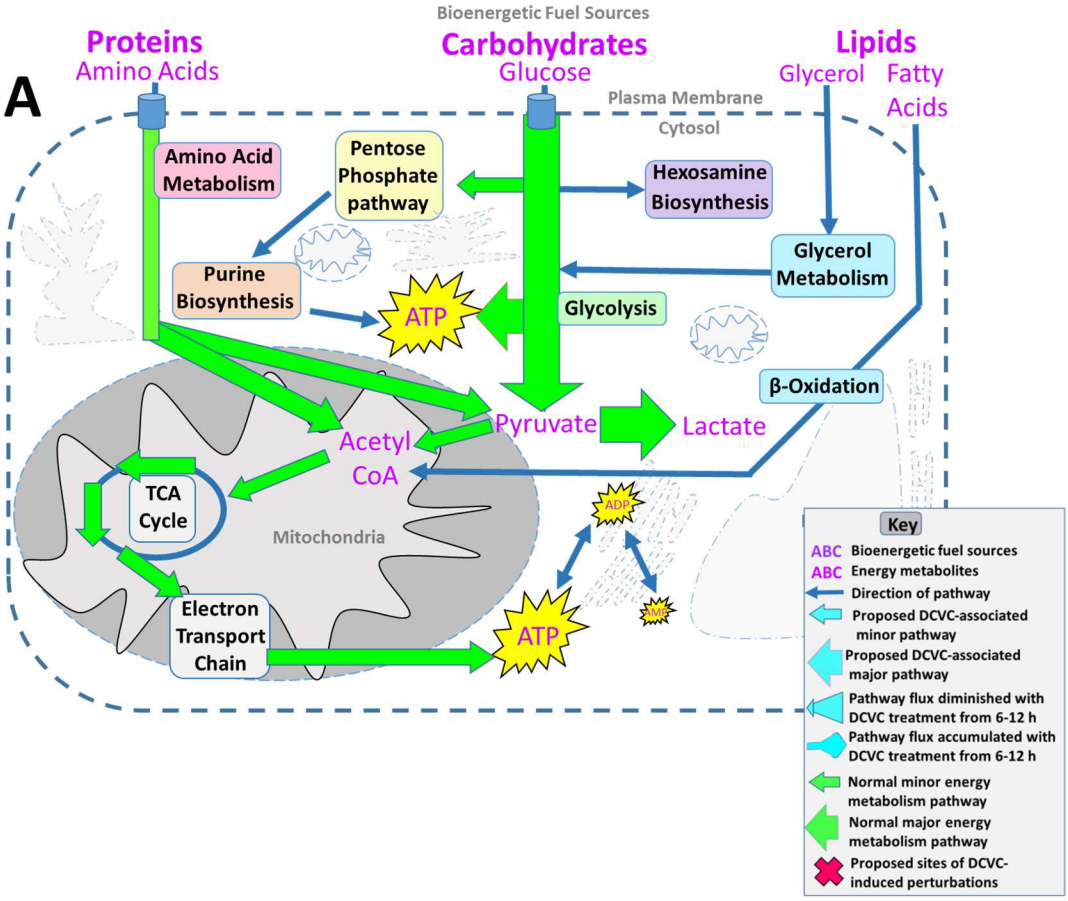
A
Bioenergetic Fuel Sources
Proteins
Amino Acids
Carbohydrates
Glucose
Lipids
Glycerol
Fatty Acids
Plasma Membrane
Cytosol
Amino Acid Metabolism
Pentose Phosphate pathway
Hexosamine Biosynthesis
Purine Biosynthesis
ATP
Glycerol Metabolism
Glycolysis
β-Oxidation
Pyruvate
Lactate
Acetyl CoA
TCA Cycle
Mitochondria
ADP
AMP
ATP
Electron Transport Chain
Key
ABC Bioenergetic fuel sources
ABC Energy metabolites
Direction of pathway
Proposed DCVC-associated minor pathway
Proposed DCVC-associated major pathway
Pathway flux diminished with DCVC treatment from 6-12 h
Pathway flux accumulated with DCVC treatment from 6-12 h
Normal minor energy metabolism pathway
Normal major energy metabolism pathway
Proposed sites of DCVC-induced perturbations

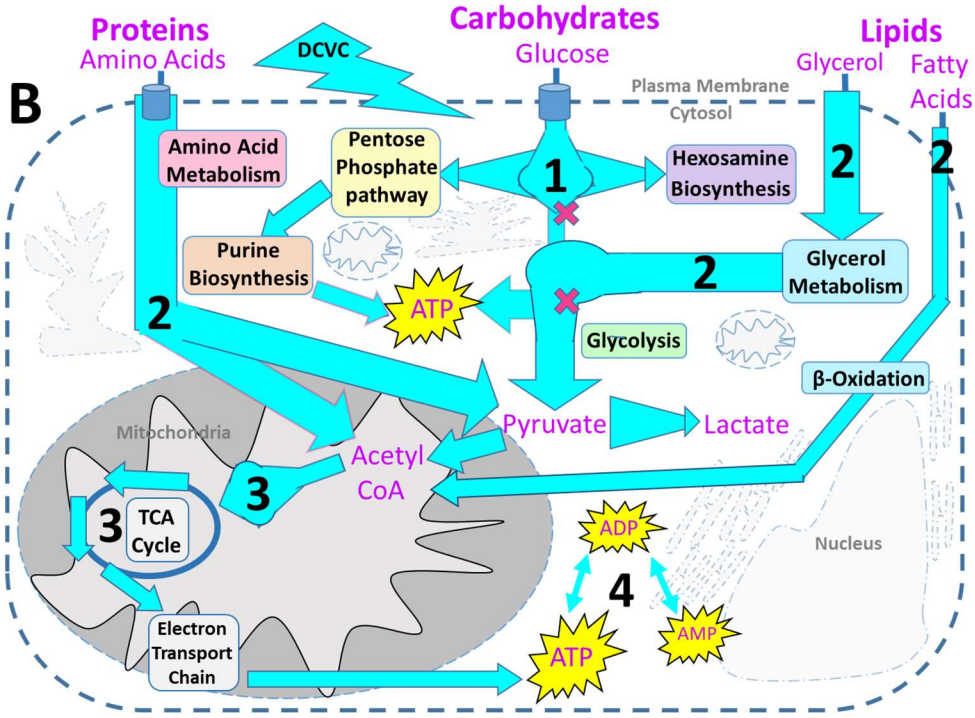
B
Proteins
Amino Acids
DCVC
Carbohydrates
Glucose
Lipids
Glycerol
Fatty Acids
Plasma Membrane
Cytosol
Amino Acid Metabolism
Pentose Phosphate pathway
1
Hexosamine Biosynthesis
2
2
Purine Biosynthesis
2
Glycerol Metabolism
ATP
2
Glycolysis
β-Oxidation
Mitochondria
Pyruvate
Lactate
Acetyl CoA
3
3
TCA Cycle
ADP
4
Nucleus
Electron Transport Chain
ATP
AMP

Figure 3.6. Proposed DCVC-induced energy metabolism alterations HTR-8/SVneo cells. **A)** Overview of normal cellular energy metabolism pathways in first-trimester placental cells. First-trimester placental cells survive in a low-oxygen environment. As a result, these cells prefer glycolysis fueled by glucose as their primary source of energy over oxidative phosphorylation. Despite this preference, the cells are capable of using other macronutrient metabolism pathways to fuel oxidative phosphorylation for additional ATP synthesis. **B)** Summary of proposed DCVC-induced energy metabolism alterations in HTR-8/SVneo cells. 1: Following glucose phosphorylation, G6P+F6P accumulated in a time-dependent manner. Conversely, PPP and HBP shunting of G6P+F6P was elevated at 6 h and diminished with time, suggesting two independent processes. 2: At 6 and 12 h, alternative bioenergentic fuel sources and pathways including amino acid, lipid and glycerol metabolism provided intermediates which enter glycolysis downstream of the G6P+F6P accumulation or enter the TCA cycle as acetyl CoA. Additionally, Ga3P and DHAP concentrations were elevated at both time points, suggesting another possible glycolytic perturbation. 3: Acetyl-CoA concentrations were increased at both time points, but TCA cycle metabolites were largely unchanged, indicating that DCVC likely does not directly affect the TCA cycle. 4: Although ATP levels are sustained, adenylate nucleotide ratios shifted down and ADP and AMP concentrations increased.

References

ATCC. 2015. Atcc product sheet: Htr8/svneo (atcc® crl3271™).American Type Culture Collection.

ATSDR. 2016. Public health statement on trichloroethylene.Agency for Toxic Substances and Disease Registry.

ATSDR. 2017. 2017 substance priority list.U.S. Agency for Toxic Substances and Disease Registry.

Berg J.M., Tymoczko J.L., Gatto J.G., Stryer L. 2015. Biochemistry. Eighth ed. Stuttgart, Germany:W. H. Freeman.

Bilban M., Tauber S., Haslinger P., Pollheimer J., Saleh L., Pehamberger H., et al. 2010. Trophoblast invasion: Assessment of cellular models using gene expression signatures. *Placenta.* **31**:989-996.

Burton G.J., Watson A.L., Hempstock J., Skepper J.N., Jauniaux E. 2002. Uterine glands provide histiotrophic nutrition for the human fetus during the first trimester of pregnancy. *J Clin Endocrinol Metab.* **87**:2954-2959.

Burton G.J., Fowden A.L. 2015. The placenta: A multifaceted, transient organ. *Philos Trans R Soc Lond B Biol Sci.* **370**:20140066.

Chen Q., Jones T.W., Brown P.C., Stevens J.L. 1990. The mechanism of cysteine conjugate cytotoxicity in renal epithelial cells. Covalent binding leads to thiol depletion and lipid peroxidation. *J Biol Chem.* **265**:21603-21611.

Chen Y., Cai J., Anders M.W., Stevens J.L., Jones D.P. 2001. Role of mitochondrial dysfunction in s-(1,2-dichlorovinyl)-l-cysteine-induced apoptosis. *Toxicol Appl Pharmacol.* **170**:172-180.

Chen Y.T., Kato T. 1985. Liver-specific glucose-6-phosphatase is not present in human placenta. *J Inherit Metab Dis.* **8**:92-94.

Chiu W.A., Jinot J., Scott C.S., Makris S.L., Cooper G.S., Dzubow R.C., et al. 2013. Human health effects of trichloroethylene: Key findings and scientific issues. *Environ Health Perspect.* **121**:303-311.

Cindrova-Davies T., van Patot M.T., Gardner L., Jauniaux E., Burton G.J., Charnock-Jones D.S. 2015. Energy status and hif signalling in chorionic villi show no evidence of hypoxic stress during human early placental development. *Molecular human reproduction.* **21**:296-308.

Crocker I.P., Cooper S., Ong S.C., Baker P.N. 2003. Differences in apoptotic susceptibility of cytotrophoblasts and syncytiotrophoblasts in normal pregnancy to those complicated with preeclampsia and intrauterine growth restriction. *Am J Pathol.* **162**:637-643.

Davies E.L., Bell J.S., Bhattacharya S. 2016. Preeclampsia and preterm delivery: A population-based case-control study. *Hypertens Pregnancy.* **35**:510-519.

Elkin E.R., Harris S.M., Loch-Caruso R. 2018. Trichloroethylene metabolite s-(1,2-dichlorovinyl)-l-cysteine induces lipid peroxidation-associated apoptosis via the intrinsic and extrinsic apoptosis pathways in a first-trimester placental cell line. *Toxicol Appl Pharmacol.* **338**:30-42.

EPA. 2017a. Tri explorer: Release trends report.Environmental Protection Agency.

EPA. 2017b. Trichloroethylene (tce); regulation of use in vapor degreasing under tsca §6(a) (rin 2070-ak11).

EPA. 2018. National priorities list.

Fisher G.J., Kelley L.K., Smith C.H. 1987. Atp-dependent calcium transport across basal plasma membranes of human placental trophoblast. *Am J Physiol.* **252**:C38-46.

Forand S.P., Lewis-Michl E.L., Gomez M.I. 2012. Adverse birth outcomes and maternal exposure to trichloroethylene and tetrachloroethylene through soil vapor intrusion in new york state. *Environ Health Perspect.* **120**:616-621.

Goodman D.R., James R.C., Harbison R.D. 1982. Placental toxicology. *Food Chem Toxicol.* **20**:123-128.

Graham C.H., Hawley T.S., Hawley R.G., MacDougall J.R., Kerbel R.S., Khoo N., et al. 1993. Establishment and characterization of first trimester human trophoblast cells with extended lifespan. *Experimental cell research.* **206**:204-211.

Guha N., Loomis D., Grosse Y., Lauby-Secretan B., El Ghissassi F., Bouvard V., et al. 2012. Carcinogenicity of trichloroethylene, tetrachloroethylene, some other chlorinated solvents, and their metabolites. *Lancet Oncol.* **13**:1192-1193.

Guimaraes-Ferreira L. 2014. Role of the phosphocreatine system on energetic homeostasis in skeletal and cardiac muscles. *Einstein (Sao Paulo).* **12**:126-131.

Hannan N.J., Paiva P., Dimitriadis E., Salamonsen L.A. 2010. Models for study of human embryo implantation: Choice of cell lines? *Biology of reproduction.* **82**:235-245.

Hardie D.G. 2003. Minireview: The amp-activated protein kinase cascade: The key sensor of cellular energy status. *Endocrinology.* **144**:5179-5183.

Hassan I., Kumar A.M., Park H.R., Lash L.H., Loch-Caruso R. 2016. Reactive oxygen stimulation of interleukin-6 release in the human trophoblast cell line htr-8/svneo by the trichlorethylene metabolite s-(1,2-dichloro)-l-cysteine. *Biology of reproduction.* **95**:66.

Hoang V.M., Foulk R., Clauser K., Burlingame A., Gibson B.W., Fisher S.J. 2001. Functional proteomics: Examining the effects of hypoxia on the cytotrophoblast protein repertoire. *Biochemistry.* **40**:4077-4086.

Ilekis J.V., Tsilou E., Fisher S., Abrahams V.M., Soares M.J., Cross J.C., et al. 2016. Placental origins of adverse pregnancy outcomes: Potential molecular targets: An executive workshop summary of the eunice kennedy shriver national institute of child health and human development. *Am J Obstet Gynecol.* **215**:S1-S46.

Illsley N.P., Caniggia I., Zamudio S. 2010. Placental metabolic reprogramming: Do changes in the mix of energy-generating substrates modulate fetal growth? *Int J Dev Biol.* **54**:409-419.

Irving J.A., Lysiak J.J., Graham C.H., Hearn S., Han V.K., Lala P.K. 1995. Characteristics of trophoblast cells migrating from first trimester chorionic villus explants and propagated in culture. *Placenta.* **16**:413-433.

James J.L., Stone P.R., Chamley L.W. 2006. The regulation of trophoblast differentiation by oxygen in the first trimester of pregnancy. *Human reproduction update.* **12**:137-144.

Khan G.A., Girish G.V., Lala N., Di Guglielmo G.M., Lala P.K. 2011. Decorin is a novel vegfr-2-binding antagonist for the human extravillous trophoblast. *Mol Endocrinol.* **25**:1431-1443.

Kilburn B.A., Wang J., Duniec-Dmuchowski Z.M., Leach R.E., Romero R., Armant D.R. 2000. Extracellular matrix composition and hypoxia regulate the expression of hla-g and integrins in a human trophoblast cell line. *Biology of reproduction.* **62**:739-747.

Lagakos S., Wessen B., Zelen M. 1986. An analysis of contaminated well water and health eff ects in woburn, massachusetts *Journal of the American Statistical Association.* **81**:583-596.

Lager S., Powell T.L. 2012. Regulation of nutrient transport across the placenta. *J Pregnancy.* **2012**:179827.

Laham S. 1970. Studies on placental transfer. Trichlorethylene. *IMS Ind Med Surg.* **39**:46-49.

Lash L.H., Anders M.W. 1986. Cytotoxicity of s-(1,2-dichlorovinyl)glutathione and s-(1,2-dichlorovinyl)-l-cysteine in isolated rat kidney cells. *J Biol Chem.* **261**:13076-13081.

Lash L.H., Anders M.W. 1987. Mechanism of s-(1,2-dichlorovinyl)-l-cysteine- and s-(1,2-dichlorovinyl)-l-homocysteine-induced renal mitochondrial toxicity. *Molecular pharmacology.* **32**:549-556.

Lash L.H., Putt D.A., Brashear W.T., Abbas R., Parker J.C., Fisher J.W. 1999. Identification of s-(1,2-dichlorovinyl)glutathione in the blood of human volunteers exposed to trichloroethylene. *J Toxicol Environ Health A.* **56**:1-21.

Lash L.H., Putt D.A., Hueni S.E., Krause R.J., Elfarra A.A. 2003. Roles of necrosis, apoptosis, and mitochondrial dysfunction in s-(1,2-dichlorovinyl)-l-cysteine sulfoxide-induced cytotoxicity in primary cultures of human renal proximal tubular cells. *J Pharmacol Exp Ther.* **305**:1163-1172.

Lash L.H., Chiu W.A., Guyton K.Z., Rusyn I. 2014. Trichloroethylene biotransformation and its role in mutagenicity, carcinogenicity and target organ toxicity. *Mutat Res Rev Mutat Res.* **762**:22-36.

Lee H.J., Jeong S.K., Na K., Lee M.J., Lee S.H., Lim J.S., et al. 2013. Comprehensive genome-wide proteomic analysis of human placental tissue for the chromosome-centric human proteome project. *J Proteome Res.* **12**:2458-2466.

Lipmann F. 1940. A phosphorylated oxidation product of pyruvic acid. *J Biol Chem.* **134**:4630464.

Liu L., Wang Y., Shen C., He J., Liu X., Ding Y., et al. 2016. Benzo(a)pyrene inhibits migration and invasion of extravillous trophoblast htr-8/svneo cells via activation of the erk and jnk pathway. *J Appl Toxicol.* **36**:946-955.

Lorenz M.A., Burant C.F., Kennedy R.T. 2011. Reducing time and increasing sensitivity in sample preparation for adherent mammalian cell metabolomics. *Anal Chem.* **83**:3406-3414.

Mando C., De Palma C., Stampalija T., Anelli G.M., Figus M., Novielli C., et al. 2014. Placental mitochondrial content and function in intrauterine growth restriction and preeclampsia. *American journal of physiology Endocrinology and metabolism.* **306**:E404-413.

March of Dimes P., Save the Children, WHO. 2012. Born too soon: The global action report on preterm birth. Geneva:World Health Organization.

McKinney L.L., Picken Jr. J.C., Weakley F.B., Eldridge A.C., Campbell R.E., Cowan J.C., et al. 1959. Possible toxic factor of trichloroethylene-extracted soybean oil meal3. *Journal of the American Chemical Society.* **81**:909-915.

Mor I., Cheung E.C., Vousden K.H. 2011. Control of glycolysis through regulation of pfk1: Old friends and recent additions. *Cold Spring Harb Symp Quant Biol.* **76**:211-216.

Morgan T. 2014. Placental insufficiency is a leading cause of preterm labor. *NewReviews.* **15**:5618-e5525.

Morgan T.K. 2016. Role of the placenta in preterm birth: A review. *Am J Perinatol.* **33**:258-266.

Murray A.J. 2012. Oxygen delivery and fetal-placental growth: Beyond a question of supply and demand? *Placenta.* **33 Suppl 2**:e16-22.

Myllynen P., Pasanen M., Pelkonen O. 2005. Human placenta: A human organ for developmental toxicology research and biomonitoring. *Placenta.* **26**:361-371.

Novakovic B., Gordon L., Wong N.C., Moffett A., Manuelpillai U., Craig J.M., et al. 2011. Wide-ranging DNA methylation differences of primary trophoblast cell populations and derived cell lines: Implications and opportunities for understanding trophoblast function. *Molecular human reproduction.* **17**:344-353.

NTP. 2015. Monograph on trichloroethylene Available: https://ntp.niehs.nih.gov/ntp/roc/monographs/finaltce_508.pdf 2016].

Oshvandi K., Jadidi A., Dehvan F., Shobeiri F., Cheraghi F., Sangestani G., et al. 2018. Relationship between pregnancy-induced hypertension with neonatal and maternal complications. *International Journal of Pediatrics.* **6**:8587-8594.

Pietrocola F., Galluzzi L., Bravo-San Pedro J.M., Madeo F., Kroemer G. 2015. Acetyl coenzyme a: A central metabolite and second messenger. *Cell Metab.* **21**:805-821.

Ruckart P.Z., Bove F.J., Maslia M. 2014. Evaluation of contaminated drinking water and preterm birth, small for gestational age, and birth weight at marine corps base camp lejeune, north carolina: A cross-sectional study. *Environ Health.* **13**:99.

Rusyn I., Chiu W.A., Lash L.H., Kromhout H., Hansen J., Guyton K.Z. 2014. Trichloroethylene: Mechanistic, epidemiologic and other supporting evidence of carcinogenic hazard. *Pharmacol Ther.* **141**:55-68.

Sharp A.N., Heazell A.E., Crocker I.P., Mor G. 2010. Placental apoptosis in health and disease. *Am J Reprod Immunol.* **64**:159-169.

Szklanna P.B., Wynne K., Nolan M., Egan K., Ainle F.N., Maguire P.B. 2017. Comparative proteomic analysis of trophoblast cell models reveals their differential phenotypes, potential uses and limitations. *Proteomics.* **17**:1700037-1700042.

Takao T., Asanoma K., Kato K., Fukushima K., Tsunematsu R., Hirakawa T., et al. 2011. Isolation and characterization of human trophoblast side-population (sp) cells in primary villous cytotrophoblasts and htr-8/svneo cell line. *PloS one.* **6**:e21990.

Tantama M., Yellen G. 2014. Imaging changes in the cytosolic atp-to-adp ratio. *Methods Enzymol.* **547**:355-371.

Tetz L.M., Cheng A.A., Korte C.S., Giese R.W., Wang P., Harris C., et al. 2013. Mono-2-ethylhexyl phthalate induces oxidative stress responses in human placental cells in vitro. *Toxicol Appl Pharmacol.* **268**:47-54.

van de Water B., Zoeteweij J.P., de Bont H.J., Mulder G.J., Nagelkerke J.F. 1994. Role of mitochondrial ca2+ in the oxidative stress-induced dissipation of the mitochondrial membrane potential. Studies in isolated proximal tubular cells using the nephrotoxin 1,2-dichlorovinyl-l-cysteine. *J Biol Chem.* **269**:14546-14552.

van de Water B., Zoeteweij J.P., de Bont H.J., Nagelkerke J.F. 1995. Inhibition of succinate:Ubiquinone reductase and decrease of ubiquinol in nephrotoxic cysteine s-conjugate-induced oxidative cell injury. *Molecular pharmacology.* **48**:928-937.

Vaughan O.R., Fowden A.L. 2016. Placental metabolism: Substrate requirements and the response to stress. *Reprod Domest Anim.* **51 Suppl 2**:25-35.

Vianta M.R., Bundy, J. G.; Pincetich, C. R.; de Ropp, J. S.; Tjeerdema, R. S. 2005. Nmr-derived developmental metabolic trajectories: An approach for visualizing the toxic actions of trichloroethylene during embryogenesis. *Metabolomics.* **1**:149-158.

Walker D.I., Uppal K., Zhang L., Vermeulen R., Smith M., Hu W., et al. 2016. High-resolution metabolomics of occupational exposure to trichloroethylene. *Int J Epidemiol.* **45**:1517-1527.

Waters E.M., Gerstner H.B., Huff J.E. 1977. Trichloroethylene. I. An overview. *J Toxicol Environ Health.* **2**:671-707.

Xu F., Papanayotou I., Putt D.A., Wang J., Lash L.H. 2008. Role of mitochondrial dysfunction in cellular responses to s-(1,2-dichlorovinyl)-l-cysteine in primary cultures of human proximal tubular cells. *Biochem Pharmacol.* **76**:552-567.

Chapter IV. Exposure to the Trichloroethylene Metabolite *S*-(1,2-Dichlorovinyl)-L-Cysteine for Short Durations Causes Progressive Mitochondrial Dysfunction in HTR-8/SVneo Trophoblasts

Abstract

Trichloroethylene (TCE) is a volatile organic solvent and common environmental pollutant. Despite ongoing efforts to ban TCE for most applications, its availability and usage persist worldwide. As a result of sustained usage in industrial settings, remediation challenges, and ongoing pollution, TCE exposure continues to be a potential human health hazard. Recent studies reported associations between maternal TCE exposure and increased risk for adverse birth outcomes, including preterm birth and low birth weight. Despite these associations, the toxicological mechanism underlying TCE adverse effects in pregnancy is not well understood. The TCE metabolite *S*-(1,2-dichlorovinyl)-L-cysteine (DCVC) induces mitochondrial-mediated apoptosis in renal cells and in a first-trimester extravillous trophoblast cell line. To gain further understanding of mitochondrial-mediated DCVC placental toxicity, this study investigated the effects of short-term DCVC exposure on mitochondrial function using non-cytolethal concentrations in placental cells. Human extravillous trophoblast cells, HTR-8/SVneo, were exposed *in vitro* to 5-20 μM DCVC for 6 or 12 h. A Seahorse XF Analyzer, which allows for concurrent real-time monitoring of oxygen consumption rates and extracellular acidification rates, was used to evaluate key aspects of mitochondrial function. Additionally, TMRE fluorochrome was used to measure changes in mitochondrial membrane potential. Following 6 h of exposure to 20 μM DCVC, elevated oxygen consumption, mitochondrial proton leak and

sustained energy coupling deficiency were observed. Similarly, 12 h of exposure to 10-20 μM DCVC decreased mitochondrial-dependent basal, ATP-linked and maximum oxygen consumption rates, and dissipation of mitochondrial membrane potential were detected. Lastly, (±)-α-tocopherol, a known suppressor of lipid peroxidation, attenuated DCVC-stimulated mitochondrial membrane depolarization but failed to rescue oxygen consumption perturbations. Taken together, these results suggest that DCVC caused progressive mitochondrial dysfunction, resulting in lipid peroxidation-associated mitochondrial membrane depolarization. Our findings contribute to the biological plausibility of DCVC-induced placental impairment and provide new insights into the role of the mitochondria in DCVC-induced toxicity.

Introduction

Trichloroethylene (TCE) is a volatile organic solvent used for decades as a dry-cleaning solvent and industrial lipophilic metal degreaser. Although still used as a solvent in industrial settings, the majority of new TCE produced is utilized as a chemical intermediate in closed-system refrigerant manufacturing (ATSDR 2016; NTP 2015). Due to longstanding industrial usage and improper disposal, TCE is a common and persistent environmental contaminant, polluting soil, air and water (Chiu et al. 2013). Confirmed TCE contamination exists in at least 1055 of 1750 current and former EPA-designated National Priorities List Superfund sites, prompting its listing as number sixteen on the U.S. Agency for Toxic Substances and Disease Registry's Priority List of Hazardous Substances (ATSDR 2017; EPA 2018) Because of steady usage in industrial settings and widespread pollution, TCE exposure continues to be potentially hazardous to human health.

TCE has proven to be a potent organ- and organ system-specific toxicant (Lash et al. 2014; Waters et al. 1977). For example, TCE is classified by the National Toxicology Program (NTP)

and International Agency for Research on Cancer (IARC) as a known human carcinogen based on epidemiological evidence and animal toxicity studies demonstrating that the compound causes kidney cancer in humans and animals (Guha et al. 2012; Lash et al. 2000; NTP 2015; Rusyn et al. 2014). Moreover, TCE has also been implicated in immunotoxicity (Bassig et al. 2013; Hosgood et al. 2011; Lan et al. 2010), neurotoxicity (Abdraboh et al. 2018; Rasmussen et al. 1993; Ruijten et al. 1991), hepatotoxicity (Christensen et al. 2013) and respiratory toxicity (Forkert and Birch 1989; Forkert et al. 2006). Additionally, TCE has been implicated in adverse pregnancy outcomes. Although an early study found no association (Lagakos et al. 1986), several recent studies reported significant associations between maternal TCE exposure and increased risk of low birth weight (Forand et al. 2012; Ruckart et al. 2014).

Optimal placental function is a critical factor for healthy fetal development during pregnancy. Abnormal placental development may play a key role in adverse birth outcomes (Ilekis et al. 2016). For example, placental insufficiency originating from deficient placental structure and/or function may contribute to preterm birth incidences (Morgan 2014; Morgan 2016). Indeed, several recent epidemiology studies found significant associations between pre-eclampsia, which involves placental abnormalities, and increased risk of preterm birth and/or low birth weight (Davies et al. 2016; Oshvandi et al. 2018).

As a highly perfused organ with abundant metabolic activity, the placenta is a probable target organ for toxicity (Goodman et al. 1982). Because the placenta has a large surface area that serves as the maternal-placental circulatory interface, it is readily exposed to TCE and it metabolites circulating in maternal blood. (Burton and Fowden 2015; Laham 1970). Moreover, the placenta expresses many enzymes required for *in vivo* TCE metabolism including cytochrome P450, glutathione-S-transferase and beta-lyase (Lee et al. 2013; Myllynen et al.

2005). The presence of these enzymes greatly increases the risk of placenta-generated toxic TCE metabolites.

Specific TCE metabolites are implicated in TCE toxicity, suggesting that TCE metabolism is required to exert its toxic effects (Lash et al. 2014). TCE is metabolized by two main pathways: cytochrome P450 oxidation and glutathione conjugation. Despite being considered a minor pathway compared to cytochrome P450 oxidation, glutathione conjugation metabolites display potent organ-specific toxicity. Notably, multiple *in vitro* studies have demonstrated that the glutathione pathway-derived metabolite *S*-(1, 2-dichlorovinyl)-L-cysteine (DCVC) is toxic to kidney proximal tubular cells in rodents and humans (Chen et al. 2001; Darnerud et al. 1989; Lash and Anders 1986; Lash et al. 2001; Xu et al. 2008). Furthermore, mechanistic studies revealed that DCVC cytotoxicity in kidney cells is mediated by mitochondrial dysfunction, aberrant reactive oxygen species (ROS) generation, and accompanying lipid peroxidation and apoptosis (Chen et al. 1990; Chen et al. 2001; Lash and Anders 1986; Lash et al. 2003; van de Water et al. 1994; van de Water et al. 1995; Xu et al. 2008). In agreement with studies of kidney cells, we recently reported that DCVC increases placental cell ROS generation, lipid peroxidation and mitochondrial-mediated apoptosis in the first trimester extravillous trophoblast cell line HTR-8/SVneo (Elkin et al. 2018; Hassan et al. 2016). Taken together, the evidence supports the mitochondria as a primary target and mediator of cytotoxicity in multiple cells types (Lash and Anders 1986).

Mitochondria are organelles that perform a diverse array of cellular functions such as calcium homeostasis, steroid hormone synthesis and ROS signaling (Meyer et al. 2013; Nicholls 2002). Most importantly, mitochondria play a role central in adenosine triphosphate (ATP) generation, the primary energy driver behind many cellular processes (Fisher et al. 1987; Lager

and Powell 2012). The majority of cellular ATP is synthesized aerobically through oxidative phosphorylation in the mitochondria (Erecinska and Wilson 1982).

Optimal mitochondrial functioning is critical for placental cells because of their sizable energy requirements for carrying out early pregnancy biological processes such tissue remodeling (Mando et al. 2014; Murray 2012; Vaughan and Fowden 2016). To date, there is considerable evidence supporting the theory that mitochondrial disruptions play a role in the pathophysiology of early pregnancy disorders. For example, mitochondria-generated ROS including lipid peroxidation and alterations in mitochondrial DNA content in placental cells have been widely observed in pregnancy disorders involving abnormal placental development, as previously reviewed (Gupta et al. 2005; Holland et al. 2017). Based on the importance of the mitochondria in placental cell function and previous studies suggesting the mitochondria as an intracellular target of DCVC toxicity, this study investigated the effects of DCVC on mitochondrial function in human extravillous trophoblasts.

Materials and Methods

Chemicals and Reagents

S-(1, 2-dichlorovinyl)-L-cysteine (DCVC), a trichloroethylene glutathione conjugation pathway metabolite, was synthesized in powder form by the University of Michigan Medicinal Chemistry Core as previously described (McKinney et al. 1959)**.** High-performance liquid chromatography (HPLC) analysis was used to determine purity (98.7%). A stock solution of 1 mM DCVC was prepared by dissolving DCVC in phosphate buffered saline and stored in small aliquots at −20°C to minimize freeze/thaw cycles. The chemical purity of the DCVC stock solution was confirmed periodically by nuclear magnetic resonance (NMR).

RPMI 1640 culture medium with L-glutamine and without phenol red, 10,000 U/mL penicillin/10,000 μg/mL streptomycin (P/S) solution, and fetal bovine serum (FBS) were purchased from Gibco, a division of Thermo Fisher Scientific (Waltham, MA, USA). Phosphate buffered saline (PBS), Hank's Balanced Salt Solution (HBSS) and 0.25% trypsin were purchased from Invitrogen Life Technologies (Carlsbad, CA, USA). Rotenone and (±)-α-tocopherol were purchased from Sigma-Aldrich (St. Louis, MO, USA). Trifluoromethoxy carbonylcyanide phenylhydrazone (FCCP) was purchased from Cayman Chemical (Ann Arbor, MI, USA). Antimycin was purchased from Enzo Life Sciences (Farmingdale, NY, USA). Dimethyl sulfoxide (DMSO) was purchased from Torcis Biosciences (Bristol, UK).

Cell Culture and Treatment

The HTR-8/SVneo cells were obtained from Dr. Charles H. Graham (Queen's University, Kingston, Ontario, Canada). This cell line was derived from first-trimester human placentae and immortalized with simian virus 40 large T antigen (Graham et al. 1993)**.** The cell line expresses markers of an extravillous trophoblast phenotype and has a female genotype. HTR-8/SVneo cells were cultured as previously described (Hassan et al. 2016; Tetz et al. 2013). Briefly, cells were cultured between passages 78–87 in RPMI 1640 medium supplemented with 10% FBS and 1% P/S at 37°C in a 5% CO_2 humidified incubator. Cells were sustained in RPMI 1640 growth medium with 10% FBS and 1% P/S prior to and during experiments to ensure optimal cell growth as previously described (Graham et al. 1993)**.** Cells were grown to 70–90% confluence for 24 h after subculture prior to beginning each experiment.

Prior to each experiment, a DCVC stock solution aliquot was quickly thawed in a 37°C water bath and then diluted in RPMI 1640 medium with 10% FBS and 1% P/S to final exposure

concentrations of 5–20 μM DCVC. The DCVC concentrations selected for study include plausible metabolite concentrations in human blood with occupational exposure to the parent compound, trichloroethylene (Lash et al. 1999). Additionally, we selected concentrations previously determined to lack overt cytotoxicity in HTR-8/SVneo cells at the times points used in the present study (Hassan et al. 2016).

Cell Line Validation

HTR-8/SVneo cells were seeded at a density of 400,000 cells per well in a 6-well cell culture plate and allowed to adhere for 24 h. Cells were incubated with culture medium for an additional 24 h. Genomic DNA was extracted using QIAamp® DNA Mini Kit (Qiagen; Hilden, Germany). DNA samples were frozen at −80°C and transported to the University of Michigan DNA Sequencing Core. Microsatellite genotyping was performed using AmpFLSTR Identifier Plus PCR Amplification Kit run on a 3730XL Genetic Analyzer purchased from Applied Biosystems (Waltham, MA, USA). DNA for 8 tetranucleotide repeat loci and the Amelogenin gender determination marker were identified. The short tandem repeat profile generated for our cells was compared to the short tandem repeat profile for HTR-8/SVneo (ATCC® CRL-3271™) published by American Type Culture Collection (Manassas, VA, USA) (ATCC 2015).The short tandem repeat profile was a match: CSF1PO: 12, D13S317: 9,12, D16S539: 13D5S818: 12, D7S820: 12, TH01: 6,9.3, vWA: 13,18, TPOX: 8, Amelogenin gender determination marker: X (ATCC 2015).

Measurement of Cellular Bioenergetics

We measured changes in cellular bioenergetics using the Seahorse XF24e or XF24 analyzers (Agilent Seahorse; Santa Clara, CA), which allowed simultaneous measurement of the oxygen consumption rate (OCR) and extracellular acidification rate (ECAR) in live cells. We plated HTR-8/SVneo cells at a density of 50,000 cells per well in Seahorse XF24 analyzer 24-well plates (Agilent Seahorse) and allowed the cells to attach for 24 h. Cells were then treated with medium alone (control) or DCVC (10 or 20 μM), 3-5 wells per treatment depending on experiment. After 6 or 12 hours, we performed a mitochondrial stress assay (Mito Stress Test) using the Seahorse analyzer and manufacturer's protocols. During the mitochondrial stress assay, the analyzer took a series of basal OCR and ECAR measurements followed by sequential injections of compounds targeting different parts of the electron transport chain: this allowed for the measurement of ATP-linked respiration rate, oxygen-linked maximum respiration rate, non-mitochondrial respiration rate and subsequent calculation of proton leak rate, reserve respiration and acidification rate and coupling efficiency (AgilentSeahorse 2017; Divakaruni et al. 2014). Briefly, the day before the assay, the Seahorse XF24 cartridge was soaked in Seahorse XF Calibrant (Agilent Seahorse) and placed in a CO_2- free incubator at 37ºC overnight. The day of the assay, the cells in the Seahorse plate were washed twice with buffer-free RPMI 1640 media (Sigma-Aldrich) and placed in a CO_2- free incubator at 37ºC for 1 h prior to reading. The mitochondrial complex V inhibitor oligomycin (1 μM) was loaded into cartridge injection port A, uncoupler FCCP (1 μM) was loaded into injection port B, and complex I and III inhibitors rotenone and antimycin A (1 μM each) were loaded into injection port C. The cartridge and Seahorse plate were placed in the Seahorse XF24e or XF24 analyzer and maintained at 37 ºC. The OCR and ECAR were measured using Wave Controller Software version 2.4 (Agilent Seahorse) at approximately 5-minute intervals, followed by measurements of OCR and ECAR

after each injection of an electron transport chain inhibitor. Following the assay, a BCA assay (Thermo Fisher Scientific) was performed to quantify total μg of protein per well for normalization purposes. At least three independent experiments were performed for each time point.

Calculation of Mitochondrial Functional Parameters

The bioenergetics parameters were measured or calculated as follows (AgilentSeahorse 2016). Non-mitochondrial respiration rate was directly measured by the Seahorse XF analyzer as the lowest OCR measurement after the rotenone/antimycin A injection. Basal respiration rate is the non-mitochondrial respiration rate subtracted from the last OCR measurement before the first injection. The maximum respiratory rate is the non-mitochondrial respiration rate subtracted from the highest OCR measurement taken after the FCCP injection. Proton leak rate is the non-mitochondrial respiration rate subtracted from the lowest OCR measurement taken after the oligomycin injection. The ATP-linked respiration rate is lowest OCR measurement taken after the oligomycin injection subtracted from the last OCR measurement before the oligomycin injection. The reserve respiration rate is the maximum respiratory rate minus the basal respiration rate. The coupling efficiency is the maximum respiratory rate divided by the basal respiration rate times 100. The calculations and relationships of these parameters are visualized in appendix figure A.2.

Measurement of mitochondrial DNA content

Relative mitochondrial DNA content, a proxy for mitochondrial copy number, was estimated by measuring the quantity of genomic DNA of two mitochondrial genes and two

nuclear genes and calculating the ratios of mitochondrial DNA to nuclear DNA. HTR-8/SVneo cells were seeded at a density of 400,000 cells per well in a 6-well cell culture plate and allowed to adhere and acclimate for 24 h. Cells were treated with medium alone (control) or DCVC (5, 10 or 20 μM) for 6 or 12 h. Following exposure, DNA was extracted using QIAamp® DNA Mini Kit (Qiagen) following the manufacturer's protocol. Briefly, cells were trypsinized with 0.25% trypsin, transferred to microcentrifuge tubes, centrifuged and resuspended in PBS. Cell were lysed in a buffer that preserves the nuclei and mitochondria of the cells, centrifuged and washed to remove any remaining cellular debris. The remaining nuclear pellet was lysed with a buffer and treated with proteinase K. The lysate was then filtered through QIAGEN Genomic tip filters to separate genomic DNA. Following filtration, the genomic DNA was washed, eluted and stored at -80 ºC in 10 mM Tris-Cl buffer with a pH of 8.5.

Following DNA extraction, real-time PCR was performed on the genomic DNA using a commercially available Human Mitochondrial DNA (mtDNA) Monitoring Primer Set (Takara Bio; Mountain View, CA) containing primers for two nuclear encoded genes; *SLCO2B1* *SERPINA1* and two mitochondrial encoded gene: *ND1* and *ND5*. real-time PCR reactions were prepared with SYBR Green Mastermix (Qiagen SABiosciences; Sioux Falls, SD, USA) and commercially purchased primers and run on a Bio-Rad (Hercules, CA) CFX96 Real Time C1000 \thermal cycler following the manufacturer's recommended protocols.

The mitochondrial content was calculated using the manufacturer's recommended procedure (Takara 2013a). Briefly, the difference in the Ct values for the *ND1/SLCO2B1* pair and *ND5/SERPINA1*was calculated separately). The $2^{\Delta Ct}$ for ΔCt1 and ΔCt2 were calculated. The mean of the two $2^{\Delta Ct}$ value was used as mitochondrial content for each DCVC exposure (Takara 2013a; Takara 2013b).

Measurement of mitochondrial membrane potential

To measure relative mitochondrial membrane potential, HTR-8/SVneo cells were seeded at a density of 20,000 cells in each well in a black, clear-bottomed plate and allowed to adhere for 24 h. After acclimation, cells were treated with medium alone (control), DCVC (5, 10, and 20 μM), or 10 μM FCCP (positive control) in quintuplicate for 3, 6, 9 or 12 h. Relative changes in the mitochondrial membrane potential were measured using the TMRE Mitochondrial Membrane Potential Assay Kit (Cayman Chemical). Because the fluorochrome tetramethylrhodamine ethyl ester (TMRE) selectively accumulates in mitochondria with normal polarized membrane potentials, the number of healthy mitochondria is proportional to TMRE fluorescence intensity (Crowley et al. 2016). The assay was performed using the manufacturer's recommended protocol with some modification, as follows. Cells were loaded with the fluorochrome by incubation with 125 nM TMRE diluted in Hank's Balanced Salt Solution (HBSS) (Thermo Fisher Scientific) at room temperature for 15 minutes followed by incubation at 37ºC for 30 minutes. Following incubation, cells were washed 3 times with HBSS and left to equilibrate to room temperature for 15 minutes. TMRE fluorescence intensity (excitation/emission=530/580 nm) was measured using a SpectraMax M2e Multi-Mode Microplate Reader (Molecular Devices). Three independent experiments were performed for each time point.

Visualization of changes in mitochondrial membrane potential

Fluorescence microscopy was used to visualize the effect of DCVC on relative mitochondrial membrane potential. HTR-8/SVneo cells were seeded at a density of 400,000 cells

per well in a 6-well clear bottom plate and allowed to adhere for 24 h. Cells were then treated with medium alone (control) or DCVC (10 or 20 μM) for 12 h. Cells were loaded with TMRE as previously described. Additionally, cellular nuclei were stained with Hoechst dye (Thermo Fisher Scientific). Cells were viewed and images were captured using an EVOS FL digital inverted fluorescence microscope (Thermo Fisher Scientific). TMRE fluorescence was visualized in the RFP fluorescence channel and Hoechst stain was visualized in the DAPI fluorescence channel. Photo images were then merged to create final images using EVOS FL software.

Treatment with (±)-α-tocopherol to assess modulation of DCVC-induced changes in mitochondrial function

The ability of (±)-α-tocopherol to attenuate DCVC-induced perturbation of mitochondrial bioenergetics and mitochondrial membrane potential were measured using the Seahorse XF Analyzer and TMRE fluorescence, respectively. For the Seahorse XF Analyzer experiment, cells were seeded at a density of 50,000 per well in Seahorse XF24 analyzer 24-well plate. For the TMRE fluorescence experiment, cells were seeded at a density of 20,000 cells per well in a 96-well black, clear-bottom plate and allowed to adhere for 24 h. To initiate treatment, cells were incubated for 15 min with 50 μM (±)-α-tocopherol, a concentration previously demonstrated to attenuate DCVC-stimulated caspase 3+7 activity in HTR-8/SVneo cells (Elkin et al. 2018). Then, cells were treated with 0.001% DMSO (solvent control for α-tocopherol), (±)-α-tocopherol (50 μM), DCVC (20 μM), or DCVC (20 μM) plus (±)-α-tocopherol (50 μM). After 12 h exposure, mitochondrial bioenergetics was measured with the Seahorse XF Analyzer and

membrane potential depolarization was measured by TMRE fluorescence intensity, as previously described.

Statistical Analysis

All experiments were performed independently and repeated three to four times. When applicable, technical replicates were averaged within each experiment, and these values were analyzed using two-way analysis of variance (ANOVA), or adjusted linear mixed-models followed by Tukey's post-hoc test for comparison of means. Two-way ANOVA analysis followed by Tukey's post-hoc comparison of means were performed with GraphPad Prism software version 7 (GraphPad Software Inc., San Diego, CA, USA). Adjusted linear mixed-models with posthoc Tukey multiple comparisons were performed with SPSS software version 22 (IBM, Armonk, New York, USA). Data are expressed as means ± SEM. N=number of independent experiments. $P < 0.05$ was considered statistically significant in all experiments.

Results

DCVC effects on cellular bioenergetics and mitochondrial function

Because DCVC decreases mitochondrial respiration in human and rat renal proximal tubular cells (Lash and Anders 1987; Lash et al. 2001; Lash et al. 2003; Xu et al. 2008), the Seahorse XF Analyzer was used to assess mitochondrial OCR perturbations in HTR-8/SVneo cells (Figs. 4.1) (AgilentSeahorse 2017; Divakaruni et al. 2014). Concomitantly, the instrument also assessed DCVC-induced changes in the extracellular acidification rate. The continuous ECAR and OCR profiles measured following treatment with medium alone (control) or 10-20 μM DCVC for 6 and 12 h are displayed in figures 4.1A and 4.1C, respectively.

Extracellular acidification rate

DCVC-induced changes in the basal ECAR were detected after 6 and 12 h of exposure (Fig. 4.1B). After 6 h of exposure, basal ECAR measurements significantly increased 26% and 63% with 10 and 20 μM DCVC, respectively, compared to time-matched controls (Fig 4.1Bi; $P<0.05$). In contrast, DCVC significantly increased basal ECAR by 37% only after 12 h of exposure to 20 μM DCVC (Fig 4.1Bi; $P=0.01$). In addition, no significant effects were observed in ECAR measured in real-time for the first 90 minutes post-DCVC treatment. These results show that DCVC exposure for 6 or 12 h disrupted the basal ECAR, which likely reflects fluctuations in intracellular pH, however imme zdiate DCVC-treatment did not affect the ECAR in placental cells. Although not directly caused by mitochondrial perturbations, changes in ECAR may be indirectly connected to declining mitochondrial dysfunction.

Mitochondrial oxygen consumption rate

Concurrent with ECAR, treatment with 10 and 20 μM DCVC for 6 or 12 h significantly altered multiple OCR parameters after one or both time points (Fig. 4.1D). Basal OCR increased 38% with 20 μM DCVC after 6 h (Fig. 4.1Di; $P=0.025$), but the opposite effect – decreased basal OCR by 57% – was observed after 12 h of DCVC exposure, compared to time-matched controls (Fig. 4.1Di; $P=0.025$). Although the maximum OCR was not impacted by DCVC treatment after 6 h, it decreased after 12 h by 45% and 64% with 10 μM and 20 μM DCVC treatment, respectively, compared to time-matched controls (Fig. 4.1Dii; $P<0.0001$). On the other hand, reserve OCR declined significantly at both time points: 72% with 20 μM after 6 h ($P=0.009$), and 55% and 73% with 10 μM or 20 μM DCVC treatment, respectively, after 12 h ($P<0.0001$), compared to time-matched controls (Fig. 4.1Diii). Proton leak OCR was significantly elevated

60% with 10 and 20 µM DCVC treatment for 6 h (P<0.0001), however, it was only elevated 32% with 10 µM DCVC treatment following 12 h of exposure (P=0.02), compared to time-matched controls (Fig. 4.1Div). Despite no change in the ATP-linked OCR after 6 h of DCVC exposure, the rate declined significantly 42% and 82% with 10 and 20 µM DCVC, respectively, after 12 h of exposure, compared to time-matched controls (Fig. 4.1Dv; P<0.002). Lastly, ATP coupling efficiency decreased significantly by 40% and 48% with 10 and 20 µM DCVC treatment, respectively, after 6 h of exposure (P<0.0001), and by 24% and 58% with 10 and 20 µM DCVC treatment, respectively, after 12 h of exposure (P<0.002), compared to time-matched controls (Fig. 4.1Dvi). The non-mitochondrial OCR was not was not significantly affect by DCVC treatment at either time point (Fig A.4). In addition, no significant effects were observed in OCAR measured in real-time for the first 90 minutes post- DCVC treatment. (Fig. A.3). These results indicate that DCVC exposure between 6 and 12 h caused progressive changes to multiple key mitochondrial OCR parameters, however immediate DCVC-treatment did not significantly affect the OCR in placental cells.

Effect of DCVC on mitochondrial DNA content

Because the mitochondria are primary targets that mediate DCVC-induced cytotoxicity in multiple cells types (Lash and Anders 1986), mitochondrial DNA content was measured as a proxy for mitochondrial copy number. Exposure to 20 µM DCVC for 12 h reduced mitochondrial DNA content by 30% compared to time-matched controls (Fig 4.2; P=0.02). There were no significant differences in the mitochondrial DNA content with 10 µM DCVC at 12 h, nor with 10 and 20 µM DCVC at 6 h, compared to time-matched controls. The results indicate a

modest decline in mitochondrial content that required at least 12 h of exposure to 20 μM DCVC for development.

Effect of DCVC on relative mitochondrial membrane potential

To further assess the impact of DCVC on mitochondrial function, the TMRE fluorochrome was used to examine DCVC-induced changes to mitochondrial membrane potential. DCVC treatment decreased the TMRE fluorescence signal in time- and concentration-dependent manners (ANOVA interaction between DCVC treatments and time, Fig. 4.3A; $P=0.0007$). Treatment with 20 μM DCVC for 12 h stimulated a 64% decline of fluorescence compared to time-matched controls ($P=0.0013$), as well as decreased fluorescence compared to other DCVC concentrations at 12 h ($P<0.002$), and earlier exposure durations with 20 μM DCVC (Fig. 4.3A; $P<0.001$). No other significant DCVC-induced changes in mitochondrial membrane potential were detected. Fluorescence microscopy with TMRE and Hoechst nuclear stain provided visual confirmation of these results (Fig. 4.3Bi-iii). These results demonstrate that the mitochondrial membrane remained polarized for at least 9 h during exposure to 20 μM DCVC, with depolarization onset between 9 and 12 h post-exposure. These results suggest an exposure duration threshold of 12 h for 20 μM DCVC-induced mitochondrial membrane depolarization.

Effect of antioxidant co-treatment on relative mitochondrial membrane potential depolarization and decline in oxygen consumption rate

Due to evidence of reactive oxygen species and lipid peroxidation involvement in the toxicological mechanism for DCVC-mediated toxicity in placental and kidney cells (Beuter et al.

1989; Chen et al. 1990; Elkin et al. 2018; Groves et al. 1991; Hassan et al. 2016), the role of lipid peroxidation in DCVC-induced mitochondrial perturbations was evaluated by including treatment with (±)α-tocopherol, an antioxidant that blocks lipid peroxidation. Co-treatment with 50 μM (±)α-tocopherol significantly rescued mitochondrial membrane depolarization caused by 20 μM DCVC exposure for 12 h (Fig 4.4A; $P < 0.001$). However, (±)α-tocopherol co-treatment did not attenuate the DCVC-induced decreases in basal OCR, ATP-linked OCR, maximum OCR and ATP coupling efficiency (Figs. 4.4Bi-iv). These results indicate that lipid-peroxidation mediates DCVC-induced depolarization of the mitochondrial membrane potential. However, the inability of (±)α-tocopherol to prevent DCVC-induced decrease in basal OCR suggests that DCVC-induced lipid peroxidation does not initially cause mitochondrial dysfunction but rather results from it.

Discussion

Several contemporary studies report associations between maternal TCE exposure and increased risk of adverse birth outcomes (Forand et al. 2012; Ruckart et al. 2014). Additionally, our laboratory reported pregnancy-related TCE toxicity in Wistar rats with impacts on the placenta (Loch-Caruso et al. 2018). Still, the mechanism of TCE-mediated toxicity in pregnancy remains poorly characterized. In order to elucidate potential TCE toxicological mechanisms during early pregnancy, we examined the effects of the TCE glutathione conjugation-derived metabolite S-(1, 2-dichlorovinyl)-L-cysteine (DCVC) on placental cells *in vitro*. In the present study, assessment of mitochondrial bioenergetics using the Seahorse XF Analyzer revealed that treatment with 10-20 μM DCVC for as little as 6 h caused multiple OCR and ECAR perturbations in HTR-8/SVneo cells. This study provides evidence that exposure to DCVC

caused progressive mitochondrial dysfunction resulting in lipid peroxidation-associated mitochondrial membrane depolarization in placental cells.

The assessment of mitochondrial bioenergetics in HTR-8/SVneo cells using the Seahorse XF Analyzer revealed that treatment with 20 μM DCVC for 6 h significantly elevated the basal OCR compared to controls, whereas the same DCVC concentration had the opposite effect – depressing basal OCR after 12 h of exposure. Because 20 μM DCVC treatment is not cytolethal after 6 or 12 h (Chapters 2 and 3) yet apoptotic caspase activity increases (Chapter 2), these results may reflect an initial adaption process that transitions to a pathological process after 12 h of DCVC exposure. To our knowledge, this is the first report of DCVC-stimulated OCR elevation in any cell type. Prior studies with renal proximal tubular cells reported DCVC-induced decreases in mitochondrial OCR, much sooner than our initial time point of 6 hour: 15 minutes with 1 mM DCVC (Lash and Anders 1986) and 1 h with 10 μM DCVC (Xu et al. 2008). The different findings in renal proximal tubular cells suggest that HTR-8/SVneo cells are more resilient than kidney cells to basal OCR perturbations. Regardless, our results indicate that DCVC disrupted mitochondrial basal OCR in HTR-8/SVneo cells, contributing novel evidence of mitochondrial involvement for DCVC-induced placental cell dysfunction.

Our bioenergetics assessment further revealed for the first time that DCVC compromised cellular bioenergetic capacity. Following 6 h of DCVC exposure, unchanged maximum OCR, elevated basal OCR and resulting diminished reserve OCR revealed that the HTR-8/SVneo cells were operating closer to their bioenergetic limit compared to non-treated cells. The maximum OCR reflects the top achievable mitochondrial respiration rate (Pereira et al. 2014), whereas spare OCR describes the cells' ability to adaptively elevate the OCR and subsequent ATP synthesis in response to increased energy demand (Brand and Nicholls 2011). These results

suggest an adaptive process occurring at 6 h, likely due to increased energy demand in response to DCVC exposure. With continuous DCVC exposure for 12 h, decreased basal, maximum and spare OCRs indicate a drop in cellular bioenergetic capacity, suggesting limited mitochondrial-mediated cellular adaptability. Consequently, these results suggest a pathological process developing with 12 h of DCVC treatment. Interestingly, other studies reported diminished spare and/or maximum OCR in pre-eclamptic placental tissue compared to normal tissue (Holland et al. 2018), or in HTR-8/SVneo cells treated with maternal serum from pregnancies complicated with pre-eclampsia compared to normal pregnancies (Sanchez-Aranguren et al. 2018). Taken together, these findings suggest that DCVC may diminish mitochondrial adaptability as a possible mechanism by which TCE exposure promotes placental toxicity.

In addition to mitochondrial bioenergetics, we demonstrated that 20 μM DCVC depolarized the mitochondrial membrane after 12 h of exposure, a finding consistent with multiple DCVC toxicity studies in kidney cells across different species (Chen et al. 2001; Lash and Anders 1987; van de Water et al. 1994; Xu et al. 2008). The mitochondrial membrane potential is maintained by proton pumping which generates a proton gradient that drives ATP production, thereby coupling proton pumping and ATP production (Zorova et al. 2018). Because a 6-h exposure to DCVC increased mitochondrial proton leak, the flow of protons back into the matrix independent of ATP production, and decreased ATP coupling efficiency, yet mitochondrial membrane depolarization did not occur until after 12 h of exposure, elevated proton leak and ATP uncoupling preceded mitochondrial membrane depolarization (Divakaruni and Brand 2011). Indeed, as demonstrated here, evidence supports mitochondrial membrane depolarization as a later event in the sequence of progressive mitochondrial injury (Heiskanen et al. 1999). Because mitochondrial membrane depolarization was not detected until 12 h-post

DCVC exposure, the data support the theory of an adaptive process occurring at 6 h with a subsequent pathological process developing and manifest at 12 h in HTR-8/SVneo cells. This finding not only demonstrates the central role of the mitochondria in DCVC-induced placental cytotoxicity, it also aids in elucidating the specific sequence of events comprising DCVC-induced adaptability and subsequent pathogenesis of mitochondrial injury.

Consistent with our previous study indicating a potential role for lipid peroxidation in DCVC-induced cytotoxicity (Elkin et al. 2018)we demonstrated that the peroxyl radical scavenger (±)-α-tocopherol, which blocks lipid peroxidation, attenuated DCVC-induced mitochondrial membrane depolarization at 12 h of exposure to 20 μM DCVC. Moreover, we observed that 12-h (±)α-tocopherol co-treatment failed to rescue DCVC-induced decreases in basal OCR, ATP-linked OCR, maximum OCR and ATP coupling efficiency. Our results agree with previous evidence of ROS-associated mitochondrial membrane depolarization following DCVC treatment in rat proximal tubular cells (van de Water et al. 1994). Lipid peroxidation, the production of lipid peroxyl radicals resulting from oxidation of lipid molecules by ROS species, damages lipid membranes within the cell and is capable of stimulating mitochondrial membrane depolarization (Ayala et al. 2014; Stark 2005). The findings reported here suggest that DCVC-stimulated mitochondrial membrane depolarization may be dependent on lipid peroxidation, likely resulting from ROS generation. Concomitantly, the inability of (±)α-tocopherol to prevent DCVC-induced decrease in basal OCR suggests that DCVC-induced lipid peroxidation does not appear to initiate mitochondrial OCR perturbations but, rather, results from them. Together, these results suggest that mitochondria may serve as both a source and target of ROS generation in DCVC-induced cytotoxicity, a phenomenon termed “ROS-induced ROS release” (Zorov et al. 2000; Zorov et al. 2014). Collectively, these findings contribute evidence to the sequence of

DCVC-induced mitochondrial pathogenesis following acute exposure and suggest the involvement of lipid peroxidation in the mechanism of DCVC toxicity.

Additionally, DCVC treatment for 12 h reduced mitochondrial DNA content in placental HTR-8/SVneo cells. To our knowledge, no other studies have reported a similar findings related to DCVC toxicity, despite extensive evidence of mitochondrial involvement in DCVC-mediated toxicity in other cell types. However, studies have shown a relationship between mitochondrial DNA content and placental impairment (Holland et al. 2017). Mitochondrial DNA content was found to be decreased in placental tissue (Poidatz et al. 2015) and cytotrophoblasts (Mando et al. 2014) isolated from pregnancies complicated with intrauterine growth restriction compared to normal pregnancies. Similarly, mitochondrial DNA content was decreased in placenta from pregnancies with small for gestational age infants (Diaz et al. 2014). In contrast, other studies reported higher mitochondrial DNA content in placenta from intrauterine growth restricted-pregnancies (Lattuada et al. 2008; Mando et al. 2014). Nevertheless, the weight of evidence supports a role for altered placental mitochondrial DNA content in pregnancy disorders with placental dysfunction, despite the need for further clarification. Consequently our finding contributes to evidence of mitochondrial involvement in DCVC-induced placental disruption.

In the current study, we observed an increase in extracellular acidification with both 6 and 12 h of DCVC exposure, likely indicating intracellular pH fluctuations. Although not directly caused by mitochondrial perturbations, ECAR alterations may be indirectly related to mitochondrial function through changes in cellular energy metabolism. For example, elevated amino acid flux may increase extracellular acidification. Indeed, we previously reported that DCVC treatment for 6 and 12 h caused a compensatory increase of intracellular concentrations of energy-relevant amino acids, likely used for energy metabolism as alternative biofuel for ATP production (Chapter 3). Additionally, lactate build-up may also explain our observed elevated ECAR. We previously reported lactate concentrations 6-h post

DCVC-treatment associated with increased glycolytic activity (Chapter 3). Although not directly investigated, ECAR perturbations may be a secondary effect of changes in energy metabolism and related mitochondrial functioning. We used DCVC concentrations relevant to potential human exposure levels in the workplace. The U.S. Occupational Safety and Health Administration Permissible Exposure Limit (PEL) is 100 ppm averaged over an 8-hour work day (ATSDR 2016). Female volunteers exposed to the PEL of TCE for 4 h by inhalation had an average peak blood concentration of 13.4 μM *S*-(1,2-dichlorovinyl) glutathione, the metabolic precursor to DCVC (Lash et al. 1999). This peak blood concentration is encompassed within the range of concentrations used in our study of 5-20 μM DCVC. Moreover, another study detected TCE concentrations up to 229 ppm, more than twice the PEL, in 80 exposed workers (29% women) wearing personal aerosolized monitoring devices (Walker et al. 2016). Lastly, the DCVC concentrations that caused mitochondrial perturbations in our study are substantially lower than those used in other *in vitro* toxicity studies which used concentrations as high as 1 mM DCVC (Chen et al. 2001; Lash et al. 2001; Lash et al. 2003; van de Water et al. 1995; Xu et al. 2008). Thus, our study contributes valuable evidence of the effects of plausible DCVC concentrations in human placental cells and possibly other cell types.

The present study used HTR-8/SVneo cells, an immortalized extravillous trophoblast cell line. These cells are easily available in contrast to first-trimester placental cells isolated from fresh placental tissue. Moreover, these cells express a combination of molecular markers that are unique to extravillous trophoblasts such as cytokeratin 7 (CK7), and histocompatibility antigen, class I, G (HLA-G) (when grown on Matrigel) (Irving et al. 1995; Khan et al. 2011; Kilburn et al. 2000; Takao et al. 2011). Additionally, these cells maintain many functional characteristics of extravillous trophoblasts (Hannan et al. 2010; Kilburn et al. 2000; Liu et al. 2016; Szklanna et al. 2017). On the other hand, although originally derived from first-trimester non-cancerous

placental tissue, the immortalization processes alters the cells to allow them to grow in culture for an extended time (Graham et al. 1993). Furthermore, *in vitro* cell culture conditions may contribute to genetic and epigenetic differences observed between HTR-8/SVneo cells and freshly isolated extravillous trophoblasts (Bilban et al. 2010; Novakovic et al. 2011). Overall, our *in vitro* experiments do not reflect the complicated *in vivo* dynamics within the fetal-uteroplacental unit, and further studies in primary first-trimester extravillous trophoblasts, villous explants and other models are needed to confirm our results.

In summary, we present evidence detailing a partial sequence of events leading to DCVC-induced adaptive and subsequently pathogenic changes in the mitochondria of HTR-8/SVneo cells (fig. 4.5). The evidence suggests that DCVC caused progressive mitochondrial OCR perturbations resulting in lipid peroxidation-associated mitochondrial membrane depolarization. To our knowledge, our study is the first to report that DCVC induced mitochondrial effects on placental cells. Our findings contribute to the biological plausibility of DCVC-induced placental toxicity, indicating that further studies into the effect of DCVC on placental cells are warranted.

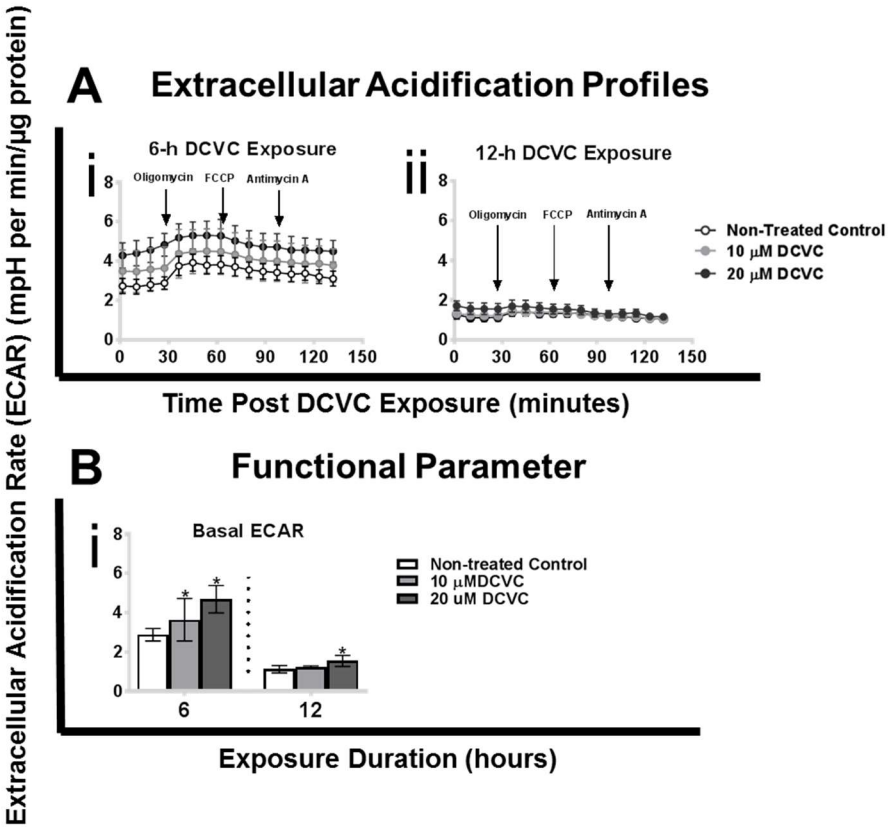
A
Extracellular Acidification Profiles
i
6-h DCVC Exposure
Oligomycin
FCCP
Antimycin A
ii
12-h DCVC Exposure
Non-Treated Control
10 μM DCVC
20 μM DCVC
Extracellular Acidification Rate (ECAR) (mpH per min/μg protein)
Time Post DCVC Exposure (minutes)
B
Functional Parameter
Basal ECAR
Non-treated Control
10 μMDCVC
20 uM DCVC
Exposure Duration (hours)

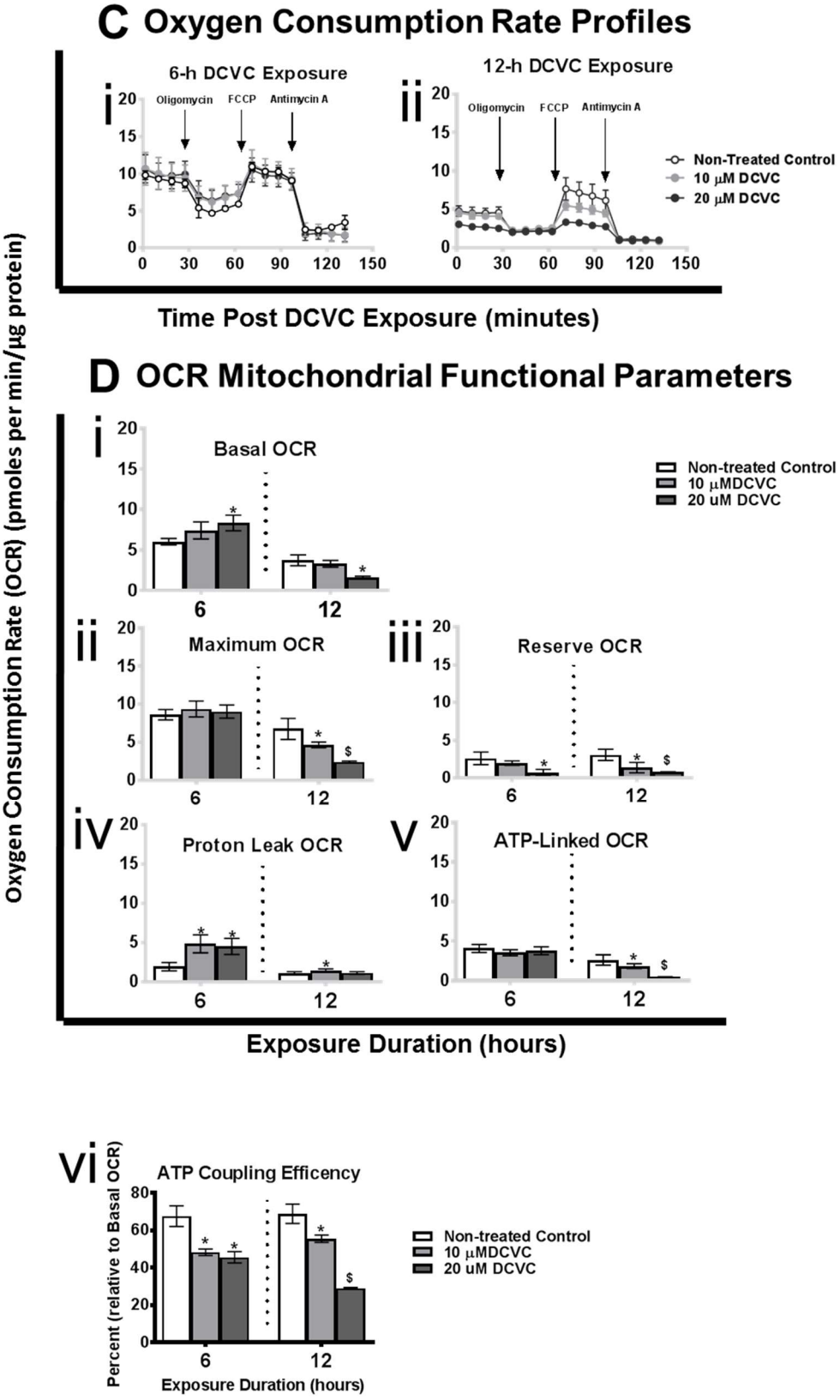
C Oxygen Consumption Rate Profiles
6-h DCVC Exposure
12-h DCVC Exposure
Oligomycin
FCCP
Antimycin A
Non-Treated Control
10 μM DCVC
20 μM DCVC
Time Post DCVC Exposure (minutes)
D OCR Mitochondrial Functional Parameters
Basal OCR
Maximum OCR
Reserve OCR
Proton Leak OCR
ATP-Linked OCR
Non-treated Control
10 μMDCVC
20 uM DCVC
Oxygen Consumption Rate (OCR) (pmoles per min/μg protein)
Exposure Duration (hours)
ATP Coupling Efficency
Percent (relative to Basal OCR)
Exposure Duration (hours)

Figure 4.1. Effects of DCVC on extracellular acidification rate (ECAR), oxygen consumption rate (OCR) and mitochondrial functional parameters.
Cells were treated for 6 or 12 h with medium alone (control), or with 10 or 20 μM DCVC. Following exposure, ECAR and OCR were measured simultaneously in real-time using the Seahorse XF24e or XF24 analyzers. Key mitochondrial functional parameters were assessed by serially injecting compounds that target specific portions of the electron transport chain (oligomycin, FCCP, antimycin A/rotenone) into wells with the cells. Mitochondrial functional parameters were measured or calculated as described in the methods section. **A)** Extracellular acidification rate ECAR profiles following DCVC treatment for **(i)** 6 h and **(ii)** 12 h. Data points represent mean ECAR ± SEM at 5-minute intervals. **B)** ECAR functional parameters: **(i)** basal ECAR, and **(ii)** reserve ECAR. **C)** Oxygen consumption rate profiles following DCVC treatment for **(i)** 6 h and **(ii)** 12 h. Data are graphed as mean OCRs ± SEM at 5-minute intervals. Arrows indicate times when electron transport chain modifiers were injected into sample wells. **D)** OCR functional parameters: **(i)** basal OCR, **(ii)** maximum OCR, **(iii)** ATP-linked OCR, **(iv)** reserve OCR, **(v)** proton leak OCR and **(vi)** ATP coupling efficiency. Bars represent means ± SEM. Data were analyzed by adjusted linear mixed-models with posthoc Tukey multiple comparisons restricted to comparison within each time point because experiments were conducted separately (as indicated by vertical dashed line on graph). Asterisk indicates significant difference compared to controls within same time point: $^{*}P<0.05$. Dollar sign indicates significant difference compared to controls and 10 μM DCVC within same time point: $^{\$}P<0.05$. N= 3 independent experiments for each time point, with 3-5 replicates per treatment in each experiment.

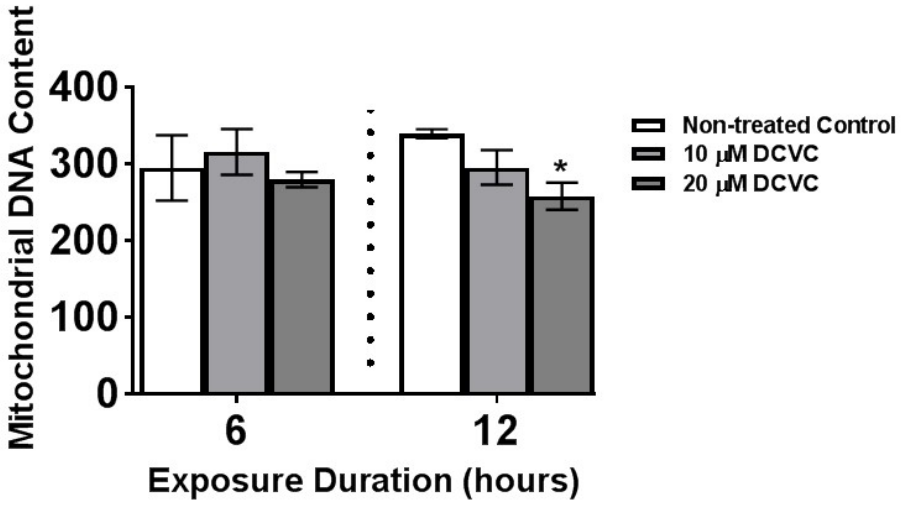

Figure 4.2. Effects of DCVC mitochondrial DNA content.
Cells were treated for 6 or 12 h with medium alone (control), or with 10 or 20 μM DCVC. Mitochondrial DNA content, a proxy for mitochondrial copy number, was estimated by measuring genomic DNA of two mitochondrial genes and two nuclear genes, and calculating the ratios: *ND1/SLCO2B1* and *ND5/SERPINA1*. Bars represent means ± SEM. Data were analyzed by one-way ANOVA with posthoc Tukey's multiple comparisons within each time point because experiments were conducted separately (as indicated by vertical dashed line on graph). Asterisk indicates significant difference compared to control within the same time point: $^{*}P \leq 0.0192$. N=3 independent experiments for 6 h time point and N=4 independent experiments for 12 h time point. Gene expression was measured in duplicate by qRT-PCR.

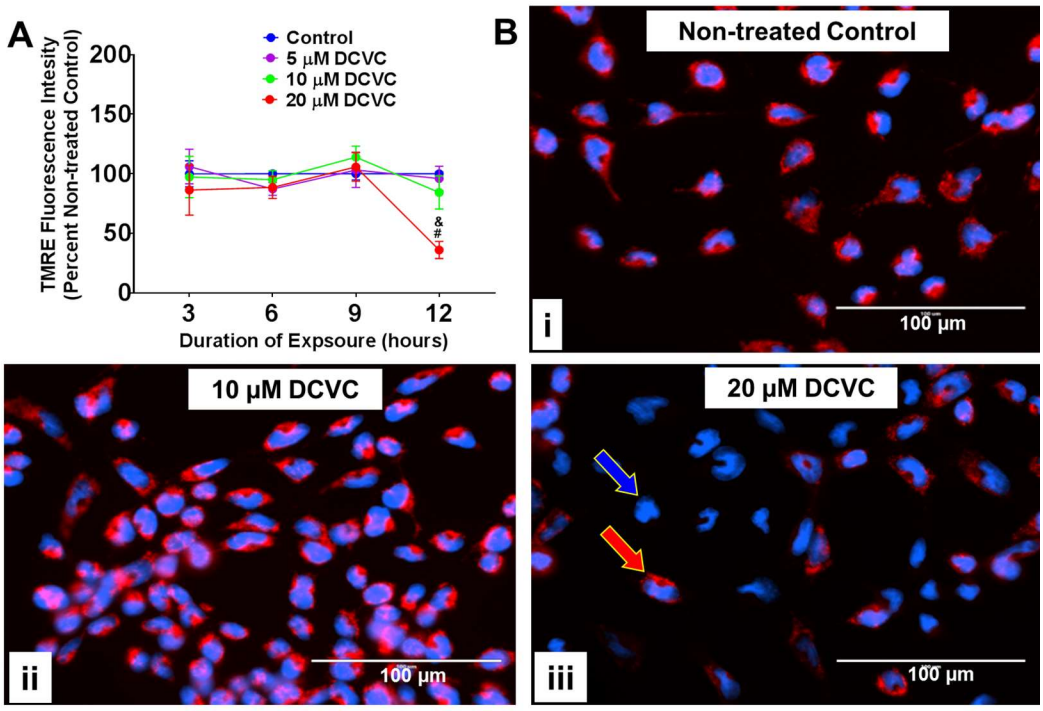

Figure 4.3. Effects of DCVC mitochondrial membrane potential.
A) Graphical representation of mitochondrial membrane potential expressed as percent non-treated control. Cells were treated for 3, 6, 9 or 12 h with medium alone (control), or with 5, 10, or 20 µM DCVC. Tetramethylrhodamine ethyl ester (TMRE), a cell-permanent fluorochrome, was used to measure relative mitochondrial membrane potential. The fluorescence signal is proportional to mitochondrial membrane polarization. N= 3 independent experiments for each time point, with 4 replicates per treatment in each experiment. Data are graphed as means ± SEM. Data were analyzed by two-way ANOVA (interaction between time and treatment, P=0.0007) with posthoc Tukey multiple comparisons. Ampersand sign indicates significant difference compared to control, 5 µM DCVC and 10 µM DCVC within the same time point: $^{\&}P$ =0.0013. Pound sign indicates significant difference compared to same treatment at all earlier time points: $^{\#}P < 0.001$. FCCP (10 µM) was included as a positive control and depolarized the mitochondrial membrane potential by 16.45% ± 4.19% at 3 h, 18.9% ± 4.16% at 6 h, 24.13% ± 7.89% at 9 h, and 8.78% ± 8.78% at 12 h. **B)** Visualization of DCVC-induced depolarization of mitochondrial membrane potential by fluorescence microscopy. Cells were treated for 12 hours with **(i)** 0 µM DCVC, **(ii)** 10 µM DCVC or **(iii)** 20 µM DCVC. Red fluorescence (TMRE) represents normal mitochondrial membrane potential (red arrow). Blue fluorescence (Hoechst stain) represents cellular nuclei (blue arrow). All images shown with 100 µm scale bars. Representative images from 3 experiments are shown.

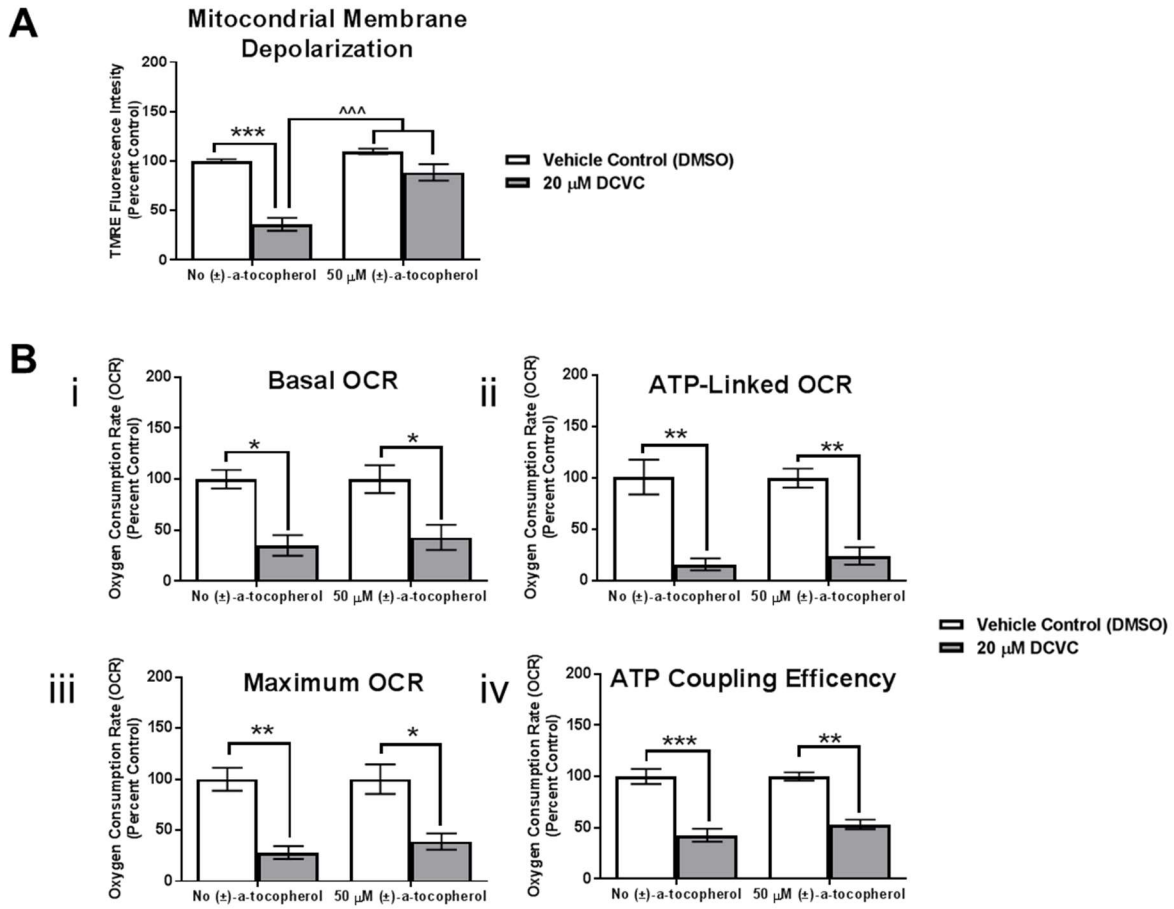

Figure 4.4. Effect of antioxidant co-treatment on DCVC-induced changes in membrane potential depolarization and OCR.
Cells were treated with DMSO (vehicle control for α-tocopherol) or 20 μM DCVC with or without 50 μM (±) α-tocopherol (pre-treatment for 15 min followed by co-treatment for 12 h). **A)** Modulation of DCVC-induced relative mitochondrial membrane potential depolarization as measured using TMRE fluorescence. **B)** Failed modulation of DCVC-induced OCR perturbations as measured by the Seahorse XF analyzer including: **(i)** basal OCR, **(ii)** ATP-linked OCR, **(iii)** maximum OCR, and **(iv)** ATP coupling efficiency. Bars represent means ± SEM as percent control. Data were analyzed by two-way ANOVA prior to percent control conversion (attenuation of membrane potential depolarization had interaction between DCVC and (±) α-tocopherol treatments, P= 0.0052; no other significant interaction calculated), followed by Tukey's multiple comparison of means. Asterisk indicates significant differences compared to vehicle control with no (±) α-tocopherol treatment or vehicle control with (±) α-tocopherol treatment: $^{*}P \leq 0.016$, $^{**}P \leq 0.0043$, $^{***}P = 0.005$. Circumflex accent sign indicates significant difference compared to 20 μM DCVC with no (±) α-tocopherol treatment: $^{\wedge\wedge\wedge}P \leq 0.0007$. N= 3 independent experiments, with 4 replicates per treatment in each experiment.

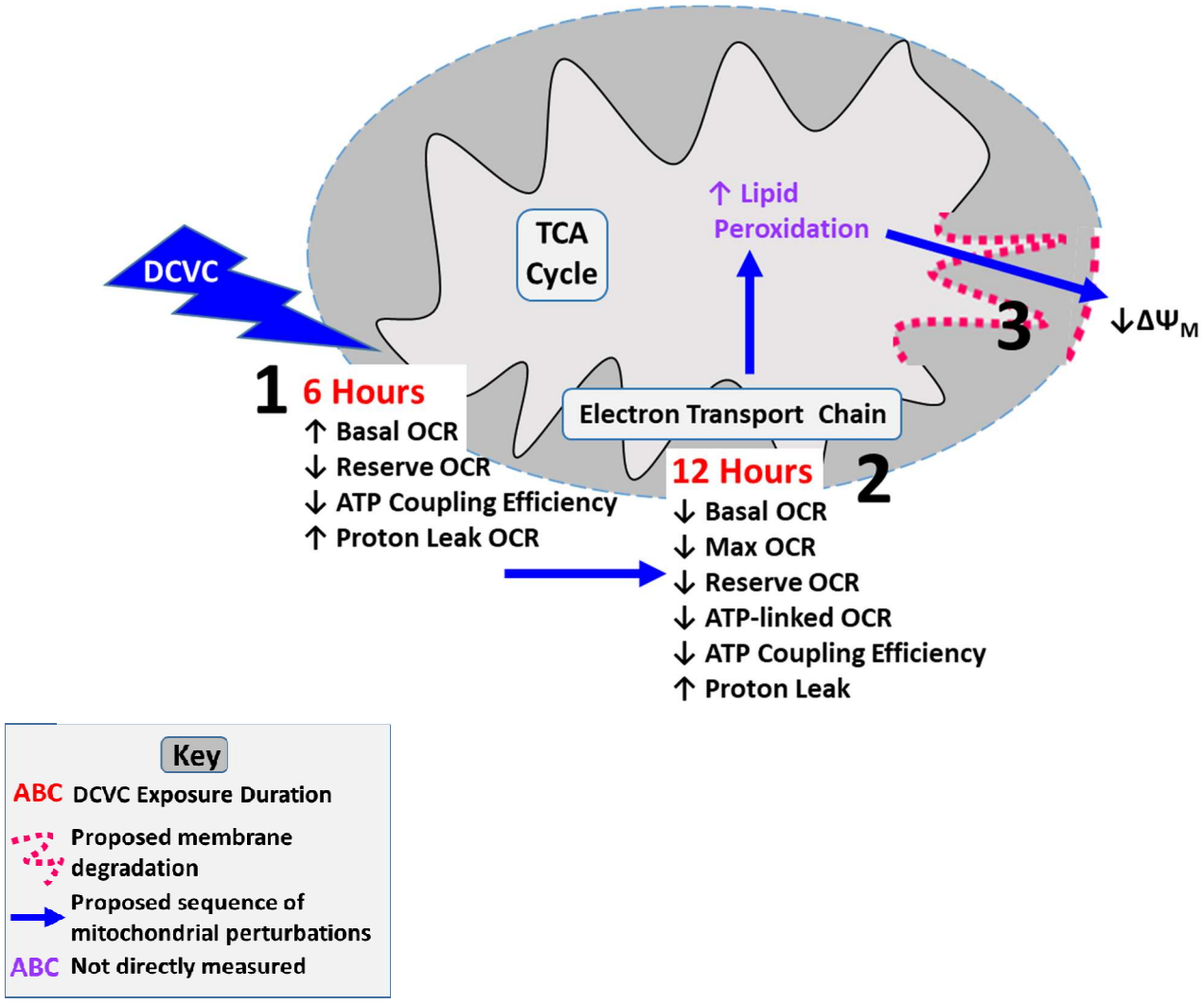

Figure 4.5. Proposed DCVC-induced mitochondrial dysfunction in HTR-8/SVneo cells. **A)** Overview and proposed partial sequence of DCVC-induced perturbations impacting mitochondrial structure and function**.** **1)** At 6 h, mitochondrial basal OCR, reserve OCR and proton leak rate were elevated, while ATP coupling efficiency dropped significantly. **2)** At 12 h, basal OCR declined significantly, accompanied by diminished maximum and reserve OCR, reduced ATP-linked OCR and decreased coupling efficiency, suggesting time-dependent progressive mitochondrial dysfunction. **3)** Between 9 and 12 h, lipid peroxidation contributed to depolarization of mitochondrial membrane potential, however it did not contribute to other oxygen consumption-related mitochondrial perturbations, indicating lipid peroxidation may be a secondary effect of mitochondrial dysfunction.

References

Abdraboh M.E., Abdeen S.H., Salama M., El-Husseiny M., El-Sherbini Y.M., Eldeen N.M. 2018. Developmental neurotoxic effects of a low dose of tce on a 3-d neurosphere system. *Biochem Cell Biol.* **96**:50-56.

AgilentSeahorse. 2016. Multi-file xf report generator user guide. Vol. 103312-400 Rev E, Part Revision E (Seahorse A, ed). United States:Agilent Seahorse.

AgilentSeahorse. 2017. Seahorse xf cell mito stress test kit user guide. Part E0:Agilent Technologies.

ATCC. 2015. Atcc product sheet: Htr8/svneo (atcc® crl3271™).American Type Culture Collection.

ATSDR. 2016. Public health statement on trichloroethylene.Agency for Toxic Substances and Disease Registry.

ATSDR. 2017. 2017 substance priority list.U.S. Agency for Toxic Substances and Disease Registry.

Ayala A., Munoz M.F., Arguelles S. 2014. Lipid peroxidation: Production, metabolism, and signaling mechanisms of malondialdehyde and 4-hydroxy-2-nonenal. *Oxid Med Cell Longev.* **2014**:360438.

Bassig B.A., Zhang L., Tang X., Vermeulen R., Shen M., Smith M.T., et al. 2013. Occupational exposure to trichloroethylene and serum concentrations of il-6, il-10, and tnf-alpha. *Environ Mol Mutagen.* **54**:450-454.

Beuter W., Cojocel C., Muller W., Donaubauer H.H., Mayer D. 1989. Peroxidative damage and nephrotoxicity of dichlorovinylcysteine in mice. *J Appl Toxicol.* **9**:181-186.

Bilban M., Tauber S., Haslinger P., Pollheimer J., Saleh L., Pehamberger H., et al. 2010. Trophoblast invasion: Assessment of cellular models using gene expression signatures. *Placenta.* **31**:989-996.

Brand M.D., Nicholls D.G. 2011. Assessing mitochondrial dysfunction in cells. *The Biochemical journal.* **435**:297-312.

Burton G.J., Fowden A.L. 2015. The placenta: A multifaceted, transient organ. *Philos Trans R Soc Lond B Biol Sci.* **370**:20140066.

Chen Q., Jones T.W., Brown P.C., Stevens J.L. 1990. The mechanism of cysteine conjugate cytotoxicity in renal epithelial cells. Covalent binding leads to thiol depletion and lipid peroxidation. *J Biol Chem.* **265**:21603-21611.

Chen Y., Cai J., Anders M.W., Stevens J.L., Jones D.P. 2001. Role of mitochondrial dysfunction in s-(1,2-dichlorovinyl)-l-cysteine-induced apoptosis. *Toxicol Appl Pharmacol.* **170**:172-180.

Chiu W.A., Jinot J., Scott C.S., Makris S.L., Cooper G.S., Dzubow R.C., et al. 2013. Human health effects of trichloroethylene: Key findings and scientific issues. *Environ Health Perspect.* **121**:303-311.

Christensen K.Y., Vizcaya D., Richardson H., Lavoue J., Aronson K., Siemiatycki J. 2013. Risk of selected cancers due to occupational exposure to chlorinated solvents in a case-control study in montreal. *J Occup Environ Med.* **55**:198-208.

Crowley L.C., Christensen M.E., Waterhouse N.J. 2016. Measuring mitochondrial transmembrane potential by tmre staining. *Cold Spring Harb Protoc.* **2016**.

Darnerud P.O., Brandt I., Feil V.J., Bakke J.E. 1989. Dichlorovinyl cysteine (dcvc) in the mouse kidney: Tissue-binding and toxicity after glutathione depletion and probenecid treatment. *Arch Toxicol.* **63**:345-350.

Davies E.L., Bell J.S., Bhattacharya S. 2016. Preeclampsia and preterm delivery: A population-based case-control study. *Hypertens Pregnancy.* **35**:510-519.

Diaz M., Aragones G., Sanchez-Infantes D., Bassols J., Perez-Cruz M., de Zegher F., et al. 2014. Mitochondrial DNA in placenta: Associations with fetal growth and superoxide dismutase activity. *Horm Res Paediatr.* **82**:303-309.

Divakaruni A.S., Brand M.D. 2011. The regulation and physiology of mitochondrial proton leak. *Physiology (Bethesda).* **26**:192-205.

Divakaruni A.S., Paradyse A., Ferrick D.A., Murphy A.N., Jastroch M. 2014. Analysis and interpretation of microplate-based oxygen consumption and ph data. *Methods Enzymol.* **547**:309-354.

Elkin E.R., Harris S.M., Loch-Caruso R. 2018. Trichloroethylene metabolite s-(1,2-dichlorovinyl)-l-cysteine induces lipid peroxidation-associated apoptosis via the intrinsic and extrinsic apoptosis pathways in a first-trimester placental cell line. *Toxicol Appl Pharmacol.* **338**:30-42.

EPA. 2018. National priorities list.

Erecinska M., Wilson D.F. 1982. Regulation of cellular energy metabolism. *J Membr Biol.* **70**:1-14.

Fisher G.J., Kelley L.K., Smith C.H. 1987. Atp-dependent calcium transport across basal plasma membranes of human placental trophoblast. *Am J Physiol.* **252**:C38-46.

Forand S.P., Lewis-Michl E.L., Gomez M.I. 2012. Adverse birth outcomes and maternal exposure to trichloroethylene and tetrachloroethylene through soil vapor intrusion in new york state. *Environ Health Perspect.* **120**:616-621.

Forkert P.G., Birch D.W. 1989. Pulmonary toxicity of trichloroethylene in mice. Covalent binding and morphological manifestations. *Drug Metab Dispos.* **17**:106-113.

Forkert P.G., Millen B., Lash L.H., Putt D.A., Ghanayem B.I. 2006. Pulmonary bronchiolar cytotoxicity and formation of dichloroacetyl lysine protein adducts in mice treated with trichloroethylene. *J Pharmacol Exp Ther.* **316**:520-529.

Goodman D.R., James R.C., Harbison R.D. 1982. Placental toxicology. *Food Chem Toxicol.* **20**:123-128.

Graham C.H., Hawley T.S., Hawley R.G., MacDougall J.R., Kerbel R.S., Khoo N., et al. 1993. Establishment and characterization of first trimester human trophoblast cells with extended lifespan. *Experimental cell research.* **206**:204-211.

Groves C.E., Lock E.A., Schnellmann R.G. 1991. Role of lipid peroxidation in renal proximal tubule cell death induced by haloalkene cysteine conjugates. *Toxicol Appl Pharmacol.* **107**:54-62.

Guha N., Loomis D., Grosse Y., Lauby-Secretan B., El Ghissassi F., Bouvard V., et al. 2012. Carcinogenicity of trichloroethylene, tetrachloroethylene, some other chlorinated solvents, and their metabolites. *Lancet Oncol.* **13**:1192-1193.

Hannan N.J., Paiva P., Dimitriadis E., Salamonsen L.A. 2010. Models for study of human embryo implantation: Choice of cell lines? *Biology of reproduction.* **82**:235-245.

Hassan I., Kumar A.M., Park H.R., Lash L.H., Loch-Caruso R. 2016. Reactive oxygen stimulation of interleukin-6 release in the human trophoblast cell line htr-8/svneo by the trichlorethylene metabolite s-(1,2-dichloro)-l-cysteine. *Biology of reproduction.* **95**:66.

Heiskanen K.M., Bhat M.B., Wang H.W., Ma J., Nieminen A.L. 1999. Mitochondrial depolarization accompanies cytochrome c release during apoptosis in pc6 cells. *J Biol Chem.* **274**:5654-5658.

Holland O.J., Cuffe J.S.M., Dekker Nitert M., Callaway L., Kwan Cheung K.A., Radenkovic F., et al. 2018. Placental mitochondrial adaptations in preeclampsia associated with progression to term delivery. *Cell Death Dis.* **9**:1150.

Hosgood H.D., 3rd, Zhang L., Tang X., Vermeulen R., Qiu C., Shen M., et al. 2011. Decreased numbers of cd4(+) naive and effector memory t cells, and cd8(+) naive t cells, are associated with trichloroethylene exposure. *Front Oncol.* **1**:53.

Ilekis J.V., Tsilou E., Fisher S., Abrahams V.M., Soares M.J., Cross J.C., et al. 2016. Placental origins of adverse pregnancy outcomes: Potential molecular targets: An executive workshop summary of the eunice kennedy shriver national institute of child health and human development. *Am J Obstet Gynecol.* **215**:S1-S46.

Irving J.A., Lysiak J.J., Graham C.H., Hearn S., Han V.K., Lala P.K. 1995. Characteristics of trophoblast cells migrating from first trimester chorionic villus explants and propagated in culture. *Placenta.* **16**:413-433.

Khan G.A., Girish G.V., Lala N., Di Guglielmo G.M., Lala P.K. 2011. Decorin is a novel vegfr-2-binding antagonist for the human extravillous trophoblast. *Mol Endocrinol.* **25**:1431-1443.

Kilburn B.A., Wang J., Duniec-Dmuchowski Z.M., Leach R.E., Romero R., Armant D.R. 2000. Extracellular matrix composition and hypoxia regulate the expression of hla-g and integrins in a human trophoblast cell line. *Biology of reproduction.* **62**:739-747.

Lagakos S., Wessen B., Zelen M. 1986. An analysis of contaminated well water and health eff ects in woburn, massachusetts *Journal of the American Statistical Association.* **81**:583-596.

Lager S., Powell T.L. 2012. Regulation of nutrient transport across the placenta. *J Pregnancy.* **2012**:179827.

Laham S. 1970. Studies on placental transfer. Trichlorethylene. *IMS Ind Med Surg.* **39**:46-49.

Lan Q., Zhang L., Tang X., Shen M., Smith M.T., Qiu C., et al. 2010. Occupational exposure to trichloroethylene is associated with a decline in lymphocyte subsets and soluble cd27 and cd30 markers. *Carcinogenesis.* **31**:1592-1596.

Lash L.H., Anders M.W. 1986. Cytotoxicity of s-(1,2-dichlorovinyl)glutathione and s-(1,2-dichlorovinyl)-l-cysteine in isolated rat kidney cells. *J Biol Chem.* **261**:13076-13081.

Lash L.H., Anders M.W. 1987. Mechanism of s-(1,2-dichlorovinyl)-l-cysteine- and s-(1,2-dichlorovinyl)-l-homocysteine-induced renal mitochondrial toxicity. *Molecular pharmacology.* **32**:549-556.

Lash L.H., Putt D.A., Brashear W.T., Abbas R., Parker J.C., Fisher J.W. 1999. Identification of s-(1,2-dichlorovinyl)glutathione in the blood of human volunteers exposed to trichloroethylene. *J Toxicol Environ Health A.* **56**:1-21.

Lash L.H., Parker J.C., Scott C.S. 2000. Modes of action of trichloroethylene for kidney tumorigenesis. *Environ Health Perspect.* **108 Suppl 2**:225-240.

Lash L.H., Hueni S.E., Putt D.A. 2001. Apoptosis, necrosis, and cell proliferation induced by s-(1,2-dichlorovinyl)-l-cysteine in primary cultures of human proximal tubular cells. *Toxicol Appl Pharmacol.* **177**:1-16.

Lash L.H., Putt D.A., Hueni S.E., Krause R.J., Elfarra A.A. 2003. Roles of necrosis, apoptosis, and mitochondrial dysfunction in s-(1,2-dichlorovinyl)-l-cysteine sulfoxide-induced cytotoxicity in primary cultures of human renal proximal tubular cells. *J Pharmacol Exp Ther.* **305**:1163-1172.

Lash L.H., Chiu W.A., Guyton K.Z., Rusyn I. 2014. Trichloroethylene biotransformation and its role in mutagenicity, carcinogenicity and target organ toxicity. *Mutat Res Rev Mutat Res.* **762**:22-36.

Lattuada D., Colleoni F., Martinelli A., Garretto A., Magni R., Radaelli T., et al. 2008. Higher mitochondrial DNA content in human IUGR placenta. *Placenta.* **29**:1029-1033.

Lee H.J., Jeong S.K., Na K., Lee M.J., Lee S.H., Lim J.S., et al. 2013. Comprehensive genome-wide proteomic analysis of human placental tissue for the chromosome-centric human proteome project. *J Proteome Res.* **12**:2458-2466.

Liu L., Wang Y., Shen C., He J., Liu X., Ding Y., et al. 2016. Benzo(a)pyrene inhibits migration and invasion of extravillous trophoblast htr-8/svneo cells via activation of the erk and jnk pathway. *J Appl Toxicol.* **36**:946-955.

Loch-Caruso R., Hassan I., Harris S.M., Kumar A., Bjork F., Lash L.H. 2018. Trichloroethylene exposure in mid-pregnancy decreased fetal weight and increased placental markers of oxidative stress in rats. *Reprod Toxicol.* **83**:38-45.

Mando C., De Palma C., Stampalija T., Anelli G.M., Figus M., Novielli C., et al. 2014. Placental mitochondrial content and function in intrauterine growth restriction and preeclampsia. *American journal of physiology Endocrinology and metabolism.* **306**:E404-413.

McKinney L.L., Picken Jr. J.C., Weakley F.B., Eldridge A.C., Campbell R.E., Cowan J.C., et al. 1959. Possible toxic factor of trichloroethylene-extracted soybean oil meal3. *Journal of the American Chemical Society.* **81**:909-915.

Meyer J.N., Leung M.C., Rooney J.P., Sendoel A., Hengartner M.O., Kisby G.E., et al. 2013. Mitochondria as a target of environmental toxicants. *Toxicol Sci.* **134**:1-17.

Morgan T. 2014. Placental insufficiency is a leading cause of preterm labor. *NewReviews.* **15**:5618-e5525.

Morgan T.K. 2016. Role of the placenta in preterm birth: A review. *Am J Perinatol.* **33**:258-266.

Myllynen P., Pasanen M., Pelkonen O. 2005. Human placenta: A human organ for developmental toxicology research and biomonitoring. *Placenta.* **26**:361-371.

Nicholls D.G. 2002. Mitochondrial function and dysfunction in the cell: Its relevance to aging and aging-related disease. *Int J Biochem Cell Biol.* **34**:1372-1381.

Novakovic B., Gordon L., Wong N.C., Moffett A., Manuelpillai U., Craig J.M., et al. 2011. Wide-ranging DNA methylation differences of primary trophoblast cell populations and derived cell lines: Implications and opportunities for understanding trophoblast function. *Molecular human reproduction.* **17**:344-353.

NTP. 2015. Monograph on trichloroethylene Available: https://ntp.niehs.nih.gov/ntp/roc/monographs/finaltce_508.pdf 2016].

Oshvandi K., Jadidi A., Dehvan F., Shobeiri F., Cheraghi F., Sangestani G., et al. 2018. Relationship between pregnancy-induced hypertension with neonatal and maternal complications. *International Journal of Pediatrics.* **6**:8587-8594.

Pereira L.C., Miranda L.F., de Souza A.O., Dorta D.J. 2014. Bde-154 induces mitochondrial permeability transition and impairs mitochondrial bioenergetics. *J Toxicol Environ Health A.* **77**:24-36.

Poidatz D., Dos Santos E., Duval F., Moindjie H., Serazin V., Vialard F., et al. 2015. Involvement of estrogen-related receptor-gamma and mitochondrial content in intrauterine growth restriction and preeclampsia. *Fertil Steril.* **104**:483-490.

Rasmussen K., Arlien-Soborg P., Sabroe S. 1993. Clinical neurological findings among metal degreasers exposed to chlorinated solvents. *Acta Neurol Scand.* **87**:200-204.

Ruckart P.Z., Bove F.J., Maslia M. 2014. Evaluation of contaminated drinking water and preterm birth, small for gestational age, and birth weight at marine corps base camp lejeune, north carolina: A cross-sectional study. *Environ Health.* **13**:99.

Ruijten M.W., Verberk M.M., Salle H.J. 1991. Nerve function in workers with long term exposure to trichloroethene. *Br J Ind Med.* **48**:87-92.

Rusyn I., Chiu W.A., Lash L.H., Kromhout H., Hansen J., Guyton K.Z. 2014. Trichloroethylene: Mechanistic, epidemiologic and other supporting evidence of carcinogenic hazard. *Pharmacol Ther.* **141**:55-68.

Sanchez-Aranguren L.C., Espinosa-Gonzalez C.T., Gonzalez-Ortiz L.M., Sanabria-Barrera S.M., Riano-Medina C.E., Nunez A.F., et al. 2018. Soluble fms-like tyrosine kinase-1 alters cellular metabolism and mitochondrial bioenergetics in preeclampsia. *Front Physiol.* **9**:83.

Stark G. 2005. Functional consequences of oxidative membrane damage. *J Membr Biol.* **205**:1-16.

Szklanna P.B., Wynne K., Nolan M., Egan K., Ainle F.N., Maguire P.B. 2017. Comparative proteomic analysis of trophoblast cell models reveals their differential phenotypes, potential uses and limitations. *Proteomics.* **17**:1700037-1700042.

Takao T., Asanoma K., Kato K., Fukushima K., Tsunematsu R., Hirakawa T., et al. 2011. Isolation and characterization of human trophoblast side-population (sp) cells in primary villous cytotrophoblasts and htr-8/svneo cell line. *PloS one.* **6**:e21990.

Takara. 2013a. Human mitochondrial DNA (mtdna) monitoring primer set cat. # 7246 product manual Vol. v201409Da. Mountain View, California:Takara Bio Inc.

Takara. 2013b. Utf-8'en-us'mtdna_copy_number_calculation In: Microsoft Excel, (UTF-8'en-us'mtDNA_Copy_Number_Calculation, ed). Mountain View, California:Takara Bio Inc.

Tetz L.M., Cheng A.A., Korte C.S., Giese R.W., Wang P., Harris C., et al. 2013. Mono-2-ethylhexyl phthalate induces oxidative stress responses in human placental cells in vitro. *Toxicol Appl Pharmacol.* **268**:47-54.

van de Water B., Zoeteweij J.P., de Bont H.J., Mulder G.J., Nagelkerke J.F. 1994. Role of mitochondrial ca2+ in the oxidative stress-induced dissipation of the mitochondrial membrane potential. Studies in isolated proximal tubular cells using the nephrotoxin 1,2-dichlorovinyl-l-cysteine. *J Biol Chem.* **269**:14546-14552.

van de Water B., Zoeteweij J.P., de Bont H.J., Nagelkerke J.F. 1995. Inhibition of succinate:Ubiquinone reductase and decrease of ubiquinol in nephrotoxic cysteine s-conjugate-induced oxidative cell injury. *Molecular pharmacology.* **48**:928-937.

Walker D.I., Uppal K., Zhang L., Vermeulen R., Smith M., Hu W., et al. 2016. High-resolution metabolomics of occupational exposure to trichloroethylene. *Int J Epidemiol.* **45**:1517-1527.

Waters E.M., Gerstner H.B., Huff J.E. 1977. Trichloroethylene. I. An overview. *J Toxicol Environ Health.* **2**:671-707.

Xu F., Papanayotou I., Putt D.A., Wang J., Lash L.H. 2008. Role of mitochondrial dysfunction in cellular responses to s-(1,2-dichlorovinyl)-l-cysteine in primary cultures of human proximal tubular cells. *Biochem Pharmacol.* **76**:552-567.

Zorov D.B., Filburn C.R., Klotz L.O., Zweier J.L., Sollott S.J. 2000. Reactive oxygen species (ros)-induced ros release: A new phenomenon accompanying induction of the mitochondrial permeability transition in cardiac myocytes. *J Exp Med.* **192**:1001-1014.

Zorov D.B., Juhaszova M., Sollott S.J. 2014. Mitochondrial reactive oxygen species (ros) and ros-induced ros release. *Physiol Rev.* **94**:909-950.

Zorova L.D., Popkov V.A., Plotnikov E.Y., Silachev D.N., Pevzner I.B., Jankauskas S.S., et al. 2018. Mitochondrial membrane potential. *Analytical biochemistry.* **552**:50-59.

Chapter V. Transcriptional Profiling of the Trichloroethylene Metabolite *S*-(1,2-Dichlorovinyl)-L-Cysteine Revealed Activation of the EIF2α/ATF4 Integrated Stress Response in the HTR-8/SVneo Trophoblast Cell Line

Abstract

Trichloroethylene (TCE) is an industrial solvent and widespread environmental contaminant. Despite its classification by multiple regulatory agencies as a known human carcinogen, industrial use of the compound continues globally, albeit mostly in a regulated capacity. Due to environmental contamination and continued usage, TCE exposure is an ongoing risk. Although epidemiological evidence associating exposure with adverse birth outcomes remains inconclusive, several recent studies demonstrated toxicity of TCE in pregnant rats. In addition, the TCE metabolite *S*-(1,2-dichlorovinyl)-L-cysteine exhibits toxicity in a placental cell line. Thus far, investigations into the mechanisms of DCVC-induced cytotoxicity have been limited to narrowly-defined methods evaluating single molecular signaling pathways and biological responses. In the current study, genome-wide transcriptomics and gene set enrichment analyses were used to identify novel biological processes and molecular signaling pathways altered by human exposure-relevant DCVC concentrations in HTR-8/SVneo cells. Transcriptomics revealed hundreds of differentially expressed genes with exposure to 20 μM DCVC for 12 h (FDR<0.1 and fold-change < -1.5 or >1.5). Gene set enrichment analyses demonstrated that the most substantially altered molecular signaling pathway was the EIF2α/ATF4 Integrated Stress Response (ISR), with the most abundantly altered biological processes including amino acid transport, metabolism and biosynthesis, transcription and

translation, and regulation of tissue development. Furthermore, western blotting confirmed the involvement of these pathways and provided insight into functional consequences in the cells. For example, decreased global protein synthesis was measured in agreement with ISR signaling. However, no changes in cell cycle progression or proliferation were detected, suggesting that a generally successful adaptive process occurred after 12 h of DCVC treatment. This study provides further insights into the mechanism of DCVC-induced cytotoxicity by revealing the involvement of a specific stress signaling pathway. However the findings should be confirmed in other models such as primary placental cells.

Introduction

Trichloroethylene (TCE) is a volatile organic compound that belongs to a class of chlorinated hydrocarbons with potent solvent properties. Throughout the twentieth century, the chemical was widely used as a dry cleaning solvent and vaporized industrial metal degreaser with little attention paid to disposal methods (Chiu et al. 2013; Waters et al. 1977). Today, over 80% of newly manufactured TCE is used as a chemical intermediate in closed-system refrigerant manufacturing processes (ATSDR 2016; NTP 2015). Despite substantial efforts in recent decades to clean up and prevent further TCE environmental contamination, legacy pollution of soil and groundwater remains, as evidenced by detection in thousands of hazardous waste sites across the United States (EPA 2017; EPA 2018). Due to ongoing usage and persistent environmental contamination, occupational and/or community-based TCE exposure continues to pose a potential risk to human health.

The weight of evidence suggests that metabolism of TCE to its reactive metabolites is required for toxic injury (Lash et al. 2014). Once TCE enters the body, it is metabolized by one of two major pathways: cytochrome P450 oxidation or glutathione conjugation (Lash et al.

2000). Bioactivation occurs primarily in the liver and kidneys, making them key targets for TCE toxicity. The glutathione conjugation-derived metabolite *S*-(1, 2-dichlorovinyl)-L-cysteine (DCVC) has proven to be particularly destructive to renal proximal tubular cells, contributing to the classification of TCE as a known human kidney carcinogen by the National Toxicology Program (NTP) and International Agency for Research on Cancer (IARC) (Guha et al. 2012; NTP 2015).

Several epidemiological studies evaluated the effects of maternal TCE exposure on pregnancy. These studies reported associations between maternal TCE exposure and adverse birth outcomes including low birth weight and preterm birth (Forand et al. 2012; Ruckart et al. 2014). Furthermore, Loch-Caruso *et al.* recently demonstrated that TCE exposure during mid-gestation in rats decreased fetal birth weights and elevated oxidative stress biomarkers in placenta (Loch-Caruso et al. 2018). Despite associations of TCE exposure with increased adverse birth outcomes in humans and rats, the toxicological mechanisms of these associations have only minimally been explored (Elkin et al. 2018; Hassan et al. 2016).

Although etiologic factors have been identified that may contribute to pregnancy complications, the pathophysiology leading to adverse birth outcomes is not well understood (March of Dimes 2012). Structural or functional abnormalities of the placenta, the multifaceted organ that supports the fetus during pregnancy, may lead to subsequent adverse birth outcomes (Ilekis et al. 2016). For example, pregnancy disorders involving placental deficiencies have been associated with adverse birth outcomes such a preterm birth in several recent epidemiology (Davies et al. 2016; Oshvandi et al. 2018) and pathology studies (Nijman et al. 2016). Similarly, toxicological injury to the placenta may also play a role in the development of adverse birth outcomes (Goodman et al. 1982; Morgan 2014).

The placenta may be at risk of toxic injury caused by TCE because it will come into direct contact with any TCE and TCE metabolites circulating in blood, blood is delivered to the placenta at a high rate, and the placenta is capable of metabolizing xenobiotics (Burton and Fowden 2015; Laham 1970). The TCE metabolite DCVC induces cytotoxicity in a first-trimester placental cell line, HTR-8/SVneo. Thus far, investigation into the mechanisms of DCVC-induced cytotoxicity in placental has been limited to specific molecular signaling pathways and biological responses including reactive oxygen species generation, lipid peroxidation, inflammatory responses and apoptotic signaling (Elkin et al. 2018; Hassan et al. 2016). Application of comprehensive data approaches such as transcriptomics allows for unbiased broad characterization of toxicity mechanisms without relying on a few pre-selected pathways. In the current study, high throughput RNA sequencing (RNAseq) was used to quantify genome-wide DCVC-induced differential gene expression in HTR-8/SVneo cells. Furthermore, gene set enrichment analysis was used to identify pathways involved in DCVC-induced cytotoxicity, including activation of a cellular stress response pathway termed the Integrated Stress Response (ISR), amino acid transport and metabolism, and regulation of biological processes involving tissue development. Finally, we validated the involvement of these pathways and investigated potential functional consequences in processes including protein synthesis, cell cycle progression, and proliferation.

Materials and Methods

Chemicals and Reagents

The trichloroethylene metabolite *S*-(1, 2-dichlorovinyl)-L-cysteine (DCVC) was synthesized as a powder by the University of Michigan Medicinal Chemistry Core according to procedures described by McKinney et al. (McKinney et al. 1959)**.** Purity of 98.7 % was

measured using high-performance liquid chromatography (HPLC) analysis. A 1 mM DCVC stock solution was prepared by dissolving DCVC powder in phosphate buffered saline (PBS), and the chemical structure was confirmed by NMR performed at the University of Michigan Biochemical Nuclear Magnetic Resonance Core. The DCVC stock solution was stored in aliquots at −20°C until use.

Cell culture reagents including RPMI 1640 culture medium with L-glutamine and without phenol red, 10,000 U/mL penicillin and 10,000 μg/mL streptomycin (P/S) mixed solution, and fetal bovine serum (FBS) were purchased from Gibco, a division of Thermo Fisher Scientific (Waltham, MA, USA). PBS and 0.25% trypsin were purchased from Invitrogen Life Technologies (Carlsbad, CA, USA).

Cell Culture and Treatment

HTR-8/SVneo cells, a gift from Dr. Charles H. Graham (Queen's University, Kingston, Ontario, Canada), were cultured as previously described (Graham et al. 1993; Hassan et al. 2016; Tetz et al. 2013). Briefly, cells were cultured between passages 78–84 in RPMI 1640 medium supplemented with 10% FBS and 1% P/S at 37°C in a 5% CO_2 humidified incubator. Cells were cultured in RPMI 1640 growth medium with 10% FBS and 1% P/S prior to and during experiments to ensure optimal cell growth as previously described by Graham et al. (Graham et al. 1993)**.** Cells were grown to 70–90% confluence at least 24 h after plating prior to use in any experiments.

A DCVC stock solution aliquot was thawed in a 37°C water bath and then diluted in RPMI 1640 medium with 10% FBS and 1% P/S to final concentrations of 10 or 20 μM DCVC. These concentrations of DCVC were adopted because we previously demonstrated that they did

not induce cytotoxicity at the time points used in the current study (Elkin et al. 2018; Hassan et al. 2016). Moreover, these concentrations are comparable to the average concentration of the DCVC precursor S-(1,2-dichlorovinyl) glutathione (DCVG), 13.4 μM, measured in the serum of female volunteers exposed to 100 ppm of the parent compound, TCE, by inhalation for 4 h (Lash et al. 1999).

Cell Line Validation

HTR-8/SVneo cells were seeded at a density of 400,000 cells per well in a 6-well cell culture plate and allowed to adjust for 48 h. DNA was extracted using QIAamp® DNA Mini Kit (Qiagen; Hilden, Germany) according to the manufacturer's published protocol. DNA samples were stored at −80°C and subsequently transported on dry ice to the University of Michigan DNA Sequencing Core. At the Core, microsatellite genotyping was performed using AmpFLSTR Identifiler Plus PCR Amplification Kit run on an 3730XL Genetic Analyzer (Applied Biosystems; Waltham, MA, USA). DNA for 8 tetranucleotide repeat loci and the Amelogenin sex determination marker were identified. The short tandem repeat profile generated for our cells was compared to the short tandem repeat profile for cells identified as HTR-8/SVneo (ATCC® CRL-3271™) by ATCC® (Manassas, VA) (ATCC 2015).The short tandem repeat profile was an exact match: CSF1PO: 12, D13S317: 9,12, D16S539: 13D5S818: 12, D7S820: 12, TH01: 6,9.3, vWA: 13,18, TPOX: 8, Amelogenin sex determination marker: X (ATCC 2015).

RNA Isolation and Sequencing

HTR-8/SVneo cells were seeded at a density of 800,000 cells per well in a 6-well cell culture plate. Twenty-four hours later, cells were treated with RPMI 1640 medium alone (control) or DCVC (10 or 20 μM) and exposed in triplicate for 6 or 12 h. Following exposure, cell were scraped and lysed with RLT lysis buffer containing beta-mercaptoethanol. Cell lysates were homogenized using QIA shredders (Qiagen; Hilden, Germany), and RNA was extracted using the RNeasy Plus Mini Kit (Qiagen) following the manufacture's recommended protocol. Briefly, homogenized cell lysates were run through gDNA eliminator spin columns to separate out genomic DNA. Following separation, one equivalent of 70% ethanol was added and lysates were loaded onto RNeasy spin columns and washed twice with RW1 and RPE buffers. RNA was eluded in RNase-free water. RNA concentrations were determined with a Nanodrop 1000 Spectrophotometer (Thermo Fisher Scientific) and stored at -80°C.

Four independent experiments were performed for each time point, with 3 replicates for each treatment group. These replicates were subsequently pooled and later transported on dry ice to the University of Michigan DNA Sequencing Core for further processing. RNA concentrations and quality were evaluated using a Bioanalyzer instrument (Agilent; Santa Clara, CA, USA). Stranded sequencing libraries were prepared with the TruSeq Stranded mRNA Library Prep Kit (lllumina; San Diego, CA, USA). Libraries were multiplexed (on two lanes) and sequenced using single-end 50 cycle reads on a HiSeq 4000 sequencer (lllumina).

RNASeq Data Analyses

The Flux high-performance computer cluster at the University of Michigan was used for computational analysis. Sequencing read quality was assessed using FastQC (Andrews 2010). Reads were aligned to the genome using STAR (Dobin et al. 2013), with the options

"outFilterMultimapNmax 10" and "sjdbScore 2". Aligned reads were assigned to GRCh37 genes using featureCounts (Liao et al. 2014). Differential gene expression testing was performed using the edgeR package for R statistical computing (Robinson et al. 2010). Prior to testing, genes with mean read counts-per-million of less than 4 across all samples were filtered out and excluded from the analysis in order to reduce the dispersion due to low expression levels. After filtering, 12,855 genes were included in the analyses. Data were also normalized using the trimmed mean of M values (TMM) method (Robinson and Oshlack 2010). Quasi-likelihood general linear modeling was utilized for differential gene expression testing (Lun et al. 2016). Comparisons were made within each time point between control and 10 or 20 μM DCVC, respectively, adjusting for experiment day as a covariate using the glmQLFit function. Because RNAseq has never been used before to evaluate DCVC effects on placental cells, genes were considered differentially expressed between non-treated and treated samples with an adjusted p-value < 0.10 using the Benjamini-Hochberg false discovery rate (FDR) method (Benjamini and Hochberg 1995) and a 1.5 fold-change in gene expression. This relaxed threshold criterion was selected in order to ensure a thorough evaluation of differentially expressed genes.

Selection and visualization of individual ATF4 gene targets from RNAseq analyses

Activating Transcription Factor 4 (ATF4) is a leucine zipper dimerizable transcription factor that regulates expression of many genes performing a myriad of different functions within the cell (Hai et al. 1989; Tsujimoto et al. 1991). ATF4 target genes were selected for individual visualization based on previously reported evidence of differential gene expression in response to well-characterized mitochondrial stressors (Bao et al. 2016; Han et al. 2013; Quiros et al. 2017; Shpilka and Haynes 2018). In order to visualize individual differential gene expression levels for

ATF4 targets from the RNAseq analyses, normalized transcriptional units, reads per kilobase of transcript, per million mapped reads (RPKM), were calculated using the rpkm function in the edgeR package for R statistical computing (Robinson et al. 2010).

Gene Set Enrichment Analyses

Gene set enrichment analysis was performed using GSEA software (Broad Institute; Cambridge, MA, USA) (Mootha et al. 2003; Subramanian et al. 2005). Specifically, we utilized GSEA pre-ranked analyses to identify treatment-related enriched processes. GSEA pre-ranked analyses are permutation-based tests that calculate a Normalized Enrichment Score (NES) and statistical FDR for each pathway within a specified gene set. For each of our analyses, all 12,855 genes included in the edgeR differential gene expression analyses were ranked according to the log fold-change value for each gene. We used 1000 permutations to test for enriched pathways within the Gene Otology (GO): Biological Processes gene set. All comparisons made during differential gene expression analysis were also tested for enriched pathways.

Western Blotting Analyses

HTR-8/SVneo cells were seeded at a density of 400,000 cells per well in a clear 6-well culture plate and allowed to adhere for 24 h. Cells were treated with medium alone (control) or DCVC (20 μM) for 12 h. Cells were lysed in RIPA lysis buffer containing both protease and phosphatase inhibitors or protease inhibitor alone, and then centrifuged at 14,000 g for 10 minutes at 4°C. Lysates were heated with loading buffer at 85°C for 2-3 minutes. Samples were loaded into commercially available Novex 4–20% Tris-Glycine Mini Gel cassettes (Invitrogen) and proteins were separated by polyacrylamide gel electrophoresis run at 140V for 1.5 h.

SeeBlue Plus2 pre-stained protein standard (Invitrogen) was used as a reference for protein molecular weight. After separation, proteins were transferred to nitrocellulose membranes at 75V for 4 h at a temperature of 4°C. Membranes were blotted at room temperature using binding immunoglobulin protein 2 (BiP) antibody [molecular weight 75; catalog no. 3177; Cell Signaling Technologies; Research Resource Identifier (RRID): AB_ 2119845], activating transcription factor 4 (ATF4) (molecular weight 49; catalog no. 11815; Cell Signaling Technologies; RRID: AB_2616025), CCAAT-enhancer-binding protein homologous protein (CHOP) [molecular weight 27; catalog no 2895 Cell Signaling Technologies; Research Resource Identifier (RRID): AB_2089254] and eukaryotic initiation factor 2 alpha subunit -phosphorylated (P-EIF2α) or non-phosphorylated (EIF2α) [molecular weight 38; catalog nos. 3597 or 9722; Cell Signaling Technologies; Research Resource Identifier (RRID): AB_ 390740 or AB_ 2230924]. Antibody complexes were detected by Alexa Fluor anti-mouse and anti-rabbit fluorescent-conjugated antibodies (Invitrogen) and visualized using an Odyssey CLx image scanner (Li-Cor Biosciences; Lincoln, NE, USA). Blots were quantified using Image Studio software version 5.2 and normalized to Revert Total Protein Stain (Li-Cor Biosciences).

Measurement of Protein Synthesis

HTR-8/SVneo cells were seeded at a density of 10,000 cells per well in a black clear-bottomed 96-well plate and allowed to acclimate for 24 h. Cells were treated with medium alone (control) or DCVC (5, 10 or 20 μM) for 6 or 12 h. Protein synthesis was measured with a Protein Synthesis Assay Kit (Thermo Fisher Scientific) according to the manufacture's recommended protocols. This assay utilizes cell-permanent O-propargyl-puromycin (OPP) which halts translation of polypeptide chains by incorporating into the C-terminus. Briefly, cells were

incubated with OPP solution for 2 h at 37°C. Following incubation, cells were fixed and incubated with FAM-Azide solution (FAM-Azide, copper sulfate and ascorbic acid) for 30 minutes in the dark at room temperature. Following incubation, protein synthesis was measured fluorescently (excitation: 485 nm; emission 535 nm) using a SpectraMax M2e Multi-Mode Microplate Reader (Molecular Devices; Sunnyvale, CA, USA).

Cell Cycle Phase Determination

HTR-8/SVneo cells were seeded at a density of 400,000 cells per well in a 6-well plate and allowed to adhere for 24 h prior to treatment. Cells were treated with medium alone (control) or DCVC (10 or 20 μM) for 12 h. The percentage of cells in each well in G_1/G_0, S, and G_2/M phases were measured using the Cell Cycle Phase Determination Kit (Cayman Chemical; Ann Arbor, MI, USA), performed according to the manufacturer's protocol. This assay uses propidium iodide (PI) to label DNA. Briefly, following exposure, cells were treated with 0.25% trypsin-EDTA and incubated for 2 minutes to detach adherent cells from the substrate. Following incubation, trypsin was deactivated with FBS-containing medium, and the suspended cells were transferred to 5-ml round-bottom fluorescence-activated cell sorting (FACS) tubes. Cells were washed twice with 1 ml of assay buffer, resuspended in 500 μl of cell fixative assay buffer solution, and chilled for 2 hours at -20°C. After fixation, cells were washed and resuspended in 500 μl PI staining solution, incubated for 30 minutes at room temperature, and transported to the University of Michigan Flow Cytometry Core for analysis. Cell phases were quantified using a LSRFortessa Flow Cytometer (BD Biosciences; San Jose, CA, USA). Quantification and dye-based visualization were performed using BD FACSDiva Software (BD Sciences) for PC. Cell aggregates and cellular debris were excluded using the forward scatter (FSC) and side scatter

(SSC) modes and the analysis was performed using 10,000 events per sample. PI was detecting using the 488 nm laser.

Effects DCVC on Cell Proliferation

HTR-8/SVneo cells were seeded at a density of 10,000 cells per well in a 96-well plate and allowed to adhere for 24 h. Cells were then treated with medium alone (control) or DCVC (5, 10 or 20 μM) in quintuplicate for 6 or 12 h. CyQUANT® Cell Proliferation Assay (Invitrogen) was used to quantify cell proliferation. The stain specifically binds to cellular DNA, and the fluorescence is proportional to the number of cells. The assay was performed according to the manufacturer's protocol. Briefly, dye binding solution was prepared by diluting CyQUANT® reagent in Hank's Balanced Salt Solution (HBSS). Following exposure to DCVC, the growth medium was removed and CyQUANT® dye binding solution was added to each well. Cells were incubated for 1 h at 37°C. Following incubation, fluorescence was measured (excitation: 485 nm; emission 530 nm) using a SpectraMax M2e Multi-Mode Microplate Reader (Molecular Devices).

Statistical Analysis

For western blotting, protein synthesis, cell cycle determination and proliferation, experiments were performed independently and repeated a minimum of three times. When applicable, technical replicates were averaged within each experiment and these values were analyzed using one-way or two-way analysis of variance (ANOVA) followed by Tukey's post-hoc test for comparison of means GraphPad Prism software version 7 was used for statistical

analysis (GraphPad Software Inc., San Diego, CA, USA). Data are expressed as means ± SEM. N=number of independent experiments. $P < 0.05$ was considered statistically significant.

Results

DCVC-induced differential gene expression

In order to evaluate DCVC-induced changes in overall gene expression, RNAseq transcriptome analyses were performed. Multidimensional scaling based on RNA expression was used to observe how individual samples clustered on relevant covarites, including treatment, duration, and experimental day (Fig. 5.1Ai-iv). Within each time point, gene expression levels were compared between non-treated cells (controls) and DCVC-treated (10 or 20 μM) cells (Fig. 5.1A). DCVC modified gene expression in both time-dependent and concentration-dependent manners (Fig 5.1Bi-iv; FDR<0.1). After a 6-hour exposure to 10 μM DCVC, only 1 gene was significantly differentially expressed compared to time-matched non-treated controls (Fig. 5.1Bi; FDR<0.1). However, exposure to 20 μM DCVC at the same time point yielded 30 significantly differentially expressed genes (Fig. 5.1Bii; FDR<0.1). Among those genes, 14 were up-regulated by 1.5 fold or greater, whereas 6 were down-regulated by 1.5 fold or more. Following 12 hour of exposure to 10 μM DCVC, 65 genes were significantly differentially expressed compared to time-matched non-treated controls (Fig 5.1Biii; FDR<0.1), with 8 genes up-regulated by 1.5 fold or greater and 11 genes down-regulated by 1.5 fold or greater. 20 μM DCVC exposure for 12 h resulted in 1268 significantly differentially expressed genes (Fig. 5.1Biv; FDR<0.1), 20 times the number within the same time point at a lower concentration and 42 times the number at an earlier time point within the same concentration. Of those 1268 genes, 132 were up-regulated by 1.5 fold or greater and 225 were down-regulated by 1.5 fold or greater.

Evaluation of dose and time-dependent transcriptional response

To characterize the relationship between specific differential gene expression and concentration level or exposure duration, a Pearson's correlation coefficient was calculated for each pairwise comparison. Within each time point, differential gene expression between non-treated controls and 10 or 20 µM DCVC, was highly correlated with r=0.51 (Fig 5.2A; $P< 1.0x10^{-15}$) at 6 h and r=0.67 (Fig 5.2B; $P< 1.0x10^{-15}$) at 12h. Consistent with these findings, the only gene differentially expressed with 10 µM DCVC, *ALAS1*, was also differentially expressed with 20 µM DCVC at 6 h (Fig. 5.2C). Similarly, 18 of the 19 differentially expressed genes with 10 µM DCVC exposure were also differentially expressed with 20 µM DCVC treatment at 12 h (Fig.5.2D). These findings indicate a concentration-dependent transcriptional response. On the other hand, differential gene expression between non-treated controls and each DCVC concentration for 6 or 12 h were weakly correlated with r=0.14 (Fig 5.2E; $P< 1.0x10^{-15}$) for 10 µM and r=0.24 (Fig 5.2F; $P< 1.0 x10^{-15}$) for 20 µM DCVC, indicating a weaker time-dependent transcriptional response.

Identification of significantly enriched biological processes

Pathway enrichment analyses utilizing the GO: Biological Processes gene set identified biological processes affected by DCVC treatment. Following a 6-h exposure to 10 µM or 20 µM DCVC, no processes were significantly positively-enriched, however 5 and 221 processes, were significantly negatively- enriched, respectively (Fig. A.5). After 12 h of exposure to 10 or 20 µM DCVC, 12 and 15 processes were significantly positively-enriched, respectively, while 397 and 596 processes were negatively-enriched (Figs 5.3A & B; FDR< 0.1), respectively. Of the 12 positively enriched biological processes occurring with 10 µM DCVC, 3 involved RNA

transcription/ribosomal translation, 3 involved amino acids and 4 involved ISR signaling, whereas 3 out of the top 15 negatively-enriched processes involved tissue development (Fig 5.3A). Additionally, of the 15 positively-enriched biological processes occurring with 20 μM DCVC treatment, 4 involved RNA transcription/ribosomal translation, 4 involved amino acids and 11 involved ISR signaling, whereas 9 out of the top 15 negatively-enriched involved tissue development (Fig. 5.3B).

Evidence of DCVC-induced Integrated Stress Response

Because multiple ISR genes were significantly up-regulated and biological processes positively-enriched with 20 μM DCVC exposure for 12 h, we further characterized the DCVC-induced ISR with this exposure (Fig. 5.4). First, we plotted differential expression of individual genes directly involved in the activation of the ISR (Fig. 5.4Ai; FDR<0.1). Second, in order to confirm ISR activation, we used western blot analysis to measure concentrations and phosphorylation levels of corresponding key ISR proteins and compared them to gene expression levels (Fig. 5.4Aii & iii; P<0.05). Among three key genes involved in activation of the ISR, DCVC increased expression of *ATF4* 1.8-fold and *DDIT3* 1.7 fold compared to non-treated controls (FDR<$8x10^{-5}$), but *EIF2A* expression was not significantly changed (Fig. 5.4Ai). Consistent with increased gene expression, DCVC increased ATF4 protein by more than 4-fold compared to non-treated controls (Fig. 5.4Aii; P=0.027). However, abundance of the protein CHOP, which is coded by *DDIT3*, was not significantly affected by DCVC treatment (Fig. 5.4Aii). Although DCVC had no significant effect on *EIF2A* gene expression, DCVC treatment increased the ratio of phosphorylated to non-phosphorylated EIF2α protein 61% compared to non-treated controls (Fig. 5.4Aii; P=0.049), indicating activation.

We next displayed significant differential expression of individual ATF4 gene targets selected based on previously reported transcriptional changes in response to well-characterized mitochondrial stressors (Fig. 5.4B & C; FDR<0.1 and logFC>0.35) (Bao et al. 2016; Han et al. 2013; Quiros et al. 2017; Shpilka and Haynes 2018). ATF4-controlled genes involved in various biological processes necessary for adaptation that were up-regulated by DCVC treatment included: metabolism genes *MTHFD2*, *PCK2, PHGDH and PSAT1* (Fig. 5.4Bi; FDR<0.1), redox balance genes *CHAC1* and *PSPH* (Fig. 5.4Bii; FDR<0.1), amino acid transport genes *SLC1A4*, *SLC1A5*, *SLC6A9* and *SLC7A11* (Fig. 5.4Biii; FDR<0.1 and amino acid biosynthesis *AARS*, *CARS*, *GARS*, *MARS*, *TARS* and *YARS* (Fig. 5.4Biv; FDR<0.1). Up-regulated genes involved in cell death signaling included: *DDIT3, PMAIP1*, *TRIB3*, and *DDIT4* (Fig. 5.4Bv; FDR<0.1).

DCVC effect on global protein synthesis

Because differential gene expression and gene set enrichment analyses revealed ISR activation, we measured global protein synthesis attenuation, a principal target of ISR signaling through phosphorylation of EIF2α. Following treatment with 0-20 μM DCVC for 6 h, protein synthesis was not significantly altered. However, treatment with 20 μM DCVC for 12 h significantly attenuated protein synthesis 37% (Fig, 5.5; P=0.0012), whereas treatment with lower DCVC concentrations had no significant effect.

Effect of DCVC on cellular proliferation or cell cycle progression

Because DCVC exposure for 12 h impacted multiple biological processes involving amino acids, RNA transcription and ribosomal translation, and these processes are closely linked

to cell cycle progression, the percentage of cells in each phase of the cell cycle was determined using a propidium iodide assay following 12 h DCVC treatment at 10 and 20 μM. No significant changes in cell cycle progression were observed (Fig 5.6). Additionally, no significant differences in cellular proliferation were observed at either 6 or 12 h comparing non-treated control cells and cells treated with 5, 10 or 20 μM DCVC for 6 or 12 h (Fig. 5.7). These results suggest that although there were changes in gene expression levels associated with these major cellular processes, they did not result in significant changes to those processes such as cell cycle progression and proliferation.

Discussion

Several recent epidemiology studies reported associations between maternal TCE exposure and increased risk of adverse birth outcomes (Forand et al. 2012; Ruckart et al. 2014). However, biological explanations for these associations have only recently been explored. To date, investigations into the mechanisms of TCE metabolite DCVC-induced cytotoxicity have been limited to specific pre-selected molecular signaling pathways and biological responses. This study utilized hypothesis-generating transcriptomic analyses to evaluate genome-wide gene expression, identify and confirm novel pathways involved in DCVC-induced toxicity, and further investigate changes to cellular function.

Here, our differential gene expression and gene set enrichment analyses revealed that DCVC treatment of HTR-8/SVneo cells for 12 h activated a cellular stress response pathway termed the Integrated Stress Response (ISR). The ISR is summarized in figure 5.8. The principal initiating event in the ISR is phosphorylation of the translation initiation factor EIF2α by one or more of the four enzymes in the EIF2α kinase family, each of which respond to different stress stimuli: GNC2 (amino acid deprivation), PKR (viral infection), HRI (heme diffency and ROS),

and PERK (endoplasmic reticulum and mitochondrial stress) (Pakos-Zebrucka et al. 2016). In our study, because we previously measured elevated amino acid concentrations (Chapter 3), GNC2 is likely not the source of EIF2α phosphorylation. In order to reestablish cellular homeostasis, EIF2α phosphorylation concomitantly suppresses global CAP-dependent protein translation while allowing for transcription and translation of selected stress response genes with open read frames in their promotors, namely the central ISR regulatory transcription factor ATF4 (Pakos-Zebrucka et al. 2016; Walter and Ron 2011; Wortel et al. 2017). Indeed, our results demonstrated EIF2α phosphorylation, global attenuation of protein synthesis and elevated ATF4 concentrations, confirming DCVC-induced ISR activation.

Although the ISR may be triggered at the cellular level by one or more different stimuli, the weight of evidence suggests that mitochondrial dysfunction is the primary stimulus driving the DCVC-induced stress response, most likely activated by EIF2α kinases HRI and/or PERK (Quiros et al. 2017; Shpilka and Haynes 2018). Specifically, we previously reported that DCVC decreases mitochondrial-dependent basal, maximum and reserve oxygen consumption rates, decreased ATP-linked respiration and coupling efficiency, increased proton leak and dissipated mitochondrial membrane potential in HTR-8/SVneo cells (Hassan et al. 2016), Chapter 4). Moreover, it is well established that mitochondria are the key target of DCVC toxicity in kidney proximal tubular cells (Chen et al. 2001; Lash and Anders 1987; Lash et al. 2003; van de Water et al. 1993; van de Water et al. 1994; Xu et al. 2008). Additionally, a comprehensive study utilizing multi-omics approaches recently established a common ATF4-mediated mitochondrial stress signature response characterized by activation amino acid biosynthesis pathways (Quiros et al. 2017). Our differential gene expression and gene set enrichment analyses demonstrated an expression pattern that resembled their mitochondrial stress signature response, lending further

evidence of mitochondrial-mediated ISR activation. Taken together, the data suggest that mitochondrial dysfunction is the most likely stimulus driving DCVC-induced ISR activation.

Molecular signaling through the ISR has a degree of complexity that allows for tight regulation and a tailored response. Although the ISR largely promotes an adaptive, pro-survival program, if restoration to equilibrium fails due to prolonged or severe stress, then apoptosis may be induced (Han et al. 2013; Pakos-Zebrucka et al. 2016; Wortel et al. 2017). Here, we report evidence of conflicting ISR pro-survival and pro-apoptotic signaling after 12 h of DCVC treatment, highlighting both adaptive and pathological processes were activated. For example, our differential gene expression analysis revealed many upregulated ATF4 transcriptional targets involved in adaptive responses including metabolism (*MTHFD2*, *PCK2, PHGDH, PSAT1*), redox balance (*CHAC1*, *PSPH*) amino acid transport (*SLC1A4*, *SLC1A5*, *SLC6A9*, and *SLC7A11*) and amino acid biosynthesis (*AARS*, *CARS*, *GARS*, *MARS*, *TARS*, *YARS*). Additionally, many of the positively enriched biological processes from our gene set enrichment analysis also involved amino acid transport, metabolism and biosynthesis. On the other hand, ATF4 transcriptional targets involved in apoptosis were also up-regulated (including *DDIT3*, *PMAIP1*, *TRIB3*, and *DDIT4*) and biological processes involving intrinsic apoptosis were positively enriched. Importantly, we observed no change in cell cycle progression or proliferation, suggesting that, overall, the cells were successfully adapting to DCVC-induced stress at 12 h of treatment. These results are consistent with several of our previous studies. First, we showed altered macronutrient and metabolic pathway utilization despite no overall change in ATP levels (Chapter 3). Additionally, we reported elevated caspase activity despite no detectable apoptosis (Elkin et al. 2018). Taken together, these results indicate that treatment with 20 μM DCVC for 12 h encompasses a critical molecular signaling transition in which, cell death

signaling increases despite ongoing adaptation, but without concomitant functional consequences.

In addition to specific cellular stresses, elevated ISR signaling components have been implicated in early pregnancy disorders characterized by placental abnormalities such as intrauterine growth restriction and pre-eclampsia. For example, two separate studies measured elevated phosphorylation levels of EIF2α and protein levels of ATF4 and/or CHOP in the placental tissue obtained from pre-eclamptic pregnancies compared to normal pregnancies (Du et al. 2017; Fu et al. 2015). Another study reported an ATF4-mediated suppression of placental growth factor (*PlGF*) mRNA expression in placentae from women diagnosed with early-onset pre-eclampsia and confirmed those results using two trophoblast cells lines (Mizuuchi et al. 2016). Furthermore, prolonged EIF2α phosphorylation decreased proliferation and invasion of trophoblast cell lines *in vitro* (Yung et al. 2008), a defining pathological characteristic of IUGR and pre-eclampsia (Brosens et al. 1972; Caniggia et al. 1999; Kadyrov et al. 2006; Meekins et al. 1994). Consequently, ISR activation in trophoblasts may be a mechanism by which the TCE metabolite DCVC contributes to placental dysfunction.

Although our differential gene expression and gene set enrichment analyses primarily involved ISR signaling for positively enriched biological processes, the most commonly represented negatively enriched biological processes involved fetal tissue development (Fig. 5.3B). Both placental trophoblasts and fetal cells originate from the blastocyst within the first week of pregnancy (Caruso et al. 2012). Moreover, recent genomic analyses revealed that placental and embryonic abnormalities in mice involved common underlying gene networks with a 70% correlation between embryonic lethal gene mutations and placental pathologies (Mohun et al. 2013; Woods et al. 2018). The common origin of placental and embryonic tissues and the

apparent underlying genetic links between abnormalities in each tissue type suggest that DCVC-induced differential gene expression in extravillous trophoblasts may also be associated with TCE-induced embryonic abnormalities. Indeed, although controversial, there have been several studies in animals reporting that maternal TCE exposure increased cardiac malformations in developing fetuses (Johnson et al. 2003; Makris et al. 2016; Rufer et al. 2010). However, other studies have not observed such a relationship (Bukowski 2014; Carney et al. 2006; Fisher et al. 2001; Watson et al. 2006). Regardless, our results indicate that the effect of TCE exposure on fetal development warrants further scrutiny.

As for any toxicology study, concentrations of the toxicant tested must be carefully selected and justifiable. For the current study, concentrations of 5-20 μM DCVC were used as relevant to potential human exposure levels. The concentrations used in our study are relevant to the Occupational Safety and Health Administration (OSHA) Permissible Exposure Limit (PEL) of 100 parts-per-million (ppm) averaged over an 8-hour work day (ATSDR 2016). TCE concentrations up to 229 ppm were reported in 80 exposed workers (29% women) wearing aerosolized monitoring devices (29% women) (Walker et al. 2016). Moreover, female volunteers exposed to the PEL of TCE for 4 h by inhalation had an average peak blood concentration of 13.4 μM for the metabolic precursor to DCVC, *S*-(1,2-dichlorovinyl) glutathione (DCVG) (Lash et al. 1999), which is comparable to the concentrations used in this study. Finally, the concentrations that caused differential gene expression in our study are considerably lower than those used previously as high as 1 mM DCVC (Chen et al. 2001; Lash et al. 2001; Lash et al. 2003; van de Water et al. 1995; Xu et al. 2008).

In addition to using low concentrations, we also investigated the effects of DCVC on placental cells for short exposure durations. Although longer exposures may more accurately

reflect real-life exposures *in vivo*, this approach enabled us to evaluate the cells' initial response to DCVC exposure, otherwise lost, and elucidate compensatory mechanisms used by the cells during the process of stress-driven adaptation. Nevertheless, studies exploring longer DCVC exposure durations on placenta should also be undertaken to understand the full range of effects on the cells.

Although the results reported here contribute new information on genes and signaling pathways affected by DCVC treatment in human placental cells, our study has a limitation of the use of an immortalized cell line, HTR-8/SVneo, to model first trimester extravillous trophoblasts *in vitro*. Although non-cancerous in origin, the immortalization processes allows cells to be cultured for extended periods in appropriate conditions (Graham et al. 1993). Furthermore, genetic and epigenetic profile changes have been reported in cell line when compared to isolated primary extravillous trophoblasts cultured *in vitro* in similar conditions (Bilban et al. 2010; Novakovic et al. 2011). Regardless, these cell are widely used to model first-trimester extravillous trophoblast cells because they express a combination of molecular markers that are unique to extravillous trophoblasts including cytokeratin 7 (CK7), α5β1 integrin, and histocompatibility antigen, class I, G (HLA-G) (when grown on matrigel) (Irving et al. 1995; Khan et al. 2011; Kilburn et al. 2000; Takao et al. 2011). Additionally, they have functional characteristics of extravillous trophoblasts such as invasive and proliferative abilities which respond to stress and oxygen deprivation, expression of adhesion molecules and a mesenchymal phenotype (Hannan et al. 2010; Kilburn et al. 2000; Liu et al. 2016; Szklanna et al. 2017). Nonetheless, due to the limitations of cell lines, further studies carried out in primary first-trimester extravillous trophoblasts or villous explants are needed to confirm our results.

In summary, we used transcriptomics and gene set enrichment analyses to identify previously unknown biological processes and molecular signaling pathways altered in response to short-term treatment with human-relevant DCVC concentrations. Furthermore, traditional methods such as western blotting were used to confirm the involvement of these pathways and to explore functional consequences in the cells. Transcriptomics revealed hundreds of differentially expressed genes with 20 μM DCVC for 12 h in HTR-8/SVneo cells (FDR<0.1 and fold-change < -1.5 or >1.5). We demonstrated that the most substantially altered molecular signaling pathway was the ISR, and the most abundantly altered biological processes included amino acid transport, metabolism and biosynthesis, transcription and translation, and regulation of tissue development. Finally, we reported decreased global protein synthesis in agreement with the ISR signaling. Despite these findings, we found no evidence for change in cell cycle progression or proliferation, suggesting a generally successful adaptive process occurring after 12 h of DCVC treatment. To our knowledge, our study is the first to report DCVC-mediated activation of the ISR in any cell type. Our findings also contribute to the biological plausibility of DCVC-induced placental toxicity, providing a compelling rationale for further studies into the effect of DCVC on placental cells.

.

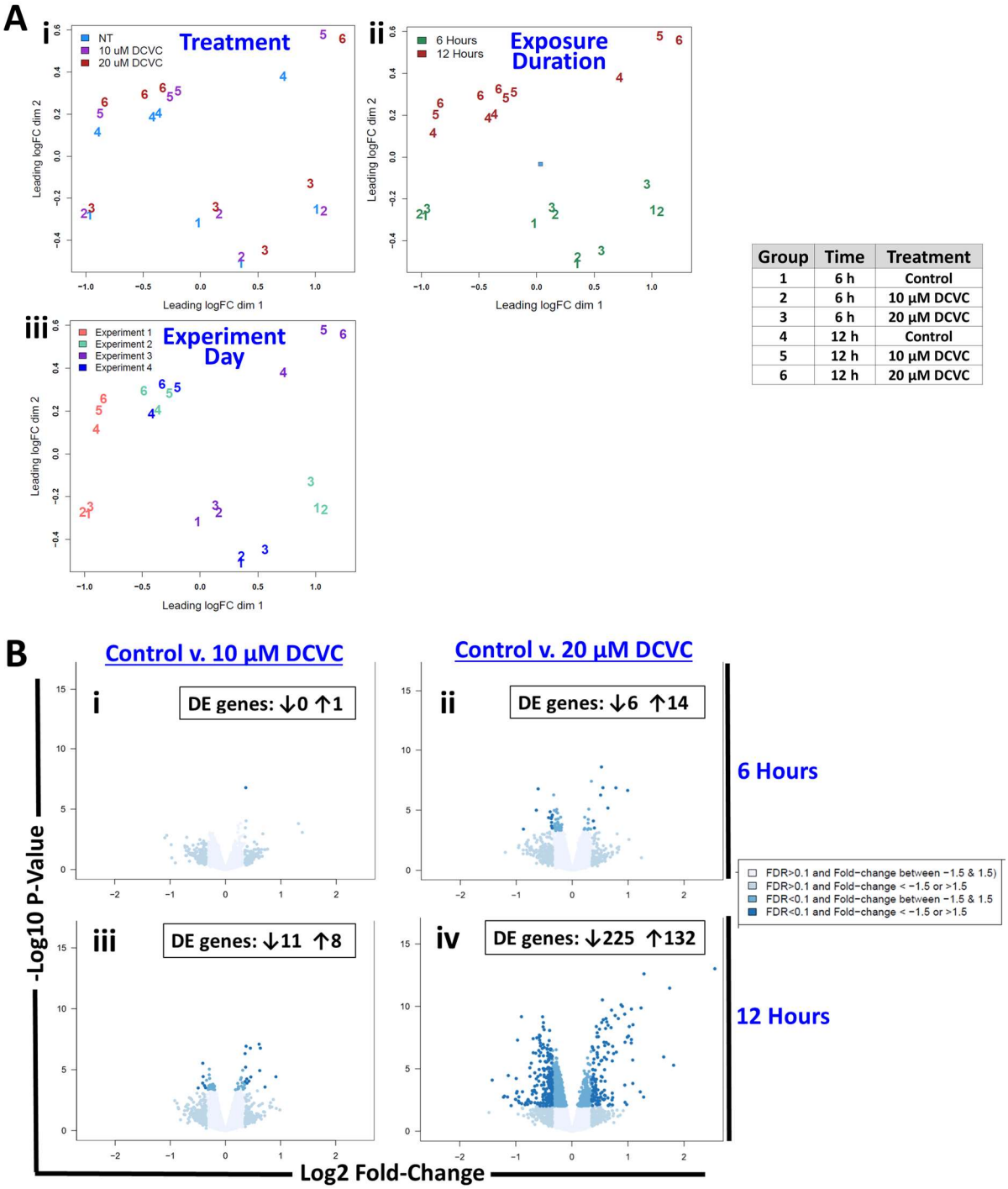
A
i
Treatment
NT
10 uM DCVC
20 uM DCVC
ii
Exposure Duration
6 Hours
12 Hours
iii
Experiment Day
Experiment 1
Experiment 2
Experiment 3
Experiment 4
Leading logFC dim 1
Leading logFC dim 2
Group | Time | Treatment
1 | 6 h | Control
2 | 6 h | 10 µM DCVC
3 | 6 h | 20 µM DCVC
4 | 12 h | Control
5 | 12 h | 10 µM DCVC
6 | 12 h | 20 µM DCVC
B
Control v. 10 µM DCVC
Control v. 20 µM DCVC
i
DE genes: ↓0 ↑1
ii
DE genes: ↓6 ↑14
iii
DE genes: ↓11 ↑8
iv
DE genes: ↓225 ↑132
6 Hours
12 Hours
FDR>0.1 and Fold-change between −1.5 & 1.5)
FDR>0.1 and Fold-change < −1.5 or >1.5
FDR<0.1 and Fold-change between −1.5 & 1.5
FDR<0.1 and Fold-change < −1.5 or >1.5
-Log10 P-Value
Log2 Fold-Change

Figure 5.1. Summary of DCVC effects on differential gene expression in HTR-8/SVneo cells.
Cells were treated with medium alone (control), 10 or 20 μM DCVC for 6 or 12 h. Following mRNA isolation and sequencing, differential gene expression was measured with edgeR package for R using quasi-likelihood general linear modeling. **A)** Multidimensional scaling clustered by **(i)** treatment group, **(ii)** exposure duration, and **(iii)** experiment day. Color keys are identified with each plot. **B)** Volcano plots comparing differential gene expression between non-treated cells and DCVC-treated cells: **(i)** 10 μM DCVC for 6 h, **(ii)** 20 μM DCVC for 6 h, **(iii)** 10 μM DCVC for 12 h, and **(iv)** 20 μM DCVC for 12 h. Genes were considered differentially expressed if FDR<0.1 and fold-change < -1.5 or >1.5.

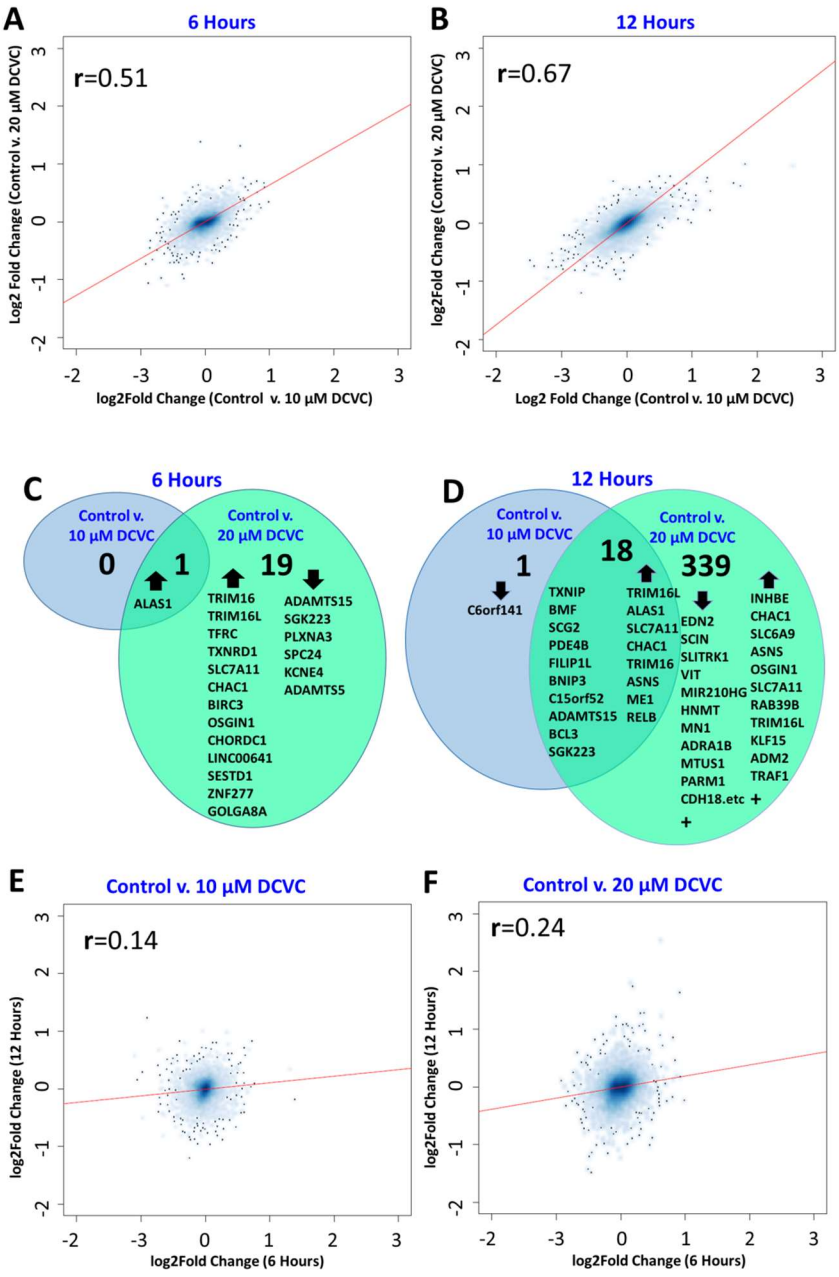

Figure 5.2. Effects of DCVC concentration and exposure duration on transcriptional response.
Pearson's correlation coefficients were calculated to evaluate the relationship between specific differential gene expression and DCVC concentration level or exposure duration. Correlation of log2 fold-change differences between control v. 10 µM and control v. 20 µM DCVC are shown ($P< 2.2x10^{-16}$) for **A)** 6 h and **B)** 12 h. Venn diagrams depicting overlap in differentially expressed genes (FDR<0.1 and fold-change < -1.5 or >1.5) between control v. 10 µM and control v. 20 µM DCVC for **C)** 6 h and **D)** 12 h. Correlation of log2 fold-change differences between 6 and 12 h ($P< 2.2x10^{-16}$) for **E)** control v. 10 µM DCVC and **F)** control v. 20 µM DCVC.

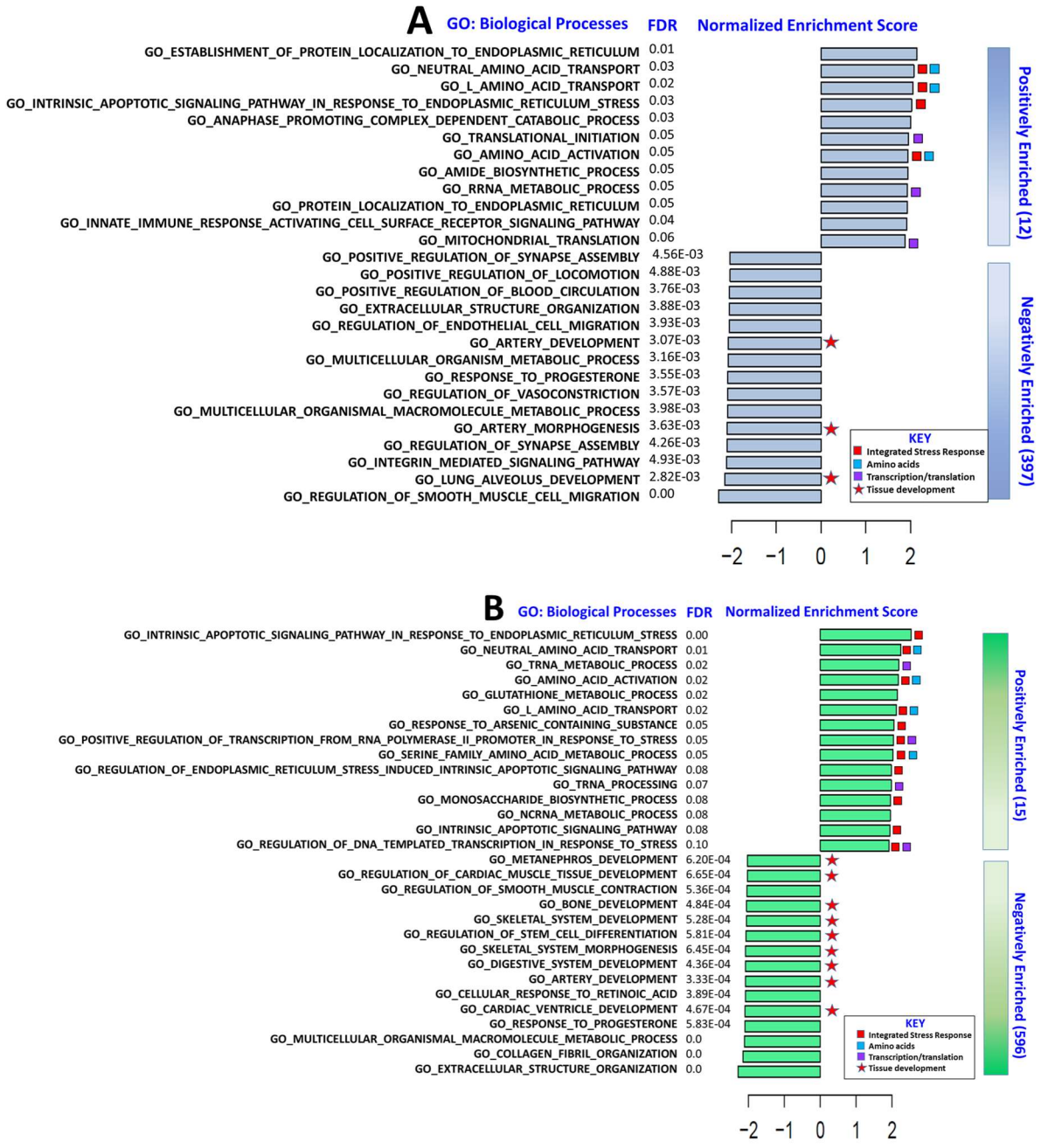

Figure 5.3. Identification of significantly enriched biological processes after 12 h treatment with DCVC.

Visualization of the top 15 positively and negatively-enriched biological processes at 12 h for **A)** 10 µM and **B)** 20 µM DCVC ranked according to normalized enrichment score (NES). Gene set enrichment analysis identified treatment-related enriched biological processes based on the GO: Biological Processes gene set. The analyses included 12,855 genes ranked according to the log fold-change value from each respective comparison. FDR<0.1 was considered significantly enriched. Biological processes associated with ISR signaling are denoted with red squares, amino acids with blue squares, transcription/translation with purple circles, and tissue development with red stars.

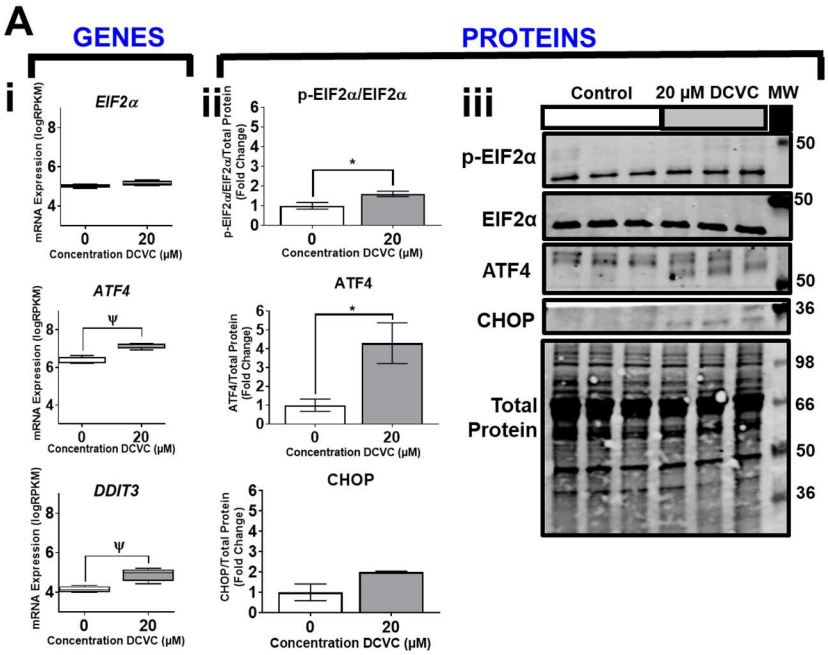

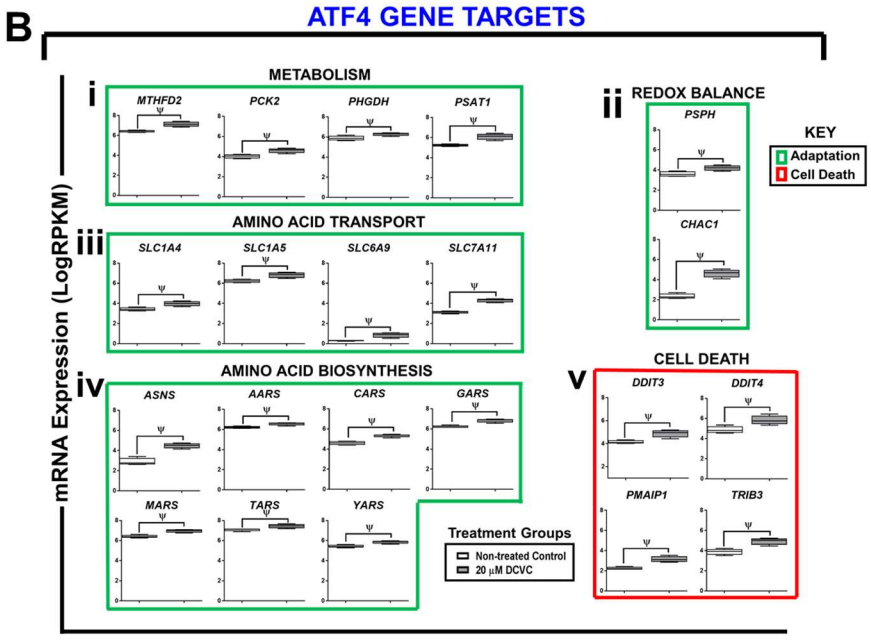

C

Gene	Log2 Fold Change	FDR
AARS	0.36	4.05E-05
ASNS	1.74	1.48E-08
CARS	0.77	6.39E-07
CHAC1	2.55	1.25E-09
DDIT3	0.79	8.52E-05
DDIT4	0.99	1.05E-05
GARS	0.62	1.34E-06
MARS	0.56	9.53E-07
MTHFD2	0.70	2.87E-07
PCK2	0.61	2.19E-05
PHGDH	0.39	3.64E-03
PMAIP1	1.06	1.47E-05
PSAT1	0.88	1.95E-07
PSPH	0.64	8.94E-05
SLC1A4	0.60	2.93E-06
SLC1A5	0.61	8.25E-07
SLC6A9	1.81	5.46E-04
SLC7A11	1.28	1.60E-09
TARS	0.37	4.61E-05
TRIB3	1.08	2.58E-04
YARS	0.45	5.60E-06

Figure 5.4. DCVC-induced Integrated Stress Response activation following 12 h treatment with DCVC.
Cells were treated with medium alone (control) or 20 μM DCVC for 12 h. **A)** DCVC effect on principle genes and proteins involved in the Integrated Stress Response**. (i)** Graphical representation of gene denoted with *italicized* titles. Boxes represent first quartile, median and third quartile; whiskers represent minimum and maximum log2 RPKM. Data were analyzed as described in the methods section. Psi symbols indicate genes considered differentially expressed: $^{\Psi}$FDR<0.1 and fold-change < -1.5 or >1.5. **(ii)** Graphical representations of selected corresponding protein levels measured by western blotting are denoted with non-italicized titles. Bars represent means ± SEM. Data were analyzed with student t-test. Asterisks indicate significant difference compared to control: *P<0.05. N= 3-4 independent experiment, with 3 replicates per treatment in each experiment. **(iii)** Representative western blot images. **B)** ATF4 transcription factor gene targets: **(i)** metabolism, **(ii),** redox balance, **(iii)** amino acid transport, **(iv)** amino acid biosynthesis, and **(v)** cell death. **C)** Table of individual ATF4 gene targets with corresponding log2 fold change and FDR.

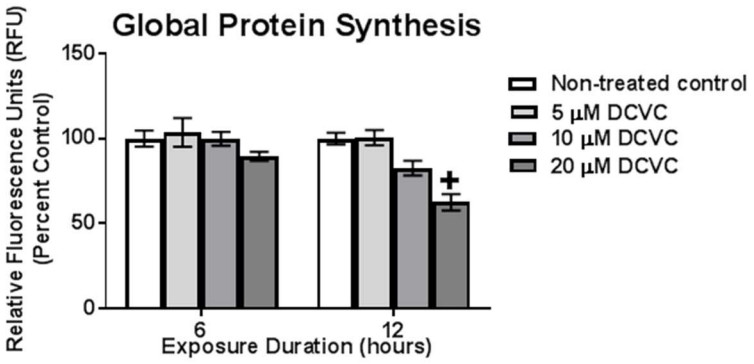

Figure 5.5. DCVC effects on protein synthesis.
Cells were treated with medium alone (control) or DCVC (10 or 20 μM) for 6 or 12 h. Protein synthesis was measured with O-propargyl-puromycin (OPP) and 5 FAM-azide fluorescent staining quantified by plate reader. Bars represent means ± SEM. Data were analyzed by two-way ANOVA (interaction between time and treatment, $P<0.0467$) with posthoc Tukey multiple comparisons. Plus sign indicates significant difference compared to control and 5 μM DCVC within same time point: $^{+}P<0.02$. N= 3 independent experiments for each time point, with 4 replicates per treatment in each experiment.

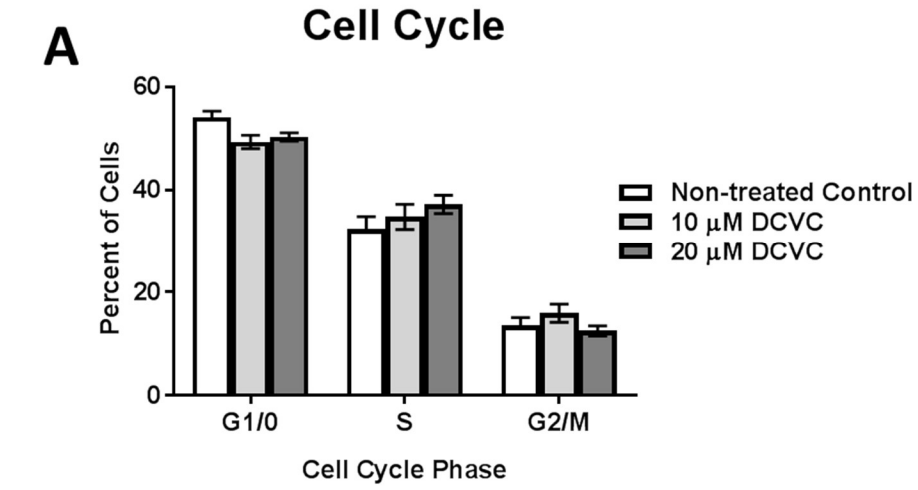

Treatment	Cell Cycle Phase		
	G1/0	S	G2/M
No Treatment	54.11%	32.35%	13.54%
10 µM DCVC	49.32%	34.78%	15.91%
10 µM DCVC	50.30%	37.20%	12.50%

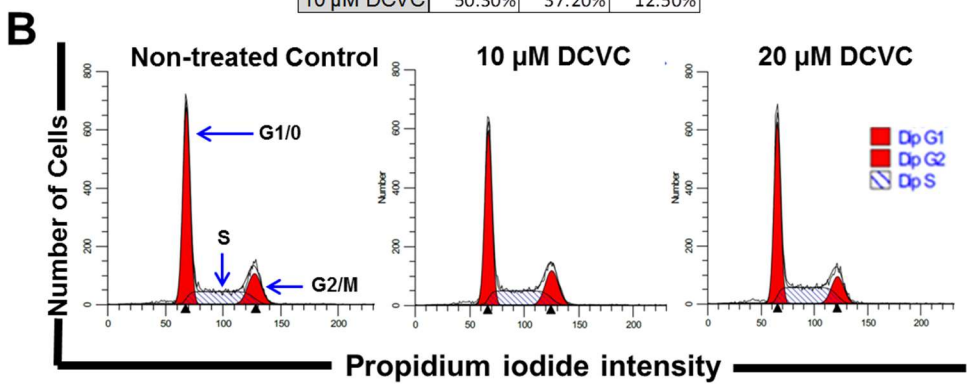

Figure 5.6. Effects of DCVC on cell cycle progression.
Cells were treated with medium alone (control) or DCVC (10 or 20 µM) for 12 h. The percentage of cells in each phase of the cell cycle was determined by propidium iodide staining and flow cytometry as described in the methods section. A) Graphical representation of cell cycle phase distribution. B) Representative cell cycle distribution histograms generated by flow cytometry and table showing percentage of cells in each phase per treatment group. Dark red represents G1/0 phase, stripes represent S phase and light red represents G2/0 phase. Bars represent means ± SEM. Data were analyzed by one-way ANOVA (no significant interaction) with posthoc Tukey's multiple comparisons. N= 3 independent experiments.

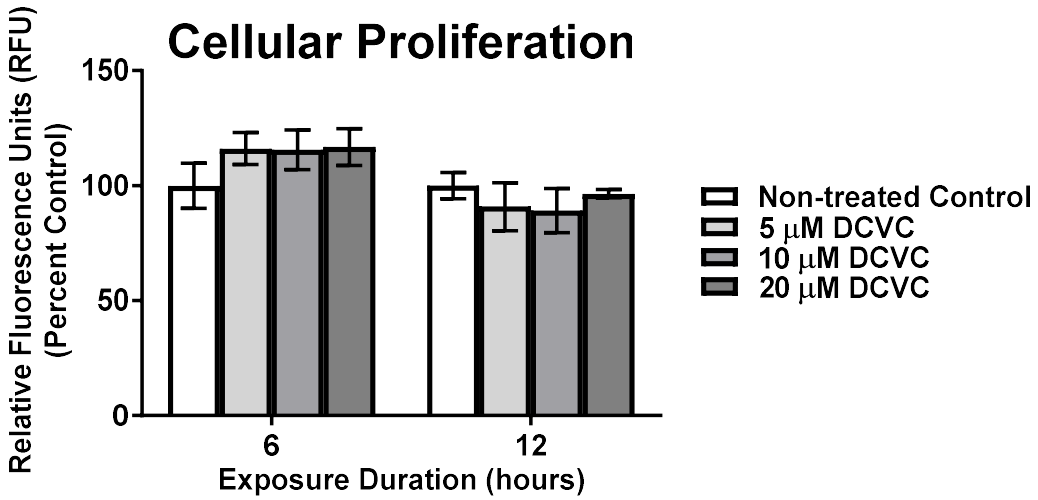

Figure 5.7. Effects of DCVC on cellular proliferation.
For cellular proliferation experiments cells were treated with medium alone (control) or DCVC (5, 10 or 20 μM for 6 or 12 h. Cellular proliferation was measured Cyquant fluorescent dye, which binds to nucleic acids. Fluorescence signal, measured by a micro plate reader, is proportional to the number of cells in each well. Bars represent means ± SEM. Proliferation was analyzed by two-way ANOVA (no significant interaction) with posthoc Tukey's multiple comparisons. N= 3 independent experiments for each time point, with 5 replicates per treatment in each experiment.

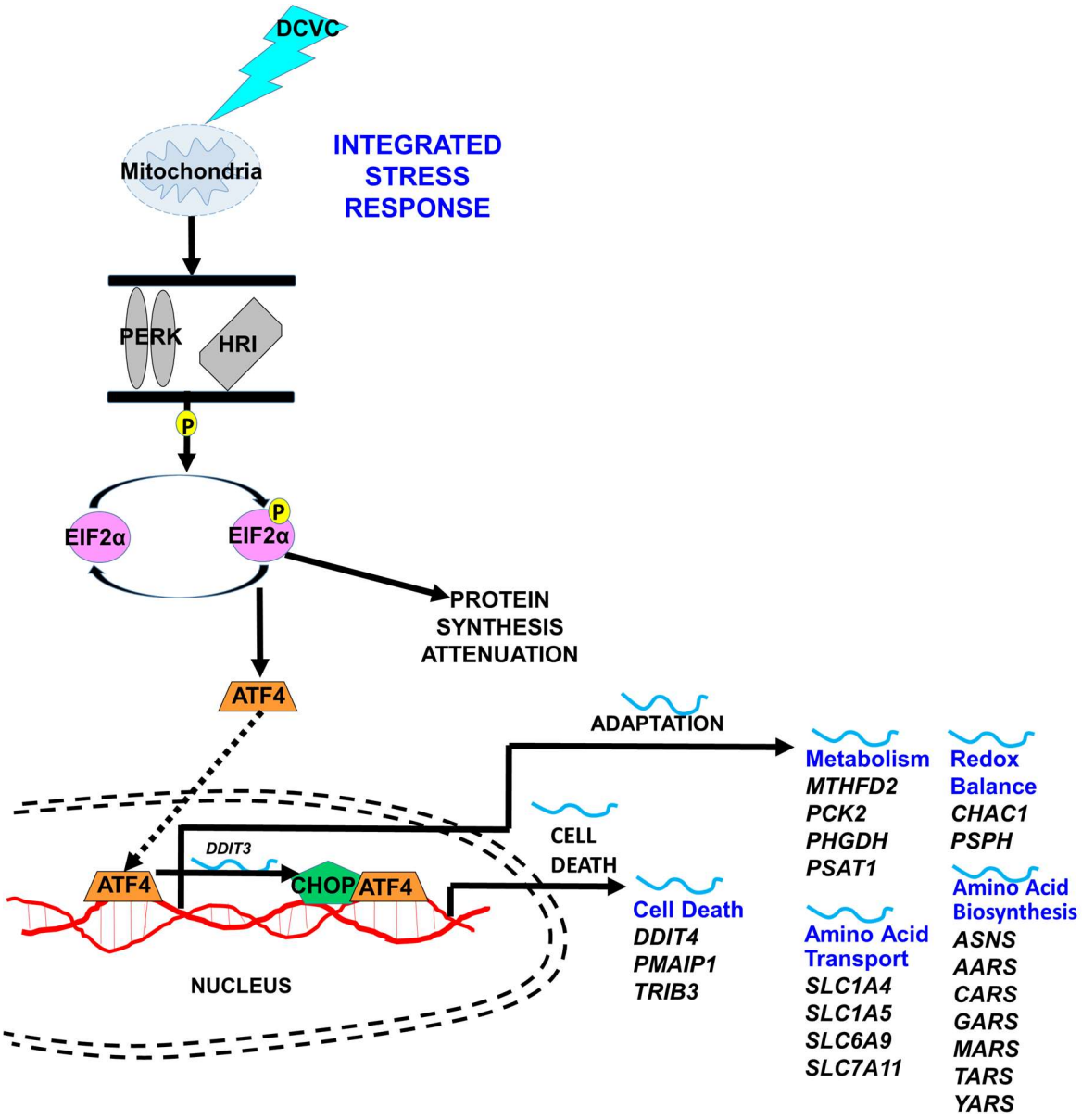

Figure 5.8. Summary of DCVC-induced activation of the Integrated Stress Response. DCVC-induced mitochondrial dysfunction activates one or more of the EIF2α kinases. Kinase(s) phosphorylate EIF2α. Phosphorylated EIF2α activates transcription and translation of ATF4 and causes global protein attenuation. ATF4 transcription factor up-regulates many genes involved in biological processes necessary to restore homeostasis. ATF4 also up-regulates transcription factor CHOP, which then interacts with ATF4 to activate transcription of genes involved in cell death signaling.

References

Andrews S. 2010. Fastqc: A quality control tool for high throughput sequence data. Available: http://www.bioinformatics.babraham.ac.uk/projects/fastqc

[accessed 2/27/19.

ATCC. 2015. Atcc product sheet: Htr8/svneo (atcc® crl3271™).American Type Culture Collection.

ATSDR. 2016. Public health statement on trichloroethylene.Agency for Toxic Substances and Disease Registry.

Bao X.R., Ong S.E., Goldberger O., Peng J., Sharma R., Thompson D.A., et al. 2016. Mitochondrial dysfunction remodels one-carbon metabolism in human cells. *Elife.* **5**.

Benjamini Y., Hochberg Y. 1995. Controlling the false discovery rate: A practical and powerful approach to multiple testing. *Journal of the Royal Statistical Society Series B (Methodological).* **57**:289– 300.

Brosens I.A., Robertson W.B., Dixon H.G. 1972. The role of the spiral arteries in the pathogenesis of preeclampsia. *Obstet Gynecol Annu.* **1**:177-191.

Bukowski J. 2014. Critical review of the epidemiologic literature regarding the association between congenital heart defects and exposure to trichloroethylene. *Critical reviews in toxicology.* **44**:581-589.

Burton G.J., Fowden A.L. 2015. The placenta: A multifaceted, transient organ. *Philos Trans R Soc Lond B Biol Sci.* **370**:20140066.

Caniggia I., Grisaru-Gravnosky S., Kuliszewsky M., Post M., Lye S.J. 1999. Inhibition of tgf-beta 3 restores the invasive capability of extravillous trophoblasts in preeclamptic pregnancies. *J Clin Invest.* **103**:1641-1650.

Carney E.W., Thorsrud B.A., Dugard P.H., Zablotny C.L. 2006. Developmental toxicity studies in crl:Cd (sd) rats following inhalation exposure to trichloroethylene and perchloroethylene. *Birth Defects Res B Dev Reprod Toxicol.* **77**:405-412.

Caruso M., Evangelista M., Parolini O. 2012. Human term placental cells: Phenotype, properties and new avenues in regenerative medicine. *Int J Mol Cell Med.* **1**:64-74.

Chen Y., Cai J., Anders M.W., Stevens J.L., Jones D.P. 2001. Role of mitochondrial dysfunction in s-(1,2-dichlorovinyl)-l-cysteine-induced apoptosis. *Toxicol Appl Pharmacol.* **170**:172-180.

Chiu W.A., Jinot J., Scott C.S., Makris S.L., Cooper G.S., Dzubow R.C., et al. 2013. Human health effects of trichloroethylene: Key findings and scientific issues. *Environ Health Perspect.* **121**:303-311.

Davies E.L., Bell J.S., Bhattacharya S. 2016. Preeclampsia and preterm delivery: A population-based case-control study. *Hypertens Pregnancy.* **35**:510-519.

Dobin A., Davis C.A., Schlesinger F., Drenkow J., Zaleski C., Jha S., et al. 2013. Star: Ultrafast universal rna-seq aligner. *Bioinformatics.* **29**:15-21.

Du L., He F., Kuang L., Tang W., Li Y., Chen D. 2017. Enos/inos and endoplasmic reticulum stress-induced apoptosis in the placentas of patients with preeclampsia. *J Hum Hypertens.* **31**:49-55.

Elkin E.R., Harris S.M., Loch-Caruso R. 2018. Trichloroethylene metabolite s-(1,2-dichlorovinyl)-l-cysteine induces lipid peroxidation-associated apoptosis via the intrinsic and extrinsic apoptosis pathways in a first-trimester placental cell line. *Toxicol Appl Pharmacol.* **338**:30-42.

EPA. 2017. Tri explorer: Release trends report.Environmental Protection Agency.

EPA. 2018. National priorities list.

Fisher J.W., Channel S.R., Eggers J.S., Johnson P.D., MacMahon K.L., Goodyear C.D., et al. 2001. Trichloroethylene, trichloroacetic acid, and dichloroacetic acid: Do they affect fetal rat heart development? *Int J Toxicol.* **20**:257-267.

Forand S.P., Lewis-Michl E.L., Gomez M.I. 2012. Adverse birth outcomes and maternal exposure to trichloroethylene and tetrachloroethylene through soil vapor intrusion in new york state. *Environ Health Perspect.* **120**:616-621.

Fu J., Zhao L., Wang L., Zhu X. 2015. Expression of markers of endoplasmic reticulum stress-induced apoptosis in the placenta of women with early and late onset severe pre-eclampsia. *Taiwan J Obstet Gynecol.* **54**:19-23.

Goodman D.R., James R.C., Harbison R.D. 1982. Placental toxicology. *Food Chem Toxicol.* **20**:123-128.

Graham C.H., Hawley T.S., Hawley R.G., MacDougall J.R., Kerbel R.S., Khoo N., et al. 1993. Establishment and characterization of first trimester human trophoblast cells with extended lifespan. *Experimental cell research.* **206**:204-211.

Guha N., Loomis D., Grosse Y., Lauby-Secretan B., El Ghissassi F., Bouvard V., et al. 2012. Carcinogenicity of trichloroethylene, tetrachloroethylene, some other chlorinated solvents, and their metabolites. *Lancet Oncol.* **13**:1192-1193.

Hai T.W., Liu F., Coukos W.J., Green M.R. 1989. Transcription factor atf cdna clones: An extensive family of leucine zipper proteins able to selectively form DNA-binding heterodimers. *Genes Dev.* **3**:2083-2090.

Han J., Back S.H., Hur J., Lin Y.H., Gildersleeve R., Shan J., et al. 2013. Er-stress-induced transcriptional regulation increases protein synthesis leading to cell death. *Nat Cell Biol.* **15**:481-490.

Hassan I., Kumar A.M., Park H.R., Lash L.H., Loch-Caruso R. 2016. Reactive oxygen stimulation of interleukin-6 release in the human trophoblast cell line htr-8/svneo by the trichlorethylene metabolite s-(1,2-dichloro)-l-cysteine. *Biology of reproduction.* **95**:66.

Ilekis J.V., Tsilou E., Fisher S., Abrahams V.M., Soares M.J., Cross J.C., et al. 2016. Placental origins of adverse pregnancy outcomes: Potential molecular targets: An executive workshop summary of the eunice kennedy shriver national institute of child health and human development. *Am J Obstet Gynecol.* **215**:S1-S46.

Johnson P.D., Goldberg S.J., Mays M.Z., Dawson B.V. 2003. Threshold of trichloroethylene contamination in maternal drinking waters affecting fetal heart development in the rat. *Environ Health Perspect.* **111**:289-292.

Kadyrov M., Kingdom J.C., Huppertz B. 2006. Divergent trophoblast invasion and apoptosis in placental bed spiral arteries from pregnancies complicated by maternal anemia and early-onset preeclampsia/intrauterine growth restriction. *Am J Obstet Gynecol.* **194**:557-563.

Laham S. 1970. Studies on placental transfer. Trichlorethylene. *IMS Ind Med Surg.* **39**:46-49.

Lash L.H., Anders M.W. 1987. Mechanism of s-(1,2-dichlorovinyl)-l-cysteine- and s-(1,2-dichlorovinyl)-l-homocysteine-induced renal mitochondrial toxicity. *Molecular pharmacology.* **32**:549-556.

Lash L.H., Putt D.A., Brashear W.T., Abbas R., Parker J.C., Fisher J.W. 1999. Identification of s-(1,2-dichlorovinyl)glutathione in the blood of human volunteers exposed to trichloroethylene. *J Toxicol Environ Health A.* **56**:1-21.

Lash L.H., Fisher J.W., Lipscomb J.C., Parker J.C. 2000. Metabolism of trichloroethylene. *Environ Health Perspect.* **108 Suppl 2**:177-200.

Lash L.H., Putt D.A., Hueni S.E., Krause R.J., Elfarra A.A. 2003. Roles of necrosis, apoptosis, and mitochondrial dysfunction in s-(1,2-dichlorovinyl)-l-cysteine sulfoxide-induced cytotoxicity in primary cultures of human renal proximal tubular cells. *J Pharmacol Exp Ther.* **305**:1163-1172.

Lash L.H., Chiu W.A., Guyton K.Z., Rusyn I. 2014. Trichloroethylene biotransformation and its role in mutagenicity, carcinogenicity and target organ toxicity. *Mutat Res Rev Mutat Res.* **762**:22-36.

Liao Y., Smyth G.K., Shi W. 2014. Featurecounts: An efficient general purpose program for assigning sequence reads to genomic features. *Bioinformatics.* **30**:923-930.

Loch-Caruso R., Hassan I., Harris S.M., Kumar A., Bjork F., Lash L.H. 2018. Trichloroethylene exposure in mid-pregnancy decreased fetal weight and increased placental markers of oxidative stress in rats. *Reprod Toxicol.* **83**:38-45.

Lun A.T., Chen Y., Smyth G.K. 2016. It's de-licious: A recipe for differential expression analyses of rna-seq experiments using quasi-likelihood methods in edger. *Methods Mol Biol.* **1418**:391-416.

Makris S.L., Scott C.S., Fox J., Knudsen T.B., Hotchkiss A.K., Arzuaga X., et al. 2016. A systematic evaluation of the potential effects of trichloroethylene exposure on cardiac development. *Reprod Toxicol.* **65**:321-358.

March of Dimes P., Save the Children, WHO. 2012. Born too soon: The global action report on preterm birth. Geneva:World Health Organization.

McKinney L.L., Picken Jr. J.C., Weakley F.B., Eldridge A.C., Campbell R.E., Cowan J.C., et al. 1959. Possible toxic factor of trichloroethylene-extracted soybean oil meal3. *Journal of the American Chemical Society.* **81**:909-915.

Meekins J.W., Pijnenborg R., Hanssens M., McFadyen I.R., van Asshe A. 1994. A study of placental bed spiral arteries and trophoblast invasion in normal and severe pre-eclamptic pregnancies. *Br J Obstet Gynaecol.* **101**:669-674.

Mizuuchi M., Cindrova-Davies T., Olovsson M., Charnock-Jones D.S., Burton G.J., Yung H.W. 2016. Placental endoplasmic reticulum stress negatively regulates transcription of placental growth factor via atf4 and atf6beta: Implications for the pathophysiology of human pregnancy complications. *J Pathol.* **238**:550-561.

Mohun T., Adams D.J., Baldock R., Bhattacharya S., Copp A.J., Hemberger M., et al. 2013. Deciphering the mechanisms of developmental disorders (dmdd): A new programme for phenotyping embryonic lethal mice. *Dis Model Mech.* **6**:562-566.

Mootha V.K., Lindgren C.M., Eriksson K.F., Subramanian A., Sihag S., Lehar J., et al. 2003. Pgc-1alpha-responsive genes involved in oxidative phosphorylation are coordinately downregulated in human diabetes. *Nat Genet.* **34**:267-273.

Morgan T. 2014. Placental insufficiency is a leading cause of preterm labor. *NewReviews.* **15**:5618-e5525.

Nijman T.A., van Vliet E.O., Benders M.J., Mol B.W., Franx A., Nikkels P.G., et al. 2016. Placental histology in spontaneous and indicated preterm birth: A case control study. *Placenta.* **48**:56-62.

NTP. 2015. Monograph on trichloroethylene Available: https://ntp.niehs.nih.gov/ntp/roc/monographs/finaltce_508.pdf 2016].

Oshvandi K., Jadidi A., Dehvan F., Shobeiri F., Cheraghi F., Sangestani G., et al. 2018. Relationship between pregnancy-induced hypertension with neonatal and maternal complications. *International Journal of Pediatrics.* **6**:8587-8594.

Pakos-Zebrucka K., Koryga I., Mnich K., Ljujic M., Samali A., Gorman A.M. 2016. The integrated stress response. *EMBO Rep.* **17**:1374-1395.

Quiros P.M., Prado M.A., Zamboni N., D'Amico D., Williams R.W., Finley D., et al. 2017. Multi-omics analysis identifies atf4 as a key regulator of the mitochondrial stress response in mammals. *J Cell Biol.* **216**:2027-2045.

Robinson M.D., McCarthy D.J., Smyth G.K. 2010. Edger: A bioconductor package for differential expression analysis of digital gene expression data. *Bioinformatics.* **26**:139-140.

Robinson M.D., Oshlack A. 2010. A scaling normalization method for differential expression analysis of rna-seq data. *Genome Biol.* **11**:R25.

Ruckart P.Z., Bove F.J., Maslia M. 2014. Evaluation of contaminated drinking water and preterm birth, small for gestational age, and birth weight at marine corps base camp lejeune, north carolina: A cross-sectional study. *Environ Health.* **13**:99.

Rufer E.S., Hacker T.A., Flentke G.R., Drake V.J., Brody M.J., Lough J., et al. 2010. Altered cardiac function and ventricular septal defect in avian embryos exposed to low-dose trichloroethylene. *Toxicol Sci.* **113**:444-452.

Shpilka T., Haynes C.M. 2018. The mitochondrial upr: Mechanisms, physiological functions and implications in ageing. *Nat Rev Mol Cell Biol.* **19**:109-120.

Subramanian A., Tamayo P., Mootha V.K., Mukherjee S., Ebert B.L., Gillette M.A., et al. 2005. Gene set enrichment analysis: A knowledge-based approach for interpreting genome-wide expression profiles. *Proceedings of the National Academy of Sciences of the United States of America.* **102**:15545-15550.

Tetz L.M., Cheng A.A., Korte C.S., Giese R.W., Wang P., Harris C., et al. 2013. Mono-2-ethylhexyl phthalate induces oxidative stress responses in human placental cells in vitro. *Toxicol Appl Pharmacol.* **268**:47-54.

Tsujimoto A., Nyunoya H., Morita T., Sato T., Shimotohno K. 1991. Isolation of cdnas for DNA-binding proteins which specifically bind to a tax-responsive enhancer element in the long terminal repeat of human t-cell leukemia virus type i. *J Virol.* **65**:1420-1426.

van de Water B., Zoetewey J.P., de Bont H.J., Mulder G.J., Nagelkerke J.F. 1993. The relationship between intracellular ca2+ and the mitochondrial membrane potential in isolated proximal tubular cells from rat kidney exposed to the nephrotoxin 1,2-dichlorovinyl-cysteine. *Biochem Pharmacol.* **45**:2259-2267.

van de Water B., Zoeteweij J.P., de Bont H.J., Mulder G.J., Nagelkerke J.F. 1994. Role of mitochondrial ca2+ in the oxidative stress-induced dissipation of the mitochondrial membrane

potential. Studies in isolated proximal tubular cells using the nephrotoxin 1,2-dichlorovinyl-l-cysteine. *J Biol Chem.* **269**:14546-14552.

Walter P., Ron D. 2011. The unfolded protein response: From stress pathway to homeostatic regulation. *Science.* **334**:1081-1086.

Waters E.M., Gerstner H.B., Huff J.E. 1977. Trichloroethylene. I. An overview. *J Toxicol Environ Health.* **2**:671-707.

Watson R.E., Jacobson C.F., Williams A.L., Howard W.B., DeSesso J.M. 2006. Trichloroethylene-contaminated drinking water and congenital heart defects: A critical analysis of the literature. *Reprod Toxicol.* **21**:117-147.

Woods L., Perez-Garcia V., Hemberger M. 2018. Regulation of placental development and its impact on fetal growth-new insights from mouse models. *Front Endocrinol (Lausanne).* **9**:570.

Wortel I.M.N., van der Meer L.T., Kilberg M.S., van Leeuwen F.N. 2017. Surviving stress: Modulation of atf4-mediated stress responses in normal and malignant cells. *Trends Endocrinol Metab.* **28**:794-806.

Xu F., Papanayotou I., Putt D.A., Wang J., Lash L.H. 2008. Role of mitochondrial dysfunction in cellular responses to s-(1,2-dichlorovinyl)-l-cysteine in primary cultures of human proximal tubular cells. *Biochem Pharmacol.* **76**:552-567.

Yung H.W., Calabrese S., Hynx D., Hemmings B.A., Cetin I., Charnock-Jones D.S., et al. 2008. Evidence of placental translation inhibition and endoplasmic reticulum stress in the etiology of human intrauterine growth restriction. *Am J Pathol.* **173**:451-462.

Chapter VI. Conclusions

Maternal exposure to TCE, an industrial solvent and pervasive environmental contaminant, has been associated with increased risk of low birth weight and preterm birth in recent epidemiology studies (Forand et al. 2012; Ruckart et al. 2014). Moreover, our laboratory recently reported decreased fetal weight and placental changes in rats exposed to TCE at a non-toxic maternal dose (Loch-Caruso et al. 2018). Placental toxicity resulting in placental insufficiency may contribute to adverse birth outcomes due to the placenta's critical role during gestation. In order to demonstrate the biological plausibility of trichloroethylene-associated placental injury, this thesis investigated effects of the trichloroethylene metabolite *S*-(1, 2-dichlorovinyl)-L-cysteine (DCVC) on extravillous trophoblasts, specific cells that play a pivotal role in tissue and maternal spiral artery remodeling during placental development. Findings revealed the sequence of DCVC-placental cell interactions resulting in compensatory and ultimately pathogenic cellular responses to short-term DCVC exposure and implicate a central role for mitochondria in DCVC-induced toxicity to placental cells, with potential implications for untoward pregnancy disorders.

Our laboratory previously reported that DCVC decreased cell viability and increased cytotoxicity in human placental cells using the HTR-8/SVneo cell line as a model for extravillous trophoblasts (Hassan et al. 2016). Here, we extended those findings by showing that DCVC treatment stimulated concentration-dependent apoptosis, a specific form of cell death, in HTR-8/SVneo cells (Chapter 2). The results further indicated for the first time that DCVC

simultaneously activated the mitochondrial-mediated (intrinsic) and cell surface receptor-mediated (extrinsic) apoptotic pathways, most likely via co-regulatory p53 signaling. Moreover, mitochondria-centered crosstalk between the two activated pathways appeared to amplify the effect on the overall apoptotic response, suggesting a regulatory role for mitochondria in the fate of cells treated with DCVC. These results are important because aberrant trophoblast apoptosis is linked to placental structural abnormalities commonly observed in early-onset pregnancy complications such as pre-eclampsia and intrauterine growth restriction (DiFederico et al. 1999; Genbacev et al. 1999; Reister et al. 2001). Therefore, DCVC-induced apoptosis in extravillous trophoblasts could be a mechanism by which TCE contributes to abnormal placental development.

Consistent with previous studies (Chen et al. 1990; Chen et al. 2001; Lash and Anders 1986; Lash et al. 2003; van de Water et al. 1994; van de Water et al. 1995; Xu et al. 2008), this thesis presented ample evidence that mitochondria are intracellular targets of DCVC toxicity in placental cells. In addition to mitochondrial-mediated apoptotic signaling (Chapter 2), DCVC altered various aspects of mitochondrial respiration that were amongst the earliest and most persistent of any other DCVC treatment effects (Chapter 4). Furthermore, the evidence suggests that DCVC-induced mitochondrial changes were predominantly adaptive after 6 h of exposure, whereas, changes after 12 h were largely pathogenic. Specifically, after DCVC treatment for 6 h, mitochondrial respiration increased accompanied by decreased spare respiration with unchanged maximum respiration, suggesting that cells were operating close to their bioenergetic limits while compensating for mitochondrial impairment. By 12 h of DCVC exposure, additional deleterious mitochondrial perturbations were detected including decreased basal OCR and dissipation of mitochondrial membrane potential, indicating a substantial decline in

mitochondrial function. These findings demonstrated compensatory and subsequently pathological changes in the mitochondria, ultimately revealing time-dependent progressive defects in mitochondrial function caused by DCVC exposure. Taken together, the evidence suggests that mitochondria are not only regulators of cell death, but significant intracellular targets for DCVC-mediated cytotoxicity in placental cells.

Previously, our laboratory reported that DCVC caused aberrant reactive oxygen species (ROS) generation in HTR-8/SVneo cells (Hassan et al. 2016). Typically, ROS generation subsequently causes lipid peroxidation (Ayala et al. 2014), which plays a key role in placental pathophysiology (Biri et al. 2007; Karowicz-Bilinska et al. 2007) and in DCVC-induced renal tubular cell toxicity (Beuter et al. 1989; Chen et al. 1990; Groves et al. 1991) by damaging cellular membranes (Stark 2005). Here, because the antioxidant (±)-α-tocopherol had no significant effect on DCVC-induced mitochondrial respiration perturbations (Chapter 4), but rescued DCVC-induced mitochondrial membrane depolarization (Chapter 4) and caspase 3+7 activation (Chapter 2), lipid peroxidation likely does not initiate mitochondrial impairment but may contribute to progressive mitochondrial decline and subsequent apoptosis. Although not directly tested, one possible explanation is that DCVC effects on mitochondrial respiration induce lipid peroxidation which, in turn, further injures the mitochondria resulting in membrane depolarization and elevated caspase 3+7 activity: that is, a scenario in which mitochondria serves as both a source and target of ROS-mediated lipid peroxidation (Zorov et al. 2000; Zorov et al. 2014). These results contribute to defining the specific role of lipid peroxidation in DCVC-induced extravillous trophoblast toxicity. However, further studies are needed for clarification and direct confirmation.

The novel assessment of cellular energy status and metabolism using targeted metabolomics revealed that DCVC treatment for 6 and 12 h altered glucose metabolism and macronutrient metabolite concentrations while maintaining adequate ATP levels in the HTR-8/SVneo cells. Because cellular ATP concentrations did not change, these results suggest an adaptive energy metabolism response to DCVC. Through evaluation of changes to intracellular metabolite concentrations and subsequent calculation of metabolite ratios, we presented evidence of a time-dependent accumulation of G6P+F6P and independent shunting of G6P+F6P directed to the pentose phosphate (PPP) and hexosamine biosynthesis (HBP) pathways that diminished with time. Furthermore, downstream glycolysis and tricarboxylic cycle (TCA) were largely unchanged with DCVC treatment, while glycerol intermediates, lipid and amino acid concentrations were elevated. These latter results suggest that DCVC stimulated compensatory utilization of alternative macronutrients to provide intermediate substrates entering downstream in the glycolytic pathway or in the TCA cycle, neither of which were altered. Although more investigation is needed to elucidate the relationships between the changes observed in various pathways, the findings suggest consequential changes to multiple interconnected bioenergetics pathways in response to DCVC treatment.

Although exposure to DCVC decreased the ratio of intracellular concentrations of ATP:ADP, indicating an energy status decline, no overall changes to ATP intracellular concentrations nor activation of the AMPK energy stress pathway were observed. These observations suggest successful energy-related compensation by the HTR-8/SVneo cells to DCVC treatment in our experimental conditions. Nonetheless, the decline in ATP:ADP ratio may be important because a previous study reported a decreased ATP:ADP ratio and subsequent increased susceptibility to apoptosis in cytotrophoblasts isolated from placentae of term

pregnancies complicated with IUGR (Crocker et al. 2003). Thus, although not directly tested, the DCVC-induced changes in the ATP:ADP ratio reported here may serve as early indicators and subsequent regulators of cell fate associated abnormal placental growth, as observed in IUGR.

Genome-wide transcriptomic and gene set enrichment analyses revealed DCVC-induced activation of the EIF2α/ATF4-mediated integrated stress response (ISR), as validated by EIF2α phosphorylation, elevated ATF4 protein levels, and differential gene expression of many ATF4 targets in HTR-8/SVneo cells. Although not directly tested, the ISR was likely stimulated by mitochondrial impairment (Quiros et al. 2017; Shpilka and Haynes 2018). We observed evidence of ISR pro-survival and pro-apoptotic signaling, based on the differential gene expression of multiple ATF4- regulated genes following 12 h of DCVC treatment. However, overall cell cycle progression and proliferation did not significantly change in response to DCVC exposure. These findings suggest that short-duration treatment with DCVC caused both adaptive and pathological processes, consistent with other findings in this thesis (Chapters 3 and 4), but largely without concomitant changes to cell cycle progression or cellular proliferation. The ISR signaling components activated in our study have been implicated in pregnancy disorders characterized by placental abnormalities. Specifically, two separate studies detected elevated phosphorylation of EIF2α (indicative of activation) and increased protein levels of ATF4 and/or CHOP in placental tissue from pre-eclamptic pregnancies compared to normal pregnancies (Du et al. 2017; Fu et al. 2015). Furthermore, prolonged EIF2α phosphorylation decreased proliferation and invasion of trophoblast cells *in vitro* (Yung et al. 2008), consistent with defining pathological characteristics of placentae from interuterine growth restriction and pre-eclampsia (Brosens et al. 1972; Caniggia et al. 1999; Kadyrov et al. 2006; Meekins et al. 1994). Consequently, ISR activation in trophoblasts may be a mechanism by which the DCVC contributes to placental dysfunction.

While contributing important new information on the effects of DCVC on trophoblasts, we readily acknowledge that our studies have some limitations. First, the *in vitro* cultured cells used in our study lack cell signaling and tissue interactions that would otherwise be present in *ex vivo* tissue models and *in vivo*. In addition, the cells used in our studies to model extravillous trophoblasts, HTR-8/SVneo, are an immortalized cell line. Even though HTR-8/SVneo were originally derived from first-trimester non-cancerous placental cells, the process of immortalization alters cells genetically to allow them to be cultured for longer periods of time than would be possible otherwise (Graham et al. 1993). Moreover, cell culture conditions may be responsible for reported changes in the genetic and epigenetic profiles of HTR-8/SVneo cells (Bilban et al. 2010; Novakovic et al. 2011). Despite these drawbacks, the HTR-8/SVneo cells retain a combination of distinctive molecular markers that are unique to extravillous trophoblasts such as cytokeratin 7 (CK7), and histocompatibility antigen, class I, G (HLA-G) (when grown on Matrigel) (Irving et al. 1995; Khan et al. 2011; Kilburn et al. 2000; Takao et al. 2011), and functional characteristics such as an invasive phenotype, (Hannan et al. 2010; Kilburn et al. 2000; Liu et al. 2016; Szklanna et al. 2017). Nevertheless, studies conducted in different models are needed to further validate our work.

Utilizing the information presented throughout this thesis, here we propose an integrated model depicting the sequence of DCVC-placental cell interactions resulting in compensatory and ultimately pathogenic cellular responses to short-term DCVC-exposure (Fig 6.1). Between 6 and 12 h of DCVC exposure to HTR-8/SVneo cells, compensatory responses including altered macronutrient and energy metabolism pathway utilization, along with elevated mitochondrial respiration, together, maintained consistent intracellular ATP concentrations. Subsequently, a transition period occurred between 12 and 24 h-post DCVC exposure in which pathogenic

responses were observed, despite ongoing compensatory activities undertaken by the cells. For example, intrinsic and extrinsic apoptotic molecular signaling began, accompanied by depressed mitochondrial respiration and lipid peroxidation-mediated mitochondrial membrane depolarization, all despite continuing energy metabolism and ISR compensatory responses. Ultimately, apoptosis occurred after 24 h of DCVC exposure, likely following failed compensatory mechanisms in the cells. Collectively, the research detailed in this thesis revealed compensatory strategies used by HTR-8/SVneo cells to adjust to DCVC exposure and the eventual pathogenic decline of the cells resulting in cell death.

In summary, the series of studies presented in this thesis utilized a first-trimester trophoblast cell line, HTR-8/SVneo, to investigate cellular responses to the TCE metabolite DCVC, ultimately contributing novel evidence to our understanding of the toxicological mechanisms. Notably, our innovative transcriptomics and targeted metabolomics analyses afforded the opportunity to simultaneously evaluate the effects of DCVC on genome-wide gene expression and multiple energy metabolism pathways. These experiments demonstrated significant alterations to energy metabolism and activation of ISR signaling, stimulated largely by adaptive cellular responses to DCVC at low concentrations and early time points. However, DCVC also disrupted mitochondrial respiration, mitochondrial membrane potential, and mitochondrial-centered apoptotic signaling. Furthermore, we established a potential role for lipid peroxidation in DCVC-induced toxicity. Taken together, the findings suggest that the mitochondria are both intracellular targets of DCVC toxicity and regulators of cell fate. Most importantly, this thesis identified potential mechanisms of DCVC-mediated trichloroethylene toxicity that provide plausible biological explanations for prior epidemiology findings associating TCE exposure with pregnancy complications and adverse birth outcomes.

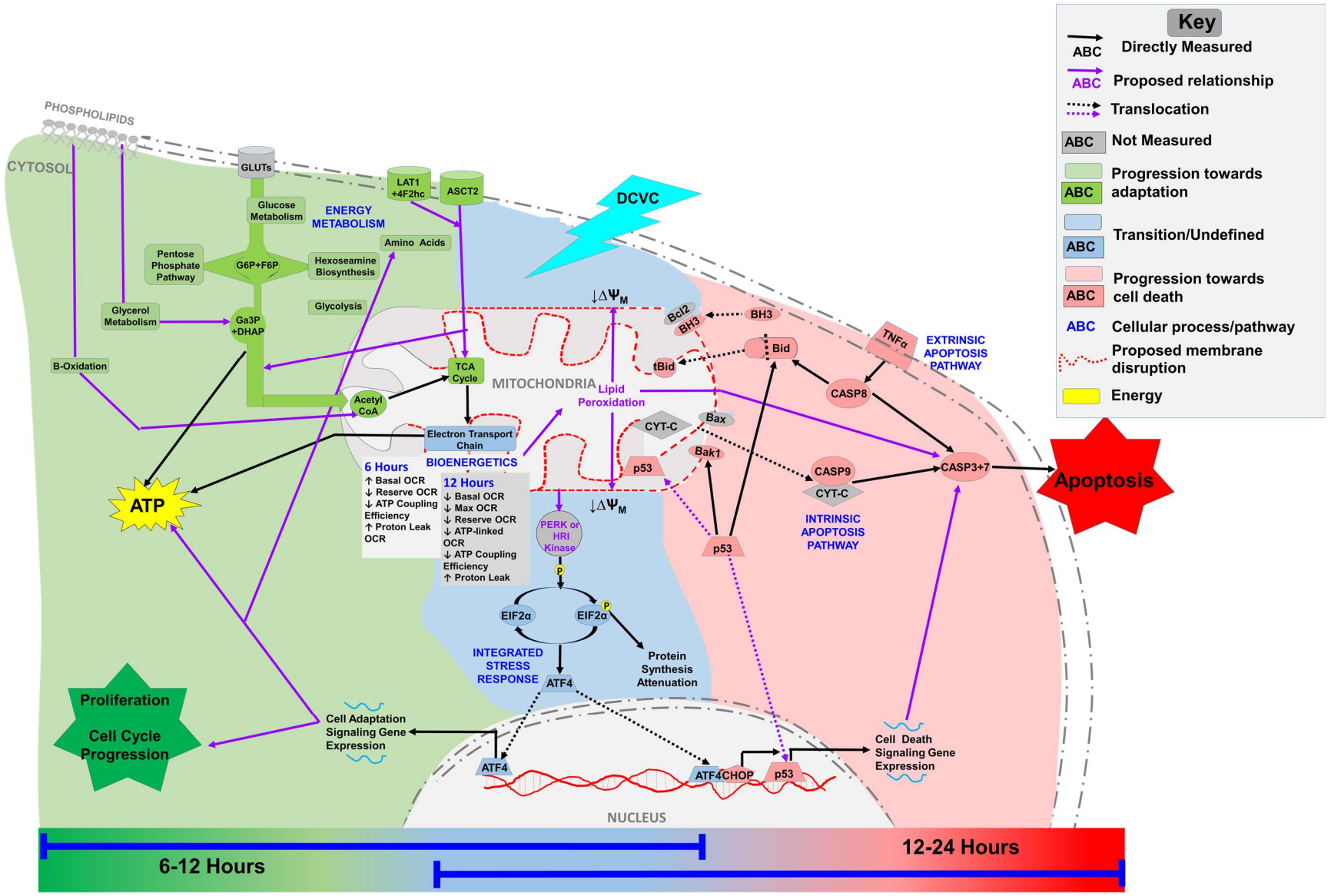
Key
Directly Measured
Proposed relationship
Translocation
Not Measured
Progression towards adaptation
Transition/Undefined
Progression towards cell death
Cellular process/pathway
Proposed membrane disruption
Energy
PHOSPHOLIPIDS
CYTOSOL
GLUTs
LAT1 +4F2hc
ASCT2
DCVC
Glucose Metabolism
ENERGY METABOLISM
Amino Acids
Pentose Phosphate Pathway
G6P+F6P
Hexoseamine Biosynthesis
Glycolysis
Glycerol Metabolism
Ga3P +DHAP
B-Oxidation
TCA Cycle
Acetyl CoA
MITOCHONDRIA
Lipid Peroxidation
Electron Transport Chain
BIOENERGETICS
ATP
6 Hours
↑ Basal OCR
↓ Reserve OCR
↓ ATP Coupling Efficiency
↑ Proton Leak OCR
12 Hours
↓ Basal OCR
↓ Max OCR
↓ Reserve OCR
↓ ATP-linked OCR
↓ ATP Coupling Efficiency
↑ Proton Leak
↓ΔΨM
↓ΔΨM
PERK or HRI Kinase
P
EIF2α
EIF2α
P
INTEGRATED STRESS RESPONSE
ATF4
Protein Synthesis Attenuation
Proliferation
Cell Cycle Progression
Cell Adaptation Signaling Gene Expression
ATF4
ATF4CHOP
p53
Cell Death Signaling Gene Expression
NUCLEUS
Bcl2
BH3
BH3
Bid
tBid
TNFα
EXTRINSIC APOPTOSIS PATHWAY
CASP8
CYT-C
Bax
Bak1
p53
CASP9
CYT-C
INTRINSIC APOPTOSIS PATHWAY
p53
CASP3+7
Apoptosis
6-12 Hours
12-24 Hours

Figure 6.1. Integrated model depicting proposed responses to DCVC exposure in HTR-8/SVneo cells.
Integrated scenario of effects of the trichloroethylene metabolite *S*-(1, 2-dichlorovinyl)-L-cysteine (DCVC) on extravillous trophoblasts, specific cells that play a pivotal role in placental development. Generally compensatory responses involving energy metabolism and mitochondrial function occurred between 6 and 12 h of DCVC exposure to HTR-8/SVneo cells, resulting in maintenance of intracellular ATP concentrations (green area). Subsequently, a critical transition period occurred between 12 and 24 h-post exposure in which apoptotic molecular signaling began, accompanied by progressive mitochondrial decline, despite ongoing energy metabolism and ISR compensation (blue area). Then, cell death occurred after 24 h of exposure to DCVC (red area).

References

Ayala A., Munoz M.F., Arguelles S. 2014. Lipid peroxidation: Production, metabolism, and signaling mechanisms of malondialdehyde and 4-hydroxy-2-nonenal. *Oxid Med Cell Longev.* **2014**:360438.

Beuter W., Cojocel C., Muller W., Donaubauer H.H., Mayer D. 1989. Peroxidative damage and nephrotoxicity of dichlorovinylcysteine in mice. *J Appl Toxicol.* **9**:181-186.

Biri A., Bozkurt N., Turp A., Kavutcu M., Himmetoglu O., Durak I. 2007. Role of oxidative stress in intrauterine growth restriction. *Gynecol Obstet Invest.* **64**:187-192.

Brosens I.A., Robertson W.B., Dixon H.G. 1972. The role of the spiral arteries in the pathogenesis of preeclampsia. *Obstet Gynecol Annu.* **1**:177-191.

Caniggia I., Grisaru-Gravnosky S., Kuliszewsky M., Post M., Lye S.J. 1999. Inhibition of tgf-beta 3 restores the invasive capability of extravillous trophoblasts in preeclamptic pregnancies. *J Clin Invest.* **103**:1641-1650.

Chen Q., Jones T.W., Brown P.C., Stevens J.L. 1990. The mechanism of cysteine conjugate cytotoxicity in renal epithelial cells. Covalent binding leads to thiol depletion and lipid peroxidation. *J Biol Chem.* **265**:21603-21611.

Chen Y., Cai J., Anders M.W., Stevens J.L., Jones D.P. 2001. Role of mitochondrial dysfunction in s-(1,2-dichlorovinyl)-l-cysteine-induced apoptosis. *Toxicol Appl Pharmacol.* **170**:172-180.

Crocker I.P., Cooper S., Ong S.C., Baker P.N. 2003. Differences in apoptotic susceptibility of cytotrophoblasts and syncytiotrophoblasts in normal pregnancy to those complicated with preeclampsia and intrauterine growth restriction. *Am J Pathol.* **162**:637-643.

Du L., He F., Kuang L., Tang W., Li Y., Chen D. 2017. Enos/inos and endoplasmic reticulum stress-induced apoptosis in the placentas of patients with preeclampsia. *J Hum Hypertens.* **31**:49-55.

Forand S.P., Lewis-Michl E.L., Gomez M.I. 2012. Adverse birth outcomes and maternal exposure to trichloroethylene and tetrachloroethylene through soil vapor intrusion in new york state. *Environ Health Perspect.* **120**:616-621.

Fu J., Zhao L., Wang L., Zhu X. 2015. Expression of markers of endoplasmic reticulum stress-induced apoptosis in the placenta of women with early and late onset severe pre-eclampsia. *Taiwan J Obstet Gynecol.* **54**:19-23.

Groves C.E., Lock E.A., Schnellmann R.G. 1991. Role of lipid peroxidation in renal proximal tubule cell death induced by haloalkene cysteine conjugates. *Toxicol Appl Pharmacol.* **107**:54-62.

Hannan N.J., Paiva P., Dimitriadis E., Salamonsen L.A. 2010. Models for study of human embryo implantation: Choice of cell lines? *Biology of reproduction.* **82**:235-245.

Hassan I., Kumar A.M., Park H.R., Lash L.H., Loch-Caruso R. 2016. Reactive oxygen stimulation of interleukin-6 release in the human trophoblast cell line htr-8/svneo by the trichlorethylene metabolite s-(1,2-dichloro)-l-cysteine. *Biology of reproduction.* **95**:66.

Irving J.A., Lysiak J.J., Graham C.H., Hearn S., Han V.K., Lala P.K. 1995. Characteristics of trophoblast cells migrating from first trimester chorionic villus explants and propagated in culture. *Placenta.* **16**:413-433.

Kadyrov M., Kingdom J.C., Huppertz B. 2006. Divergent trophoblast invasion and apoptosis in placental bed spiral arteries from pregnancies complicated by maternal anemia and early-onset preeclampsia/intrauterine growth restriction. *Am J Obstet Gynecol.* **194**:557-563.

Karowicz-Bilinska A., Kedziora-Kornatowska K., Bartosz G. 2007. Indices of oxidative stress in pregnancy with fetal growth restriction. *Free Radic Res.* **41**:870-873.

Khan G.A., Girish G.V., Lala N., Di Guglielmo G.M., Lala P.K. 2011. Decorin is a novel vegfr-2-binding antagonist for the human extravillous trophoblast. *Mol Endocrinol.* **25**:1431-1443.

Kilburn B.A., Wang J., Duniec-Dmuchowski Z.M., Leach R.E., Romero R., Armant D.R. 2000. Extracellular matrix composition and hypoxia regulate the expression of hla-g and integrins in a human trophoblast cell line. *Biology of reproduction.* **62**:739-747.

Lash L.H., Anders M.W. 1986. Cytotoxicity of s-(1,2-dichlorovinyl)glutathione and s-(1,2-dichlorovinyl)-l-cysteine in isolated rat kidney cells. *J Biol Chem.* **261**:13076-13081.

Lash L.H., Putt D.A., Hueni S.E., Krause R.J., Elfarra A.A. 2003. Roles of necrosis, apoptosis, and mitochondrial dysfunction in s-(1,2-dichlorovinyl)-l-cysteine sulfoxide-induced cytotoxicity in primary cultures of human renal proximal tubular cells. *J Pharmacol Exp Ther.* **305**:1163-1172.

Liu L., Wang Y., Shen C., He J., Liu X., Ding Y., et al. 2016. Benzo(a)pyrene inhibits migration and invasion of extravillous trophoblast htr-8/svneo cells via activation of the erk and jnk pathway. *J Appl Toxicol.* **36**:946-955.

Loch-Caruso R., Hassan I., Harris S.M., Kumar A., Bjork F., Lash L.H. 2018. Trichloroethylene exposure in mid-pregnancy decreased fetal weight and increased placental markers of oxidative stress in rats. *Reprod Toxicol.* **83**:38-45.

Meekins J.W., Pijnenborg R., Hanssens M., McFadyen I.R., van Asshe A. 1994. A study of placental bed spiral arteries and trophoblast invasion in normal and severe pre-eclamptic pregnancies. *Br J Obstet Gynaecol.* **101**:669-674.

Quiros P.M., Prado M.A., Zamboni N., D'Amico D., Williams R.W., Finley D., et al. 2017. Multi-omics analysis identifies atf4 as a key regulator of the mitochondrial stress response in mammals. *J Cell Biol.* **216**:2027-2045.

Ruckart P.Z., Bove F.J., Maslia M. 2014. Evaluation of contaminated drinking water and preterm birth, small for gestational age, and birth weight at marine corps base camp lejeune, north carolina: A cross-sectional study. *Environ Health.* **13**:99.

Shpilka T., Haynes C.M. 2018. The mitochondrial upr: Mechanisms, physiological functions and implications in ageing. *Nat Rev Mol Cell Biol.* **19**:109-120.

Stark G. 2005. Functional consequences of oxidative membrane damage. *J Membr Biol.* **205**:1-16.

Szklanna P.B., Wynne K., Nolan M., Egan K., Ainle F.N., Maguire P.B. 2017. Comparative proteomic analysis of trophoblast cell models reveals their differential phenotypes, potential uses and limitations. *Proteomics.* **17**:1700037-1700042.

Takao T., Asanoma K., Kato K., Fukushima K., Tsunematsu R., Hirakawa T., et al. 2011. Isolation and characterization of human trophoblast side-population (sp) cells in primary villous cytotrophoblasts and htr-8/svneo cell line. *PloS one.* **6**:e21990.

van de Water B., Zoeteweij J.P., de Bont H.J., Mulder G.J., Nagelkerke J.F. 1994. Role of mitochondrial ca2+ in the oxidative stress-induced dissipation of the mitochondrial membrane potential. Studies in isolated proximal tubular cells using the nephrotoxin 1,2-dichlorovinyl-l-cysteine. *J Biol Chem.* **269**:14546-14552.

van de Water B., Zoeteweij J.P., de Bont H.J., Nagelkerke J.F. 1995. Inhibition of succinate:Ubiquinone reductase and decrease of ubiquinol in nephrotoxic cysteine s-conjugate-induced oxidative cell injury. *Molecular pharmacology.* **48**:928-937.

Xu F., Papanayotou I., Putt D.A., Wang J., Lash L.H. 2008. Role of mitochondrial dysfunction in cellular responses to s-(1,2-dichlorovinyl)-l-cysteine in primary cultures of human proximal tubular cells. *Biochem Pharmacol.* **76**:552-567.

Yung H.W., Calabrese S., Hynx D., Hemmings B.A., Cetin I., Charnock-Jones D.S., et al. 2008. Evidence of placental translation inhibition and endoplasmic reticulum stress in the etiology of human intrauterine growth restriction. *Am J Pathol.* **173**:451-462.

Appendix. Supplementary Figures

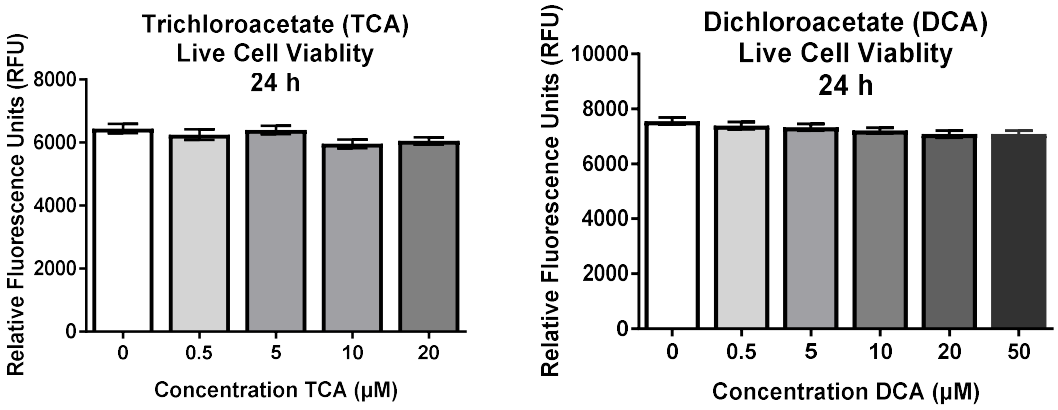

Figure A.1. Effects of trichloroacetate (TCA) and dichloroacetate (DCA) treatment on cell viability.
Cells were treated with medium alone or TCA or DCA (0.5-50 uM) for 24 h. Cell viability was measured fluorescently with ApoLive-Glo™ Multiplex Assay (Promega). Data were analyzed by one-way ANOVA. N= 3 independent experiments, with 3 replicates per treatment in each experiment. Camptothecin (4 µM) was included as a positive control and decreased live cell fluorescence to 3378±53.57 for the TCA experiments and 3682±106.4 for DCA experiments.

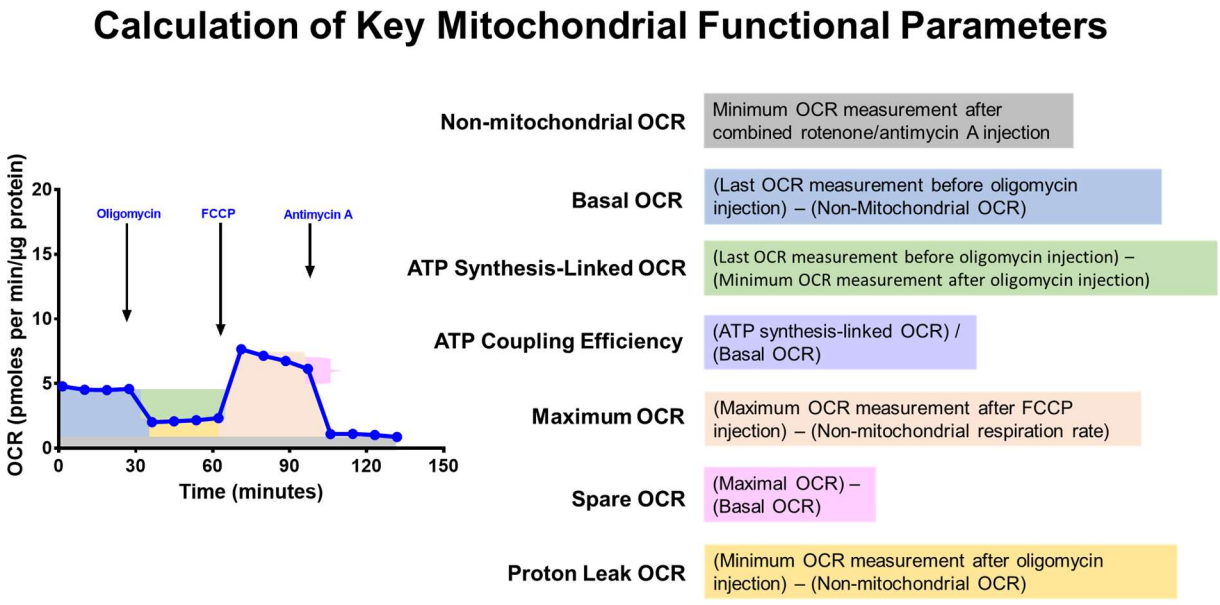

Figure A.2. Mitochondrial OCR function parameters.
Visualization of mitochondrial functional parameter calculations as described in the methods section of Chapter 4. This figured is modified from the Seahorse XF Cell Mito Stress Test Kit User Guide (AgilentSeahorse 2017).

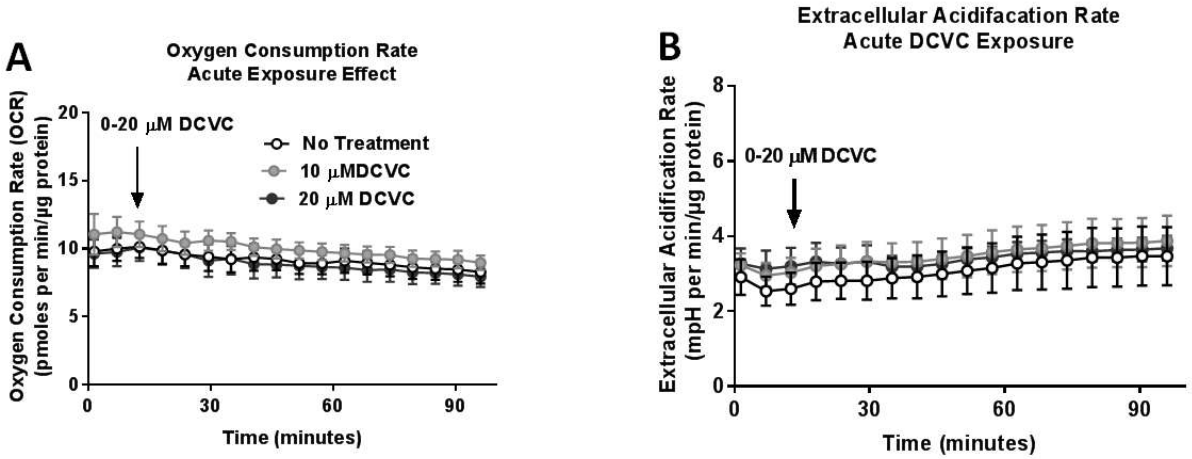

Figure A.3. Effects of acute DCVC treatment on OCR and ECAR.
DCVC treatment on mitochondrial function in HTR-8/SVneo cells. Different concentrations of DCVC (5-20 µM) were injected directly into wells containing live-intact cells and A) oxygen consumption rates and B) extracellular acidification rates were measured simultaneously for 90 minutes. N= 3 independent experiments for each time point, with 3-5 replicates per treatment in each experiment.

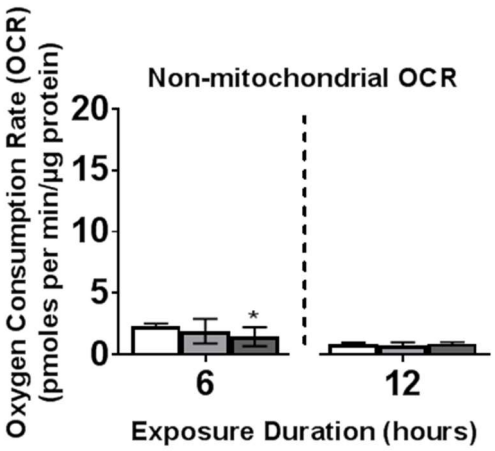

Figure A.4. Non-mitochondrial OCR.
Cellswere treated for 6 or 12 h with medium alone (control), or with 10 or 20 µM DCVC. Non-mitochondrial respiration (cellular oxygen consumption not attributed to mitochondrial activity) was measured with the Seahorse XF24 Analyzer. Bars represent means ± SEM. Data were analyzed by adjusted linear mixed-models with posthoc Tukey multiple comparisons restricted to comparison within each time point because experiments were conducted separately (indicated by vertical dashed line on graph). N= 3 independent experiments for each time point.

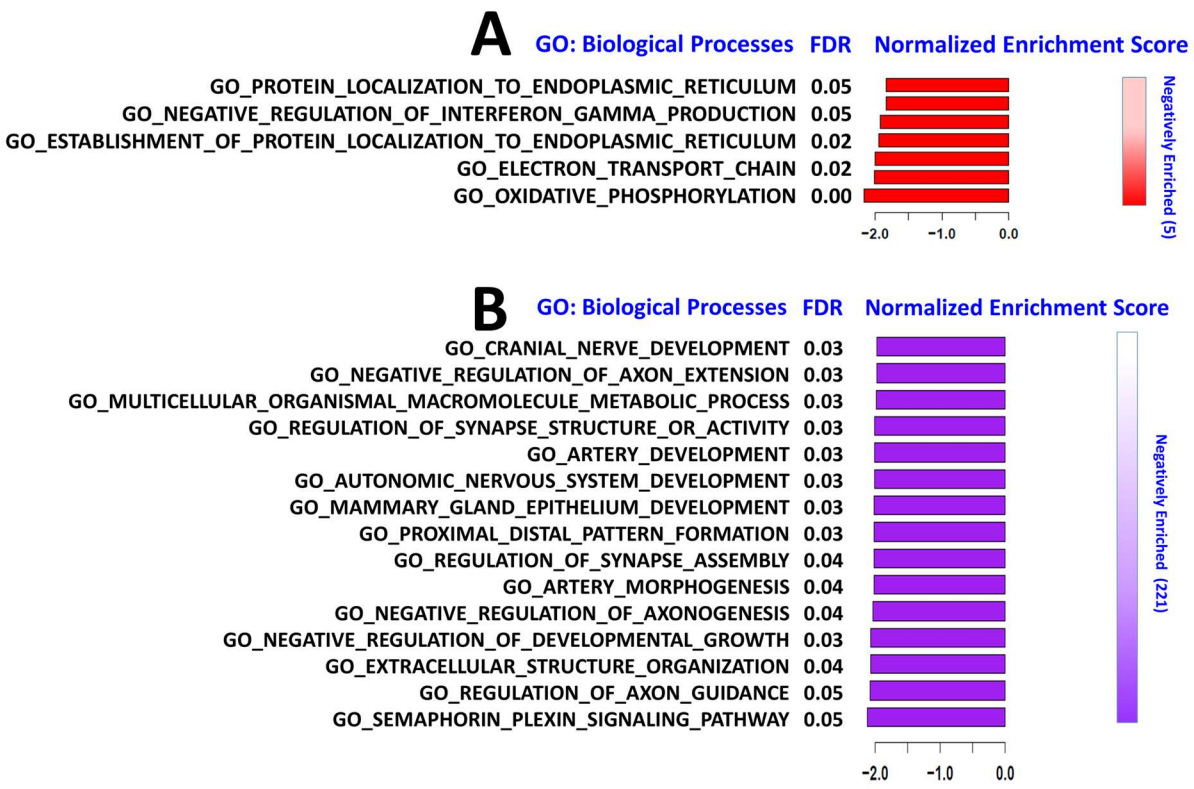

Figure A.5. Identification of significantly enriched biological processes after 6 h treatment with DCVC.

Visualization of the top 15 negatively-enriched biological processes at 6 h for **A)** 10 µM and **B)** 20 µM DCVC ranked according to normalized enrichment score (NES). Gene set enrichment analysis identified treatment-related enriched biological processes based on the GO: Biological Processes gene set. The analyses included 12,855 genes ranked according to the log fold-change value from each respective comparison. FDR<0.1 was considered significantly enriched.